
Tuning the Singlet-Triplet Splitting in Eu-Quinolinolate Complexes

Diplomarbeit

am Fachgebiet Theoretische Chemie

Institut für Physikalische und Theoretische Chemie

Technische Universität Graz

vorgelegt von

Johannes Kreutzer

Betreuerin: Ass.-Prof Dr. Anne-Marie Kelterer

Johannes Kreutzer

Matrikelnummer: 0230447

Eidesstattliche Erklärung

Ich erkläre hiermit an Eides statt, dass ich die vorliegende Arbeit ohne Hilfe Dritter und ohne Benutzung anderer als der angegebenen Hilfsmittel angefertigt habe; die aus fremden Quellen direkt oder indirekt übernommenen Gedanken sind als solche kenntlich gemacht. Die Arbeit wurde bisher in gleicher oder ähnlicher Form keiner anderen Prüfungsbehörde vorgelegt und auch noch nicht veröffentlicht.

Graz, 1.8.2009

Unterschrift

Meinen Eltern

Acknowledgment

My special thanks to Ass.-Prof. Dr. Anne-Marie Keltere for giving me the possibility to work on this diploma thesis, for guidance through the whole working process and for the possibilities to participate on conferences.

I would also like to thank all the people at the institute for their help and for support during the work on this project. Special thanks to the technical engineer Helmut Eisenkölbl, who always gave a helping hand when technical problems occurred. Thanks also to Prof. M. Ramek and Prof. K. Gatterer for assistance and fertile discussions and to my colleague K. Punyain for scientific support.

I also want to express my gratitude to Prof. E. Zojer from the Institute of Solid State Physics, Dr. K. Zojer from the Institute of Theoretical and Computational Physics and Prof. C. Slugovc from the Institute of Chemistry and Technology of Materials for their support during the working process.

Many thanks to Dr. F. Niedermair for recording the UV-VIS spectra. Thanks also to Dr. U. Rosspeintner, who gave me support in experimental matters.

I am also grateful to L. Payrer and K. Georgieva for doing corrections on the manuscript.

In the end I want to thank my family for their support and aid during my studies. Without them none of this would have been possible.

Abstract

The main topic of this work was the theoretical investigation on the photophysics and especially the singlet and triplet states of Eu-complexes. Homoleptic Eu(III) complexes comprising three bidentate 8-quinolinolate ligands (Q) in the structure (EuQ₃) were investigated. Complex systems composed of extended organic π -systems and bearing a lanthanide ion in the center are of high interest in sensor and OLED technology due to their photophysical properties. Energy transfer occurs via the so called "antenna-effect", where the ligand system is excited and transfers the energy via ISC to the triplet state of the ligand followed by an energy transfer to the 4f electrons of the Eu(III) ion. Emission occurs from the ⁵D₀ level of the Eu(III) ion to the ⁷F₂ level at 2.023 eV (614 nm).

The main topic of the work was to test standard quantum chemical methods (DFT and TD-DFT) for their applicability to describe the ligand and complex systems, to investigate the singlet-triplet splitting energetically and to estimate the error relative to experimental data.

A series of 8-hydroxyquinoline molecules with different substituents in 5-position and with selected substituents (NH₂, -NO₂, -Ph, -HSO₃ and Py) in the remaining positions were calculated. For three substituents (-HSO₃, -NH₂ and -NO₂) and the unsubstituted 8-quinolinolate ligand, the Eu complexes were calculated and the different absorption energies were compared with UV experiments. Solvent studies with a continuum model and with explicit solvent molecules were performed for ethanol and dichloromethane, respectively. The photophysics of the singlet and triplet states is discussed and all results are compared with available experimental data.

Density Functional Theory (TD-B3LYP) was used for the investigation of the photophysics and the singlet and triplet state of both, the ligands and the complexes. Based on the knowledge, that the 4f electrons do not participate in the ligand to Eu bonding, Eu is described by relativistic ECPs including the 4f electrons in the core. The triple-zeta-basis set TZVP was used for the ligand system. Additionally the semiempirical AM1 model was employed to optimise the complex structures and the goodness of the results is compared to the ab initio calculations.

It could be shown that donor substituents decrease the HOMO-LUMO gap and shift the excitation energy to lower wavelength. There is evidence that the charges on the oxygen of the Eu-oxoquinolinolate

complexes can be estimated by calculation on ligands only. These charges correlate with the Eu-O bond length in the complex system and with the HOMO-LUMO energy and the triplet energy. It could be proved that the applied method is able to describe the systems correctly with an error of approximately 5% for the gas phase calculation and 3% for the solvent calculation.

Zusammenfassung

In der vorliegenden Arbeit wurden homoleptische Eu(III) Komplexe der Form EuQ_3 untersucht. Q ist hierbei ein bidentater 8-hydroxychinolinat Ligand. Lanthanid-Ion Komplexe mit ausgedehnten π -Systemen erwecken durch ihre speziellen photophysikalischen Eigenschaften vor allem Interesse in der OLED und Sensortechnologie. Energietransfer findet durch den sogenannten "Antennen-Effekt" statt, wobei das Ligandensystem angeregt wird und die Energie nach einem ISC zum Triplettzustand der Liganden an die 4f Elektronen des Eu-Ions übertragen wird. Emission findet vom $^5\text{D}_0$ zum $^7\text{F}_2$ Niveau des Eu(III)-Ions bei ca. 2,023 eV (614 nm) statt.

Von größtem Interesse ist die Frage nach der Auswirkung verschiedener Substituenten auf den HOMO-LUMO Abstand im Liganden System. Weiters ist die Lage des Triplettzustandes in den verschiedenen Komplexen wichtig, da ein vollständiger Energie Transfer nur zustande kommen kann, wenn der Triplettzustand der Liganden nahe am Resonanz Niveau des Eu(III)-Ions liegt. In Bezug auf die Rechenmethode stellt sich die Frage, in wie weit Resultate der Liganden Eigenschaften der Komplexe vorhergesagen können.

Eine Reihe von 8-Hydroxychinolin Molekülen mit verschiedenen elektronenziehenden und -drückenden Substituenten in Position 5 der Chinolinstruktur wurde untersucht. Für ausgewählte Substituenten wurden Rechnungen in anderen Substitutionspositionen durchgeführt. Vier Substituenten ($-\text{HSO}_3$, $-\text{NH}_2$, $-\text{NO}_2$ und $-\text{H}$) wurden gewählt, um Rechnungen an den Komplexsystemen durchzuführen. Hierbei wurden die Triplett- und Singlettenergien ermittelt und Lösungsmittelleffekte mit dem Continuum Modell (PCM) und durch explizite Lösungsmittelmoleküle für Ethanol (ETOH) und Dichlormethan (DCM) untersucht. Die photophysikalischen Eigenschaften der Singlett- und Triplettzustände wurden diskutiert und alle Ergebnisse wurden mit vorhandenen experimentellen Werten verglichen.

Für die Untersuchung der Triplett- und Singlettzustände wurde die Dichtefunktional-Theorie (TD-B3LYP) verwendet. Da 4f Elektronen nicht an der Bindung im Komplex beteiligt sind, wurde für Eu(III) ein relativistisches Effective-Core Potential (ECP) verwendet. Der Triple-Zeta Basissatz (TZVP) wurde zur Beschreibung der Ligandenatome verwendet. Zusätzlich wurde das semiempirische Modell AM1 zur Untersuchung der Geometrie getestet.

Es konnte gezeigt werden, dass die verwendete Methode experimentelle Resultate mit einem Fehler von 5% für Gasphasenrechnungen und mit einem Fehler von 3% für Lösungsmittelrechnungen reproduzieren kann. Weiters konnte gezeigt werden, dass Donorsubstituenten in der Lage sind den, HOMO-LUMO Abstand zu verkleinern und die Anregungsenergie dadurch weiter in den sichtbaren Bereich des elektromagnetischen Spektrums zu schieben. Es gibt Anzeichen dafür, dass die Ladungen an den Sauerstoffatomen im Komplex durch Rechnungen an den reinen Liganden abschätzbar sind. Diese Ladungen wiederum korrelieren mit der Eu-O Bindungslänge und mit dem HOMO-LUMO Abstand im Komplex.

Contents

1	Introduction	1
2	Methods in Computational Chemistry	4
2.1	HF-SCF Theory	4
2.2	Basis Sets	11
2.3	Semiempirical Methods	14
2.4	Ab Initio Methods	15
2.4.1	Configuration Interaction	16
2.4.2	Many-Body Perturbation Theory	17
2.4.3	Density Functional Theory	18
2.4.3.1	Functionals	22
2.4.3.2	Time Dependent Density Functional Theory (TD-DFT)	23
2.5	Calculating Properties	24
2.5.1	Structure Optimisation	24
2.5.2	Population Analysis	26
2.6	Solvation Models	27
2.7	Relativistic Effects	32
3	Description of the Methodology	37
4	Results	40
4.1	Calculation on the Ligand Systems	40
4.1.1	Singlet and Triplet State Geometry of the Ligands	43
4.1.2	Geometry of the Singlet Ground State	43
4.1.3	Geometry of the Triplet State	48
4.1.4	Difference in the Singlet and Triplet Geometry	52
4.2	Evaluation of the Electrical and Chemical Parameters	55
4.3	Absorption Spectra of the Ligands	58
4.3.1	8-Hydroxyquinoline	58

4.3.2	5-Formyl-8-hydroxyquinoline	61
4.3.3	5-nitro-8-hydroxyquinoline	65
4.3.4	Other ligand systems	71
4.4	Jablonski Diagram for Ligand Structures	76
4.5	Calculation on Complex Systems	81
4.5.1	Singlet and Triplet State Geometry of the Complexes	82
4.5.2	Difference in the geometry of the isomers	84
4.5.3	Effect of the substituents	85
4.5.4	Singlet and triplet geometries	85
4.5.5	Solvent effects	85
4.5.6	AM1 geometries	87
4.6	Absorption Spectra of the Complexes in Gas Phase	89
4.6.1	Unsubstituted complexes - Eu(Q) ₃	89
4.6.2	NH ₂ substituted complexes - Eu(NH ₂ Q) ₃	95
4.6.3	NO ₂ substituted complexes - Eu(NO ₂ Q) ₃	101
4.6.4	HSO ₃ substituted complexes - Eu(HSO ₃ Q) ₃	105
4.7	Explicit solvent models	110
4.7.1	EuQ ₃ (X) ₃ (X=DCM, ETOH)	110
4.7.2	Eu(NH ₂ Q) ₃ (X) ₃ (X=DCM or ETOH)	113
4.7.3	Eu(NO ₂ Q) ₃ (X) ₃ (X=ETOH, DCM)	115
4.7.4	Eu(Q) ₄ (X) ₂ (X=H ₂ O or ETOH)	117
4.8	Jablonski Diagram for Complex Structures	124
4.9	Conclusion	129
4.9.1	Error introduced in the calculation	129
4.9.2	Geometry of the ligand and complex structures	132
4.9.3	Singlet and Triplet state energies of the ligands and complexes	132
5	Summary and Outlook	137
	Bibliography	XII
A	Tables	XVI
B	List of Tables	LVI
	List of Tables	LVII
C	List of Figures	LX

List of Figures

LXI

D List of Symbols

LXIV

Chapter 1

Introduction

Matter of this work is the investigation of structure and photophysical properties of Europium-8-oxoquinolinolate complexes (EuQ_3). Complexes of lanthanide ions with organic ligands comprising an extended π -system are of high interest in OLED and sensor technology due to their special electron transfer and emissive properties. VanSlyke was the first who reported an OLED which used an AlQ_3 complex in the emitting layer and showed in this way the excellent photochemical properties of this compound class. Following the publication of VanSlyke more and more work was done regarding the application of metal-complex compounds in technology [1, 2, 3, 4, 5] and regarding the investigation of photophysical and structural properties of such complexes [6, 7].

In newer publications the application of lanthanide ions as central ion in the complex structures is reported [8, 9, 10]. The big advantage of this lanthanide complexes is a relatively sharp emission line due to f-f transitions [3]. The energy levels of the 4f orbitals do not change in dependence of the chemical environment in the complex, since the 4f electrons are shielded by energetically higher lying 5s and 5p orbitals. Emission from the 4f levels occurs with a narrow spectral line at a well defined wavelength. Other advantages compared to organic dyes, which were used in the emissive layer of OLEDs before, is the good thermal stability of lanthanide complexes and long decay times. A drawback is that due to Laporte forbidden transitions the excitation of lanthanide ions is unsatisfactory. To overcome this problem excitation happens in the organic ligand system, which transfers the energy via an inter system crossing (ISC) process to the triplet state. From the triplet state energy of the ligand system, transfer to the resonance level of the lanthanide ion occurs. This process of energy transfer is also called "antenna-effect" and exhaustingly discussed in literature [11, 12].

8-hydroxyquinoline and its derivatives emerged to be a good ligand system and are often reported in literature [13, 14, 15]. Three bidentate 8-oxoquinolinolate can coordinate to the lanthanide ion, giving

a distorted octahedral structure. However, structural investigations on lanthanide halogenides show that 9-fold coordinated complexes are possible [16]. In case where the ligand system of the octahedral complex is sterically not very demanding, solvent molecules can saturate the coordination sphere and can be the reason for nonradiative decay and a diminished quantum yield during the energy transfer. However, Kottas et al. reported a ninefold coordinated complex where the coordination sphere is occupied by bipyridine ligand molecules only [6]. Therefore the behaviour of different ligand systems and its influence on the complex structure is of high interest.

There is an increasing number of publication which deal with computing such complex systems and there is an interest to find ways to predict structural and photophysical properties of different complexes. The special way to excite this systems via the antenna effect gives good possibilities to alter the ligand system chemically and enhance the performance of the compounds but leave the emission wavelength unchanged at the same time. A drawback of the 8-oxoquinolinolate ligands is the absorption maximum at short wavelength. UV light sources have a lower brightness and are more expensive than VIS light sources. In sensor technology UV light sources are the reason for a high level of background fluorescence in biological media. Additionally cheap fibers to the excitation light have generally a low transparency in the UV range. Therefore development of complexes with high quantum yield and absorption characteristics in the visible range of the spectrum attracted research interest.

In this work the Density Functional Theory (DFT) was applied to predict structural and absorption characteristics of EuQ_3 complex systems and to investigate the singlet and triplet splitting of such complex systems. By introducing substituents with different electron pushing and pulling abilities in the backbone of the 8-oxoquinolinolate ligand the singlet and triplet energies of the complex system can be shifted. The investigation of the HOMO - LUMO splitting is of special interest since the substituents are able to change the position of the frontier orbitals. In this way the excitation energy can be shifted to smaller or larger wavelength. Another aspect of this work was to find a reliable, but referring to computational cost, still cheap method to compute Eu-oxoquinolinolate systems. Therefore interest exists in how far results from calculations on the ligand system only can be used to predict properties of the complex systems.

The method of choice was DFT and TD-DFT in combination with the B3LYP functional. This method was proposed before for similar calculations [17, 18, 19] and emerged to be appropriate to calculate the complex systems with an adequate accuracy. Previously it was reported that 4f electrons do not participate in bonding in the complex [20, 21]. This allows to employ effective core potentials (ECP) which comprise the 4f electrons in the core during calculation on the Eu(III) ion. In this work the 52MWB rela-

tivistic ECP published by Dolg [22] was used. The TZVP and 6-31G* basis set was used for calculation on the ligand systems and for calculation on the light atoms in the complex system.

In a first step, calculations on 8-hydroxyquinoline derivatives with different substituents in 5-position of the backbone were performed. The electron pulling or pushing ability of the ligands was investigated by determining electronic parameters such as the ionisation potential, electron affinity and chemical hardness parameter. In a second step, the selected substituents were placed on different positions of the ligand backbone, to investigate the influence of the substitution position. Finally, four complex systems were investigated and the absorption spectra and singlet and triplet energies were computed. Freire et al. published a set of AM1 Sparkle parameters for europium complexes [23]. This parameter set was used to optimise the complex structures semiempirically and results were compared to DFT calculated structures. Solvent effect was accounted for by energy refinement while employing the polarisable continuum model (PCM) for ethanol and dichloromethane. Additionally solvent effects were investigated by explicit putting three solvent molecules in the first coordination sphere of the complex.

To get an understanding about the methods of computation which were applied in this work Chapter 2 is dedicated to the theoretical principles. Here, starting with the Schrödinger equation the different methods are explained, such as the HF-SCF method as fundamental method and consequently the approximations in form of the semiempirical methods. Since calculation for this work were performed with DFT, a subchapter explains the principles of DFT and its time dependent form (TD-DFT). The theory of solvation models can be found in chapter 2 as well as a short overview about relativistic effects in general and models how to handle them during computation.

Chapter 3 gives an overview of the methodology. Here it is explained how the calculations were performed, and which programs were used for calculation and evaluation of the results.

Chapter 4 is devoted to the interpretation of the results. Presentation of the ligand and complex results are separated in two parts and each part starts with a comparison of structural characteristics of the systems of investigation. After discussing the absorption spectra interpretation of the singlet and triplet energies is given, as well as a close look on the HOMO - LUMO splitting in the ligand and complex systems. Tables containing all results are presented in the Appendix.

Chapter 2

Methods in Computational Chemistry

The improvement of computational possibilities during the last decades made it possible to accomplish calculations even for bigger sized systems with high accuracy. Nevertheless, methods which do not solve the Schrödinger equation ab initio but fall back on approximations, show their advantage in respect of computational cost and give in some cases as good results as the ab initio methods. During the years the models applied in computational chemistry became manifold and knowing which method to use is one of the key features of a successful calculation. Some methods will not be able to describe the system in the best way or will fail for calculating special properties. Knowledge about the methods, their excellence and drawbacks is therefore most important.

All of the following described methods are based on quantum mechanical methods. Generally, one can distinguish between two major groups, semi-empirical and ab initio methods. While in ab initio methods only the geometry and the charges are used as input, and all other parameters like the wavefunction coefficients are determined during the calculation, semi-empirical methods estimate some integrals during the calculation or even fall back on empirically gained parameters. The following chapter gives a short outline on common up-to-date methods.

2.1 HF-SCF Theory

[24, 25, 26]

At the beginning of every quantum chemical calculation stands the Schrödinger equation, which is given here in its time dependent short-hand operator form:

$$\left[-\frac{1}{2m} \left(\frac{\delta^2}{\delta x^2} + \frac{\delta^2}{\delta y^2} + \frac{\delta^2}{\delta z^2} \right) + \mathbf{V} \right] \Psi = i \frac{\delta \Psi}{\delta t} \quad (2.1)$$

The term in brackets on the left hand side of equation 2.1 is abbreviated as \mathbf{H}_{tot} , speak total Hamilton operator, and is the sum of the kinetic and potential energy operators of the nuclei and electrons as shown in its expanded form in equation 2.2

$$\mathbf{H}_{tot} = \sum_K -\frac{\hbar^2}{2M_K} \Delta_K + \sum_{\mu} -\frac{\hbar^2}{2m_{\mu}} \Delta_{\mu} + \sum_{K \neq L} -\frac{Z^2 e^2}{4\pi\epsilon_0 r_{K,L}} + \sum_{K,\mu} -\frac{Z e^2}{4\pi\epsilon_0 r_{K,\mu}} + \sum_{\mu \neq \nu} -\frac{e^2}{4\pi\epsilon_0 r_{\mu,\nu}} \quad (2.2)$$

The first term corresponds to the kinetic energy of the nuclei, the second term gives the kinetic energy of the electrons and the last three terms correspond to the potential energy of the nucleus-nucleus, nucleus-electron and electron-electron interaction, respectively. With equation 2.2 a special notation has been introduced which will be used from now on. All operators are written as capital, bold letters. The indices referring to nuclei are K and L, those referring to the electrons are μ and ν . Δ is the square of the nabla operator and is shown in equation 2.3:

$$\Delta = \nabla^2 = \left(\frac{\delta^2}{\delta x^2}, \frac{\delta^2}{\delta y^2}, \frac{\delta^2}{\delta z^2} \right) \quad (2.3)$$

For convenience the operator notation will be used and atomic units will be introduced, that means:

- Charge of an electron as 1 unit of charge = $|e|$
- 1 kg as 1 unit of mass = $|m_e|$
- Bohr radius as 1 unit of length = a_0
- 1 Hartree as 1 unit of energy = E_a

The kinetic and potential energy operators of the electronic Hamiltonian have now the following form:

$$\mathbf{T}_e = - \sum_{\mu=i}^N \frac{\hbar^2}{2m_i} \nabla_i^2 \quad (2.4)$$

$$\mathbf{T}_n = - \sum_{\mu=i}^N \frac{\hbar^2}{2M_i} \nabla_i^2 \quad (2.5)$$

$$\mathbf{V}_{ne} = - \sum_{\mu=i}^N \sum_K \frac{Z_K}{r_{\mu K}} \quad (2.6)$$

$$\mathbf{V}_{nn} = - \sum_{K=i}^N \sum_{L>K}^N \frac{Z_K Z_L}{r_{KL}} \quad (2.7)$$

$$\mathbf{V}_{ee} = - \sum_{\mu=i}^N \sum_{\nu>i}^N \frac{1}{r_{\mu\nu}} \quad (2.8)$$

Letting \mathbf{H}_{tot} act on the wavefunction in equation 2.1 gives the energy as an eigenvalue. Unfortunately, it is not possible to solve this form of the Schrödinger equation exactly if more than 2 particles interact with each other, e. g. more than one electron and one nucleus. Hence, even for the simplest molecule, the H_2^+ molecule, equation 2.1 can not be solved exactly. The time dependent form of the wavefunction describes the situation of an electron moving through the space under an external field (e. g. the electrostatic potential arising from the nuclei). Generally, the problems in computational chemistry show, referring to the potential, a time independent behavior. The wavefunction therefore can be separated in a time dependent part and a spatial part, according to equation 2.9

$$\Psi(r,t) = \Psi(r) \mathbf{T}(t) \quad (2.9)$$

Nuclei have a much higher mass than electrons and therefore electrons can adjust to a change of the nuclear coordinates very easily. The molecular backbone can be seen as fixed on the timescale of electron motion. Therefore the whole equation can be separated in an electronic part which is dependent on the nuclear position only, and a nuclear part, which is known as Born-Openheimer approximation in literature. These two equations can now be solved separately.

$$\mathbf{H}_e \Psi_e = E_e \Psi_e \quad (2.10)$$

$$\mathbf{H}_n \Psi_n = E_n \Psi_n \quad (2.11)$$

with

$$\mathbf{H}_e = \mathbf{T}_e + \mathbf{V}_{ne} + \mathbf{V}_{ee} + \mathbf{V}_{nn} \quad (2.12)$$

and

$$\mathbf{H}_n = \mathbf{T}_{nn} \quad (2.13)$$

\mathbf{T} will be used for the kinetic energy operators and \mathbf{V} for the potential energy operators from now on. This approximation simplifies the problem significantly, since the electronic energy E_e can be calculated

by using the electronic operators from equation 2.12 for solving the Schrödinger equation, which is dependent on a fixed nuclear position only.

Wavefunctions are expected to be orthogonal and normalized, which can be expressed by using the Kronecker δ for the overlap matrix:

$$\mathbf{S}_{\mu\nu} = \int \Psi_{\mu}^* \Psi_{\nu} d\tau = \delta_{\mu\nu} \quad (2.14)$$

The Schrödinger equation is only valid if the wavefunction is an eigenfunction of the Hamilton operator, that is the case if the wavefunction exactly describes a system. For approximated wavefunctions the expectation value for the energy is given as

$$\langle E \rangle = \frac{\int \Psi^* \mathbf{H} \Psi d\tau}{\int \Psi^* \Psi d\tau} \quad (2.15)$$

Recalling that wavefunctions are orthonormal functions, equation 2.15 simplifies to

$$\langle E \rangle = \langle \Psi | \mathbf{H} | \Psi \rangle \quad (2.16)$$

The bra-ket notation used in equation 2.16 expresses the integrals. Bra $\langle x |$ is a complex conjugate function standing on the left, while $|y\rangle$ means a function standing on the right. The operator in the middle acts on the right function as usual.

Everything needed to successfully solve the Schrödinger equation is a suitable wavefunction. Unfortunately, the exact form of the wavefunction is not known a priori. However, Hartree and Fock developed a recursive method which takes approximative wavefunctions as input and gives coefficients for a better function. This method can be repeated with the new set of functions until the function becomes self consistent, that is when the energy difference meets a certain threshold criterion.

When constructing trial wavefunctions one has to bear in mind that electrons are fermions with a spin of $\frac{1}{2}$. Therefore, the wavefunction must be antisymmetric, that means, it must change the sign when two electrons are exchanged. The Hartree product which is shown in equation 2.17 where the one electron functions of the system are multiplied is not an appropriate form since interchange of two electrons will not change the sign.

$$\Psi(1, 2, \dots, N) = \chi(1)\chi(2)\dots\chi(N) \quad (2.17)$$

One possible form to overcome this problem is to use a matrix representation. The so called Slater determinant is a scheme comprising the orbital functions at which the rows of the matrix refer to the electron coordinates and the column to single electron functions. χ stands now for a spin orbital where a spin function is multiplied with a single electron function and the factor $\frac{1}{\sqrt{N!}}$ is a normalisation factor.

$$\Phi_{\text{SD}} = \frac{1}{\sqrt{N!}} \begin{vmatrix} \chi_1(1) & \chi_2(1) & \dots & \chi_N(1) \\ \chi_1(2) & \chi_2(2) & \dots & \chi_N(2) \\ \dots & \dots & \dots & \dots \\ \chi_1(N) & \chi_2(N) & \dots & \chi_N(N) \end{vmatrix}$$

Exchanging two electrons is equivalent with exchanging two rows and the determinant will change its sign, as proposed from the antisymmetry principle. Furthermore, two equivalent rows would mean that two electrons with same spin occupy one orbital, which is not allowed by the Pauli exclusion and the determinant will vanish. In the electronic Hamiltonian given in equation 2.12 two operators are dependent on one electron function only, that is \mathbf{T}_e and \mathbf{V}_{ne} . \mathbf{V}_{ee} depends on two electrons and the nuclear potential energy operator \mathbf{V}_{nn} gives a constant for a fixed geometry. Therefore, it is possible to combine the one electron operators to a so called one electron Hamiltonian. Letting it act on the system will give the sum of the potential and the kinetic energy of each electron in the field of the nuclei as eigenvalue.

$$E^{\text{core}} = \sum_{i=1}^N \langle \chi_i(1) | \mathbf{H}_{ii}^{\text{core}} | \chi_i(1) \rangle \quad (2.19)$$

with

$$\mathbf{H}_{ii}^{\text{core}} = -\frac{1}{2} \nabla_i^2 - \sum_{K=1}^N \frac{Z_K}{r_{iK}} \quad (2.20)$$

The two electron Hamiltonian refers to the electron correlation in the system and gives, acting on χ , two contributions to the energy. The first describes the electrostatic repulsion of two electrons and has, summed over all electrons, the form of:

$$E^{\text{coulomb}} = \sum_{\mu=1}^N \sum_{\nu=i+1}^N \left\langle \chi_{\mu}(1) \chi_{\mu}(1) \left| \frac{1}{r_{\mu\nu}} \right| \chi_{\nu}(2) \chi_{\nu}(2) \right\rangle \quad (2.21)$$

The other contribution is called the exchange interaction and refers to the fact that electrons with the same spin avoid each other. The exchange energy is given as:

$$E^{\text{exchange}} = \sum_{\mu=i}^N \sum_{\nu=i+1}^N \left\langle \chi_{\mu}(1) \chi_{\nu}(2) \left| \frac{1}{r_{\mu\nu}} \right| \chi_{\mu}(2) \chi_{\nu}(1) \right\rangle \quad (2.22)$$

The final operator giving the energy for a closed shell system, that means all N electrons are paired and occupy $\frac{N}{2}$ orbitals is called Fock operator and can be written as

$$\mathbf{F} = 2 \sum_{i=1}^{\frac{N}{2}} \mathbf{H}_{ii}^{\text{core}} + \sum_{\mu=1}^{\frac{N}{2}} \sum_{\nu=1}^{\frac{N}{2}} (2\mathbf{J}_{\mu\nu} - \mathbf{K}_{\mu\nu}) \quad (2.23)$$

$\mathbf{J}_{\mu\nu}$ and $\mathbf{K}_{\mu\nu}$ are the two electron integrals describing the Coulomb and the exchange energy.

$$\mathbf{J}_{\mu\nu} = \left\langle \chi_{\mu}(1) \chi_{\nu}(1) \left| \frac{1}{r_{\mu\nu}} \right| \chi_{\mu}(2) \chi_{\nu}(2) \right\rangle \quad (2.24)$$

and

$$\mathbf{K}_{\mu\nu} = \left\langle \chi_{\mu}(1) \chi_{\nu}(2) \left| \frac{1}{r_{\mu\nu}} \right| \chi_{\mu}(2) \chi_{\nu}(1) \right\rangle \quad (2.25)$$

As mentioned before the exact wavefunction of the system must be known to be able to calculate the exact energy of the system. Unfortunately, the form of this function is unknown and an approximate function has to be introduced. The variation principle states, any approximate wavefunction gives a higher energy than the exact function. The method of Lagrange multiplier gives mathematically a way to handle this problem by using the orthonormality condition which was introduced in equation 2.14 as constraint. In the Hartree-Fock equation the Lagrange multiplier represents the energy of the molecular orbitals and so the constraint can be written as

$$\delta E - 2\delta \sum_{\mu} \sum_{\nu} \epsilon_{\mu\nu} S_{\mu\nu} = 0 \quad (2.26)$$

For constructing the trial wavefunctions for the molecular orbitals, it is most easy to fall back on the Linear Combination of Atomic Orbitals ansatz (LCAO). Trial molecular wavefunctions can be constructed through a linear combination of atomic orbital wavefunctions as shown in equation 2.27. These functions are known as basis set and can have basically any form, although some practical aspects speak in the favour of Gaussian type functions.

$$\psi_i = \sum_{\nu=1}^K c_{\nu i} \phi_{\nu} \quad (2.27)$$

Letting now act the Fock operator on the system gives the sum of the core, coulomb and exchange energies in form of matrix elements. After introducing the LCAO ansatz and approximating the molecular wavefunctions with a set of AO, the coefficients can be singled out and can be represented through the density matrix \mathbf{P} . The form of the Fock matrix elements is shown below:

$$\mathbf{F}_{\mu\nu} = \mathbf{H}_{\mu\nu}^{\text{core}} + \sum_{\lambda=1}^K \sum_{\sigma=1}^K \mathbf{P}_{\lambda\sigma} [\langle \mu\nu | \lambda\sigma \rangle - \frac{1}{2} \langle \mu\lambda | \nu\sigma \rangle] \quad (2.28)$$

with

$$\mathbf{P}_{\lambda\sigma} = 2 \sum_i^{\text{occupied}} a_{\lambda i} a_{\sigma i} \quad (2.29)$$

where a is the contribution of the basis function (here specified through greek letters) to the molecular orbital i .

With these operators the Roothan-Hall equation, which is the fundamental equation for the Hartree Fock Self Consistent Field ansatz, can be formed as followed

$$\mathbf{FC} = \mathbf{SCE} \quad (2.30)$$

The Roothan-Hall equation is a matrix equation, containing the Fock matrix \mathbf{F} , the coefficient matrix \mathbf{C} , the energy matrix \mathbf{E} , which is a diagonal matrix and whose elements refer to the molecular energy and the overlap matrix \mathbf{S} . Solving the Roothan-Hall equation and refining the energy is best shown in a scheme:

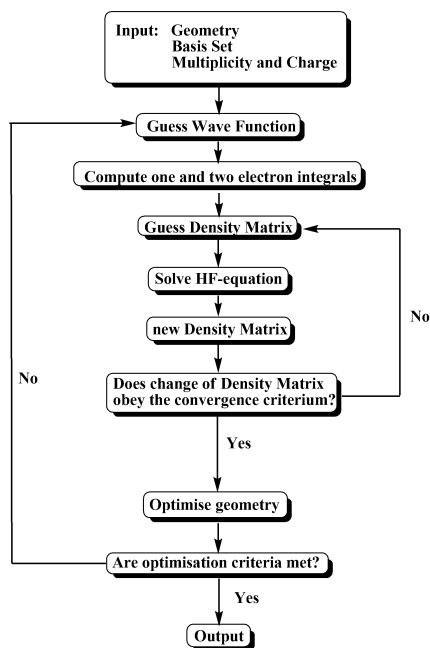


Figure 2.1: Scheme of HF calculation for optimising the geometry.

2.2 Basis Sets

[24, 25, 26]

Equation 2.27 shows how the molecular wavefunction can be constructed from atomic orbitals (AO). Fortunately the form of AO is in principle known and best described with a function proposed by Slater (STO).

$$\phi = Nr^n e^{-\alpha r} Y_l^m(\theta, \phi) \quad (2.31)$$

The radial part ($r^n e^{-\alpha r}$) does not describe any nodes and so orbitals with a higher principal quantum number than one have to be modelled through a linear combination of STOs. The mathematical form of the STOs does not allow it to solve the three and four centered integrals analytically. On the other hand a numerical solution of this integrals would be demanding in matter of computational cost. One way to overcome this problem is to use Gauss type functions (GTO) to approximate the STO. The mathematical form is shown in equation 2.32

$$\phi = Nx^l y^m z^n e^{-\beta r^2} \quad (2.32)$$

The drawback when using GTO is that the spin and charge distribution close to the nucleus and the long range distribution can not be described correctly (see Figure 2.2).

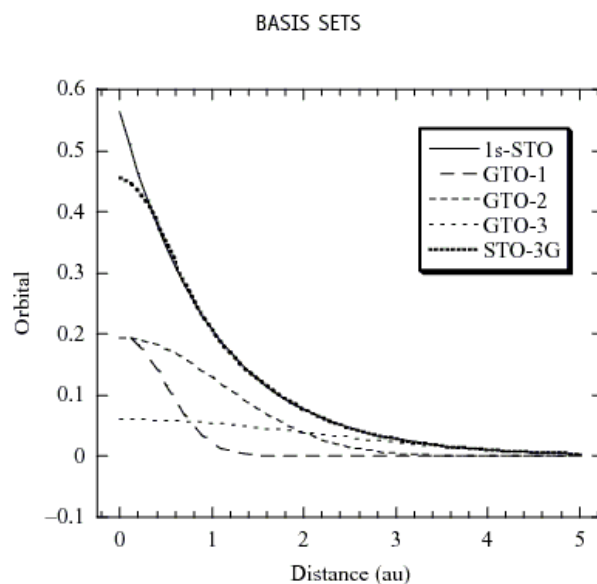


Figure 2.2: A 1s-STO function approximated by three GTO functions. Taken from Jensen "Introduction to Computational Chemistry" p. 194

Using a linear combination of at least three gaussian type orbitals gives a quite good fit regarding the overlap, but one has to bear in mind that the cusp at the nucleus can never be described exactly in this way. However, the save in computational cost compensates the error introduced by using GTO. There are different approaches how to approximate STOs using GTO from which the most common will be presented here. A *minimal basis set* consists only of the minimal amount of atomic orbitals which are needed to accommodate all the filled orbitals of each atom. The STO-3G basis uses the minimal number of orbitals and approximates it with three GTO. That means for hydrogen a 1s orbital is modelled with three gaussian functions. In general a STO-nG basis set uses n GTO per atomic orbital to model the minimum number of orbitals. Minimal basis sets give problems for heavier atoms, since they use the same number of basis functions for elements standing at the beginning or at the end of a period. One way to overcome this problem is to double the number of basis functions. A double zeta basis set for the H atom uses two 1s functions for example. The benefit is that using more than one function allows to modify the coefficients during the SCF optimisation more flexible. Using three functions per orbital gives a triple Zeta basis set and there are even higher ordered basis sets available, although increasing the size gives better results in general, but can also introduce artefacts in the calculation. This type of basis sets can describe the behaviour near the nucleus very well. However, for chemical problems the valence orbitals play an important role. Describing the behaviour far from the nucleus with the same accuracy like the inner orbital electrons can result in quite large basis sets. It is useful to simplify this problem by

using contracted functions and by splitting the basis set in a core and a valence part. Contracting basis functions means that a set of functions is seen as fixed, and the coefficients are not optimised separately during the optimisation. The degree of contraction states how many primitive gaussians (PGTO) enter the contracted GTO (CGTO).

Split valance basis set use a number of CGTO to describe the core and a different set of GTO to describe the valence part. In principal it is enough to use the minimal set of functions for each atom, depending on the angular momentum. Introducing functions with a higher angular momentum becomes important if different types of bonds are present in a molecule. The so called Polarisation function has for example a much higher ability to model distorted electron clouds which can be found in π bonds. For long range effects far from the nucleus diffuse functions are used. Those functions have a radial part which expands far in the space and are employed when loosely bond electrons are matter of interest, like in ionic structures or excitation calculations. Problems can occur during the SCF optimisation since diffuse functions converge very slowly.

A special notation has been found for describing basis sets. The 6-31G basis set uses 6 gaussians to approximate the core orbitals, and four gaussians describing the valence part. Three gaussians of the four valence functions are employed for the contracted part and one gaussian is used as diffuse function. Polarisation functions are signed with a "*" and diffuse functions are noted with a "+" after or the the phrase "aug-" before the notation.

Elements from the third row or higher of the PSE have a large number of core electrons. To model these systems would need a large number of functions, even if contracted functions are applied. For even more heavy elements relativistic effects have to be taken into account and things get complicated very fast. One way to deal with this problem is to apply Effective Core Potentials (ECP). The electrons are separated in core and valence electrons, respectively. The core electrons are treated with one wavefunction while the valence electrons are described explicitly. The approach is to do an all electron calculation, accounting for relativistic effects where needed, and replacing the valence orbitals with a set of pseudo-orbitals. Those pseudo-orbitals behave correctly in the outer part but are nodeless in the core region. The core orbitals are simulated with a potential and solving the Schrödinger equation gives valence orbitals and the potential comprising relativistic effects. The potential can then be fitted with gaussian functions.

During this work the following basis sets were used:

- 6-31G* for geometry optimisation on the ligands and the ligand system in the complex and for frequency calculations
- TZVP Triple Zeta valance split basis set for energy refinement on ligands and complexes and for TD-DFT calculations

- 52MWB Relativistic ECP from Dolg [22] for Eu, 52 electrons in the core

2.3 Semiempirical Methods

[24, 25]

In the computational less expensive semiempirical ansatz three and four center integrals, which need long time for calculating, are approximated and empirical parameters are introduced in the calculation. The most important methods for the semiempirical approach are described in this chapter. The basic principle behind semiempirical methods is the Zero Differential Overlap (ZDO). All products of the basis function for the same electron but on different nuclei is set equal to zero. As result the overlap matrix becomes the unity matrix, $S_{\mu\nu}=\delta_{\mu\nu}$, and all three- and four-center integrals are set to zero. Taking the overlap matrix as unity matrix simplifies the Roothan-Hall equation to $\mathbf{FC}=\mathbf{CE}$. This approximation saves a lot of computational cost, but good results can not be obtained. To compensate the approximation, some integrals are set as parameters. The semiempirical methods are all based on the ZDO approach, but differ in the parametrisation and in the choice of integrals which are set to zero.

The Complete Neglect of Differential Overlap (CNDO):

CNDO was the first method which based on the ZDO. The two-electron integrals which are centered on different atoms were replaced by a parameter (γ_{KL}). The Fock matrix can be divided in three groups now, $\mathbf{F}_{\mu\mu}$, the diagonal elements, $\mathbf{F}_{\mu\nu}$, the off diagonal elements centered on the same nucleus and $\mathbf{F}_{\mu\nu}$, the off diagonal element centered on different nuclei. The first term can be written as following and describes the diagonal elements of the Fock matrix:

$$\mathbf{F}_{\mu\mu} = \mathbf{U}_{\mu\mu} + \sum_{K \neq L} \mathbf{V}_{KL} + \left(\mathbf{P}_{KK} - \frac{1}{2} \mathbf{P}_{\mu\mu} \right) \gamma_{KK} + \sum_{L \neq K} \mathbf{P}_{LL} \gamma_{KL} \quad (2.33)$$

The core hamiltonian is separated in two terms $\mathbf{U}_{\mu\mu}$ and $\sum_{K \neq L} \mathbf{V}_{KL}$. The first one describes the interaction between the electron and the nucleus where it is centered, the second one describes the potential which the electron can experience from the other nuclei. The other terms describe the two center integrals on the same nucleus (γ_{KK}) and on different nuclei (γ_{KL}). The off diagonal fock matrix elements where μ and ν are centered on one nucleus is described in equation 2.34

$$\mathbf{F}_{\mu\nu} = -\frac{1}{2} \mathbf{P}_{\mu\nu} \gamma_{KK} \quad (2.34)$$

Here the core potential is zero due to the orthonormality condition for the atomic orbitals. The last term stands for the off diagonal fock matrix elements where the electrons are centered on different nuclei.

$$\mathbf{F}_{\mu\nu} = \beta_{KL}^0 \mathbf{S}_{\mu\nu} - \frac{1}{2} \mathbf{P}_{\mu\nu} \gamma_{KL} \quad (2.35)$$

The resonance part of the core hamiltonian is proportional to the overlap matrix $\mathbf{S}_{\mu\nu}$ and the proportionality factor β_{KL}^0 is a parameter which depends on K and L.

The parameters for the CNDO approach are γ , which simulates the average electrostatic repulsion between electron centered on nucleus K and L, the potential $\mathbf{U}_{\mu\mu}$ which is the energy of an atomic orbital in the field of the nucleus where it is centered, similarly the potential V_{KL} which gives the energy of an atomic orbital regarding to the field of all other nuclei and the bonding parameter β_{KL}^0 .

The failors of CNDO are the underestimation of predicted equilibrium distances for diatomic molecules and the overestimation of the dissociation energy.

In the CNDO approach the interaction of electrons regarding to their spin state can not be modelled. The Intermediate Neglect of Differential Orbitals (INDO) method overcomes this problem by including monoatomic differential overlap for one center integrals centered on the same atom. This allows electrons with unpaired spin to interact energetically favourably and states with different multiplicity can be distinguished.

The next step is to neglect only integrals of orbitals which are centered on different atoms. All four electron integrals where $\mu\nu$ and $\sigma\lambda$ are centered on the same center retain in the calculation. This method is known as Neglect of Diatomic Differential Overlap (NDDO). All these methods discussed so far suffered from the same drawbacks: results could not be obtained with the needed accuracy and they were limited to a small class of molecules only. Some modifications like Modified Intermediate Neglect of Atomic Orbitals (MINDO/3) and Modified Neglect of Diatomic Orbitals (MNDO) were developed and were responsible for spreading semiempirical methods to a wider audience. MNDO, AM1 and PM3 are very common methods for routine calculation and give, a good parametrisation prefaced, reliable results. For calculations on excited states the ZINDO method is the method of choice. If heavy elements are present in the structure a Sparkle method can be applied. Sparkles replace the heavy atoms and represent the charge of the ion.

2.4 Ab Initio Methods

The Fock Matrix elements which were used before in the Roothan-Hall equation can not be applied to systems with unpaired spin. Two different ways were developed to solve this problem. The first attempt is to use single and double occupied molecular orbitals and is known as Restricted Hartree Fock (RHF) theory. The second way is to treat the spin orbitals separately, that means a spatial orbital is connected

with one spin orbital. The latter one is also known as Unrestricted Hartree Fock (UHF) theory. So far, the effect of electron correlation was neglected. The energy was derived from a mathematical formulation where one electron "sees" all the other electrons as a charge density. Three methods are most important to deal with correlation effects and will be briefly discussed here.

2.4.1 Configuration Interaction

[25, 24, 26]

The one determinant approach which was described above limits the possibilities of calculating excited states. An excited state can be represented by using more than one Slater determinant to construct the wavefunction. Using more determinants allows to put one or more electrons in former unoccupied orbitals and the different excitation states can be modelled. Mathematically one gets a linear combination of different wavefunctions (comparable to the LCAO ansatz).

$$\Psi = a_0\phi_{HF} + \sum_{i=1} a_i\phi_i \quad (2.36)$$

The first Slater determinant ϕ_{HF} is the known ground state determinant. The expression ϕ_i are determinants where former occupied orbitals were replaced by virtual orbitals. The coefficient a_0 is normally close to one since solving the one determinant Roothan-Hall equation gives almost 99% of the energy. This equation can be solved in the same way like the LCAO ansatz using the method of Lagrange multipliers. The constraint is that the total CI wavefunction is normalized. Minimizing the energy is done by variation of the coefficients. Theoretically all combinations of different states can be varied, but bearing in mind that the total number of possibilities to alter the states for N electrons and K orbitals is $\frac{2K!}{N!(2K-N)!}$ and gives a bigger number of elements and coefficients in equation 2.36. Considering all states is called Full Configuration Interaction and is not recommended unless for very small systems and using a minimal basis set. Therefore, only a limited number of states are normally considered. In Configuration Interaction Singlets (CIS) only a single spin orbital is altered. Double substitution gives CID and so on. Even with this approximation the calculation can become oversized and a further approach would be to separate the orbitals in a frozen core, incorporating the occupied molecular orbitals until the HOMO-1 orbital and the valence orbitals which are matter of variation. Normally only the HOMO and LUMO orbitals are altered.

In a traditional CI calculation only the coefficients of equation 2.36 are optimised. Knowing that the determinants in the linear combination of equation 2.36 consist of a linear combination of atomic orbitals one would assume to get better energies when both coefficients, those from the determinant linear combination and for each determinant the coefficients of the LCAO ansatz are optimised. This method

is known as Multi Configuration Self-Consistent Field method (MCSCF). However, this approach can be quite demanding. Splitting the set of molecular orbitals in three types, those which are fully occupied in each state, those which are unoccupied in each state and the remaining active orbitals leads to the Complete Active Space SCF method. For the last type of orbitals, also referred to as active space, all possible states can be calculated.

2.4.2 Many-Body Perturbation Theory

[24, 25]

One method proposed by Møller and Plesset adds a so called perturbation term V to the hamiltonian which is multiplied with a factor λ . The true hamiltonian can be written then as

$$\mathbf{H} = \mathbf{H}_0 + \lambda \mathbf{V} \quad (2.37)$$

λ can have values between 0 and 1. $\lambda=0$ means the zeroth order Hamiltonian \mathbf{H}_0 becomes the true Hamiltonian \mathbf{H} . The eigenfunctions and eigenvalues are given as powers of λ :

$$\Psi_{i\mu} = \sum_{n=0} \lambda^n \Psi_{\mu}^{(n)} \quad (2.38)$$

$$E_{\mu} = \sum_{n=0} \lambda^n E_{\mu}^{(n)} \quad (2.39)$$

where the indices on E describe the order of correction. \mathbf{H}_0 is the known one electron fock operator. \mathbf{V} is given as in equation 2.40

$$\mathbf{V} = \sum_{\mu=1}^N \sum_{\nu=\mu+1}^N \frac{1}{r_{\mu\nu}} - \sum_{\mu=1}^N (\mathbf{J}_{\mu} + \mathbf{K}_{\mu}) \quad (2.40)$$

The energies are now given as

$$E_{\mu}^0 = \int \Psi_{\mu}^{(0)} \mathbf{H}_0 \Psi_{\mu}^{(0)} d\tau \quad (2.41)$$

$$E_{\mu}^1 = \int \Psi_{\mu}^{(0)} \mathbf{V} \Psi_{\mu}^{(0)} d\tau \quad (2.42)$$

$$E_{\mu}^2 = \int \Psi_{\mu}^{(0)} \mathbf{V} \Psi_{\mu}^{(1)} d\tau \quad (2.43)$$

The sum of the first two terms, that is $E_{\mu}^0 + E_{\mu}^1$ is exactly the HF energy. To get better energy values, perturbation to at least an order of two must be applied. This method is known as MP2 method. Perturbation methods going to higher order are known as well and are named as MP3 and MP4, respectively.

2.4.3 Density Functional Theory

[24, 25]

One method which is sometimes referred to as ab initio method, although it sometimes employs empiric parameters, is the Density Functional Theory (DFT). The underlying principle is the proof of Hohenberg and Kohn that the non-degenerated ground state energy is fully determined by the electron density [27]. However, the first attempts to describe energetic properties by only the electron density were done by Thomas and Fermi in 1927 proposing a uniform electron gas (UEG), that is an infinite number of electrons moving in an infinite space which is characterised by an equally distributed positive charge.

The kinetic density of this system is given according to equation 2.44. Here the kinetic energy is a functional dependent on the electron density $\rho(\mathbf{r})$.

$$\mathbf{T}_{ueg}[\rho(r)] = \frac{3}{10} (3\pi^2)^{\frac{2}{3}} \int \rho^{\frac{5}{3}}(\mathbf{r}) d\mathbf{r} \quad (2.44)$$

with

$$\rho(r) = N \int \dots \int |\Psi(x_1 x_2 \dots x_N)|^2 dx_1 dx_2 \dots dx_N \quad (2.45)$$

The Thomas-Fermi approach is the first attempt to build up the Hamiltonian operator by using the electron density instead of the wavefunction. Three major things are necessary to build up the Hamiltonian: the position of the nuclei, the charge of the nuclei and the total number of electrons. While the position of the nuclei is given a priori when defining the system of interest, the number of electrons is just the integral over all space of the electron density (equation 2.46) and the charge of the nuclei is connected with the electron density according to equation 2.47 where $\rho_A(r_A)$ is the spherical averaged density.

$$N = \int \rho(r) dr \quad (2.46)$$

$$\frac{\delta \rho(r_A)}{\delta(r_A)}_{r_A=0} = -2Z_A \rho(r_A) \quad (2.47)$$

In equation 2.2 all the relevant terms of the Hamiltonian are given. The Thomas-Fermi approach handles all terms in a classical way with only the kinetic energy term being expressed via equation 2.44. This description however shows some crucial drawbacks since the potential energy term \mathbf{V}_{ee} from equation 2.8 is described in a classical way and does not include any correlation or exchange effects. For describing the correlation and exchange effects the concept of Fermi- and Coulomb holes is necessary. This is best done with a so called hole function $h(\mathbf{r}_\mu; \mathbf{r}_\nu)$ which corrects the error which is introduced due to the classical description of the electronic potential energy term.

Two effects arise in the correlation of electrons. The first comes from the antisymmetry of the wavefunction of fermions and refers to the Pauli principle that two electrons with equal same spin can not be found at the same place. The Fermi hole also accounts for the self interaction of the electrons. The Fermi hole has negative values everywhere, it integrates to -1 over the whole space, and does not necessarily have a spherical shape since it is dependent on the density of the reference electron (r_ν). One further characteristic is that the Fermi hole also accounts for the self interaction of electrons. The Coulomb hole integrates to zero, that means it must have positive values somewhere in the space. It will be largest

and negative at the place of the reference electron and the density is not independent from the reference atom, that means if the distance is elongated the function must change abruptly. The exchange term in the Hamilton operator can thus be written in its most correct form as

$$\mathbf{E}_X = \frac{1}{2} \int \int \frac{\rho(r_\mu) h_X(r_\mu; r_\nu)}{r_{\mu\nu}} dr_\mu dr_\nu \quad (2.48)$$

This rather complicated term was simplified first by Slater in 1951 by assuming a spherical shaped exchange hole situated around the reference electron. Further improvements were done by introducing an empirical parameter in the exchange term which is called X_α or Hartree-Fock-Slater method according to equation 2.49.

$$\mathbf{E}_{X\alpha}[\rho] = -\frac{9}{8} \left(\frac{3}{\pi}\right)^{\frac{1}{3}} \alpha \int \rho(r_\mu)^{\frac{4}{3}} dr_\mu \quad (2.49)$$

The big win is that the complicated expression in equation 2.48 is simplified to a functional which is only dependent on the local value of the density. The breakthrough for chemical application is based on the work of Kohn and Sham who set up two important theorems.

In the first theorem, the "The proof of Existence" Hohenberg and Kohn showed that the ground state density specifies uniquely the external potential [27]. This means that the ground state energy can be written in terms of the ground state density only and this can also be applied to its individual compounds.

$$\mathbf{E}_0[\rho] = \mathbf{T}[\rho_0] + \mathbf{E}_{ee}[\rho_0] + \mathbf{E}_{Ne}[\rho_0] \quad (2.50)$$

where the nuclear-electron interaction functional ($\mathbf{E}_{Ne}[\rho_0]$) is the only system dependent term. The other two system independent terms, the functional of the kinetic energy ($\mathbf{T}[\rho_0]$) and the functional contributing to the electron-electron interaction ($\mathbf{E}_{ee}[\rho_0]$) are often combined to $\mathbf{F}_{HK}[\rho_0]$, the Hohenberg-Kohn functional. Knowing the form of this functional would made it possible to exactly solve the Schrödinger equation irrelevant which system is matter of investigation. Unfortunately, there is no indication to how this functional should look like.

The second theorem of Hohenberg and Kohn deals with the problem to be sure which density is really the ground state density. It is equivalent to the variation principle, that means the energy calculated by an electron density is the lowest energy only and only if the density used is the ground state density. The proof is rather simple. A given electron density is enough to build up a Hamiltonian which in return gives a wavefunction. Proof can be done according to the variational principle which was developed for wavefunctions then.

Those two theorems by Hohenberg and Kohn prove that the Hamiltonian can be obtained by the electron density only. They do not give any description how to apply this theory in practice. In 1965 Kohn and Sham published a paper which gives directions to direct application [28]. The Hohenberg-Kohn functional can be divided in a term describing the classical coulomb energy and a functional which comprises all non classical effects. The ulterior motive is that non interacting contributions can be described exactly like in HF theory with a Slater determinant and the non-classic contributions are added by applying a potential so that the energy calculated from the electron densities exactly equals the ground state energy. The operator introduced is called Kohn-Sham operator \mathbf{F}^{KS} and is given as:

$$\mathbf{F}^{\text{KS}} = -\frac{1}{2}\nabla^2 + \mathbf{V}_S(r) \quad (2.51)$$

The potential \mathbf{V}_S from equation 2.51 is given as

$$\mathbf{V}_S(r) = \int \frac{\rho(r_v)}{r_{\mu v}} dr_v + \mathbf{V}_{XC}(r_\mu) - \sum_K^N \frac{Z_K}{r_{\mu K}} \quad (2.52)$$

If a solution of this equation can be found, it can be employed in the Kohn-Sham operator, let it act on the Kohn-Sham orbitals and will get the electron density, which is in return necessary to determine \mathbf{V}_S . As already known from the HF theory this leads to an iterative process. DFT shows two major strength: if the exact exchange functional is known, an exact solution of the Schrödinger equation is possible and since DFT is based on electron densities the method is much less demanding in terms of computational cost. The exact functional however is elusive but there are several approaches how to develop approximate functionals. A special notation for the functional form is used where the functional $\mathbf{E}_{XC}[\rho(r)]$ is dependent on the energy density ϵ_{XC} which has the unit of "particles per volume".

$$\mathbf{E}_{XC}[\rho(r)] = \int \rho(r) \epsilon_{XC}[\rho(r)] dr \quad (2.53)$$

Furthermore, although not completely proved to be correct, the exchange functional is often separated in an exchange term ($\mathbf{E}_X[\rho(r)]$) and a correlation term ($\mathbf{E}_C[\rho(r)]$), respectively.

$$\mathbf{E}_{XC}[\rho(r)] = \mathbf{E}_X[\rho(r)] + \mathbf{E}_C[\rho(r)] = \int \rho(r) \epsilon_X[\rho(r)] dr + \int \rho(r) \epsilon_C[\rho(r)] dr \quad (2.54)$$

The potential which is used in equation 2.51 is the derivative of the energy with respect to the density.

$$\mathbf{V}_{XC}(r) = \frac{\delta \mathbf{E}_{XC}[\rho]}{\delta \rho(r)} \quad (2.55)$$

Finally, the spin is accounted for via a function of the spin polarisation (ζ) as given in equation 2.56

$$\zeta = \frac{\rho^\alpha - \rho^\beta}{\rho^\alpha + \rho^\beta} \quad (2.56)$$

2.4.3.1 Functionals

Different approaches are used to find functionals describing the correlation and exchange effects. The Local Density Approximation (LDA) is based on the fact that the energy density can be calculated at a certain point from the electron density on this point only. This local approach has the only constrain that the electron density must be single valued everywhere, however, the only functionals used were derived from the uniform electron gas model introduced before, thus the electron density is a function showing a constant value everywhere, or in some cases also slowly changing functions of the electron density were allowed. The exchange functional is given as

$$\mathbf{E}_{XC}^{LDA}[\rho] = \int \rho(\mathbf{r}) \varepsilon_{XC}(\rho(\mathbf{r})) dr \quad (2.57)$$

The LDA functional can also be written for open shell systems in a spin polarized form and is referred to then as Local Spin Density Approximation (LSDA). Modifications on the LDA functional were done by Vosko, Wilk and Nusair (VWN) who used an interpolation function and fall back on energy densities which were determined for the uniform electron gas via Monte Carlo calculations. To gain better functionals a better model must be applied since in true systems the electron density is not uniformly distributed. This is done in the Generalized Gradient Approximation (GGA). The improvement is given through calculating the gradient of the electron density ($\nabla\rho$), that means the density is not taken as a constant through the space, but it allows the density to vary dependent on the location which is matter of observation. Most of the generalized gradient approximations take the energy density from the LDA approach and add a correction term which is dependent on the gradient. For example, Perdew and Wang proposed the corrected functional (PW86) given in equation 2.58.

$$\varepsilon_x^{PW86} = \varepsilon_x^{LDA} (1 + ax^2 + bx^4 + cx^6)^{\frac{1}{15}} \quad (2.58)$$

with x being

$$x = \frac{|\nabla\rho|}{\rho^{\frac{4}{3}}} \quad (2.59)$$

The most widely used correction term was proposed by Becke in 1988 and is abbreviated as B88 where the correction energy density is

$$\Delta_x^{B88} = -\beta\rho^{\frac{1}{3}} \frac{x^2}{1 + 6\beta x \sinh^{-1}x} \quad (2.60)$$

The parameter β is a fitting parameter to the exactly known exchange energies of the noble gases He-Rn and x is described in equation 2.59.

The correlation functional proposed by Lee Yang and Parr in 1988 (LYP) is not a correction to the LDA approach but computes the correlation energy completely. It is also the only functional which completely eliminates the self correlation. In the literature the acronyms are put together to describe which functional forms are used. The BLYP functional for example uses the Becke exchange functional and the LYP correlation functional. One of the most robust and nowadays widest used functionals is the hybrid functional B3LYP. Hybrid functionals are based on the fact that the completely uncorrelated state and the completely correlated state can be connected through a switching function λ . Thus one can determine the degree of correlation in the system by adjusting the parameters. $\lambda=0$ describes the uncorrelated state while $\lambda=1$ describes the fully correlated one. The connection between those two states is given via the Adiabatic Connection Formula (ACF).

$$E_{XC} = \int_0^1 \langle \psi_\lambda | V_{XC}(\lambda) | \psi_\lambda \rangle d\lambda \quad (2.61)$$

The B3LYP model which was also employed in our calculations is defined as

$$E_{XC}^{B3LYP} = (1-a)E_X^{LSDA} + aE_X^{HF} + b\Delta E_X^{B88} + (1-c)E_C^{LSDA} + cE_C^{LYP} \quad (2.62)$$

The parameters a , b and c can be different for different programs. In the gaussian program package used for this work [29] the weight of the different terms is: $0.8E_X^{LSDA} + 0.2E_X^{HF} + 0.7\Delta E_X^B + 0.19E_C^{LSDA} + 0.81E_C^{LYP}$

2.4.3.2 Time Dependent Density Functional Theory (TD-DFT)

The theorems of Kohn and Hohenberg discussed before are only valid for the ground state. This is a big drawback, since the DFT theory can not be applied in this form to photochemical problems. A way to overcome this problem is to lead back electronic states to ground state properties. This method is also referred as time dependent response approach.

One imagine an external time dependent field, such as the electric field \mathbf{E} of a light beam oscillating with

a frequency ω . If this lightbeam interacts with a molecule it alters the electronic charge and the electron density of the molecule. The electron density is described by the one-particle density matrix $\mathbf{P}(t)$ which starts to oscillate around its ground state $\mathbf{P}(t_0)$. The amplitude of this oscillation can be expressed in an Fourier transformation and is then dependent on the frequency ($\mathbf{P}(\omega)$).

Taking the case that the frequency ω of the perturbation comes close to the excitation energy of the system (ω_i) results in a so called resonance catastrophe where the amplitude of the oscillation diverges. The ω_i frequencies are computed in form of an electronic Hessian matrix, which is the second derivative of the electron energy with respect to the electronic degree of freedom [30]. This ω_i energies are also known as vertical transition energies. Calculations are done by solving the time dependent Kohn-Sham equation as given in equation 2.63

$$i \frac{\partial}{\partial t} \phi_j(t, x) = \mathbf{H}[\rho](t, x) \phi_j(t, x) \quad (2.63)$$

where the one particle Hamiltonian $\mathbf{H}[\rho](t, x)$ is composed of the external, the coulomb and the exchange-correlation potential. The oscillator strength can be computed as

$$f = \frac{2}{3} \Omega |\langle \mu | X, Y \rangle|^2 \quad (2.64)$$

Ω is the transition energy and X and Y refers to the orbitals which are involved in the transition step.

2.5 Calculating Properties

2.5.1 Structure Optimisation

[25]

The first step in calculating properties is the optimisation of the molecule geometry. Once a minimum geometry with sufficient accuracy is found, all other properties can be calculated. At the beginning a guess geometry is given as input, either in cartesian coordinates or in form of a Z-Matrix. The energy can be calculated for one geometry, thus giving one point of a 3N dimensional function, if cartesian coordinates are used, or a 3N-6 dimensional function if internal coordinates is applied. This function is called Potential Energy Surface (PES) and connects the energy of different geometries to its energetically state. Exploring the PES becomes important if a molecule can show different isomers or if transition states are of interest. One method to find the geometry corresponding to the minimal energy is to use a derivative method. Different algorithms have been developed from them, only the most important will be matter of discussion here. All the algorithms have in common that they only can go downwards on the

PES. That means, if the way down leads to a local minimum, and the global minimum is separated by a maximum, e. g. transition state, from the starting point, the minimisation procedure will never end up in finding the global minimum. Thus different geometries should be taken as starting point for exploring the energy surface. Taking into account very basic chemical principles, e. g. a sp^3 carbon will have bond angles close to 120° , a good starting structure can be set up and in most cases the optimisation will result in finding the global minimum. The derivative methods use either the first or the second derivative with respect to the coordinates. Applying the first derivative method gives the gradient of the function in a certain point, which is equivalent to the negative of the force vector acting on the nucleus on this point. The magnitude of the gradient is referred to the steepness of the slope of function in the environment around the point. The potential as function of the coordinates is expanded in a Taylor series normally. The first derivative with respect to the coordinates gives $3N$ matrix elements in a vector form. The second derivative gives a $3N \times 3N$ matrix and is known as Hessian matrix. Cutting the Taylor expansion after the third term gives a quadratic function and is not a good approximation for modelling the PES. However, close to a minimum, the behaviour of the PES is close to a parabel and allows to use the approach via the truncated Taylor expansion. If the optimization cycle fails, e. g. if the starting point is too far from the minimum, other, more robust methods can be applied. The steepest descent method is commonly used in the Gaussian program. Taking the starting point, a $3N$ dimensional vector is constructed and the gradient is calculated. The direction of the shift of the coordinates is given by equation 2.65

$$\mathbf{s}_k = -\frac{\mathbf{g}_k}{|\mathbf{g}_k|} \quad (2.65)$$

with

$$\mathbf{g}_k = \mathbf{V}' \mathbf{x}_k \quad (2.66)$$

The stepsize is a parameter present in the program, but can be changed if needed.

The Newton Raphson method is a second derivative method and uses the Taylor expansion up to the first quadratic term. The step size is now determined by the Hessian matrix and the direction is again the gradient of the function, as can be seen in equation 2.67.

$$(\mathbf{x} - \mathbf{x}_0) = -\mathbf{g}\mathbf{H}^{-1} \quad (2.67)$$

In the case where one element of the inverse Hessian becomes close to zero the stepsize can become infinitely large. Thus moving the point outside the quadratical behaviour of the PES will make the method fail. It became useful to use a trust radius which allows only certain stepsizes. The big advantage

of the Newton Raphson method is that if an exact quadratical behaviour is present the minimum will be found within one step. In general calculating the Hessian takes more time, but the method can be considered as rather fast.

2.5.2 Population Analysis

[24, 25]

One property of interest are multipoles, since it gives an idea of the charge distribution in molecules. The dipole moment can be split up in a nuclear and an electronic part, both given in equation 2.68 and equation 2.69

$$\mu^{\text{nuc}} = \sum_{K=1}^L Z_K \mathbf{R}_K \quad (2.68)$$

$$\mu^{\text{elec}} = \sum_{\mu=1}^K \sum_{\nu=1}^K \mathbf{P}_{\mu\nu} \langle \phi_{\mu} | -\mathbf{r} | \phi_{\nu} \rangle \quad (2.69)$$

\mathbf{r} , the dipole moment operator consists of components in x, y and z direction and the dipole components acting in each direction can be written in vector form. Higher order multipoles are calculated in the same way and are represented in matrix form. Equation 2.5.2 gives such a matrix for a quadrupole moment.

$$\theta = \begin{pmatrix} \sum q_i x_i^2 & \sum q_i x_i y_i & \sum q_i x_i z_i \\ \sum q_i y_i x_i & \sum q_i y_i^2 & \sum q_i y_i z_i \\ \sum q_i z_i x_i & \sum q_i z_i y_i & \sum q_i z_i^2 \end{pmatrix}$$

Electronic charges on atoms are calculated via Population Analysis. According to equation 2.71 the electron density is calculated using the density matrix $\mathbf{P}_{\mu\mu}$ on the atom and subtract it from the two center density matrix $\mathbf{P}_{\mu\nu}$ times the overlap matrix $\mathbf{S}_{\mu\nu}$. Subtracting the electron density from the nuclear charge gives the charge on the atom.

$$q_A = Z_K - \sum_{\mu=1}^K \mathbf{P}_{\mu\mu} - \sum_{\mu=1}^K \sum_{\nu=1}^K \mathbf{P}_{\mu\nu} \mathbf{S}_{\mu\nu} \quad (2.71)$$

A shortcoming of the Mulliken Population Analysis is the strong dependence on the basis set. In this way sometimes artefacts can occur, where one orbital gets populated by more than two electrons.

Bearing in mind that the above introduced Hessian matrix is the second derivation of the PES regarding the nuclear coordinates and the Taylor expansion truncated after the quadratic term gives an approximation which is similar to the harmonic oscillator in the one dimensional space one can refer to the elements of the Hessian matrix to the vibrational states of the system. The eigenvalues give the force constant of the vibration and the eigenvectors show the direction in which each atom moves. In case the structure shows a minimum on the PSE all eigenvalues of the Hessian matrix must be positive. The mathematical principle behind it is rather trivial. In a minimum the first derivative must be zero and the second derivative must be positive. If there are negative frequencies the structure corresponds to a transition state, e. g. a saddle point or a maximum. However, having all frequencies positive does not tell anything about if the minimum is of local or global kind.

2.6 Solvation Models

[24, 25, 31]

Calculations done on molecules always assume a single molecule bare of any external forces. This model is comparable to the gas phase. In chemistry most of the reactions are done in condensed phase and also photochemical observations are measured in most of the cases in solution. Therefore, it is necessary to include solvent effects in the calculation. Different models have been developed so far, and their accuracy and adaptability is dependent on the system subject of investigation.

When placing a molecule in a solvent, the solvent molecules which are very close to the solute will arrange themselves in an ordered matter. Commonly one speaks from first, second and third solvation sphere. Specially for the europium complexes which are described in this work the first coordination sphere plays an important role. From Eu(III) halogenide crystal structures it is known that europium complexes show a coordination number of nine [16], that means three solvent molecules can possibly coordinate to the sixfold coordinated 8-hydroxyquinolinolate europium complexes. And it is obvious that coordinated solvent molecules will have an impact on the geometry of the primal complex. The order of the solvent sphere decreases with increasing distance to the solute so that solvent spheres higher than three are not important for short range effects. The long range effects arise due to shielding of charges and polarisation of the solute.

The first approach to account solvent effects for would be to simply place explicitly solvent molecules around the solute. In this way short range effects can be modelled in a good way. The explicit solvent molecules will interact with the solute during the optimisation procedure and, using an appropriate method, hydrogen bonds and weak interactions can be modelled. However, following this approach only short range effects are considered, such as influence on the structure of the solute. If bigger sized

molecules such as bioactive compounds are matter of investigation the number of solvent molecules around the surface of the solute will increase very fast resulting in an unmanageable number of minimum structures. The problem would get too demanding in terms of computational cost very soon, even if statistical sampling techniques are applied.

Another approach, which is today's common state of the art, sees the solvent as continuum which encloses the solute and which is determined by its bulk properties, e. g. dielectric constant. This ansatz is called Continuum Model (CM) in the literature. The solute is enclosed in a cavity, a space which defines the dimension of the solute and sets the border to the solvent. Creating a cavity in a dielectric costs energy. Rearrangements and dispersion in the solvent create a favourable term in the energy balance. Since the overall charge of the solution must be zero a net charge or local charge distribution of the solute must be compensated by the solvent. Same applies for dipole moments or higher order moments. A permanent dipole moment of the solute will influence the solvent in this way that the overall dipole moment will be zero. Furthermore the system shows a dynamic behaviour. The solute dipole moment will cause an induced dipole moment in the dielectric which re-acts on the solute. This idea of interchange is commonly known as *reaction field*. The electrostatic energy term acts stabilising and thus the solvation energy can be written as shown in equation 2.72

$$\Delta G_{\text{solvation}} = \Delta G_{\text{cavity}} + \Delta G_{\text{dispersion}} + \Delta G_{\text{elec.}} + \Delta G_{\text{mm}} \quad (2.72)$$

The term ΔG_{mm} contributes to all molecular motions. Since continuum models are normally time averaged systems following a Boltzmann distribution at a certain temperature, the latter term will not be implemented for the following considerations. The term $\Delta G_{\text{elec.}}$ is the contribution of the electrostatic interaction of the solvent with the solute according to equation 2.73 [32]

$$G_{\text{elec.}} = \left\langle \psi \left| \mathbf{H}(\psi) - \frac{1}{2} \mathbf{V}(\psi) \right| \psi \right\rangle \quad (2.73)$$

and $\mathbf{H}(\psi)$ being

$$\mathbf{H}(\psi) = \mathbf{H}_0 + \mathbf{V}(\psi) \quad (2.74)$$

where $\mathbf{V}(\psi)$ is the solute-solvent interaction potential. The solvation models differ mainly in the size and shape of the cavity and in the way how this last electrostatic energy term is described. The Poisson Equation (equation 2.75) describes the response of the continuum to a solute in terms of a polarisation of a charge density in a cavity which is embedded in a homogeneous dielectric.

$$\nabla \varepsilon(r) \nabla \phi(r) = 4\pi \rho(r) \quad (2.75)$$

where $\phi(r)$ is the electrostatic scalar potential. Solutes which show an ionic strength can be described by the Poisson-Boltzmann equation. Its linearised form which can be applied for solvents with low ion strength is widely used for reaction field calculations nowadays [33].

$$\nabla \varepsilon(r) \nabla \phi(r) - \varepsilon(r) \lambda(r) \kappa^2 \phi(r) = -4\pi \rho(r) \quad (2.76)$$

with κ being the Debye-Hückel parameter and λ being a switching function ($\lambda = 0$ for areas not accessible for the solvent and $\lambda = 1$ for all other cases). The charge density on the surface of a spherical cavity $\rho(s)$ can be described as

$$\rho(s) = \frac{q}{4\pi r_{1,2}} \quad (2.77)$$

The electrostatic potential which is built up between the continuum and the cavity is given as

$$\phi(r) = -\frac{q}{\varepsilon |r|} \quad (2.78)$$

with r being the radius of the cavity. The work which is necessary to create the cavity can be described as

$$G = -\frac{q^2}{2\varepsilon r} \quad (2.79)$$

and the polarisation energy is given as the difference between the work in the gas phase and the solvent

$$G_p = -\frac{1}{2} \left(1 - \frac{1}{\varepsilon}\right) \frac{q^2}{r} \quad (2.80)$$

Equation 2.80 is the so-called Born equation and describes the polarisation energy of a spherical ion in the continuum. Onsager extended this approach for the effect of a dipole in a solution and equation 2.81 is now known as Kirkwood-Onsager equation [34].

$$G_p = -\frac{1}{2} \left[\frac{2(\varepsilon - 1)}{2(\varepsilon + 1)} \right] \frac{\mu^2}{r^3} \quad (2.81)$$

From equation 2.81 one can establish the Hamiltonian for a dipole in a solute according to equation 2.82

$$\mathbf{H}_{\text{solv}} = \mathbf{H}_{\text{gas}} - \frac{1}{2} \left[\frac{2(\epsilon - 1)}{2(\epsilon + 1)} \right] \frac{\langle \psi |}{r^3} \quad (2.82)$$

Letting \mathbf{H}_{solv} act on the wavefunction results in a nonlinear equation system which can be solved according to the HF procedure described in chapter 1.1. Solving the Schrödinger equation with \mathbf{H}_{solv} by employing the HF ansatz is called Self Consistent Reaction Field (SCRF). The Kirkwood-Onsager model deals with spherical cavities and only accounts for dipoles. The extension to multipoles is known as the Kirkwood model, where the polarisation model is given as

$$G_p = -\frac{1}{2} \sum_{l=0}^L \sum_{m=-l}^l \sum_{l'=0}^L \sum_{m'=-l'}^{l'} M_l^m f_{ll'}^{mm'} M_{l'}^{m'} \quad (2.83)$$

For ellipsoid cavities the Kirkwood-Westheimer model can be used. In equation 2.83 l is the order of the multipole M and f is the reaction field factor which is dependent on the cavity radius and the dielectric constant of the continuum. Generally the order is not limited but typically multipoles up to an order of 6 are relevant. The Onsager model gives a good description of the reaction field but it has also to deal with different drawbacks. Dispersion interactions are completely neglected. No description of the solvent-solute charge transfer can be done and solvent static field effects are omitted [35]. However, the biggest drawbacks are the slow convergence in respect of the order of the multipole and that there is no unifying way how to determine the radius for the spherical cavity. Taking an ellipsoidal cavity gives only small improvement. Better improvements give cavities which are closely shaped as the molecule, such as the overlap surface of the Van-der-Waals radii of the solute atoms. For such systems equation 2.76 can not be solved analytically anymore and a numerical approach is necessary. The most common numerical approach is the finite difference Poisson-Boltzmann technique [33]. At this technique the solute surface is subdivided in a grid and the potentials on the surface and in the solvent are calculated for charges on the grid points. Another approach is the surface boundary element approach, often referred to as Polarizable Continuum Model (PCM) developed by Miertus, Scrocco and Tomasi. There the term in equation 2.78 is calculated as the potential which arises from point charges placed on small surface elements [36, 32]. This method was modified in different ways, in terms of computational performance (IEF-PCM, Cossi in 2002) and extensions like accounting for liquid-gas phase interactions. The cavity in the PCM model is constructed of overlapping Van der Waals spheres with a 20 % bigger radius and distinguishing between polarized and non-polarized hydrogen atoms. An alternative is to take the electron density as measure for the cavity radius (IPCM). One quite common approach is the United Atom topological model. There only the Van der Waals radii of the heavy atoms are used to build up the cavity in dependence of the connectivity, number of hydrogen atoms bonded and overall charge of the molecule. Another kind of surface represents the Solvent Accessible Surface. A surface of combined Van der Waals radii will always have small holes where no solvent can interact. The SAS is comparable to the surface described by ball

rolling over the van der Waals surface but not touching the small holes between the connection of the Van der Waals spheres. Solvent accessible surfaces are mostly used for calculating the dispersion-repulsion energy term in equation [2.72](#).

2.7 Relativistic Effects

[25, 37, 38]

Depending on the principal quantum number, electrons in a molecule move with different velocities. Effects resulting from this are that orbitals shrink and binding energies are increased. These effects are generally summarised as relativistic effects. In relativistic theory the mass increases dependent on the velocity according to equation 2.84. Recalling that the expectation value for the radius $\langle r \rangle$ is proportional to $\frac{1}{m}$ and the eigenvalues of the Schrödinger equation scale proportional to m , it becomes understandable that the mass increase can not be neglected anymore for electrons moving with a notable fraction of the speed of light.

$$m = m_0 \left(\sqrt{1 - \frac{v^2}{c^2}} \right)^{-1} \quad (2.84)$$

In relativity theory the speed of light is invariant to the inertia frame. A further requirement is that physical laws are independent of such frames. Thus following a Lorentz transformation of any system must show invariance in respect of the speed of light and the physical laws applied in this system. The time dependent form of the Schrödinger equation 2.1 is clearly not invariant in Lorentz transformations, since the derivative in respect of the coordinates is of second order and the derivative in respect of time is of first order.

The contraction of the orbital expansion is most commonly seen in s type orbitals, mainly those close to the nucleus resulting in a shielding of the outer orbitals (e. g. p and d type orbitals). This shielding is responsible that the p, d and f electrons experience a smaller potential from the nucleus and increase in size. In p type orbitals spin-orbit interactions counteract the shielding effect and thus they mainly stay unaltered. Orbital expansion can only be seen for d and f type orbitals. Accounting for relativistic effects for geometries and energy calculations is not important up to the third row in the periodic table of elements. The fourth row elements show a transition area and from the fifth row elements on relativistic effects can not be neglected anymore.

In classical terms the relativistic energy of an electron moving in an electromagnetic field is given as

$$\{E + q\phi(r)\}^2 = c^2 \{p + qA(r)\}^2 + m^2c^4 \quad (2.85)$$

with $A(r)$ and $\phi(r)$ being the magnetic and electric potential and q the charge of the electron. Applying equation 2.85 to quantum mechanic effects is known as the Klein-Gordon equation

$$\{E + q\phi(r)\}^2 \Psi(r) = \left(c^2 \{p + qA(r)\}^2 + m^2 c^4 \right) \Psi(r) \quad (2.86)$$

Unfortunately the Klein-Gordon equation, beside other drawbacks, does not account for the spin states and so Dirac proposed a form of a relativistic Hamiltonian which accounts for the spin states of the electron as well

$$c\alpha \{p + qA(r)\} - q\phi(r) + \beta mc^2 \quad (2.87)$$

with α and β being two 4x4 matrices written in terms of the 2x2 Pauli spin matrices $\sigma_{x,y,z}$ for α and in terms of the unity matrix I for β , respectively. c in equation 2.87 is the speed of light and \mathbf{p} is the momentum operator in its known form $\mathbf{p} = -i\hbar \nabla$.

$$\alpha_{x,y,z} = \begin{pmatrix} 0 & \sigma_{x,y,z} \\ \sigma_{x,y,z} & 0 \end{pmatrix} \quad \beta = \begin{pmatrix} I & 0 \\ 0 & I \end{pmatrix}$$

and the Pauli spinmatrices being

$$\sigma_x = \begin{pmatrix} 0 & 1 \\ 1 & 0 \end{pmatrix} \quad \sigma_y = \begin{pmatrix} 0 & -i \\ i & 0 \end{pmatrix}$$

$$\sigma_z = \begin{pmatrix} 1 & 0 \\ 0 & -1 \end{pmatrix}$$

Since the Dirac equation bears more information than the Gordon-Klein equation, all of the solutions of the Dirac equations are solutions of the Gordon-Klein equation, but not the same is true for the conversion. Two conditions must be met by the matrices α and β

$$[\alpha_x, \alpha_y]_+ = [\alpha_y, \alpha_z]_+ = [\alpha_z, \alpha_x]_+ = 0 \quad (2.88)$$

and

$$[\alpha_x, \beta]_+ = [\alpha_y, \beta]_+ = [\alpha_z, \beta]_+ = 0 \quad (2.89)$$

This commutation conditions can only be met if the Dirac equation is a four component equation in terms of the matrices. In the interpretation of the four components two can be assigned to the spin states "up" and "down", the two other components are commonly referred to as two different particles namely electron and positron. Expectedly solving the Dirac equation gives two solutions, one referring to the energy of the electron, called as large solution, and one referring to the energy of the positron, called small solution, respectively. It is quite common to split up the four-spinor from equation 2.87 in two two-spinor equations so that

$$(E - mc^2) \Psi^L(r) = c\sigma \{p + qA(r)\} \Psi^S(r) - q\phi(r) \Psi^L(r) \quad (2.90)$$

and

$$(E + mc^2) \Psi^S(r) = c\sigma \{p + qA(r)\} \Psi^L(r) - q\phi(r) \Psi^S(r) \quad (2.91)$$

The second equation can be solved for the smaller component Ψ^S and can be inserted in the upper equation giving

$$\left[\frac{1}{2m} (\sigma\pi) K (\sigma\pi) + (-E + V) \right] \Psi^L = 0 \quad (2.92)$$

with K

$$K = \left(1 + \frac{E - V}{2mc^2} \right)^{-1} \quad (2.93)$$

and π is the generalized momentum operator $\pi = \mathbf{p} + \mathbf{A}$. \mathbf{A} is the vector potential dependent on the magnetic field \mathbf{B} according to $\mathbf{B} = \nabla \times \mathbf{A}$.

In the nonrelativistic limit K is one and equation 2.92 becomes

$$\left[\frac{\pi^2}{2m} + V + \frac{\sigma\mathbf{B}}{2m} \right] \Psi^L = E\Psi^L \quad (2.94)$$

Equation 2.94 is exactly the Schrödinger equation with exception of the $\sigma\mathbf{B}$ term, which is also called Zeeman interaction and which describes the interaction of an external magnetic field with an internal magnetic field of the electron. The Dirac operator for relativistic corrections is often written in form of the Pauli equation

$$\left[\frac{\pi}{2m} + V - \frac{\pi^4}{8m^3c^2} + \frac{ZsL}{2m^2c^2r^3} + \frac{Z\pi\delta(r)}{2m^2c^2} \right] \Psi^L = E\Psi^L \quad (2.95)$$

The first two components represent the kinetic and potential energy operators in its classical form. The third term is the so called mass-velocity term and sets the mass of the electron in dependence of the velocity. The next accounts for the interaction of the electronic spin with the magnetic moment generated by the electron and is called spin-orbit term and the last term is called Darwin correction and defines a correction due to the Zitterbewegung of the electron. The Zitterbewegung can be observed even in the nonrelativistic limit and is a purely non classical observation where the electron oscillates around the median with a certain frequency. The Pauli equation is only valid if $E-V \ll mc^2$ which is definitely not valid in regions near the nucleus. A modified operator can be formulated for this case which is called Zero-Order Regular Approximation (ZORA) or First-Order Regular Approximation (FORA).

Above given equations describe the relativistic energy operators for an electron in the field of a nucleus, but no interaction with other electrons is included. One approach is to describe every electron relativistically as shown above and to sum up the individual energy terms. However, effects such as electron-electron repulsion must also be included and since the repulsion term in classical quantum mechanics just given as the coulomb potential which is time independent it is clear that this term must be modified for relativistic calculations. The Quantum Electro Dynamic describes this interaction in a form where photons, exchanged between the electrons, carry the same information as the potential in the classical description. The potential energy factor in relativistic terms has a rather complicated form but can be expanded in a Taylor series and truncated after the second term with good accuracy. Other terms which must be included are spin-other-orbit correction, accounting for the interaction of the electronic spin of electron μ with the magnetic field due to motion of electron ν , spin-spin correction between two electrons and orbit-orbit interaction. Since nuclei also show an internal structure, the same terms must be defined for the electron-nucleus interaction. Recalling the Born-Oppenheimer approximation the interaction of the electronic spin with the nuclear magnetic field arisen from nuclear motion can be neglected. But the same is not true for the interaction of the nuclear spin with the magnetic field coming from the electron. This term is called Paramagnetic Spin-Orbit operator. And of course the same terms can be defined for the nuclear-nuclear interaction. But again, after falling back on the Born-Oppenheimer approximation, only the spin-spin coupling survives. Solving the Dirac equation equivalent to the Hartree-Fock equation bears some difficulties. First of all a suitable form of the wavefunction must be found. Basis set functions were described before and by applying this concept to relativistic calculations the same aspects come into consideration. The function should describe the real system as good as possible in an easy integrable form. Since the Dirac Hamiltonian is a four component function, also basis sets for the small solution must be defined. The boundary condition for the small component basis functions is given in

the kinetic balance condition

$$\chi_{\mu}^S = \frac{\sigma P}{2c} \chi_{\mu}^L \quad (2.96)$$

In most computer programs GTO type functions are used to expand the wavefunction. In relativistic terms the flat spot at near nucleus region which can be observed in the nonrelativistic case is not a good approximation anymore. The relativistic function shows a singularity close to the nucleus. On the other hand side this can not be modelled correctly by applying GTO's. The solution is, to represent the nuclei as finite sized particles with a positive charge. Of course by doing this, one has to come up with an idea how the positive charge is distributed in the nucleus, in most cases a gaussian type distribution where the exponent depends on the nuclear mass, is accepted. In this case isotope effects are not negligible anymore.

Performing a full relativistic calculation is much more demanding in terms of computational costs than non relativistic Hartree Fock calculations. However approximations are possible, most of them neglecting the small component part of the four component function to a certain order. The most used approximation beside others is the Douglas-Kroll approximation where the positive and negative parts are decoupled in second order in the external potential. Two other approximations, the ZORA and FORA approximation, were described before.

Electronic calculations can be reduced to the valence electrons only for heavy elements. In our calculations Effective Core Potentials from Dolg [22] for Eu were used. Beside the savings in computation time ECPs have the advantage that relativistic effects can be included via parametrisation of the potential.

Chapter 3

Description of the Methodology

The calculations focused on the determination of the singlet and triplet state energies of the ligands and complexes. Furthermore the effect of the chemical environment on the $S_0 - S_1$ transitions in the ligands was investigated. Therefore optimisation and excitation calculations were done for 12 complex structures and 50 ligand systems in gas phase. Calculations were also performed with the Polarizable Continuum Model (IEF-PCM) and additionally, in case of the complex structures, by putting explicitly three solvent molecules in the outer coordination sphere of the Eu complex to account for solvent effects. Calculations with explicit solvent molecules were necessary, since the three solvent molecules can be incorporated in the complex structure between the ligands and can have an influence on the structure of the complex. This effect can not be simulated via continuum models. It is known that europium can form nine fold coordinated complexes, mainly due to its extended radius [6, 16]. Therefore solvent molecules are able to coordinate directly to the Eu atom in cases where the ligand system is not sterically very demanding. Other effects which can not be investigated in terms of continuum models are those resulting from the formation of weak bonds between solvent molecules and some functional groups of the ligand system. For both solvent models (IEF-PCModel and explicit solvent model) ethanol (ETOH) and dichloromethane (DCM) was used as solvent.

The method of choice is the density functional theory (DFT) with the B3LYP functional in its spin unrestricted form (UB3LYP) and was earlier reported for similar problems in literature [17, 18, 19], dft4. For the excitation calculations the DFT method was used in its time dependent form (TD-DFT). All DFT calculations were carried out by using the Gaussian03 program package, revision C.02 [29]. In a second study changes in the geometry were investigated with the semiempirical AM1 model employing a sparkle model for the Eu atom as previously reported by Freire [23]. AM1 calculations were done with the Mopac2009 [39] program.

For evaluation of the results MOLDEN [40] and Origin 8.0 have been used. Molecular Orbitals were visualised with GaussView (Gaussian 03, revision-B01) and convoluting absorption spectra was done with

the program Voigt, developed by Stefan Kontur [41]. Gaussian line shape was used for the broadening of the transition lines with a half width of 0.22eV. The half width was estimated from the experimental spectra of the ligands. Experimental spectra were recorded on a Cary 50 Bio UV-Visible spectrophotometer.

Calculating Ligand properties To find the minimum structure different starting geometries of the ligands were optimised by using the 6-31G* basis set for the neutral, the cationic and the anionic structure. Optimisation calculations were done without symmetry restriction and the normal default convergence criteria were used.

The singlet structures corresponding to the minimum energy served as input structures for the optimisation of the triplet geometries. Afterwards frequency calculations were run for all stationary points and checked for imaginary modes. The energy was refined using the bigger, polarised triple zeta valence basis set (TZVP) in form of a single point calculation.

Excitation calculations were performed for 40 States giving singlet and triplet transitions, to cover the entire visible spectrum in gas phase and in solvent. For solvent calculations the IEF-PCM model was employed. Dielectric constants are shown in Table 3.1.

Table 3.1: Dielectric constant of the solvents.

Solvent	Dielectric Constant (ϵ)
Dichloromethane	8.93
Ethanol	24.55

Calculating Complex properties Four choosing the complex structures, four ligand types were used. The unsubstituted quinoline as a reference, the NH₂ and NO₂ substituted ligands due to their strong electron pulling and pushing ability and the HSO₃ substituted ligand since experimental data were available for this system. To build up the complex structure, three bidentate quinoline molecules of the same structure were coordinated around the Eu atom giving an octahedron like complex geometry. The geometries were again optimised without any symmetry constraint on UB3LYP/6-31G* level for the light ligand atoms (C, H, N, O, S) and with the 52MWB effective core potential published by Dolg [22] for the Eu atom. Frequency calculations were done for the optimised structures to show that the geometries correspond to a minimum on the PES. Energy refinement was done with a single point calculation on UB3LYP/TZVP level for the ligand atoms and UB3LYP/52MWB level for the Eu atom. Excitations were calculated in the same way as described before in gas phase and by applying the IEF-PCM model.

For calculations with explicit solvent molecules optimisation, frequency calculation, energy refinement and excitation calculations were performed as described before. 40 states were computed in the excita-

tion calculations. The 6-31G* basis for optimisation and frequency calculation and the TZVP basis for energy refinement and excitation calculations were applied to the light atoms of the ligands and solvent molecules (C, H, N, O, S, Cl) and the 52MWB effective core potential for the Eu atom in all cases.

Since the bonding of the ligands to the Eu atom is mainly of electrostatic nature [20], research has been done previously by other groups on semiempirical calculations using the AM1 model, which is known for giving good structures for organic molecules [23]. The Eu atom is hereby replaced by a sparkle. In this work geometry optimisations were performed using the AM1 Hamiltonian and the Eu(III) sparkle implemented in the Mopac2009 program package. Values for the sparkle parameters are given in Table 3.2

Table 3.2: Parameters for the Eu sparkle implemented in Mopac2009. See also [23].

Parameter	Value	Parameter	Value
a ₁	0.5695122475	a ₂	0.3286619046
b ₁	7.4680207642	b ₂	7.8009779599
c ₁	1.7319729855	c ₂	2.9641285490
GSS	55.6059122033	ALP	2.1247188613

MOPAC keywords were set according to the work of Freire [42] as: GNORM=0.25, SCFCRT=10⁻¹⁰. Optimisation was done in Cartesian coordinates only.

Chapter 4

Results

4.1 Calculation on the Ligand Systems

A total of 50 different ligand structures were optimised on the UB3LYP/6-31G* level in their ground state. The ligand backbone is the 8-hydroxyquinoline as shown in Figure 4.1 ($R'=H$). In a first step, different substituents were introduced in 5-position of the molecule, such as amino (NH_2), cyano (CN), formyl (CHO), sulfonic acid (HSO_3), methoxy (MeO), nitro (NO_2), phenyl (Ph) and pyridino (Py).

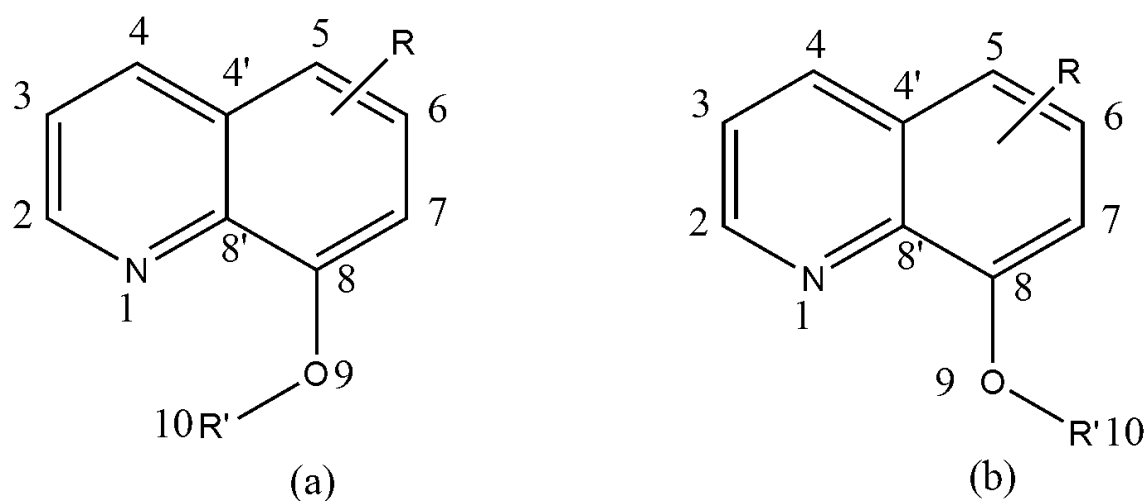


Figure 4.1: Structures of the isomers of 8-hydroxyquinoline with $\theta_1=0^\circ$ (a) and $\theta_1=180^\circ$ (b) with the labeled substitution positions.

The functional groups were selected according to their electron pulling and pushing ability. The Ph and Py groups were chosen due to their ability to extend the delocalised π - system. The Py substituent also exhibits some interest because of the quarternised Py nitrogen and was calculated in its cationic form. Furthermore, one ligand showing the deprotonated sulfonic acid group (SO_3^-) introduced in 4-position and the disubstituted quinoline 5,7-dimethyl-8-hydroxyquinoline (5,7-DiMe) was investigated.

The SO_3^- was introduced in 4-position because of available experimental data. The method of calculation was validated by comparing calculated geometry parameters with experimental values, as given in Table 4.1.

Two isomers can be distinguished when the dihedral angle θ_1 (H(10)-O(9)-C(8)-C(8')), see Figure 4.1, is turned from 0° to 180° . The first structure (Figure 4.1 (a)) with $\theta_1 = 0^\circ$ where the OH group faces the heterocycle nitrogen and a second one with $\theta_1 = 180^\circ$ (Figure 4.1 (b)) where the OH group is directed away from the ring system.

The change in energy for the torsion mode was calculated for the unsubstituted 8-hydroxyquinoline and shows a minimum for the first structure with $\theta_1 = 0^\circ$. At $\theta_1 = 105^\circ$ and $\theta_1 = 255^\circ$ two maxima exist which lie 13.9 kcal/mol above the minimum. These two barriers are separated by a local minimum at $\theta_1 = 180^\circ$ which lies energetically 9.28 kcal/mol above the global minimum. For all calculations the structure based on the local minimum at $\theta_1 = 180^\circ$ was taken because of the possibility that the OH group interacts with the ring nitrogen in the global minimum structure. Furthermore, the hydroxy group is not present in the complex structure. A ligand geometry where the hydroxy group shows weak bonding characteristics can therefore not be used to predict energetic behaviour of the ligands in the complex structure. The PES along the θ_1 mode is shown in Figure 4.2.

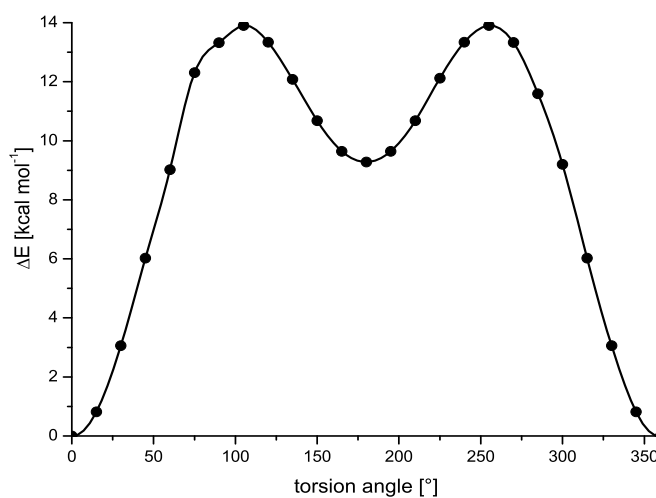


Figure 4.2: Potential Energy Surface (PES) along the C(8')-C(8)-O(9)-H(10) torsion mode. Calculated on UB3LYP/6-31G* level of theory (optimisation) and UB3LYP/TZVP level of theory (energy refinement).

The geometry parameters of the calculated global minimum and local minimum structures are compared to experimental XRD-structures [43] and selected values are depicted in Table 4.1. The whole data set is given in the Appendix, Tables A.1 and A.2.

Table 4.1: Comparison of experimental and calculated bond length of 8-hydroxyquinoline. Experimental data taken from [43]. Calculations were done on UB3LYP/6-31G* level of theory.

Bond	experimental value [Å]	calculated for $\theta_1 = 0^\circ$ [Å]	calculated for $\theta_1 = 180^\circ$ [Å]
C(8')-C(8)	1.411	1.433(8)	1.430(2)
C(8')-N(1)	1.383	1.360(3)	1.360(4)
C(8)-O(9)	1.390	1.358(9)	1.350(9)
Angle	experimental value [°]	calculated for $\theta_1=0$ [°]	calculated for $\theta_1=180$ [°]
C(8)-C(8')-N(1)	119.1	116.3(4)	118.6(5)
C(8')-C(8)-C(7)	121.2	119.7(9)	119.9(6)
C(8')-C(8)-O(9)	120.3	118.3(8)	116.9(3)

As presented in Table 4.1 the bond lengths calculated on UB3LYP/6-31G* level of theory are predicted too long with an average error of 0.01 Å, which proves that the applied method is sufficiently accurate for calculating the ligands.

Regarding the two values calculated for the two isomers, the average error is with 0.001 Å insignificant. In general, the structure based on the local minimum converges to smaller bond lengths than the global minimum structure. The largest deviation shows the C(8)-O(9) bond length which is shrunk in the local minimum structure.

Regarding the bond angles (Table 4.1) the average error between experimental and calculated results is 1.6° which is within an acceptable range.

The angles which are most important in the complex structure, are the angles between C(8')-C(8)-O(9) and C(8)-C(8')-N(1), since they form the pentamorous ring with the Eu ion. Those angles are calculated much too small with an error of 2° and 2.8° compared to the XRD-structure. Comparing the calculated isomers, the average error is with 1° quite acceptable.

However, the C(8')-C(8)-O(9) angle shows again the highest deviation with 2.3°.

In Tables A.3 - A.10 (see Appendix pages XVI - LVI) the geometry data for all ligand singlet and triplet state geometries are depicted. For some of the 5-substituted ligands, structures were calculated comprising both the OH and MeO function in 8-position of the quinoline. The MeO function was chosen to calculate a structure similar to the global minimum structure of the 8-hydroxyquinoline ($\theta_1 = 0^\circ$) but still to prevent H-bonding to N(1). Important structure data are the C(8')-C(8), C(8')-N(1) and C(8)-O(9) bond lengths and N(1)-C(8')-C(8) and C(8')-C(8)-O(9) angles. The O(9)-H(10) bond length (or O(9)-C(10) bond length in case of the 8-MeO derivatives) is expected to give an idea about the influence of the altered charge distribution on the oxygen atom. In the following the structures of the different ligands in their singlet and triplet state are discussed.

4.1.1 Singlet and Triplet State Geometry of the Ligands

4.1.2 Geometry of the Singlet Ground State

The change in geometry due to substituent influence is of high interest. Tables comprising the full data set are displayed in the Appendix (Table A.3 - A.6 on page XVI - XVI).

Regarding the **C(8')-C(8) bond length** (see Figure 4.4) similarities can be found for the electron withdrawing groups (CN, NO₂, Py). Going from substitution position 2 to position 3, the bond shrinks and becomes elongated when substitution takes place in 3- to 5-position. Substitution in 7-position shows a decrease in the bond length. The exception is the 7-NO₂ substituted hydroxyquinoline, due to the H-bridge between the NO₂ oxygen and the OH hydrogen atom.

Considering the substitution in 2-position the Py compound behaves differently than the other acceptors and shows a low value. One reason may be the interaction of the Py hydrogen with the quinoline nitrogen. The distance between the pyridino H closest to the quinoline nitrogen is around 2.3 Å and the torsion angle from the quinoline plane is with 26° rather low. Torsion angles out of the quinoline plane for the Py ring for other substitution positions are around 52°-72° (see Figure 4.3 for the 2 and 4 substituted pyridino quinoline). This atypical behaviour let us suggest a weak interaction between the Py ring and N(1) if substituted in 2-position.

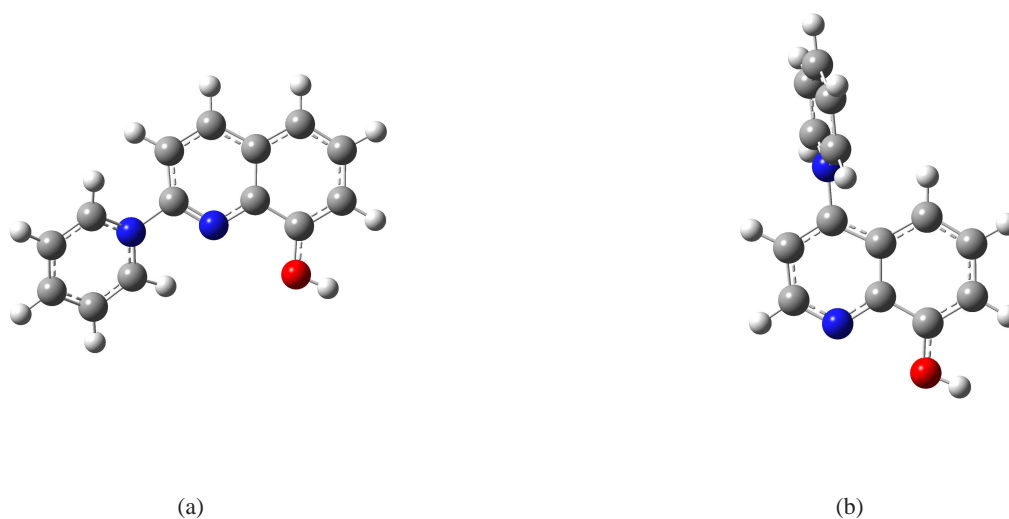


Figure 4.3: Torsion angle of the pyridino group out of the quinoline plane in (a) 2-pyridino-8-hydroxyquinoline (26.86°) and (b) 4-pyridino-8-hydroxyquinoline (72.92°). Calculated on UB3LYP/6-31G* level of theory.

When the OH group is exchanged by a MeO group, the C(8')-C(8) bond elongates.

For the electron pushing groups (NH₂, Ph, HSO₃) no general trend is observed regarding the C(8')-C(8) bond. For the NH₂ substituted structures an alternating behaviour is shown with elongated bond lengths in the even numbered substitution positions. The Ph group follows the trend of the NH₂ group, although

the elongation in 2-position is more distinct. The torsion angle out of the quinoline plane for the Ph group is similar to the Py substituted molecule. In 2-position the Ph torsion angle out of the quinoline plane is with 26° smaller than in other positions. It is expected, that a smaller torsion angle gives a better overlap between the two conjugated systems and shows therefore a more distinct electronic effect. However, in 6- and 7-positions the effect clears out. The torsion angle in these positions is around 53° - 63° , but the bond length does not change significantly. In case of HSO_3 substitution the bond length increases with increasing substitution position, becomes slightly shorter in the 6-substituted compound and increases again in 7-position. The high value in 7-position is again a result of the intermolecular H-bridge formation. A deprotonation of the HSO_3 group in 4-position results in a shortening of the bond length.

Generally speaking, electron withdrawing groups elongate the C(8')-C(8) bond compared to electron donating groups. Interactions with the quinoline nitrogen, when substituted in 2-position, or formation of H-bonds, if substituted in 7-position, result in an elongated C(8')-C(8) bond. A trend can better be seen for the electron withdrawing groups. The bond length is elongated if substituted in 5- or 6-position and compressed in 2- and 7-position. Electron donating groups show an alternating pattern, with bond elongation if substituted in even positions.

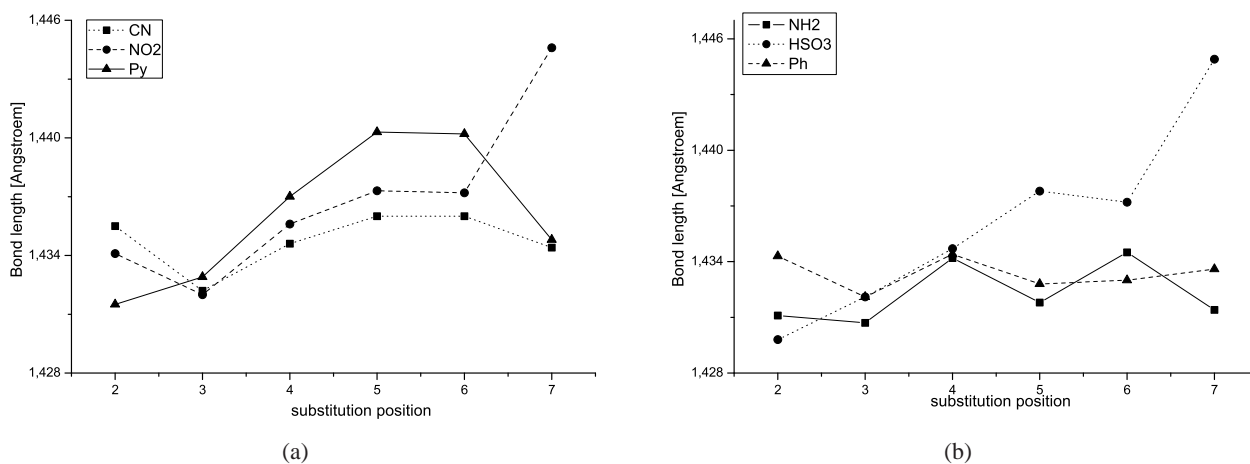


Figure 4.4: Bond length of the C(8')-C(8) bond for the (a) acceptor and (b) donor substituted 8-hydroxyquinoline in its singlet state geometry. Calculated on UB3LYP/6-31G* level of theory.

Regarding the C(8')-N(1) bond length (see Figure 4.5) the acceptors show a trend for the first three substitution positions with the smallest value in 2-position and the largest in 3-position. For all other positions no correlation is observed. However, in 7-position the presence of the OH group effects all three substituents. In case of the CN group a small deviation from the linearity is observed. The nitrogen is bent with 3.82° towards the OH group. The NO_2 group builds again a hydrogen bond to the OH group and the Py group shows an increased torsion angle with 59° . Examining the donor groups, no trend is apparent. In general, the bond shrinks if substitution takes place in 2- and 6-position and is elongated in 3-position. The Ph group displays the highest torsion angle, same as the Py group, in 4-position. However, this does not result in a conspicuous shortening of the bond length, as observed in case of the Py substituent. Generally speaking, acceptor groups show shortened bond lengths compared to the donor groups, which is contrary to the above discussed C(8')-C(8) bond.

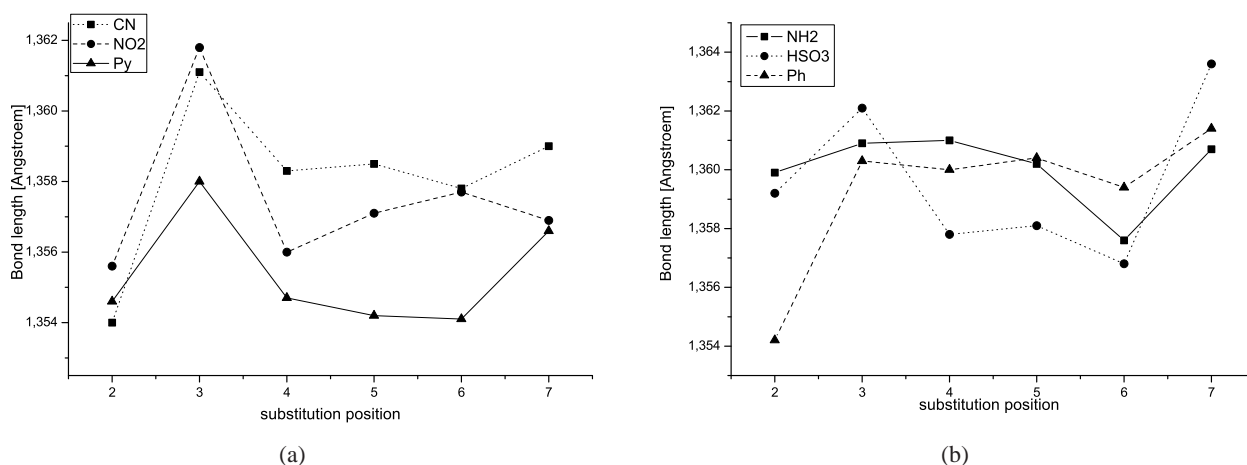


Figure 4.5: Bond length of the **C(8')-N(1)** bond for the (a) acceptor and (b) donor substituted 8-hydroxyquinoline in its singlet state geometry. Calculated on UB3LYP/6-31G* level of theory.

The **C(8)-O(9)** bond length (see Figure 4.6) however, shows a better correlation regarding the acceptor groups. Bond lengths are longer in 2-,3-,4- and 6-position, while in 5- and 7-position a shortening of the bond length takes place. The NO₂ group in 7-position shows a remarkable shortening, again due to the intramolecular interaction. The Py derivatives do not follow exactly this trend. While the values for substitution in 3- and 4-position decrease, the molecule substituted in 7-position shows a much longer C-O distance.

Regarding the donor groups the influence on the bond length is rather small, which can be seen in case of the Ph substitution. The deflecting values for the NH₂ and HSO₃ substituents can again be explained with characteristics in the geometry. In case of the NH₂ substituent the bond length decreases in 7-position, mainly due to a rotation of the NH₂ group with an angle of 89°. Also the wagging angle, which is an indication for the degree of pyramidalisation, is highest in this position, giving free the lone pair of the NH₂ for interaction with the OH group. The N-H distance between amino nitrogen and hydroxy hydrogen is 2.03 Å.

To sum up, the donor derivatives show a longer bond distance than the acceptor derivatives, which is also stated by Hoge [44] for the phenyl derivatives.

Surprisingly, the **O(9)-H(10)** bond length (see Figure 4.7) is not effected by the substitution pattern. Bond length remains uniformly over all substitution positions with exception of the known substituents showing an interaction with the OH group. Intramolecular interaction in 7-position results expectedly in an increased bond length. However, acceptors show in general a slightly longer bond distance compared to donor molecules.

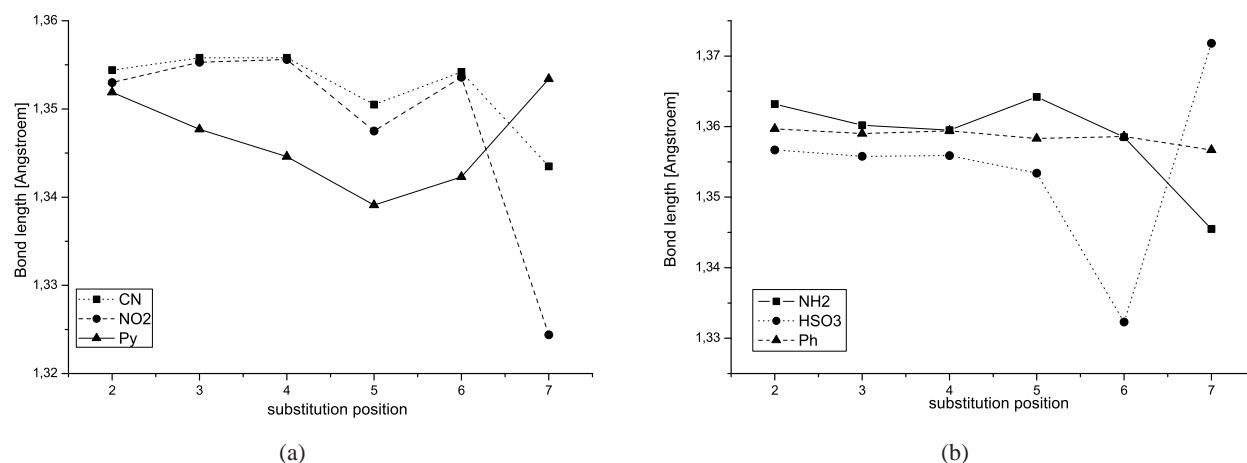


Figure 4.6: Bond length of the C(8)-O(9) bond for the (a) acceptor and (b) donor substituted 8-hydroxyquinoline in its singlet state geometry. Calculated on UB3LYP/6-31G* level of theory.

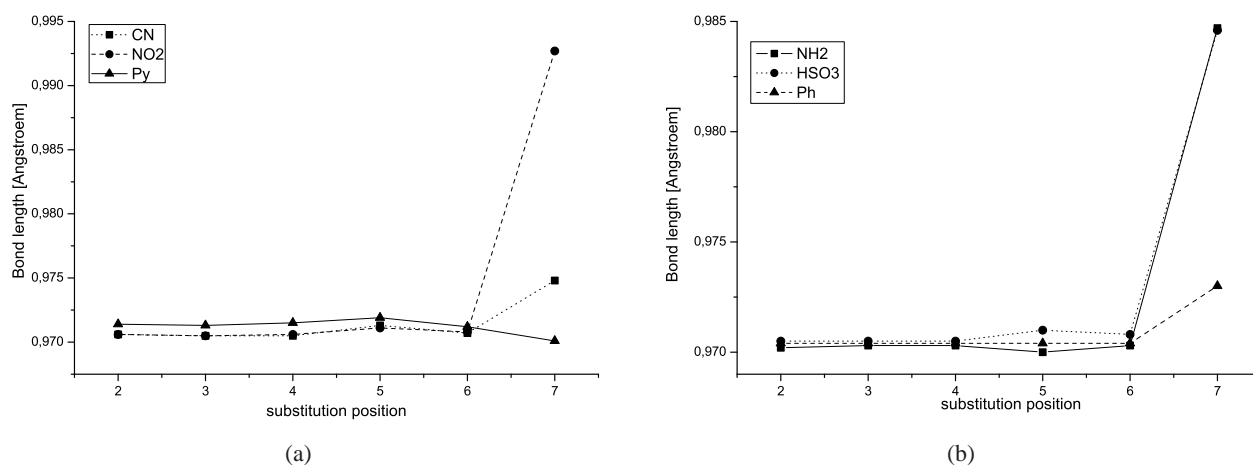


Figure 4.7: Bond length of the O(9)-H(10) bond for the (a) acceptor and (b) donor substituted 8-hydroxyquinoline in its singlet state geometry. Calculated on UB3LYP/6-31G* level of theory.

As mentioned before, the angles which form the cyclic structures with the Eu ion in the complex are matter of interest and were investigated as well. Having a look on the donor systems a clear trend can be seen with narrow angles in 4-,5- and 7-position and widened angles in 1-,3- and 6-position for the N(1)-C(8')-C(8) angle (see Figure 4.8). In the HSO₃ substituted structure the angle is again smaller due to interaction with the quinoline nitrogen when substituted in 2-position.

However, the influence of the acceptor systems is less clear. Going from substitution in 2-position, the angles become more narrow and reach their minimum in 5-position, showing a value similar to that in position 7. The most distinct influence is observed in case of the NO₂ substituent.

Changes regarding the angles are seen more drastically in case of the donor substituents, where the minimum values reach a magnitude much below the acceptor values. Factoring out the substituents with intramolecular bonding ability, the influence on the $C(8')-C(8)-O(9)$ angle (see Figure 4.9) is very small. In fact the angles remain almost unchanged in terms of different substitution patterns or different donor - acceptor ability.

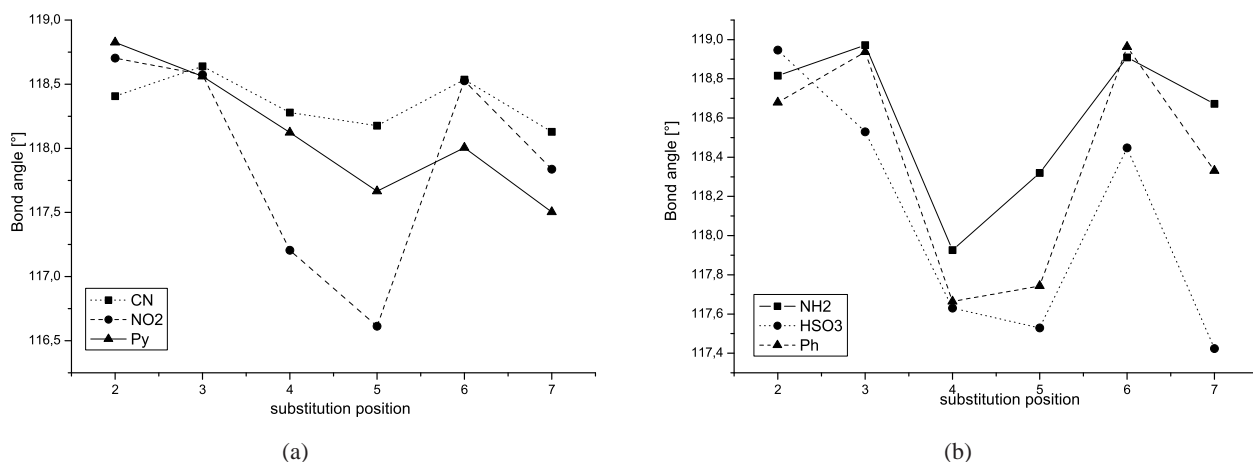


Figure 4.8: Values for the $N(1)-C(8')-C(8)$ angle for the (a) acceptor and (b) donor substituted 8-hydroxyquinoline in its singlet state geometry. Calculated on UB3LYP/6-31G* level of theory.

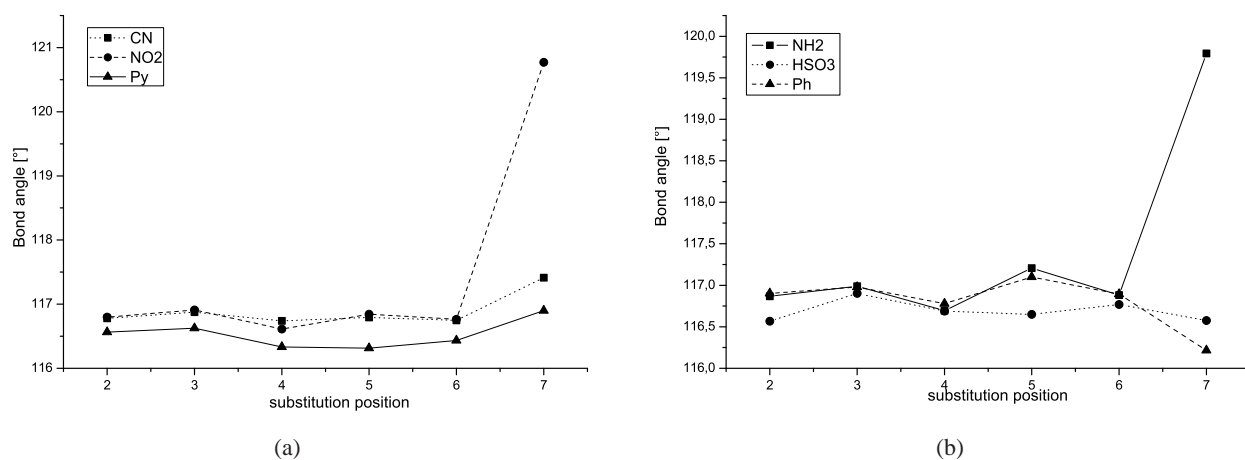


Figure 4.9: Values for the $C(8')-C(8)-O(9)$ angle for the (a) acceptor and (b) donor substituted 8-hydroxyquinoline in its singlet state geometry. Calculated on UB3LYP/6-31G* level of theory.

4.1.3 Geometry of the Triplet State

Special attention should be given on geometry changes when the molecule is excited to its triplet state. As mentioned before, energy transfer takes place in the complex structure from the triplet state of the ligands to the Eu ion. Geometry data for the ligands in their triplet states are depicted in Tables A.7 - A.10 on pages LVI - LVI in the Appendix.

For the **C(8')-C(8)** bond (see Figure 4.10) both donor and acceptor substituents show the same correlation. The bond shrinks dramatically if substitution takes place in 3-position of the quinoline backbone. Going further to 4-, 5- and 6-position, the bond length elongates continuously showing a maximum in substitution 6-position. Only the NH_2 substituent shows a maximum elongation in 5-position. Remarkable is the consistency in 7-position throughout all substituents. Values for the 7- NO_2 derivative were excluded since optimisation calculations remained without success. In case of an unrestrained optimisation, a breakdown of the molecule occurs. When the NO bond of the NO_2 group is constrained during the optimisation process, the hydrogen from the OH group migrates to the NO_2 oxygen. The bond lengths are generally longer compared to the singlet geometry, with exception of donor substituents in 3-position of the hydroxyquinoline. Here the bond is compressed if compared to the singlet structure.

Interestingly, extension of the π -system by substituting with Ph or Py results in a smaller change of the bond length regarding 4- and 5-position. The HSO_3 substituent, when attached in 7-position, interacts expectedly with the OH group in form of H-bridge bonding. Interestingly, this does not show any effect on the bond length as observed in the singlet state. No conclusion can be done regarding the difference in the bond length referring to the donor and acceptor ability. Ph and Py rings are twisted similar to the singlet structures although to a much less degree. In 2-position the Ph ring is planar with the quinoline system (0.036° compared to 14.4° in the singlet structure), while the Py ring is slightly twisted (4.3° compared to 26.8° in the singlet structure). With increasing position number the twisted structure becomes more apparent but stays with a maximum value of 36.9° for the Ph ring (55.75° in the singlet structure) in 4-position and 37.5° for the Py ring in 5-position (72.9° in 4-position in the singlet structure) far behind the singlet structure values. The NH_2 group in 7-position however shows the same geometry as in the singlet structure (59.77° in triplet and 60.3° in singlet structure for the wagging angle and 89.91° in triplet and 89.96° in singlet state structure for the rotation angle).

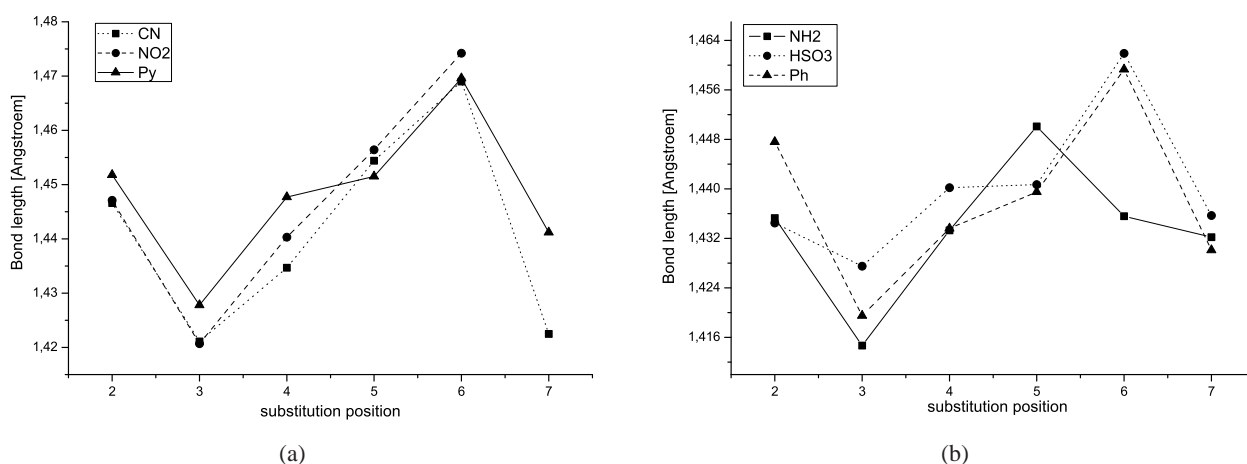


Figure 4.10: Bond length of the **C(8')-C(8)** bond for the (a) acceptor and (b) donor substituted 8-hydroxyquinoline in its triplet state geometry. Calculated on UB3LYP/6-31G* level of theory.

The trend for the **C(8^{*})-N(1) bond** length (see Figure 4.11) is opposite to the trend of the former discussed C(1)-C(2) bond. Electron pulling and pushing groups show a similar behaviour. Starting from 2-position, the bond length increases in 3-position and decreases again slowly for substitution in 4- and 5-position, and shows its minimum in 6-position. Substitution in 7-position increases the bond length. Again the Ph and Py systems show an abnormality in 4- and 5-position. While all substituents show a diminished bond length in 5-position compared to 4-position, derivatives containing a conjugate substitution system show a longer bond in 5-position.

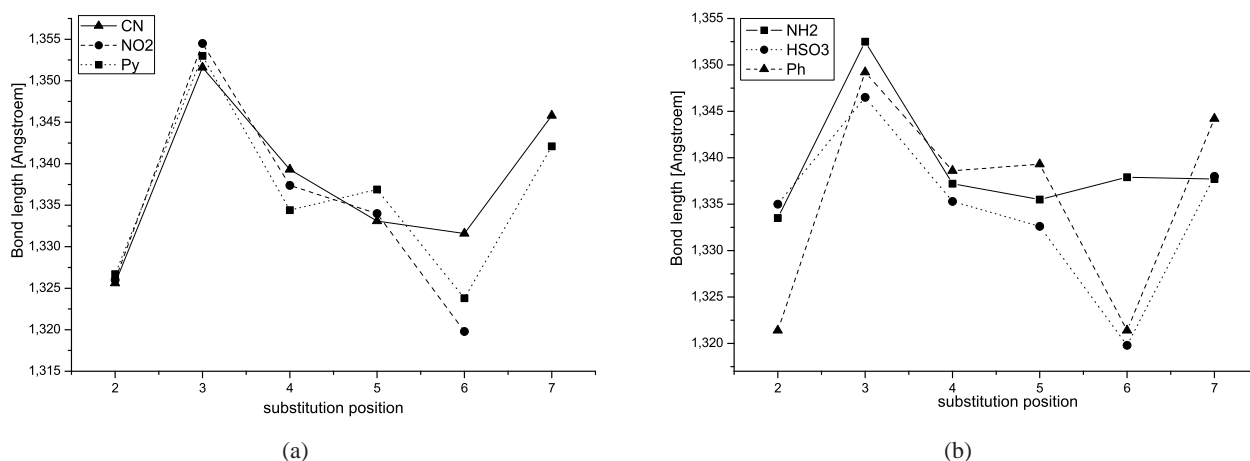


Figure 4.11: Bond length of the **C(8^{*})-N(1)** bond for the (a) acceptor and (b) donor substituted 8-hydroxyquinoline in its triplet state geometry. Calculated on UB3LYP/6-31G* level of theory.

The **C(8)-O(9) bond** (see Figure 4.12) shows a minor dependence regarding the substitution pattern in case of the acceptor ligands. Generally, the bond length stays constant and reduces in 6- and 7-position. However, the acceptor strength of the substituents has an effect. Strong acceptors like Py shorten the C(8)-O(9) bond. Donor systems however, show a much less distinct effect. The bond length stays quite constant for the first three substitution positions, increases in 5-position and decreases for the 6- and 7-position. The NH₂ substituted ligand system does not exactly follow this trend. Generally, donor groups increase the bond length compared to the acceptor substituents.

The **O(9)-H(10) bond** (see Figure 4.13) of the OH group stays, as seen for the singlet state, unaltered regarding the substitution pattern. However, the donor ligands show an increased bond length when substituted in 7-position. Acceptors show generally a slightly longer O-H bond.

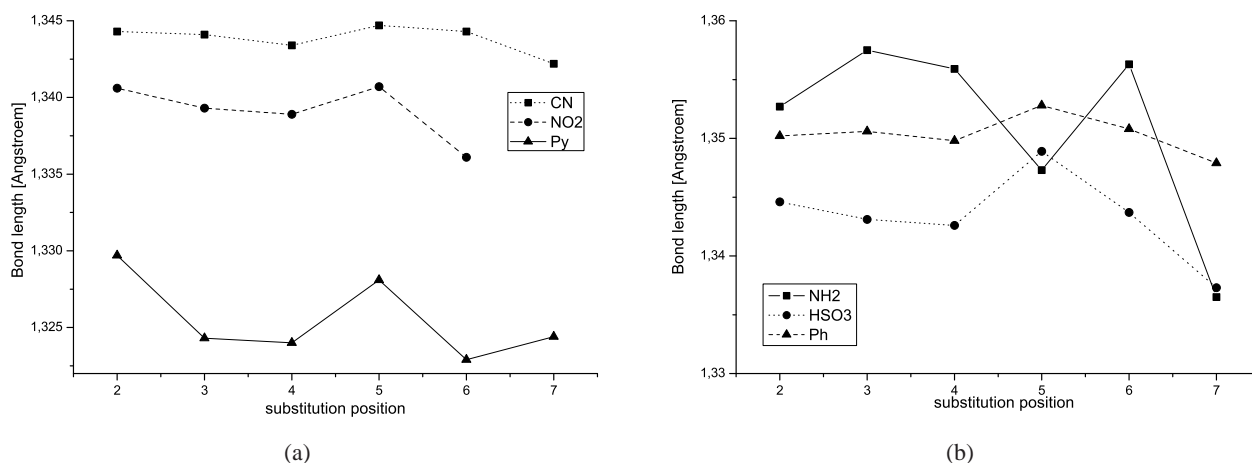


Figure 4.12: Bond length of the C(8)-O(9) bond for the (a) acceptor and (b) donor substituted 8-hydroxyquinoline in its triplet state geometry. Calculated on UB3LYP/6-31G* level of theory.

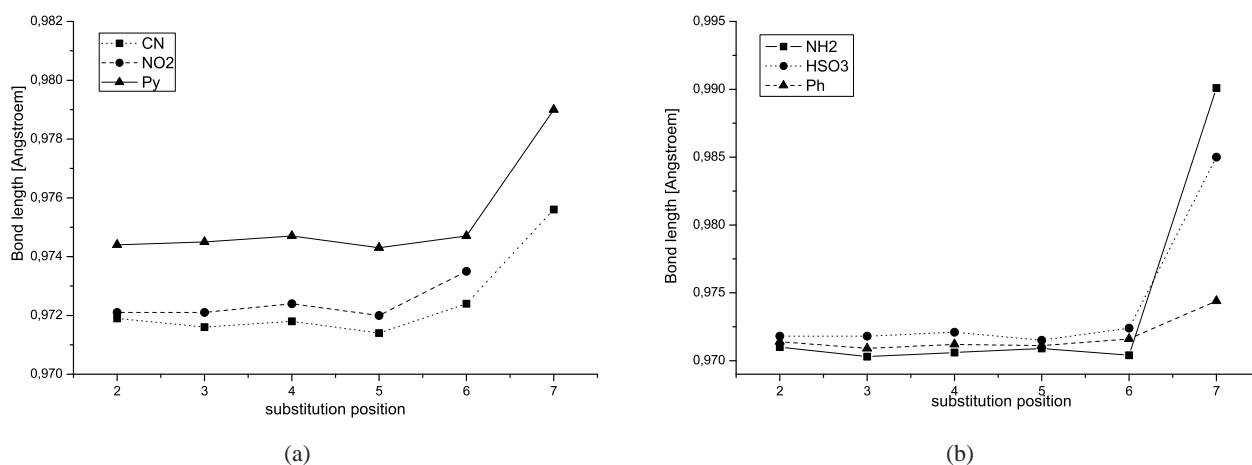


Figure 4.13: Bond length of the O(9)-H(10) bond for the (a) acceptor and (b) donor substituted 8-hydroxyquinoline in its triplet state geometry. Calculated on UB3LYP/6-31G* level of theory.

Regarding the N(1)-C(8')-C(8) angle (see Figure 4.14) acceptors decrease the angle if substituted in 4- or 5-position. The CN substituent does not follow this trend. Donor substituents show a similar behaviour, however, they also display a more narrow angle if substituted in 2-position. Generally donors widen the angle slightly.

For the C(8')-C(8)-O(9) angle (see Figure 4.15) donors and acceptors show again the same trend in form of a zig-zag pattern. This can be seen most distinct for the conjugated substituents, specially for the pyridine group. In even numbered positions a compression of the angle can be found, in odd numbered positions the angle seems widened.

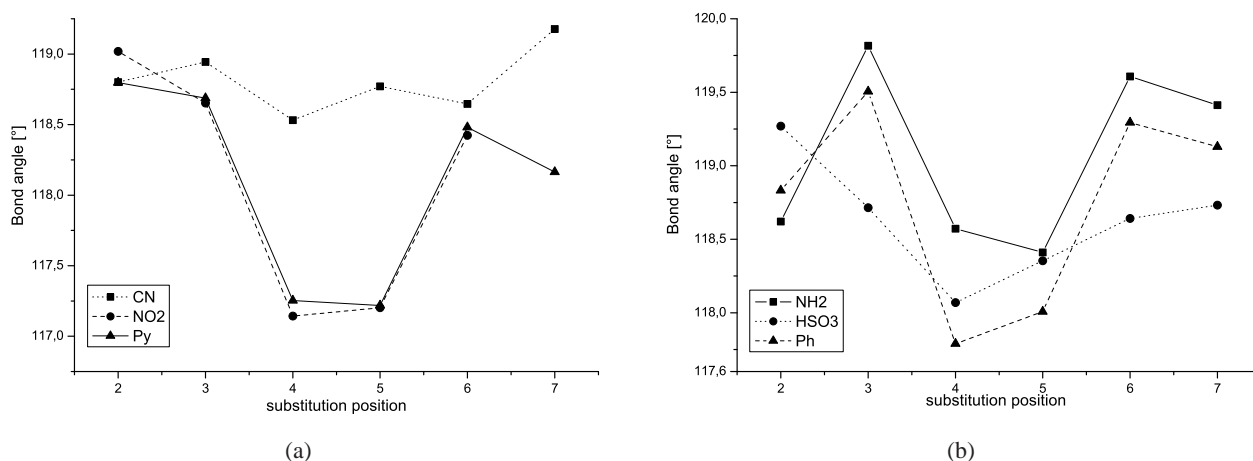


Figure 4.14: Values for the N(1)-C(8')-C(8) angle for the (a) acceptor and (b) donor substituted 8-hydroxyquinoline in its triplet state geometry. Calculated on UB3LYP/6-31G* level of theory.

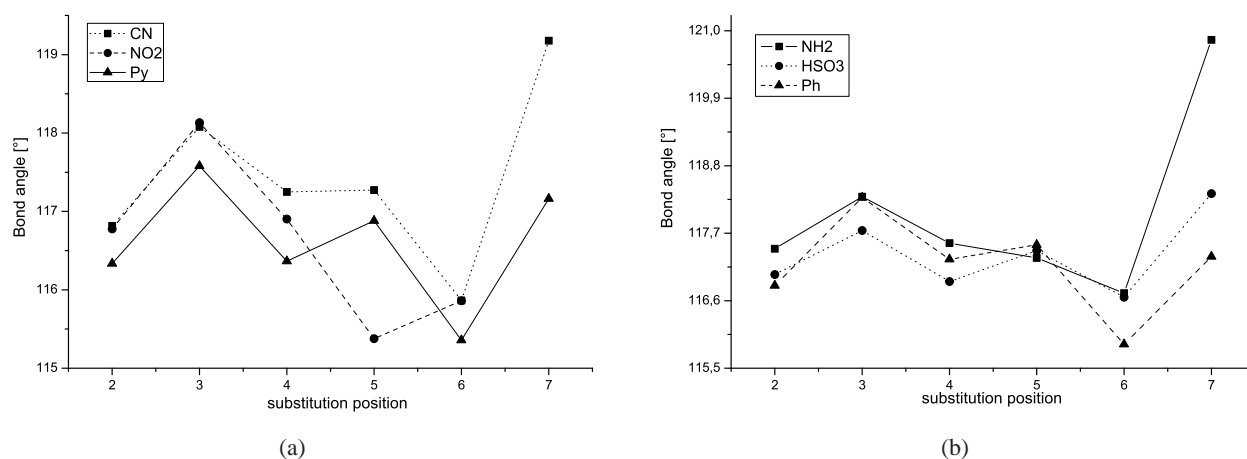


Figure 4.15: Values for the C(8')-C(8)-O(9) angle for the (a) acceptor and (b) donor substituted 8-hydroxyquinoline in its triplet state geometry. Calculated on UB3LYP/6-31G* level of theory.

4.1.4 Difference in the Singlet and Triplet Geometry

The difference in the bond length and angles between the singlet and triplet states was investigated. Donor molecules have an influence on the bond length as described before. In Figure 4.16 the difference in the singlet and triplet geometry regarding the C(8')-C(8) bond length is depicted.

In cases where the substituent is a donor (NH₂, Ph, HSO₃), the bond length is shortened in the triplet state if substitution takes place in 3-, 4- or 7-position of the 8-hydroxyquinoline backbone and is elongated if the substituents are in 2-, 5- or 6-position. The biggest change can be seen in 5-position for the NH₂ substituent and in 6-position for the Ph and HSO₃ substituents (elongation). If substitution in 3-position of the hydroxyquinoline backbone occurs, an inter system crossing (ISC) to the triplet state results in a shortening of the C(8')-C(8) bond length for all substituents (see Figure 4.16 (b)). Acceptor substituted

ligands show the same bond lengths in the singlet and triplet state as depicted in Figure 4.16 (a). The same can also be observed for other bond lengths (C(8')-N(1), C(8)-(O(9) and O(9)-H(10)). Therefore, it was refrained to depict further figures of the acceptor substituted ligands in the following discussion.

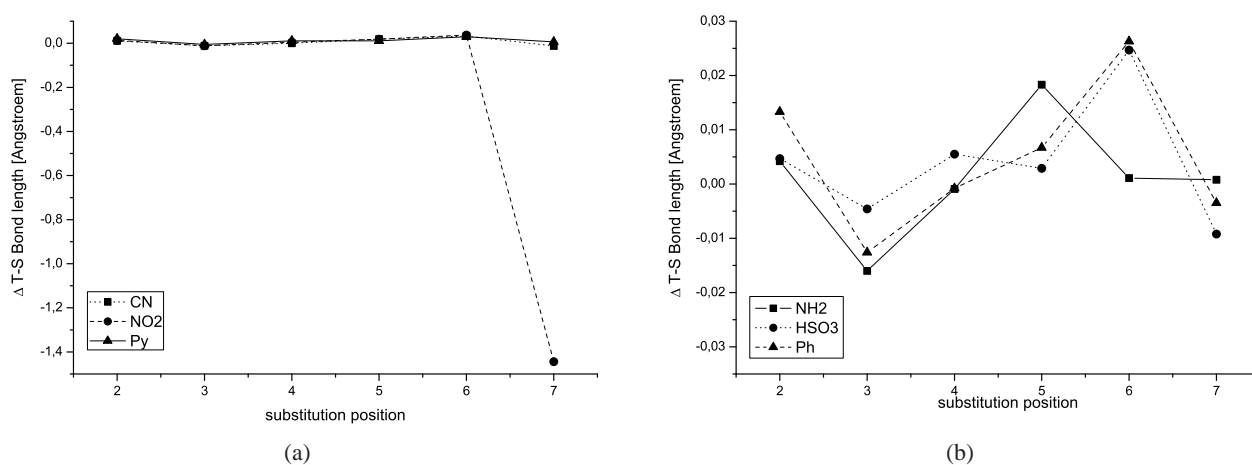


Figure 4.16: Difference in the C(8')-C(8) bond length between the singlet and the triplet state for acceptor molecules (a) and donor molecules (b). Calculation on UB3LYP/6-31G* level of theory.

The C(8')-N(1) bond length shows a shortening after ISC for all substitution positions if the substituent is a donor group. In substitution of 3-position the C(8')-N(1) bond length for all three donor substituents (NH₂, Ph and HSO₃) shows the smallest deviation to the singlet state with a difference of 0.01 Å - 0.016 Å. The highest deviation can be observed at 6-substituted hydroxyquinoline for the Ph and HSO₃ substituents.

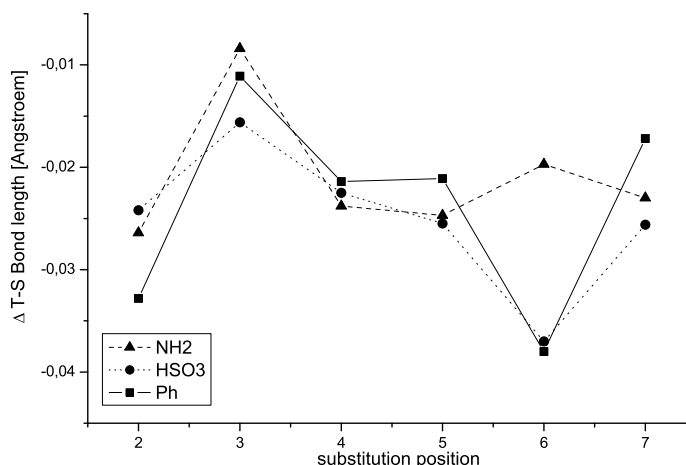


Figure 4.17: Difference in the C(8')-N(1) bond length between the singlet and the triplet state for donor molecules. Calculation on UB3LYP/6-31G* level of theory.

In the C(8)-O(9) bond the bond length in the triplet state is around 0.01 Å shorter than in the singlet state for the NH₂ and the Ph substituent in all substitution positions (see Figure 4.18). The HSO₃ substituent shows a more distinct shortening compared to the other donors with exception of substitution 6-position

where the bond is elongated. In 7-position the bond length of the HSO₃ substituted ligand in the triplet state is 0.04 Å shorter than in the singlet state, which is a result of the H-bonding of the HSO₃ substituent with the hydroxy group.

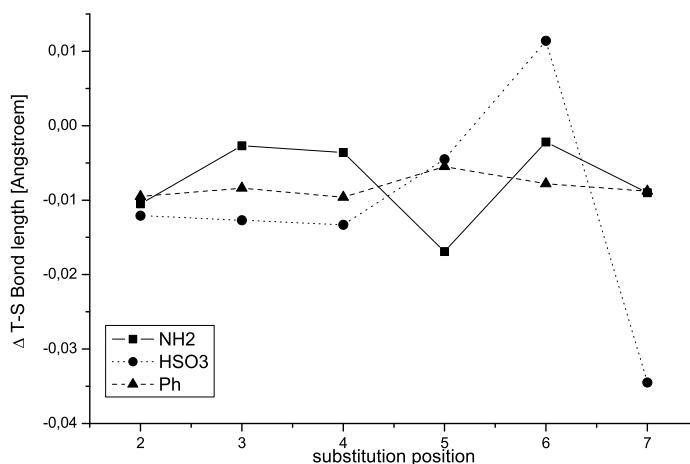


Figure 4.18: Difference in the C(8)-O(9) bond length between the singlet and the triplet state for donor molecules. Calculation on UB3LYP/6-31G* level of theory.

In donor substituted ligands the O(9)-H(10) bond length is elongated in the triplet state. An exception are the NH₂ derivatives if substitution occurs in 3- and 6-position (see Figure 4.19). The approximate difference is around 0.001 Å and therefore quite small compared to the difference in the bonds discussed before. In 7-position the NH₂ group shows an elongation of 0.005 Å which is a quite high value when compared to other donor substituents. A Reason for this behaviour might be the higher degree of hybridisation of the NH₂ group and H-bonding to the hydroxy O.

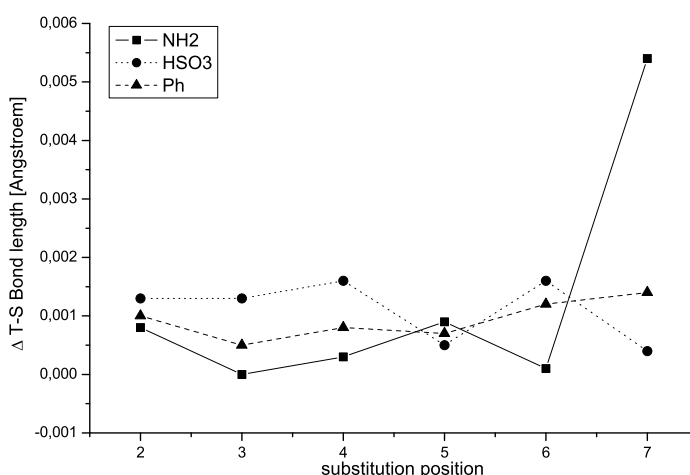


Figure 4.19: Difference in the O(9)-H(10) bond length between the singlet and the triplet state for donor molecules. Calculation on UB3LYP/6-31G* level of theory.

4.2 Evaluation of the Electrical and Chemical Parameters

Hoge reports in his work on phenyl derivatives [44] that a correlation between the Hammett parameters and the C-O bond length, in ortho substituted X-C₆H₄-OH phenyl derivatives exists. Although a correlation between bond distances and substituent and substitution position can be seen, as proved in the chapter before, sterical effects can not be singled out and a deeper investigation of the Hammett parameters and related key data is indispensable. DFT calculation gives easily a set of information on the ionisation potential or electron affinity of a molecule, which can be read out from the energies of the frontier orbitals. Following the Koopmans theorem, the ionisation potential (IP) can be calculated as the negative HOMO orbital energy of the neutral species. Accordingly the electron affinity (E_{ea}) is the negative HOMO orbital energy of the charged molecule. However, this description lacks in terms of accuracy. The effect of relaxation due to taking an electron from the neutral species is not described in the Koopmans theorem and IP's calculated on this level are naturally underestimated. One way how to account for the relaxation effect is taking the energies of the optimised geometries of the charged and uncharged species and subtract them according to equation 4.1 and 4.2.

$$IP = E(N-1) - E(N) \quad (4.1)$$

$$E_{ea} = E(N+1) - E(N) \quad (4.2)$$

$E(N+1)$ is the total HF energy of the anionic species, $E(N)$ refers to the neutral molecule and $E(N-1)$ to the cationic form of the molecule.

Taking the IP and the E_{ea} one can calculate the chemical potential (μ_S) according to equation 4.3, which gives evidence of the electron donating or accepting ability. The chemical potential is the negative of the absolute electronegativity (χ_S).

$$\mu_S = \left(\frac{\delta E}{\delta N} \right) = -\chi_S = \left(\frac{IP + E_{ea}}{2} \right) \quad (4.3)$$

Another parameter, the chemical hardness (η_S) is defined similar to the chemical potential, but takes the second derivative of the energy with respect to changes in the numbers of electrons and is given in equation 4.4.

$$\eta_S = \left(\frac{IP - E_{ea}}{2} \right) = \left(\frac{\delta^2 E}{\delta N^2} \right) \quad (4.4)$$

The hardness parameter is defined in the HSAB theory by Pearson [45] and measures the resistance of a molecule in changes of its electron cloud.

E_{ca} and IP's for all ligand systems were calculated and the results were checked for any correlation with known Hammett parameters. The full data set is presented in Tables A.11 - A.14 in the Appendix (see pp. LVI - LVI).

For the *hardness* no direct correlation to donor or acceptor strength can be made. However, *absolute electronegativity* and the *chemical potential* correlate with the acceptor and donor ability of the substituents as depicted in Figure 4.20.

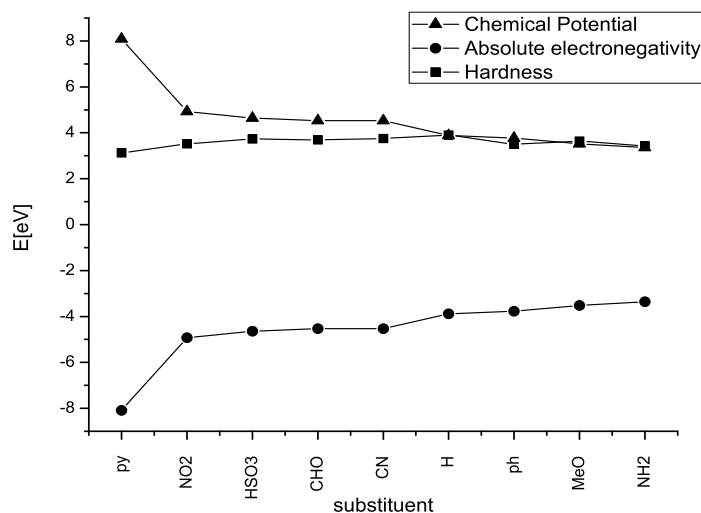


Figure 4.20: μ_S , χ_S and η_S values in eV for different substitution groups in 5-position of the 8-hydroxyquinoline molecule. Values are calculated on UB3LYP/TZVP level of theory.

The pyridino group shows the highest electron withdrawing ability (low absolute electronegativity in Figure 4.20). The order is $\text{Py} > \text{NO}_2 > \text{HSO}_3 > \text{CHO} > \text{CN} > \text{H} > \text{Ph} > \text{MeO} > \text{NH}_2$. The *hardness parameter* is almost uniform for all substitution groups, but shows a slightly lower value for the Py and NH₂ group, that means the electron cloud in this groups can resist better a change if electrons are taken or given to the molecule. The *ionisation potential* and *electron affinity* also correlate with the donor and acceptor strength of the substituents as depicted in Figure 4.21. Electron pulling groups such as Py show higher values for IP and E_{ca} . Values for electron donors are smaller. In case of the electron affinity the unsubstituted hydroxyquinoline shows a lower value than the Ph group, which does not necessarily mean that Ph acts as an acceptor. Here the fact that charges in conjugated systems can move more easily in both directions (from the quinoline backbone in the Ph ring and from the Ph group to the backbone), increases the value for the electron affinity.

Referring to the substitution pattern it is harder to draw a conclusion. None of the parameters shows a

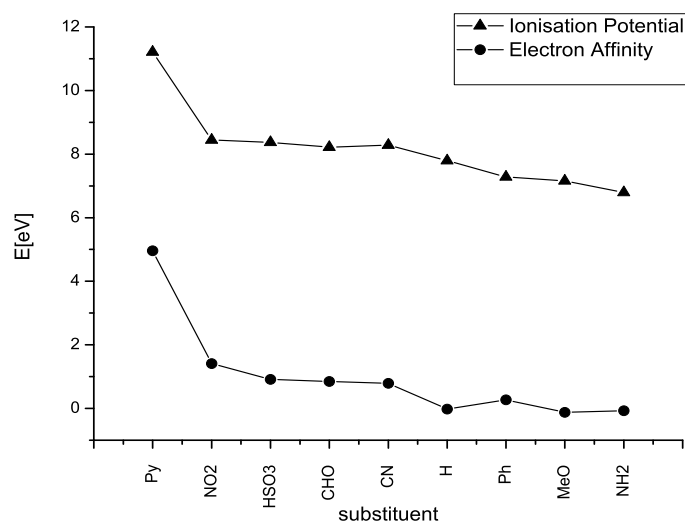


Figure 4.21: IP and E_{ea} values in eV for different substitution groups in 5-position of the 8-hydroxyquinoline molecule. Values are calculated on UB3LYP/TZVP level of theory.

significant change in dependence of substitution positions.

One key aspect of the Hammett parameters is a dependence according to the shift of the HOMO - LUMO orbitals or excitation energies, since a correlation between these molecular characteristics and the Hammett parameters would make it easy to select appropriate candidates for further calculations. With the here available data no correlation can be found. To find a dependence a bigger test set would be necessary. This work is done normally in QSAR studies, which use a set of more than hundred test molecules.

4.3 Absorption Spectra of the Ligands

Absorption spectra of the ligands were calculated in gas phase and with the IEF-PCM model of solvation. To evaluate the method, four experimental spectra were recorded and compared with calculated spectra.

4.3.1 8-Hydroxyquinoline

In Figure 4.44 the experimental spectra of **8-hydroxyquinoline** in ETOH and the calculated gas phase and PCM-ETOH spectra are depicted. Two major peaks can be distinguished. The higher energetic peak in the experimental spectra is attributed as the S_0-S_5 transition and lies at 5.08 eV (244 nm, $\epsilon=31.78 \text{ l mol}^{-1} \text{ cm}^{-1}$). The weaker peak at 3.92 eV (316 nm, $\epsilon=5.80 \text{ l mol}^{-1} \text{ cm}^{-1}$) is attributed as the S_0-S_1 transition. The calculated spectra shift to higher energies for the stronger peak and vice versa for the weaker one. The error is with approximately 5% in an acceptable range. For the S_0-S_1 transition the gas phase calculation shows a bigger shift and a higher error with 7%. Using the PCM model increases the quality of the results and the error, if compared to the experimental spectrum with an error of 1%. This behaviour can be observed for $n-\pi^*$ transitions normally, where different solvents cause a shifting of the absorption bands, but the relatively high oscillator strength of $f=0.0486 \text{ a.u.}$ in this case indicates more a $\pi-\pi^*$ transition. The S_0-S_1 transition comes mainly from a HOMO - LUMO excitation with smaller contributions from HOMO-2 - LUMO+1 and HOMO - LUMO+2 excitations. As can be seen in Figure 4.23 the orbitals show a node in the molecular plane which underlines the assumption of a $\pi-\pi^*$ transition.

The excitation from the HOMO to the LUMO orbital goes from the phenoxy part of the molecule to the pyridino part. In the HOMO orbital the oxygen shows an electron density, which decreases in the LUMO orbital. In the LUMO+1 orbital the electron density is distributed in the ring systems only without any electron density on the OH group. The HOMO-2 - LUMO+1 transition is mainly a charge redistribution in the ring system, where the π^* orbitals of the LUMO+1 show a very localised characteristic on the ring carbon atoms. In the HOMO - LUMO+2 transition electron density goes again from the OH group in the ring system and from the phenoxy part to the central C(8')-C(4') bond. In contrast to the LUMO+1 orbital, the LUMO+2 orbital shows a small electron density on the OH group.

Exchange of the OH group in 8-position with a MeO group does not shift the spectrum noteworthy. The composition of the S_0-S_1 transition is the same as in case of the 8-hydroxyquinoline, however the oscillator strength with $f=0.0628 \text{ a.u.}$ is slightly increased.

In the S_0-S_5 transition of the 8-hydroxyquinoline the main contribution comes from an excitation from the HOMO-2 to the LUMO orbital and goes again from the phenoxy part to the pyridino part of the molecule. The density shifts from the C(8')-C(4') bond to the nitrogen and the carbon atom opposed to

the nitrogen. With an oscillator strength of $f=0.6482$ a.u. the S_0 - S_5 transition is much stronger than the S_0 - S_1 transition.

Again, substituting the OH group with MeO does not significantly effect the transition, although the oscillator strength in the MeO derivative is with $f=0.5976$ a.u. slightly smaller than in the 8-hydroxyquinoline. The nodes of the orbitals in the molecular plane and the relatively high oscillator strength gives reason to attribute both transitions as π - π^* excitation. Table 4.4 compares the experimental and calculated energies of the main transitions and shows the dominating excitations and their attributions.

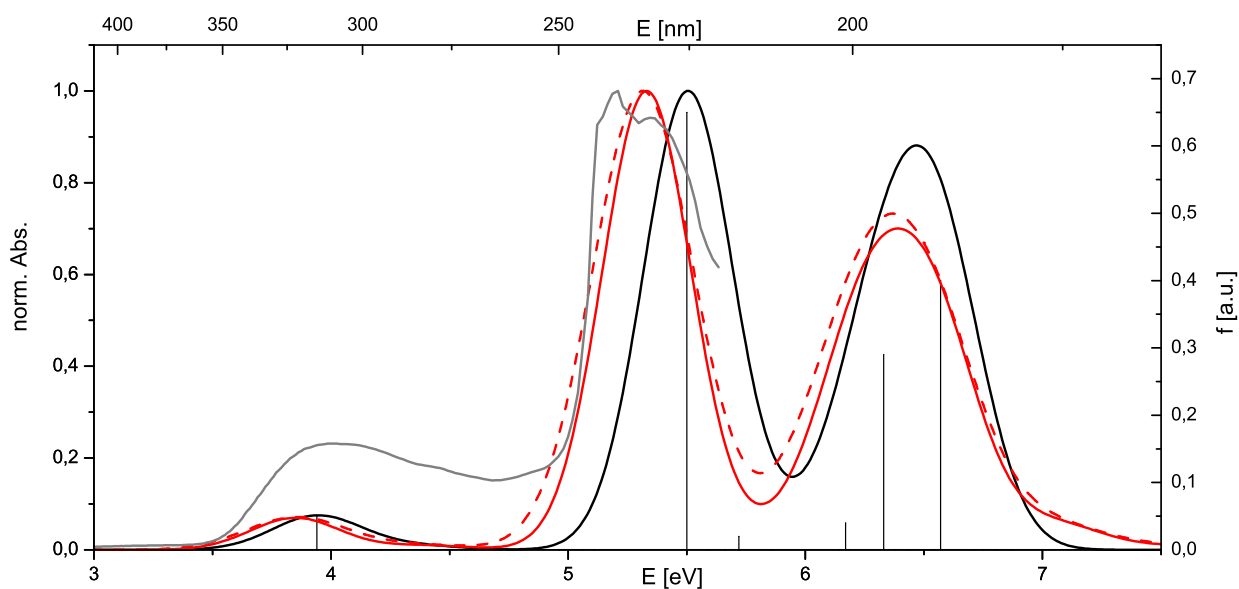


Figure 4.22: Experimental and calculated spectra of 8-hydroxyquinoline (8HQ). Grey: Experimental spectra in ETOH ($c=2.62 \times 10^{-3} \text{ mol l}^{-1}$, $\epsilon_{244}=31.78 \text{ l mol}^{-1} \text{ cm}^{-1}$); Black: Calculated gas phase spectrum; Red: Calculated solvent spectra: IEF-PCM ETOH: red solid line; IEF-PCM DCM: red dashed line. Vertical lines: calculated gas phase transitions. All calculations were done on UB3LYP/TZVP level of theory.

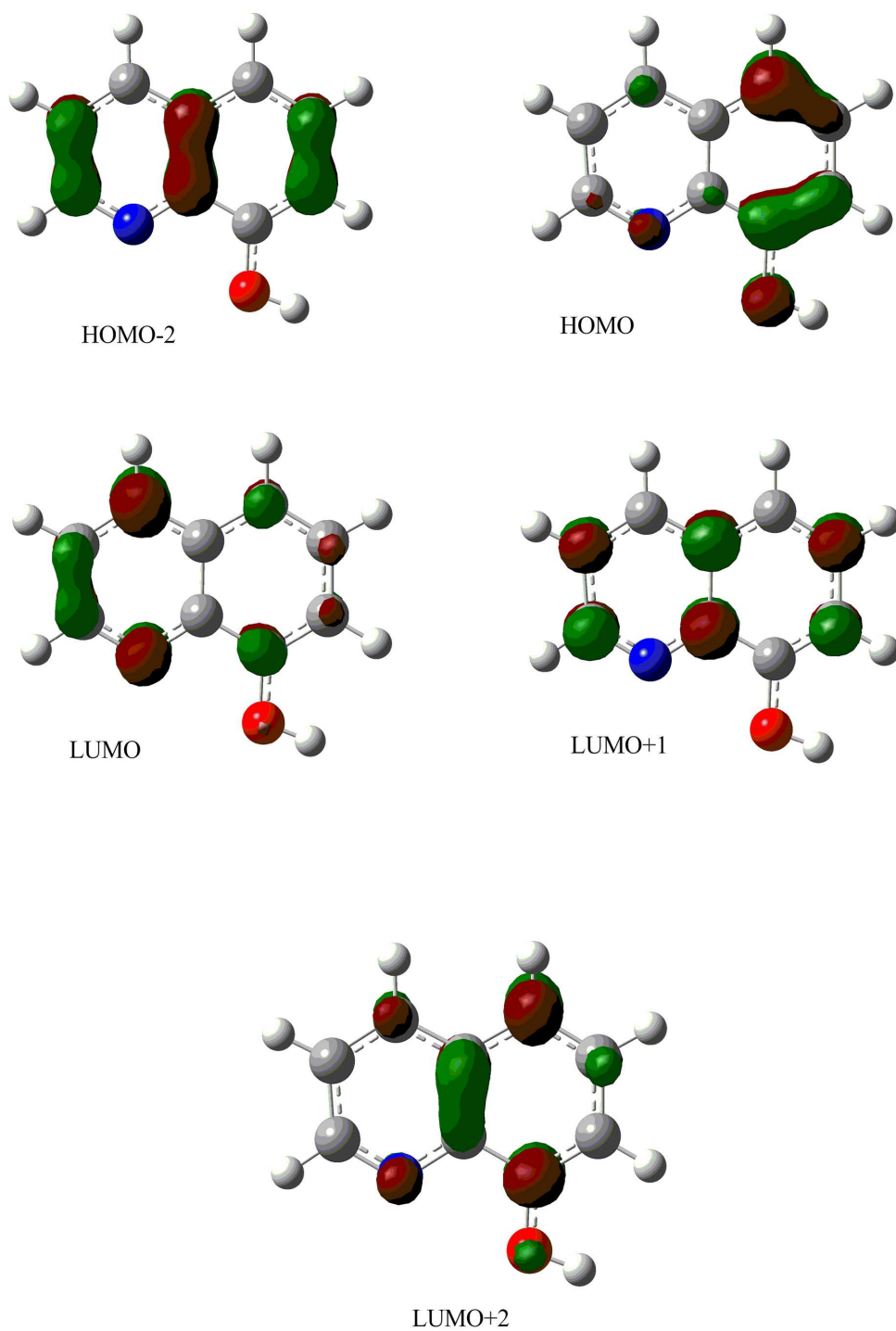


Figure 4.23: Molecular orbitals of the **8-hydroxyquinoline**. Calculated on UB3LYP/TZVP level of theory in gas phase.

Table 4.2: Main absorption energies, oscillator strengths, dominant contributions of the excitation and attributions of the **8-hydroxyquinoline** spectra. Experimental spectra in ETOH ($c=2.62 \times 10^{-3} \text{ mol l}^{-1}$), calculated spectra in gas phase (UB3LYP/TZVP).

E_{exp} [nm]	E_{exp} [eV]	ϵ [$\text{l mol}^{-1} \text{cm}^{-1}$]	Excitation	E_{calc} [eV]	f [a.u.]	Contribution	CI coefficient [a.u.]	Attribution
316	3.92	5.80	S_0-S_1	3.94	0.0486	H - L	0.64987	$\pi-\pi^*$
						H - L+2	0.11743	$\pi-\pi^*$
						H-2 - L+1	-0.11633	$\pi-\pi^*$
244	5.07	31.78	S_0-S_5	5.50	0.6482	H-2 - L	0.45119	$\pi-\pi^*$
						H - L+1	-0.35142	$\pi-\pi^*$
						H-3 - L+1	-0.22849	$\pi-\pi^*$
						H-2 - L+2	0.14149	$\pi-\pi^*$

Table 4.3: Summary of calculated and experimental absorption energies of **8-hydroxyquinoline**. Calculation on UB3LYP/TZVP level of theory.

E_{exp} [nm]	E_{exp} [eV]	E_{calc} gas phase [eV]	f [a.u.]	E_{calc} ETOH [eV]	f [a.u.]	E_{calc} DCM [eV]	f [a.u.]
316	3.92	3.94	0.0486	3.84	0.0609	3.86	0.0643
244	5.07	5.50	0.6482	5.33	0.8735	5.31	0.9051

4.3.2 5-Formyl-8-hydroxyquinoline

In Figure 4.24 the spectra of 5-formyl-8-hydroxyquinoline in ETOH is given. Four peaks can be distinguished from which the weakest at 3.12 eV (397 nm) comes from the S_0-S_1 transition. The next one at 3.74 eV (331 nm) can be identified as the S_0-S_2 transition. At 4.73 eV (262 nm) the experimental spectrum shows a peak which is not well described in the convoluted spectrum. In the calculated solvent spectrum clearly a shoulder can be seen, which is not really present in the gas phase spectrum. However, taking a close look on the calculated transition lines shows an excitation at this energy which is shifted towards smaller wavelengths and might be superposed with the peak originating from the next energetically higher lying transition. Comparison with the line spectra shows that the peak at 4.73 eV (262 nm) comes from the S_0-S_6 transition. The last and strongest peak at 5.14 eV (241 nm) is the S_0-S_8 transition. The error between experimental and calculated spectra is quite small (3% for the gas phase spectrum and 1% for the PCM-ETOH spectrum referring to the strongest peak). Again, applying the solvent model increases the quality of the results. The intensity is slightly overestimated for the S_0-S_2 transition in case of the calculated solvent spectrum. All peaks are shifted towards shorter wavelengths. The S_0-S_1 transition is present in the calculation at 3.47 eV (357 nm). The oscillator strength with $f=0.0004$ a.u.

is much too weak to be observed in the spectra. This transition comes mainly from excitations from the HOMO-1 - LUMO orbital with a smaller contribution from a HOMO-3 - LUMO excitation. As depicted in Figure 4.25 both HOMO-1 and HOMO-3 orbitals show a n-bonding orbital characteristic at the pyridino nitrogen and the aldehyde function, respectively. The LUMO orbital is a π^* orbital with the electron density distributed uniformly over the whole molecule. n- π^* transitions are known to possess low intensities and show a bathochromic shift in more polar solvents. n- π^* transitions are not well described by DFT calculations and the energies are generally underestimated. The same transition in the PCM-ETOH calculation can be found at 3.60 eV (344 nm) and at 3.58 eV (346 nm) in the PCM-DCM calculation. This underlines the assumption that the S_0 - S_1 transition has the attribution of a n- π^* excitation. The S_0 - S_2 is mainly a HOMO - LUMO excitation with contributions from HOMO-2 - LUMO+1 and HOMO - LUMO+2 excitations. These excitations are attributed as π - π^* transitions as clearly depicted in the MO pictures. The HOMO - LUMO excitation goes from the phenoxy part to the π^* orbital located at the aldehyde function and also pushes the electron density in the pyridino ring. A similar characteristic shows the HOMO - LUMO+2 excitation. Here the electron density in the π^* orbital is more localised on the aldehyde function and no density is present on the OH group, whereas the LUMO orbital shows a contribution of the hydroxy function in the orbital. The HOMO-2 - LUMO+1 shows a similar characteristic as the HOMO-2 - LUMO+1 transition of the 8-hydroxyquinoline. In both cases the HOMO-2 orbital is a π orbital where the electron density is located along the C(8')-C(4') bond. In the LUMO+1 orbital the electron density is distributed in the ring system only.

The S_0 - S_6 transition at 4.88 eV (244 nm) is mainly a HOMO - LUMO+2 excitation, which is a redistribution of the electron density from the phenoxy ring to the whole molecule. A small contribution also comes from a HOMO - LUMO+1 excitation, where the electron density in the π^* orbital is more pronounced in the pyridino part of the molecule and does not show any contribution of the OH group or the aldehyde function. The oscillator strength is with $f=0.1286$ a.u. smaller than in the S_0 - S_2 transition. The strongest band in the spectrum comes from the S_0 - S_8 transition at 5.23 eV (237 nm, $f=0.3557$ a.u.) and is composed in equal parts of three excitations. Two of them were found and described in the S_0 - S_6 transition before. The third one is the HOMO-2 - LUMO excitation. All excitations show π - π^* characteristics. The HOMO-2 - LUMO excitation shows a behaviour which is different to the HOMO-2 - LUMO+1 excitation. The electron density redistributes from the HOMO-2 orbital to the phenoxy ring in the LUMO orbital embedding the formyl- and the hydroxy group. A comparison of the calculated and experimental transitions with its attribution is given in Table 4.5.

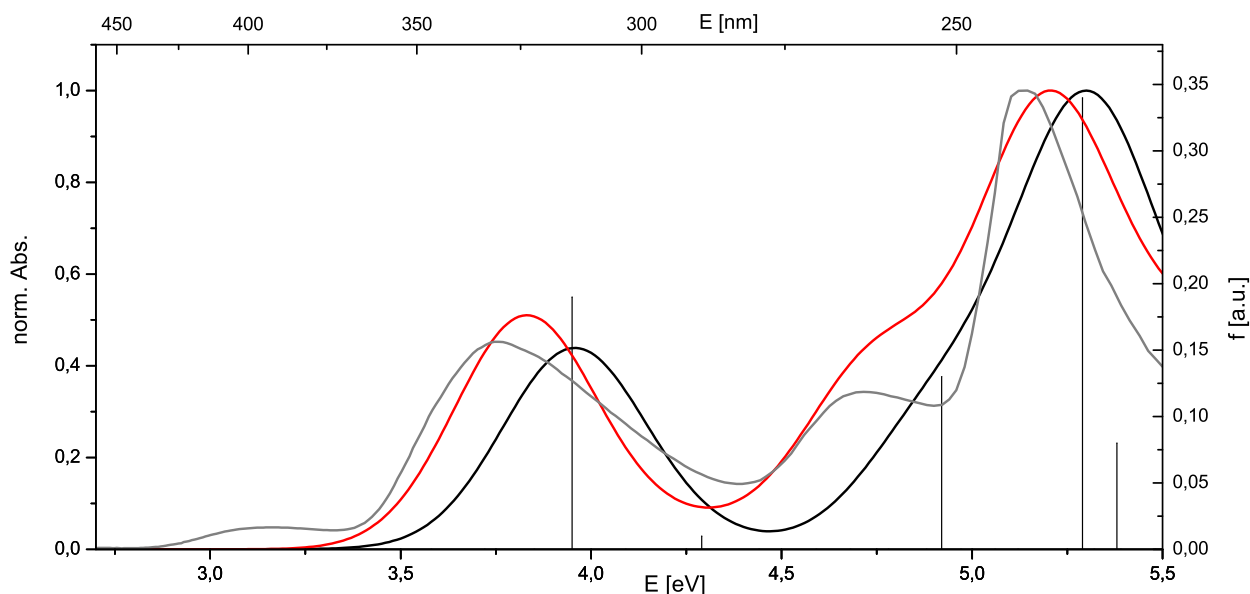


Figure 4.24: Experimental and calculated spectra of **5-formyl-8-hydroxyquinoline**. Grey: Experimental spectra in ETOH ($c=1.47 \times 10^{-3} \text{ mol l}^{-1}$, $\epsilon_{241}=17.68 \text{ l mol}^{-1} \text{ cm}^{-1}$); Black: Calculated gas phase spectra; Red: Calculated PCM-ETOH spectra; vertical lines: transitions of the gas phase calculation. Calculated on UB3LYP/TZVP/52MWB level of theory.

Table 4.4: Summary of calculated and experimental absorption energies of **5-formyl-8-hydroxyquinoline**. Calculation on UB3LYP/TZVP level of theory, experimental spectra were recorded in ETOH ($c=1.47 \times 10^{-3} \text{ mol l}^{-1}$).

E_{exp} [nm]	E_{exp} [eV]	E_{calc} gas phase [eV]	f [a.u.]	E_{calc} ETOH [eV]	f [a.u.]	E_{calc} DCM [eV]	f [a.u.]
396	3.13	3.46	0.0004	3.61	0.0005	3.59	0.0005
330	3.75	3.95	0.1855	3.82	0.2502	3.83	0.2617
262	4.73	4.92	0.1258	4.75	0.2001	4.75	0.2041
241	5.14	5.29	0.3371	5.19	0.4400	5.18	0.4640

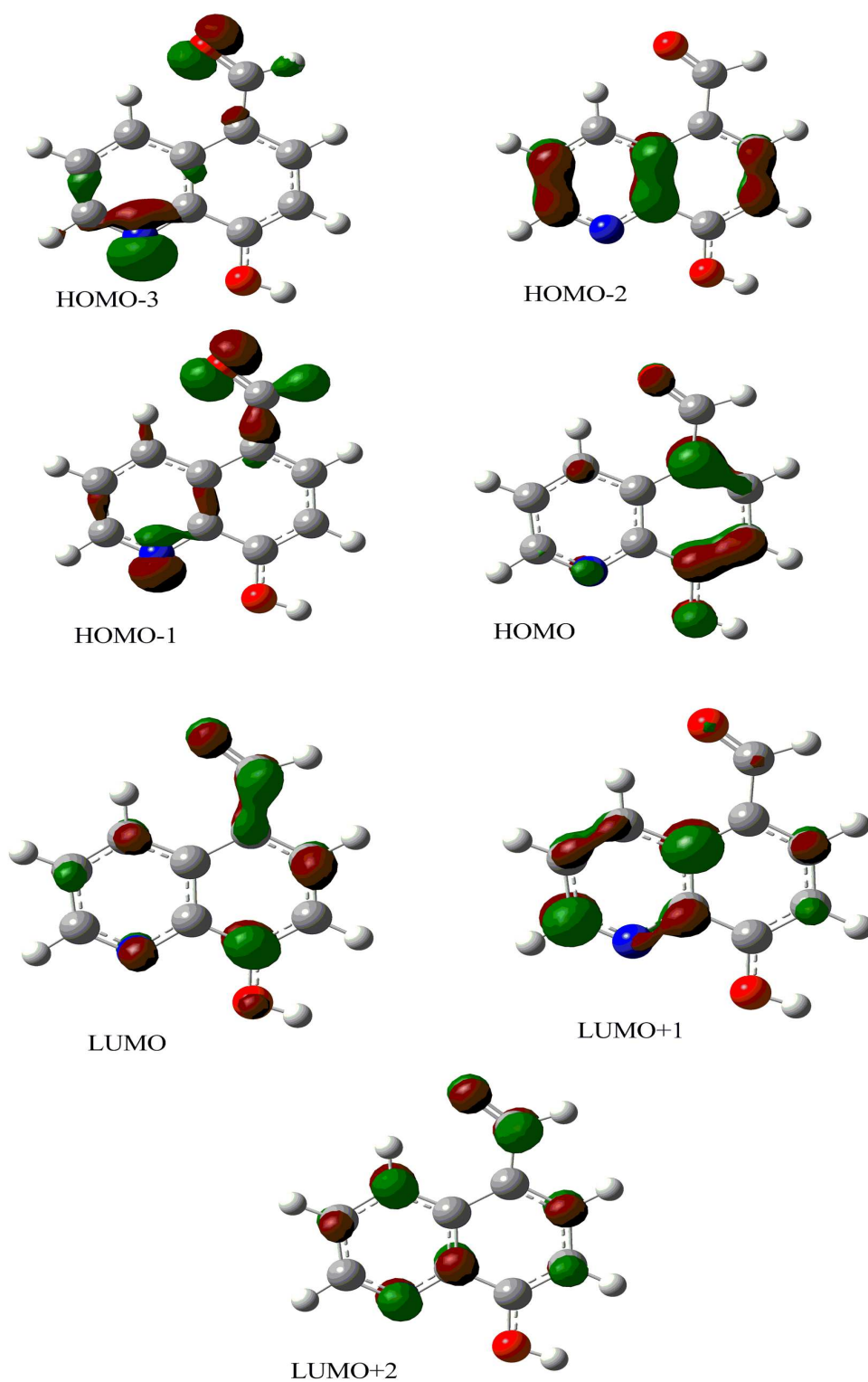


Figure 4.25: Molecular orbitals of the **5-formyl-8-hydroxyquinoline**. Calculated on UB3LYP/TZVP level of theory in gas phase.

Table 4.5: Main absorption energies, oscillator strengths, dominant contributions of the excitation and attributions of the **5-formyl-8-hydroxyquinoline** spectra. Experimental spectrum in ETOH ($c=1.47 \times 10^{-3} \text{ mol l}^{-1}$), calculated spectrum in gas phase (UB3LYP/TZVP).

E_{exp} [nm]	E_{exp} [eV]	ϵ [$\text{l mol}^{-1} \text{cm}^{-1}$]	Excitation	E_{calc} [eV]	f [a.u.]	Contribution	CI coefficient [a.u.]	Attribution
396	3.13	0.522	S_0-S_1	3.46	0.0004	HOMO-1 - LUMO	0.66368	$n-\pi^*$
						HOMO-1 - LUMO+2	0.10370	$n-\pi^*$
						HOMO-3 - LUMO	0.10370	$n-\pi^*$
330	3.75	5.84	S_0-S_2	3.95	0.1855	HOMO - LUMO	0.62122	$\pi-\pi^*$
						HOMO-2 - LUMO+1	-0.12721	$\pi-\pi^*$
						HOMO - LUMO+2	-0.10908	$\pi-\pi^*$
262	4.73	5.57	S_0-S_6	4.92	0.1258	HOMO - LUMO+2	0.51262	$\pi-\pi^*$
						HOMO - LUMO+1	-0.35688	$\pi-\pi^*$
						HOMO-4 - LUMO	-0.18259	$\pi-\pi^*$
						HOMO-2 - LUMO	0.14375	$\pi-\pi^*$
241	5.14	17.68	S_0-S_8	5.29	0.3371	HOMO - LUMO+1	0.36152	$\pi-\pi^*$
						HOMO-2 - LUMO	-0.31037	$\pi-\pi^*$
						HOMO - LUMO+2	0.29098	$\pi-\pi^*$
						HOMO-4 - LUMO	-0.24482	$\pi-\pi^*$
						HOMO-2 - LUMO+2	-0.16015	$\pi-\pi^*$
						HOMO-5 - LUMO	0.12223	$\pi-\pi^*$

4.3.3 5-nitro-8-hydroxyquinoline

Experimental spectra of 5-nitro-8-hydroxyquinoline were recorded in ETOH and DCM and are depicted in Figure 4.26. Comparing the spectra in the two solvents one can see that the peaks do not show a strong shift. Remarkable is that the peak at 2.83 eV (438 nm) in the ETOH spectra is absent in the DCM spectra. The relevant molecular orbitals are depicted in Figure 4.27 and the results are listed in Tables 4.7 and 4.6. The calculated spectra show the strongest band at 5.47 eV (227 nm, solvent calculation) and 5.68 eV (218 nm, gas phase calculation). Taking a close look on the involved orbitals shows that excitation goes mainly from the HOMO-2 to the LUMO+1 and from the HOMO to the LUMO+2 orbital. This transition is attributed to the S_0-S_{13} excitation in the gas phase calculation. In case of the solvent calculations a similar transition is the S_0-S_{11} transition at lower energy. Here excitation goes from the HOMO-1 to the LUMO+1 and again from the HOMO to the LUMO+2 orbital. The oscillator strengths for the

S_0-S_{11} (solvent calculation, $f=0.4872$ a.u. in ETOH and $f=0.4845$ a.u. in DCM) and S_0-S_{13} (gas phase calculation, $f=0.3864$ a.u.) are similar.

Interestingly the transitions are exchanged in the gas phase and solvent calculations. The solvent S_0-S_{11} transition involves the same orbitals as the S_0-S_{13} gas phase transition and goes from the HOMO-3 to the LUMO+1 orbital mainly. However, the oscillator strengths are much lower than in the above discussed transition, giving evidence, that the S_0-S_{13} gas phase transition equals in terms of involved orbitals the S_0-S_{11} solvent transition and gives the main contribution to the strongest peak in the absorption spectra. This difference in excited states between the solvent and gas phase calculation also explains the relatively strong shift of 0.20 eV between the corresponding peaks in the calculated gas phase and solvent spectra. The error of the solvent calculations to the experimental spectra is with 7% higher than in the before discussed spectra, but still acceptable.

The S_0-S_{13} transition in the gas phase consists mainly of an excitation from the center of the ring system to the pyridino part of the molecule and goes from the HOMO-2 to the LUMO+1 orbital. The second contribution is the HOMO - LUMO+2 excitation, where charge moves from the phenoxy ring to the ring carbon atoms. MO pictures are depicted in Figure 4.27.

Both excitations can be attributed to $\pi-\pi^*$ transitions. The S_0-S_{11} transition in the gas phase calculation is a transition from the π type orbitals located at the NO_2 oxygen to the pyridino part of the ring system (HOMO-3 - LUMO+1) and to the phenoxy ring of the quinoline (HOMO-3 to the LUMO) and shows a $\pi-\pi^*$ characteristic. The lower oscillator strength of $f=0.0030$ a.u. can be explained by the slightly rotated NO_2 group, which does not positively effect a charge transfer from the group in the ring system. The weaker band at 4.33 eV (286 nm) in the experimental spectra shows a solvent dependency. In the ETOH spectra it is shifted slightly towards higher energy (4.40 eV, 310 nm). In the convoluted spectra it is clearly visible in the gas phase (4.87 eV, 255 nm) and the PCM-ETOH spectra (4.79 eV, 259 nm) and can merely be guessed in the PCM-DCM spectrum. In general the bands are blue shifted in the calculated spectra compared to the experimental one and the oscillator strength is overestimated in the gas phase spectrum ($f=0.0923$ a.u.) and underestimated in the ETOH solvent calculation ($f=0.0559$ a.u.). One reason is that one of the main contributions in the solvent calculation comes from the HOMO-1 - LUMO+1 $n-\pi^*$ transition. This excitation is absent in the gas phase calculation, where the main contribution comes from a HOMO - LUMO+2 $\pi-\pi^*$ transition and smaller contributions from HOMO-2 - LUMO+1 and HOMO-2 - LUMO transition respectively. These three $\pi-\pi^*$ excitations make 85% of the transition in the gas phase calculation, while in the solvent calculation the $n-\pi^*$ excitation makes around 33% of the transition. The biggest contribution however comes from the HOMO - LUMO+2 excitation and makes 46% of the transition in the PCM-ETOH calculation. In the DCM spectrum this transition shows a slightly higher oscillator strength if compared with the ETOH calculation ($f=0.0679$ a.u. in DCM and $f=0.0559$ a.u. in ETOH). This let us assume that the $\pi-\pi^*$ transition has a higher contribution to the

transition in the DCM calculation, and truly, with roughly 50% it is more pronounced than in the ETOH calculation. However, the $n-\pi^*$ contribution from the HOMO-1 - LUMO+1 orbital makes 30% of the transition in the calculated DCM spectrum. Comparing the results of the two solvent calculations shows that the band is not shifted, as can be observed in the experimental spectrum. For the gas phase calculation the peak is shifted slightly to higher energy.

The peak lowest in energy in the experimental DCM spectrum lies at 3.49 eV (355 nm) and is almost not shifted to the corresponding peak in the ETOH spectrum, where it lies at 3.45 eV (359 nm). The convoluted solvent spectra show a quite good fit regarding the intensity and are shifted towards lower energy (3.41 eV, 364 nm, for DCM and 3.40 eV, 365 nm, for ETOH). The computed transition corresponds to the S_0-S_1 transition and is in both cases a pure HOMO - LUMO excitation with oscillator strengths of $f=0.3037$ a.u. for DCM and $f=0.3013$ a.u. for ETOH. The gas phase spectrum shows a peak shifted towards higher energy at 3.68 eV (337 nm). From the line spectra it can be seen that the single band in the gas phase spectrum can be split up in three transitions at 3.57 eV (S_0-S_1 , 347 nm, $f=0.0870$ a.u.), 3.69 eV (S_0-S_2 , 336 nm, $f=0.0533$ a.u.) and 3.77 eV (S_0-S_3 , 329 nm, $f=0.0801$ a.u.). Comparing the oscillator strength, the S_0-S_1 and S_0-S_3 transitions are the more dominant ones. The S_0-S_1 transition comes mainly from a HOMO-3 - LUMO, where the electron density migrates from the NO_2 group to the phenoxy ring system, and a noteworthy contribution from the HOMO - LUMO excitation. The S_0-S_2 transition shows components of excitations from the HOMO-3, the HOMO-1 and the HOMO orbitals to the LUMO orbital and shows due to participation of the n type HOMO-3 and HOMO-1 orbitals a lower oscillator strength. The S_0-S_3 transition is mainly an excitation from the HOMO-1 and the HOMO orbitals to the LUMO orbital. Comparing to the S_0-S_1 state, the oscillator strength is slightly decreased. One reason might be that the excitations coming from the n -type orbitals, go from the NO_2 group to the adjoining phenoxy ring in case of the S_0-S_1 transition, while in the S_0-S_3 transition the n -type orbital is located on the pyridino N atom.

The experimental spectrum recorded in ETOH shows the energetically lowest lying band at 2.83 eV (324 nm). This band is not present in the spectrum recorded in DCM and is not computed in any of the theoretically obtained spectra. Although the appearance of the band in ETOH remains unclear we assume a special effect on the quinoline structure caused by protic solvents, which can not be modelled with continuum solvation models. Possible is a weak interaction of the ETOH solvent with the heterocycle nitrogen. Calculation for the extreme case of a protonation on the heterocycle showed a tailing of the energetically lowest lying absorption band, coming from very weak $n-\pi^*$ transitions from lower lying HOMO orbitals to the LUMO and LUMO+1 orbital, respectively. However, a deeper investigation of structural and solvent effects lies beyond the scope of this work.

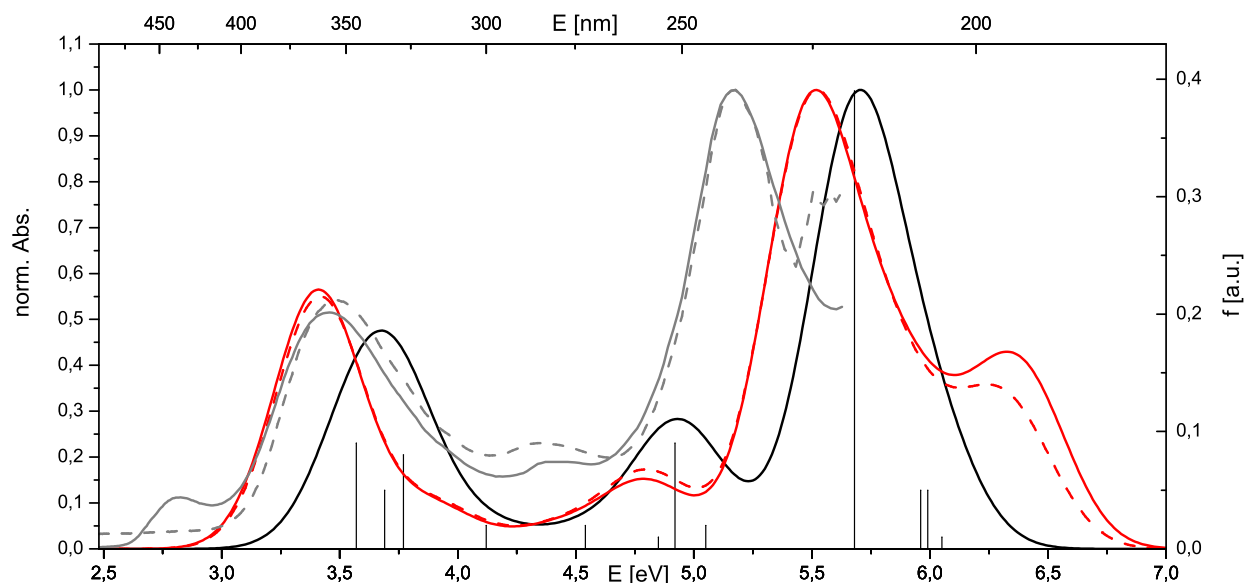


Figure 4.26: Experimental and calculated spectra of **5-nitro-8-hydroxyquinoline**. Grey: Experimental spectra in ETOH (solid line) and DCM (dashed line) with $c=1.3235 \times 10^{-3} \text{ mol l}^{-1}$, $\epsilon_{239}=15.41 \text{ l mol}^{-1} \text{ cm}^{-1}$ for ETOH and $\epsilon_{239}=14.20 \text{ l mol}^{-1} \text{ cm}^{-1}$ for DCM, normalised); Black: Calculated gas phase spectra; red: Calculated PCM-ETOH spectra (solid line) and calculated PCM-DCM spectra (dashed line); vertical lines: transitions of the gas phase calculation. Calculation on UB3LYP/TZVP level of theory.

Table 4.6: Summary of calculated and experimental absorption energies of **5-nitro-8-hydroxyquinoline**. Calculation on UB3LYP/TZVP level of theory. Experimental spectra were recorded in ETOH ($c=1.32 \times 10^{-3} \text{ mol l}^{-1}$).

E_{exp} [nm]	E_{exp} [eV]	E_{calc} gas phase [eV]	f [a.u.]	E_{calc} ETOH [eV]	f [a.u.]	E_{calc} DCM [eV]	f [a.u.]
436	2.84						
355	3.49	3.57	0.0870	3.41	0.3013	3.41	0.3037
280	4.43	4.92	0.0923	4.40	0.0232	4.41	0.0237
239	5.19	5.68	0.3864	5.48	0.4872	5.48	0.4845

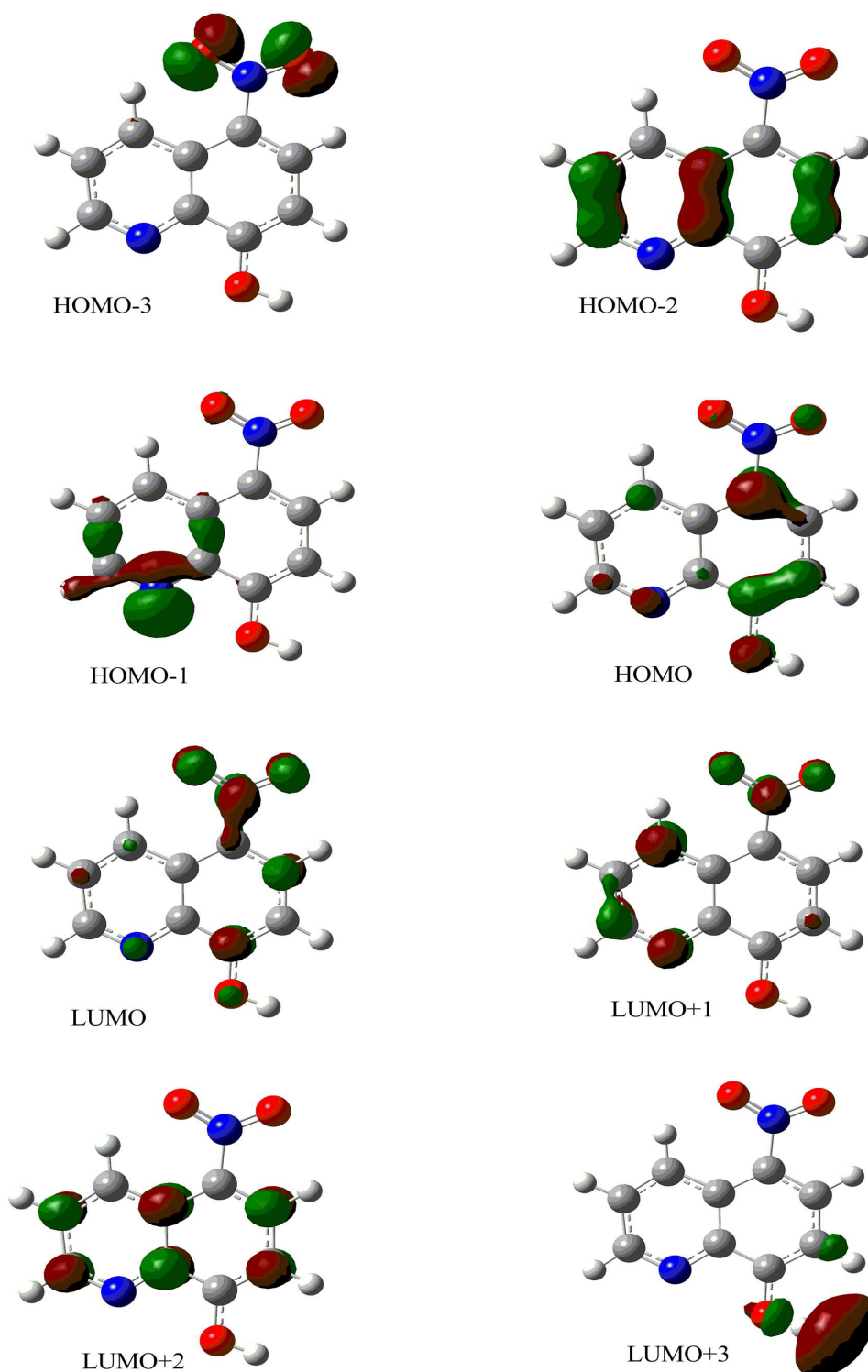


Figure 4.27: Molecular orbitals of the **5-nitro-8-hydroxyquinoline**. Calculated on UB3LYP/TZVP level of theory in gas phase.

Table 4.7: Main absorption energies, oscillator strengths, dominant contributions of the excitation and attributions of the **5-nitro-8-hydroxyquinoline** spectra. Experimental spectra in ETOH ($c=1.32 \times 10^{-3} \text{ mol l}^{-1}$), calculated spectra in gas phase (UB3LYP/TZVP).

E_{exp} [nm]	E_{exp} [eV]	ϵ [$\text{l mol}^{-1} \text{cm}^{-1}$]	Excitation	E_{calc} [eV]	f [a.u.]	Contribution	CI coefficient [a.u.]	Attribution			
436	2.84	0.96	-	-	-	-	-	-			
355	3.49	5.37	S_0-S_1	3.57	0.0870	HOMO-3 - LUMO	0.48373	$n-\pi^*$			
						HOMO - LUMO	0.42052	$\pi-\pi^*$			
						HOMO-3 - LUMO+1	0.14684	$n-\pi^*$			
			S_0-S_2	3.69	0.0533	HOMO-1 - LUMO	0.52074	$n-\pi^*$			
						HOMO - LUMO	0.31967	$n-\pi^*$			
						HOMO-3 - LUMO	-0.25635	$\pi-\pi^*$			
			S_0-S_3	3.77	0.0801	HOMO-1 - LUMO	0.42544	$n-\pi^*$			
						HOMO-3 - LUMO	0.35344	$\pi-\pi^*$			
						HOMO - LUMO	-0.34746	$\pi-\pi^*$			
						HOMO-3 - LUMO+1	0.10435	$\pi-\pi^*$			
			280	4.43	2.54	S_0-S_8	4.92	0.0923	HOMO - LUMO+2	0.46663	$\pi-\pi^*$
									HOMO-2 - LUMO+1	-0.39842	$\pi-\pi^*$
HOMO-2 - LUMO	-0.22763	$\pi-\pi^*$									
HOMO-1 - LUMO+1	0.11867	$n-\pi^*$									
HOMO-5 - LUMO	0.11492	$n-\pi^*$									
239	5.19	15.53	S_0-S_{13}	5.68	0.3864	HOMO-2 - LUMO+1	0.43310	$\pi-\pi^*$			
						HOMO - LUMO+2	0.26445	$\pi-\pi^*$			
						HOMO-4 - LUMO+2	-0.18892	$\pi-\pi^*$			
						HOMO-3 - LUMO+2	0.17561	$\pi-\pi^*$			
						HOMO-4 - LUMO	-0.13816	$\pi-\pi^*$			
						HOMO-7 - LUMO	-0.13600	$\pi-\pi^*$			
						HOMO-6 - LUMO+2	-0.11446	$n-\pi^*$			
						HOMO-5 - LUMO	-0.10581	$n-\pi^*$			
						HOMO-4 - LUMO+1	0.10246	$\pi-\pi^*$			
HOMO-2 - LUMO+4	0.10166	$\pi-\pi^*$									

4.3.4 Other ligand systems

Absorption spectra have been calculated for all 50 ligand systems in gas phase and with the PCM model in ETOH and DCM. An exact analysis of the transitions and molecular orbitals would go far beyond the scope of this work. Instead in Figure 4.28 the energies of the S_0 - S_1 transitions are depicted and a deeper analysis of the excitation will be presented for selected ligands only. The exact values can be found in Tables A.15 - A.26 on Pages LVI - LVI in the Appendix.

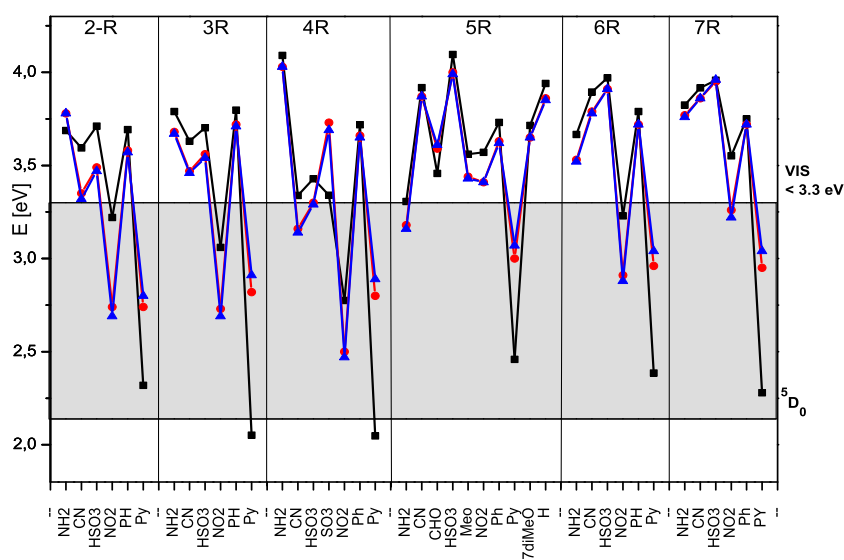


Figure 4.28: Calculated S_0 - S_1 energies of the ligands in gas phase (black) and with PCM-DCM (red) and PCM-ETOH (blue). Energies are grouped according to their substitution position on the quinoline backbone. The highlighted area in the diagram marks the area from begin of the visible spectral region at 3.30 eV and the energy of the 5D_0 state of the Eu^{3+} ion.

The by far most important contribution to the S_0 - S_1 transition for the ligands is the HOMO - LUMO excitation. An exception are the ligands with NO_2 and CHO substituent since they show n - π^* transitions from lower lying n -type orbitals in the S_0 - S_1 transition. However, investigation of the frontier orbitals of different donor and acceptor substituted derivatives gives an idea about the substitution effect on the absorption characteristics.

Starting with the NH_2 derivative, the HOMO orbital shows electron density mainly in the phenoxy ring of the system and around the substitution group. In cases where the substitution takes place on the pyridino ring, the orbitals expand on the side of the pyridino ring where the substitution took place. The opposed side of the ring does not show any electron density. Excitation goes from the phenoxy ring and from the NH_2 group to the pyridino ring. In the LUMO orbital almost no electron density can be found in the phenoxy ring and in none of the substitution positions electron density can be found on the NH_2 group. Exception is the derivative with substitution in 6- and 7-position. Here the NH_2 group does neither par-

ticipate in the HOMO nor in the LUMO orbital. The electron density is distributed over the ring carbons only and redistributes to π^* LUMO orbitals which are strictly located on the ring carbons. One reason why in 6- and 7-position the NH_2 group is not involved might be the higher degree of hybridisation. If the NH_2 group shows a smaller wagging angle, as can be found in substitution in 2-, 3-, 4- and 5-positions, the N-p orbitals are closer to a sp^2 hybridisation, giving the p_z orbital a better possibility to overlap with the ring system. An increased wagging angle means a more sp^3 like hybridisation and therefore the hybrid orbitals are not perpendicular to the molecular plane anymore, making it more difficult to pull from - or insert charge in the ring system. If substituted in 4-position, the HOMO orbital expands over the whole molecule. The S_0 - S_1 energy shows the highest value and also the oscillator strength is with 0.1178 a.u. much higher than in the other substitution positions where it is uniformly around 0.004 a.u.

The **Ph** substituent is of high interest as well, since it introduces an additional chromophoric group in the molecule. The S_0 - S_1 energies are similar with the NH_2 substituent and clearly higher than the strong electron withdrawing groups NO_2 and Py. The transition is only composed of one excitation from the HOMO to the LUMO orbital. If substituted in 2-position HOMO-1 - LUMO and in 5-position a HOMO - LUMO+2 excitation occurs as well. As seen before for the NH_2 group, the excitation goes from the phenoxy to the pyridino part of the molecule. If substituted on the pyridino ring of the quinoline backbone, the phenyl ring is not involved in the HOMO and LUMO orbitals. But the position of substitution effects the distribution of the density in the ring. An interesting exception in this series is the 5-phenyl-8-hydroxyquinoline, where the HOMO - LUMO excitation goes from the pyridino part to the phenoxy part and the phenyl system. Oscillator strengths are not as uniform as in the case of the NH_2 substituted quinoline and differ from $f=0.11$ a.u. (2-, 4- and 5-position) and $f=0.07$ a.u. (6-position) to $f=0.04$ a.u. (3- and 7-position).

For the **CN** substituent a similar pattern can be found. The most important excitation is the HOMO - LUMO transition and excitation goes from the phenoxy ring to the pyridino ring. The CN group does not participate in the HOMO orbital, but shows some contribution in the LUMO orbital, most distinct if substituted in 4-position. In 5-position the effect reverses and electron density on the CN group is present in the HOMO orbital. In this substitution position the oscillator strength is also the highest for this series with $f=0.1176$ a.u.

The **NO_2** group shows a high electron density in the LUMO orbital and almost none in the HOMO orbital if substituted on the pyridino ring. From substitution 5-position and higher on, NO_2 is involved in both, the HOMO and LUMO orbitals. Excitation goes again from the phenoxy ring to the pyridino ring.

Oscillator strengths are slightly increased if substituted in 5-position or higher.

A very promising substituent is the **Py** group, since all derivatives show absorption in the visible range of the spectra. HOMO - LUMO excitation takes part from the phenoxy ring system to the pyridino ring mainly. If substituted in 5-position or higher also the pyridino ring of the quinoline has some electron density in the HOMO orbital, in lower substitution positions the electron density is only located in the phenoxy ring and goes to the attached pyridino ring during the excitation. The pyridino derivatives are the only ligands which strictly show only HOMO - LUMO excitation for the S_0 - S_1 transition. No other orbitals are involved here.

The high deviation of the absorption energy between gas phase and solvent calculations show clearly that the PCM model has a certain problem to handle charged molecules.

In Figure 4.29 the orbital energies of the HOMO and LUMO orbitals are depicted for the 5-substituted hydroxyquinoline. The most right substituent is H and represents the unsubstituted 8-hydroxyquinoline. It can clearly be seen that introducing electron withdrawing groups (NO_2 , Py, CHO, CN) lowers the energy of the HOMO and LUMO orbital depending on the electron pulling ability, while electron donating groups (NH_2 , MeO, Ph) do not change the energy of the frontier orbitals significantly compared to the unsubstituted 8-hydroxyquinoline. If electron pulling groups are introduced in the quinoline backbone the HOMO - LUMO gap is smaller and the S_0 - S_1 transition can be shifted in the visible range of the spectra.

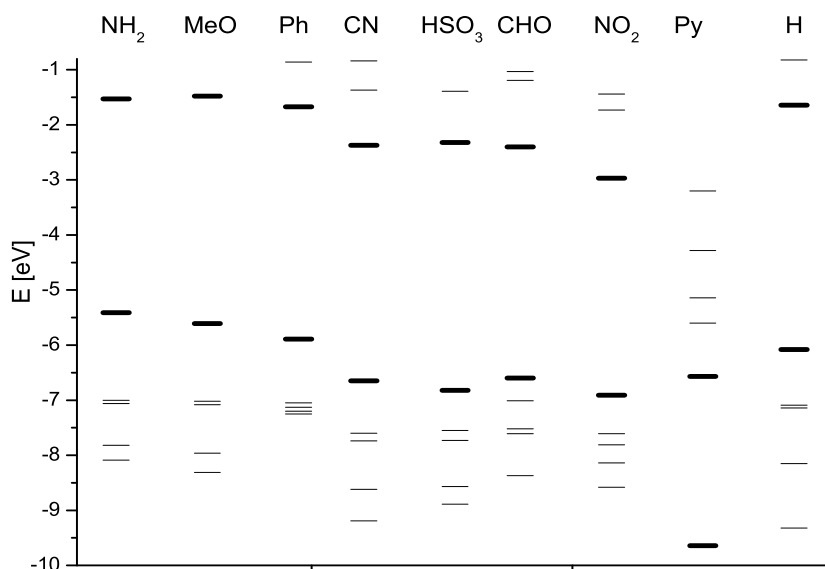


Figure 4.29: Orbital energies of the HOMO and LUMO orbitals for different substituents. Calculated for the 5-substituted 8-hydroxyquinoline.

More complicated to answer is the question of the best substitution position, since steric effects can

influence electronic interaction between substituent and backbone structure. Furthermore, in this work a too small number of ligand structures was calculated to make a clear statement. From the present data a trend can be estimated which does not claim to be an exact description of the position effect. In Figure 4.30 (a) the HOMO - LUMO splitting of the pyridino substituted 8-hydroxyquinoline is depicted. The HOMO - LUMO gap of the less strong NO_2 acceptor substituent can be seen in Figure 4.30 (b).

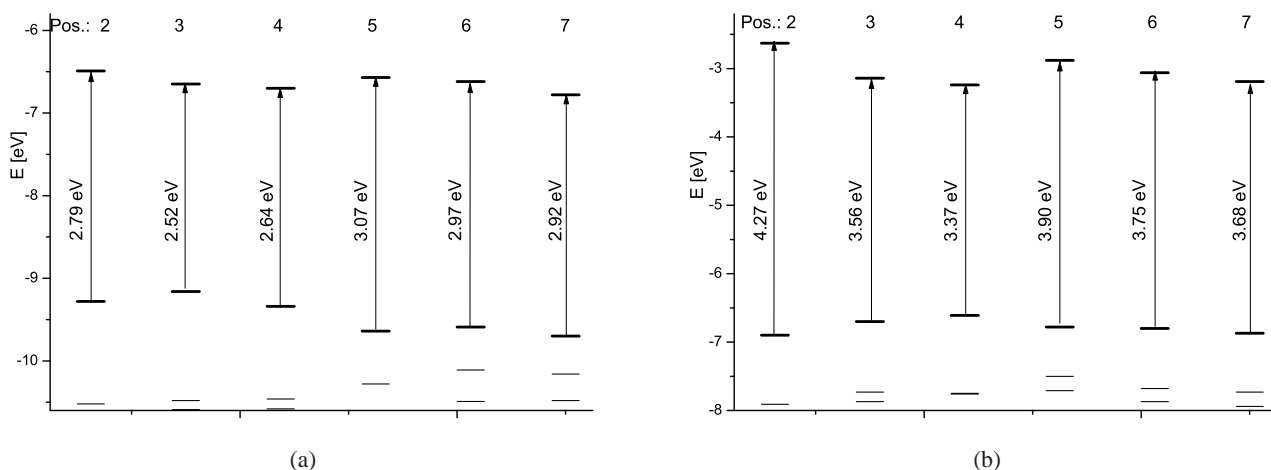


Figure 4.30: HOMO - LUMO splitting for the pyridino (a) and nitro (b) substituted ligand system. Substitution position is marked on the top.

Very generally, acceptor substitution in 3- and 4-position lowers the HOMO - LUMO gap and shifts the excitation energy more to the visible range of the spectra. In both cases the LUMO orbital is shifted downwards if substitution takes place in 4-position. The HOMO orbital has lower energies in 5-,6- and 7-position. At the same time the LUMO orbital in this position shifts to higher energy and increases the HOMO - LUMO gap. For the analysis of the donor influence the NH_2 and Ph substituted systems were compared. Figure 4.31 depicts the orbital energies for the NH_2 (a) and the Ph substituent (b).

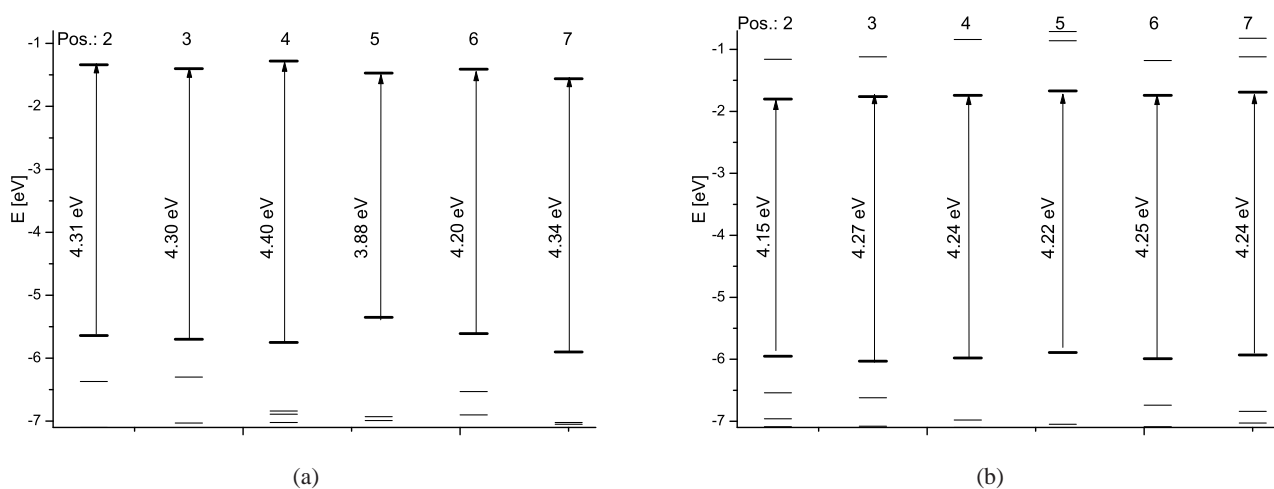


Figure 4.31: HOMO - LUMO splitting for the amino (a) and phenyl (b) substituted ligand system. Substitution position is marked on the top.

Here the difference regarding the substitution position is less clear visible. In case of the NH_2 the HOMO orbital is slightly lowered in 4- and 7-position while the LUMO orbital energy is increased. In case of the Ph substituent the orbital energies stay almost uniformly and do not differ significantly.

In case of the weak acceptor HSO_3 (see Figure 4.32 (a)) the HOMO - LUMO gap is increased if substitution takes place in 5-,6- or 7-position. Here the HOMO orbital is lowered in terms of energy while at the same time the LUMO orbital is lifted. The lowest HOMO - LUMO gap can be seen for substitution 4-position, where the LUMO is energetically lower and the HOMO orbital has a higher energy. The CN substituted derivative (Figure 4.32 (b)) has the lowest HOMO - LUMO energy in substitution position 4. As seen before for the acceptor derivatives, the LUMO orbital is shifted towards lower energy in 4-position while the HOMO orbital shows an increased energy. In 5-, 6- and 7-position the LUMO orbital is shifted towards higher energy, a trend which was seen before for the NO_2 and Py ligands.

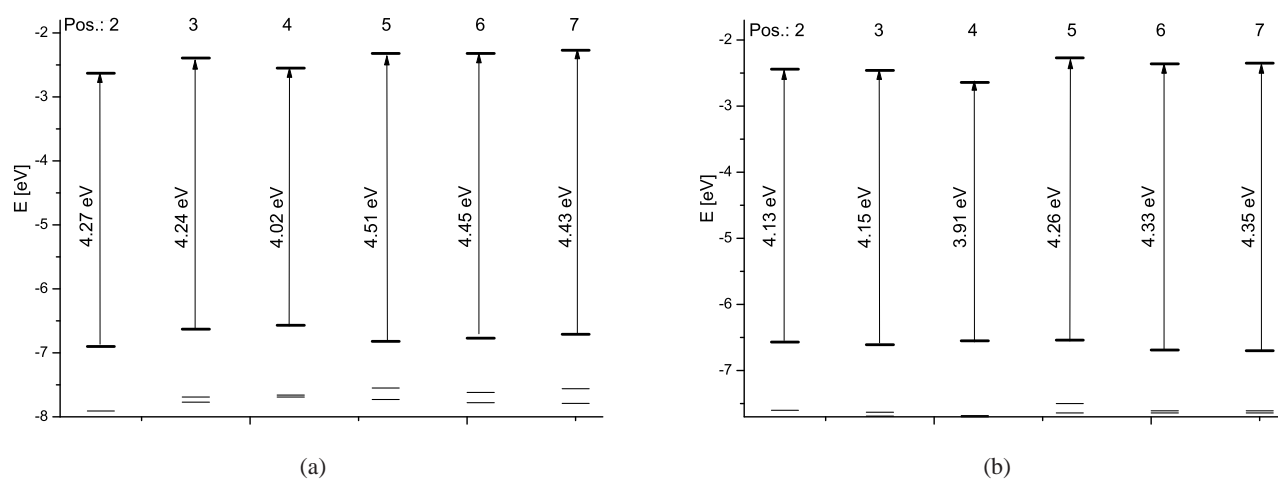


Figure 4.32: HOMO - LUMO splitting for the sulfonic acid (a) and cyano (b) substituted ligand system. Substitution position is marked on the top.

4.4 Jablonski Diagram for Ligand Structures

Important for an effective energy transfer in the complex system is the position of the triplet state of the ligands which should lie slightly above the 5D_0 state of the Eu(III) ion. Ligands which have a triplet state below this level can not transfer energy to the Eu(III) ion. If the triplet state lies too high, an effective transfer is not possible. In the best case the triplet state should lie a few hundred wavenumbers above the 5D_0 state to avoid a back reaction and formation of the antenna triplet state again [11]. The two main points of interest are the singlet-triplet splitting in the different ligand systems and the optimal way how to compute these energies. To prevent confusion, the different states will be labeled with the symbol S or T referring to the multiplicity singlet and triplet, followed by the description of the state (0 for ground state, 1 for the first excited state etc.) and a label referring to the underlying geometry. Excitation calculations based on the singlet state geometry gives also triplet state energies which are referred to as vertical triplet state (T_{1S^*}). Optimising the triplet geometry gives a triplet state (T_{1T}) which lies energetically below the T_{1S^*} state. The energy difference between T_{1T} and S_{0S} is referred to as adiabatic triplet state energy. Another way to calculate the triplet state is taking the optimised singlet geometry and use a triplet wavefunction to compute the energy in a single point calculation. This triplet energy is also a vertical energy and refers to the T_{1S} state. The difference to the first vertical triplet state (T_{1S^*}) is that for the calculation a triplet wavefunction is used, based on a singlet geometry. That means, the orbital coefficients are optimised with a triplet wavefunction, which is not the case when computing the T_{1S^*} state. In Figure 4.33 the Jablonski diagram of the 5-amino-8-hydroxyquinoline is depicted to demonstrate the different states.

The triplet states were calculated for all ligand systems in gas phase, and in DCM and ETOH with the PCM solvent model. Results are presented in Figure 4.34 - 4.36 and in Tables A.15 - A.26 in the Appendix on pages LVI - LVI.

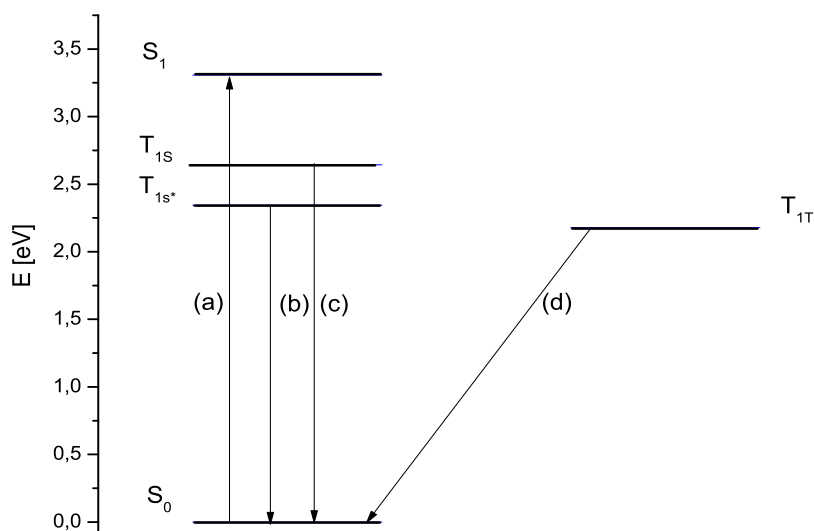


Figure 4.33: Jablonski diagram of 5-amino-8-hydroxyquinoline: (a) Absorption from S_0 to S_1 , (b) vertical phosphorescence from T_{1S^*} to the singlet ground state, (c) vertical phosphorescence from T_{1S} to the S_0 , (d) adiabatic transition from T_{1T} to the S_0 state.

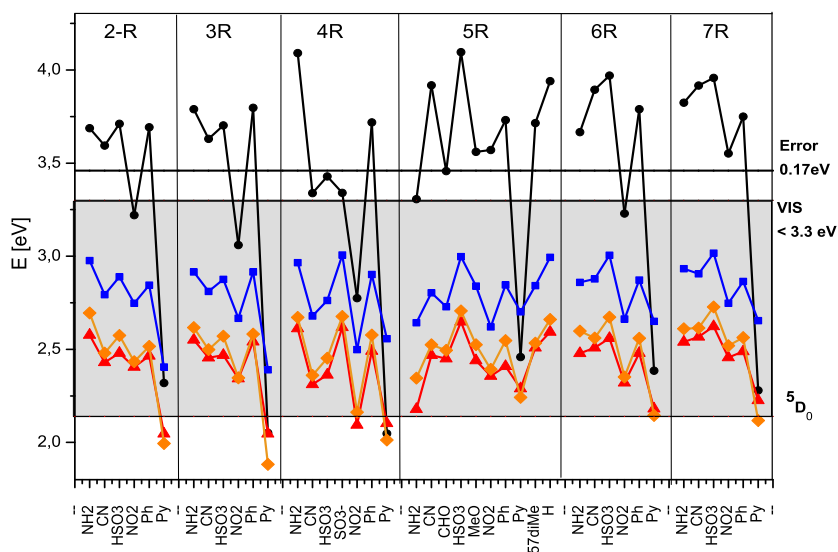


Figure 4.34: Absorption and triplet state energies of the ligand systems in **gas phase**. Black: Absorption energies; blue: Vertical phosphorescence from T_{1S} to S_0 ; orange: Vertical phosphorescence from T_{1S^*} to S_0 , red: Adiabatic transition from T_{1T} to S_0 ; The error of 5% is marked as line.

In the gas phase calculation the electron withdrawing NO_2 and Py group show a good absorption characteristic. The absorption energy of the pyridino substituted ligand lies in the visible spectrum in all substitution positions. The NO_2 group shows the same characteristic except if substituted in 5- or 6-position. Considering the expected error of approximately 5% to higher energy also other ligand systems such as CN, CHO or HSO_3 substituted ligands show absorption in the visible range.

A good choice is also the 5-amino-8-hydroxyquinoline. As a strong donor, the triplet level lies at higher energy. In 5-position however, both T and S_1 states are lowered, making it on the one side possible to excite in the visible range while the triplet state stays above the 5D_0 level of the Eu(III) ion. The most promising candidate however is the pyridino substituent. The T_{1S^*} triplet state, which is based on a singlet geometry comes quite close to the energies which are build on the optimised triplet geometry. The second, less time expensive possibility, to take the T_{1S} state which is based on the S_0 geometry and uses the triplet wavefunction for the single point calculation computes the energies too high.

In the solvent calculations the absorption energies are shifted towards lower wavelength compared to the gas phase calculation. Charged molecules like the Py derivatives or the 4- SO_3^- ligand show higher absorption energies. However, it is known that the PCM solvent model shows some problems to deal with ions. This trend is more distinct in the ETOH calculations. Triplet states are also shifted to lower energies in ETOH. This trend is more pronounced for the electron accepting groups than for the donors. Regarding the triplet states the same trend as before can be seen. The adiabatic triplet energies are lowest in energy. Triplet energies gained from singlet excitation are close to the T_{1T} energies and the triplet energies based on singlet geometry are shifted to higher energy.

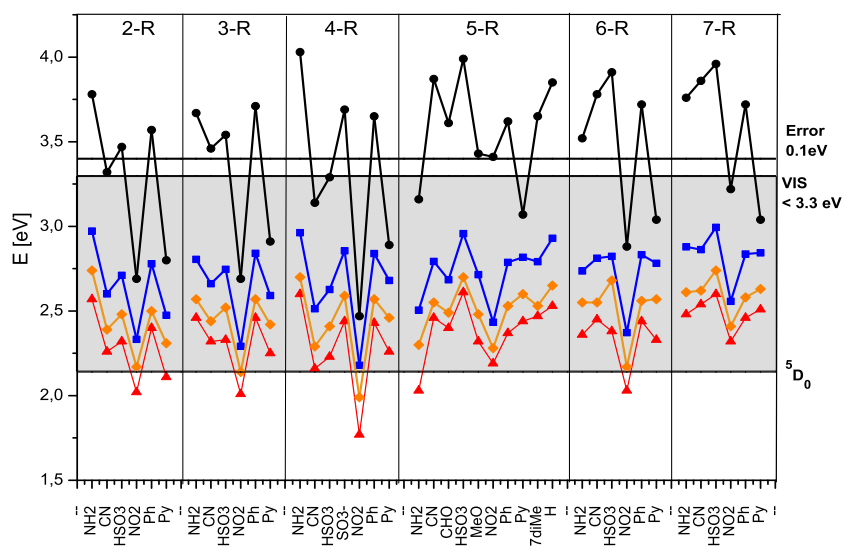


Figure 4.35: Absorption and triplet state energies of the ligand systems in ETOH. Black: Absorption energies; blue: Vertical phosphorescence from T_{1S} to S_0 ; orange: Vertical phosphorescence from T_{1S^*} to S_0 , red: Adiabatic transition from T_{1T} to S_0 . The error of 0.1eV is marked as line.

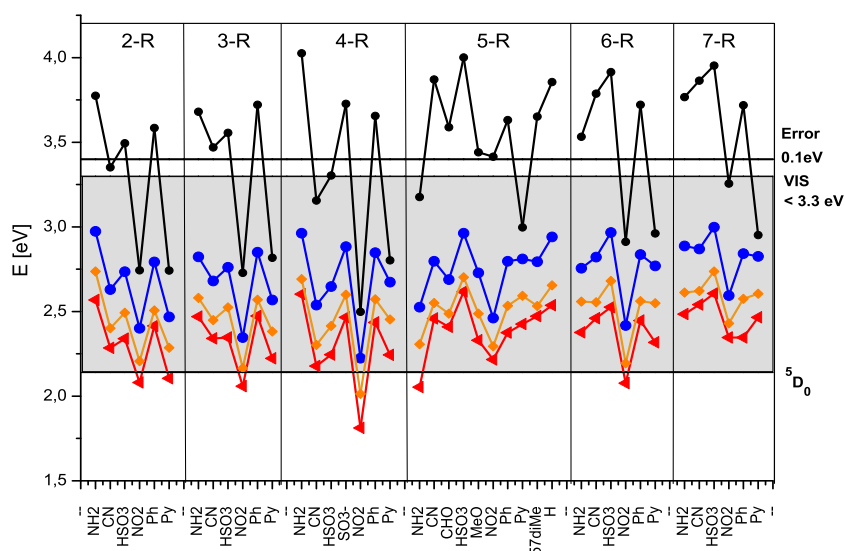


Figure 4.36: Absorption and triplet state energies of the ligand systems in **DCM**. Black: Absorption energies; blue: Vertical phosphorescence from T_{1S} to S_0 ; orange: Vertical phosphorescence from T_{1S^*} to S_0 , red: Adiabatic transition from T_{1T} to S_0 . The error of 0.1 eV is marked as line.

Figure 4.37 gives an overview over the singlet and triplet- α and β orbitals of the ligand system with different substituents in 5-position of the 8-hydroxyquinoline backbone. It is clearly visible that for the donor systems (NH_2 , Me, Ph) the HOMO orbital is higher in energy if compared to the unsubstituted 8-hydroxyquinoline. At the same time the energy of the LUMO orbital stays unaltered compared to the unsubstituted species. This decreases the HOMO-LUMO gap for strong donor systems. The energy of the SOMO orbital for donor substituted complexes is increased.

For acceptor substituents the LUMO orbital is lower in energy, corresponding to the acceptor ability. The energy of the HOMO orbital decreases as well, however the effect on the LUMO orbital is more distinct. Same applies for the SOMO orbital in the acceptor substituted ligand systems.

An exception is the MeO substituted ligand, where the HOMO orbital lies energetically too low. Still MeO is attributed as donor, which can also be seen by means of the relatively high lying SOMO orbital (see Figure 4.37).

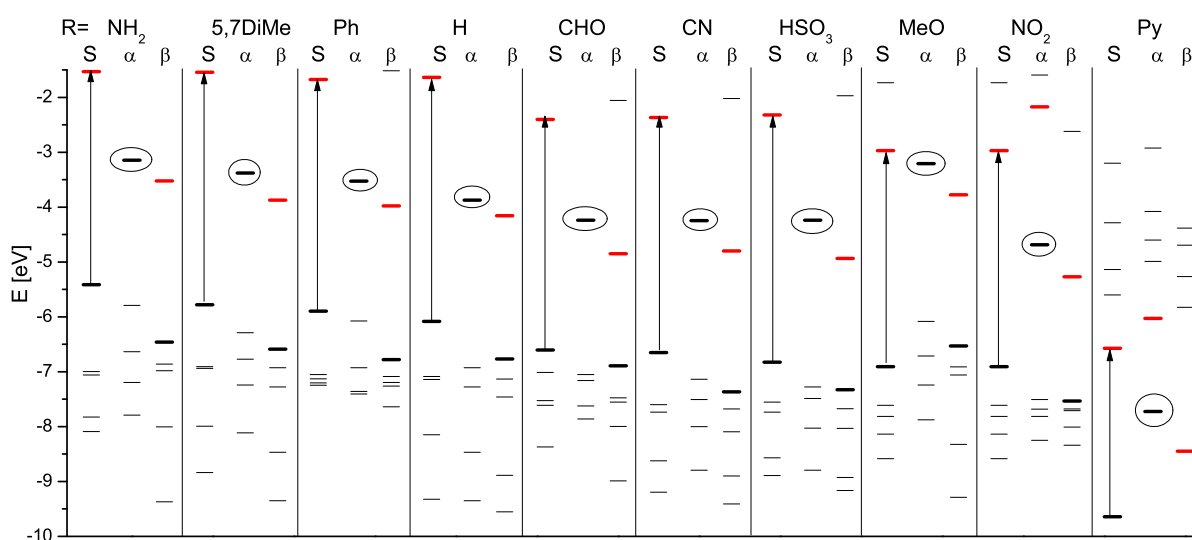


Figure 4.37: HOMO (black), LUMO (red) and SOMO (circled) orbitals of the 5 substituted 8-hydroxyquinoline. Calculation in gas phase on UB3LYP/TZVP level of theory.

4.5 Calculation on Complex Systems

The homoleptic quinolinolate complex AlQ_3 was one of the first complexes reported to show emission after excitation of the ligand system [46]. The underlying principle is an excitation of the ligand system which serve as sensitiser and subsequent ISC to its triplet state. Energy is transferred for the triplet state of the ligand system to the emitting state of the metal ion. This principle of excitation and energy transfer is called *Antenna Effect* in literature [47] and it overcomes the problem of low intensity f-f transitions which are laporte forbidden. The ligand system serves as "antenna", can be excited easily and transfers the energy to the metal ion. The process of the antenna effect is depicted in Figure 4.38.

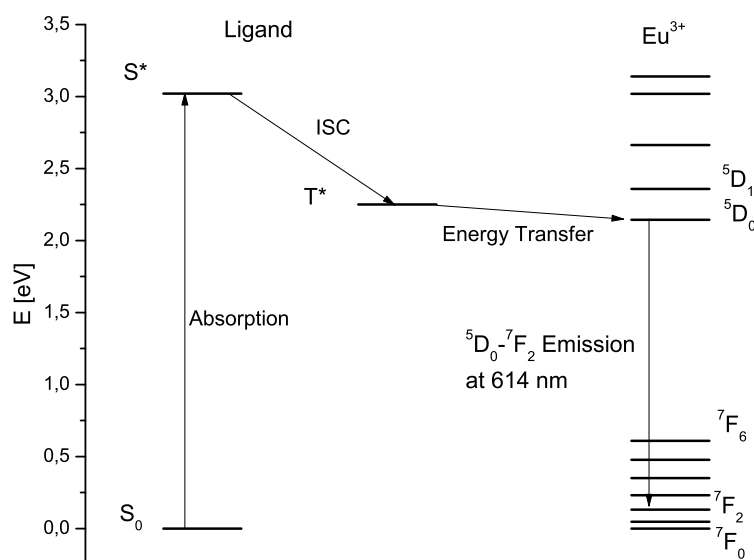


Figure 4.38: Scheme of the "Antenna Effect".

In case of the Eu(III) ion both, the $^5\text{D}_0$ and the $^5\text{D}_1$ state are reported as resonance levels [48]. In best case the triplet state of the ligand should lie above the $^5\text{D}_0$ but below the $^5\text{D}_1$ state to achieve a pure emission line. Emission goes from the resonance level to the $^7\text{F}_J$ ($J=0-4$) levels, however, the transition form $^5\text{D}_0$ to the $^7\text{F}_2$ state shows the highest intensity and lies at 614 nm (2.02 eV).

Important for a good energy transfer is a triplet state energy of the ligand system which lies close above the resonance level of the metal ion. The energy transfer which forms the excited lanthanide state is a reversible reaction. The backreaction from the metal to the ligand occurs when the ligand triplet state is too close to the resonance level and diminishes the quantum yield.

In case of the Eu(III) ion, the energy of the $^5\text{D}_0$ state can change according to the chemical nature of the ligand system [49]. However, since the 4f electrons are shielded by fully occupied 5s and 5p orbitals, the effect is rather small.

4.5.1 Singlet and Triplet State Geometry of the Complexes

In the complex structure, three bidentate quinoline ligands are coordinated in a distorted octahedral geometry to the central Eu(III) ion. Three isomers can be distinguished as shown in Figures 4.39. In the first structure the ligands are coordinated in a symmetric like fashion, showing a distorted octahedral structure bearing almost a C_3 symmetry. If one of the ligands is flipped (oxygen and nitrogen coordination points exchange their positions) the second isomer is obtained. Twisting another ligand gives a chiral of isomer 2.

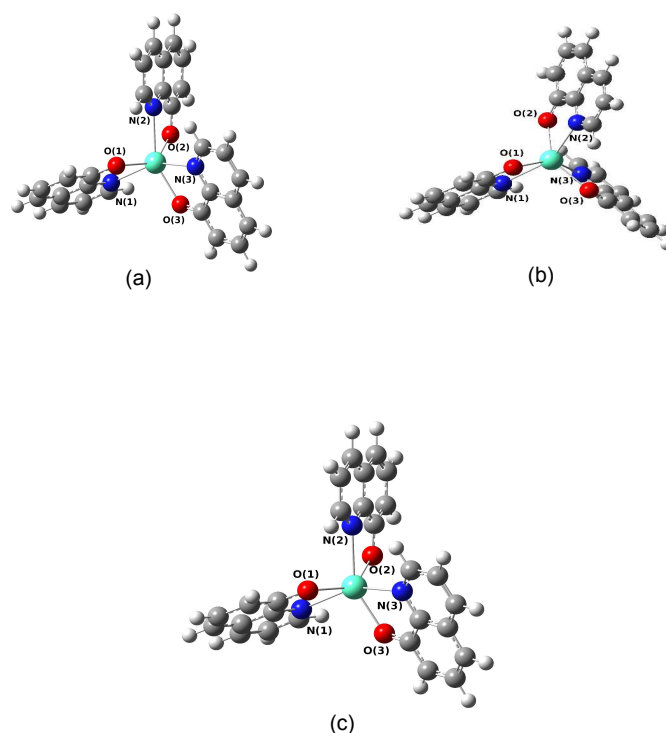


Figure 4.39: Complex structure of the three isomers: (a) isomer 1; (b) isomer 2; (c) isomer 3

The octahedral geometry was chosen because of previously reported sixfold coordinated Eu complexes. Eu is existent in its Eu(III) ionic form and coordination of 3 quinolinate ligands gives a neutral species. However, the Eu halides show often a 9 fold coordination. For the gas phase and IEF-PCM calculation the octahedral geometry was taken. In the explicit solvent models a coordination of the solvent molecules can be observed giving also nine fold coordinated complexes, such as in the case of the $\text{Eu}(\text{NO}_2)_3(\text{EtOH})_3$ complex (see Figure 4.42 on page 85). The relative energies for gas phase, PCM-solvent model and explicit solvent model are displayed in Table 4.8 and are referred to the most stable isomer. Substitution in the ligand system is always in 5-position of the quinolinate backbone. To give a detailed description

of different bonds and angles in the complex structure, the ligands are numbered as depicted in Figures 4.40 and 4.41.

Table 4.8: Relative energies of the calculated complexes and its isomers in gas phase and in solvent. Energies in kcal/mol

Complex	Gas phase	PCM/DCM	PCM/ETOH	Expl. DCM	Expl. ETOH
isomer 1	1.849	0.000	0.000	0.003	0.000
isomer 2	0.000	0.001	0.001	0.000	0.004
isomer 3	$< 10^{-4}$	0.001	0.001	-	-
isomer 1 NH ₂	1.750	0.000	0.000	0.009	0.000
isomer 2 NH ₂	0.000	0.001	0.001	0.000	0.000
isomer 3 NH ₂	0.000	0.001	0.001	-	-
isomer 1 NO ₂	2.500	0.000	0.000	0.000	0.000
isomer 2 NO ₂	0.000	$< 10^{-4}$	$< 10^{-4}$	0.001	0.070
isomer 3 NO ₂	0.000	$< 10^{-4}$	$< 10^{-4}$	-	-
isomer 1 HSO ₃	2.822	0.000	0.000	-	-
isomer 2 HSO ₃	0.324	$< 10^{-4}$	$< 10^{-4}$	-	-
isomer 3 HSO ₃	0.000	0.001	0.002	-	-

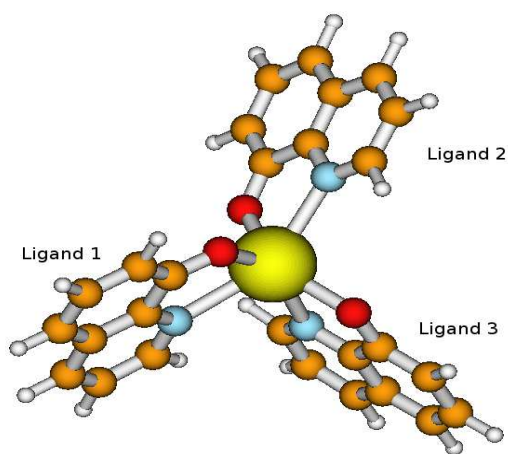


Figure 4.40: Structure of isomer 2 of the unsubstituted Eu(Q)₃ complex. Calculated on UB3LYP/6-31G* level of theory.

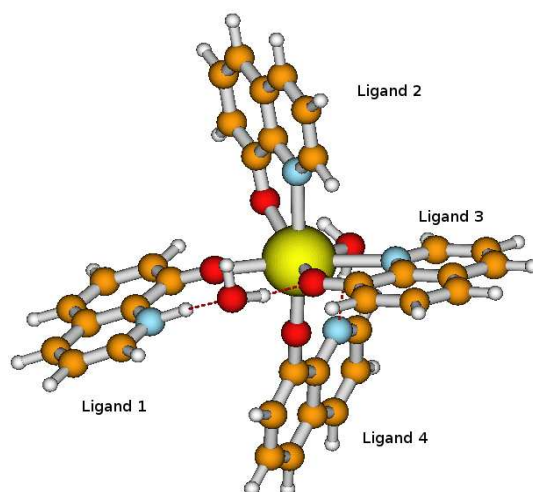


Figure 4.41: Structure of the unsubstituted $\text{Eu}(\text{Q})_4(\text{H}_2\text{O})_2$ complex. Calculated on UB3LYP/6-31G* level of theory.

4.5.2 Difference in the geometry of the isomers

The data for the following section are displayed in the Appendix on pages [LVI](#) and [LVI](#) (Tables [A.27](#) and [A.28](#)).

From the energetic characteristics of the isomers we can expect a similar structure for isomer 2 and isomer 3. Regarding the **Eu-N bond** length, isomer 1 exhibits a longer bond length with 2.636 Å. In isomers 2 and 3 the Eu-N bond is shrunk and two of the bonds display a similar value with 2.613 Å and 2.617 Å, while the third bond with 2.579 Å is smaller. The Eu-O bond is smaller in isomer 1 (2.251 Å) compared to the other two isomers (2.265 Å for two of the bonds and one showing 2.274 Å).

The **axial angles** are compressed and differ from the ideal octahedral geometry in all isomers. In isomer 1 the axial angles are uniformly 149.9° while in isomer 2 and 3 one axial angle is with 137.3° smaller than in isomer 1, one angle is almost the same (149.3°) and one is expanded (152.3°). Here again the difference in the values for isomer 2 and 3 is marginal.

The **equatorial angles** are uniform for isomer 1 and show with 66.9° a bigger deviation from the 90° angles in an ideal octahedron. The difference in the angles comparing isomers 1 and 2 is negligible. Only one angle in these structures seems to be slightly expanded with 67.5°. The above given values correspond to the unsubstituted 8-hydroxyquinoline europium complexes, however also the substituted complex structures follow this trend. Isomer 1 of the unsubstituted species shows for each of the three equivalent bond lengths and angles exactly the same value. The substituted version of the complexes exhibit some steric effect. Also the degree of divergence between the isomers is dependent on the sub-

stitution. Expansion of the axial angle in isomer 2 and 3 is less distinct, if NO₂ or HSO₃ is present as a substituent.

4.5.3 Effect of the substituents

Data for this section are displayed in the Appendix on pages LVI in Table A.27. Considering the electron pushing or withdrawing ability of the substituents one can observe an elongation of the **Eu-N** bond length induced by electron pushing groups (NH₂ or HSO₃). The effect is bigger for the HSO₃ substituent. The NO₂ group in 5-position contracts the bond.

Referring to the **axial angles** the electron withdrawing groups tend to widen the angle. However, the effect is more pronounced for the HSO₃ group, which shows a wider angle than the NH₂ substituent although it possesses a more distinct electron donating ability. In this case steric effects might play a role. The HSO₃ is sterical much more demanding than the NH₂ group.

The **equatorial angles** decrease in the following order: NH₂ > HSO₃ > NO₂. Here steric effects might have a bigger influence than electronic effects.

4.5.4 Singlet and triplet geometries

Data for this section are displayed in the Appendix on page LVI - LVI in Tables A.27 - A.28. Comparing the singlet and triplet geometry of the complexes a compression of the **Eu-N** and **Eu-O bond** lengths occurs in the triplet state for isomer 1. Referring to isomer 2 and 3 no conclusion can be done. Two of the axial angles are compressed in the triplet state, however, one is expanded, compared to the singlet ground state geometry. The same is valid for the **equatorial angle**. Triplet state geometry optimisation with solvent molecules showed that the distance between solute and solvent remains the same.

4.5.5 Solvent effects

Data are displayed in the Appendix on pages LVI - LVI (Tables A.31) and A.30. Optimisation was done by putting 3 explicit solvent molecules, either dichloromethane (DCM) or ethanol (ETOH) in the first coordination sphere of the complex structure. Here changes in the structure, mainly due to incorporation of the solvent molecule to the coordination shell of the Eu(III) ion, are very pronounced. Isomer 2 of the NO₂ substituted complex shows a 9-fold coordination when putting explicitly 3 ETOH molecules around the complex. This is an interesting observation since it is known that Eu(III) forms 9-fold complexes with halides. The structure of the ninfold coordinated EU(NO₂Q)₃(ETOH)₃ complex is depicted in Figure 4.42

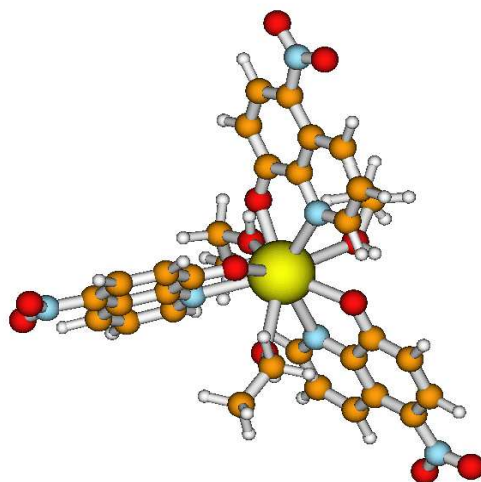


Figure 4.42: Structure of the ninefold coordinated $\text{EU}(\text{NO}_2\text{Q})_3(\text{ETOH})_3$ complex (isomer 2). Calculated on UB3LYP/6-31G* level of theory.

In most cases the solvent molecule builds H-bonds with the ligand system or the Eu ion. In case of ETOH the distance between the solvent molecule (measured as Eu-O bond) is smaller than in the case of DCM (Eu-C bond). One reason is that the prolate ETOH molecule can be more easily incorporated in the structure than the roundish DCM. Another reason is that the oxygen as electron rich atom is bonded closer to the Europium ion than the carbon of the DCM. The distances do not show any trend and are in the range of 2.5 Å - 4 Å. In isomer 1 of the NO_2 species one chloro atom of the DCM binds directly to the europium ion as depicted in figure 4.43.

Compared to the gas phase calculation, the **Eu-N bond** length is elongated when ETOH and compressed when DCM is used as solvent. However, the effect is biggest for the ETOH calculations and always more distinct in the unsubstituted structure.

The above discussed trends concerning the difference between the isomers is conserved in the solvent calculations. The Eu-N bond length is smaller in isomer 2 and the Eu-O bond length is elongated. Comparing the substituent effects the Eu-N bond length is elongated in isomer 1 for ETOH calculations with electron withdrawing groups (contrary to the trend observed in gas phase). The trend for isomer 2 is according to the gas phase observation. The same applies for the DCM calculations, where in both isomers electron withdrawing groups show an elongation of the Eu-N bond.

Calculation was also performed on one complex comprising four ligands and two H_2O molecules. The primal structure comes from a 2-methyl-8-quinolinolate scandium complex, where the scandium ion in

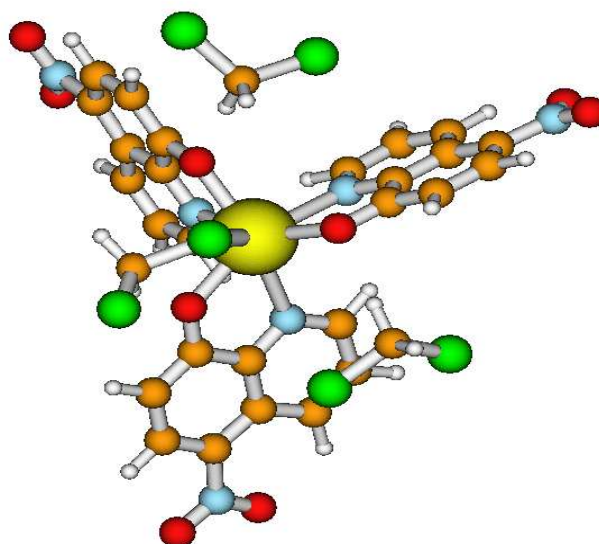


Figure 4.43: Structure of isomer 1 of the $\text{Eu}(\text{NO}_2\text{Q})_3(\text{DCM})_3$ complex. Calculated on UB3LYP/6-31G* level of theory.

the reported XRD structure [50] was replaced by the Eu ion. The ligand system consists of four 8-hydroxyquinolinolate molecules, each two of them coordinating in a bidentate fashion and the other two coordinating with the oxygen only (see Figure 4.41). The geometry data are given in Table A.37 in the Appendix (page LVI). One H_2O molecule coordinates directly to the coordination center with a bond length of 2.52 Å while the second one fills the gap between the two single coordinated ligands and is in a 4.3 Å distance to Eu. Differences in the singlet and triplet state are quite small. The axial angles are slightly compressed in the triplet state. Bond lengths or the equatorial angles remain almost the same. Compared to the EuQ_3 structures, the Eu-N bonds are smaller in the EuQ_4 structure and the Eu-O bonds are slightly longer.

4.5.6 AM1 geometries

Geometry data for the AM1 optimised structures are displayed in Tables A.29 - A.30 and A.35 - A.36 in the Appendix. Also the semiempirical AM1 model with a sparkle for Eu was used to optimise the structure. In the work of Freire et al. [23] a parametrisation for the Eu sparkle is given and shows good results in optimising geometries. One big advantage of using semiempirical methods on the stage of geometry optimisation, is the save of computation time. To compare the different methods, optimisation for the singlet and triplet geometries in gas phase were performed with the AM1 Hamiltonian and the reported Eu sparkle. Solvent calculations for DCM and ETOH with explicit solvent model were done on the semiempirical level for the singlet state only. Here results are compared with the DFT optimised geometries. Furthermore, one excitation calculation on UB3LYP/TZVP/52MWB level based on a AM1

structure was done. The small changes in the DFT and AM1 optimised structures however shift the absorption energies for the AM1 geometry to higher energy. Structures optimised on AM1 level of theory can therefore not be used to calculate the absorption energies.

Generally, the **Eu-N bond** lengths are underestimated in the AM1 model by 0.1 Å, while the O-Eu bond lengths are elongated by the same factor. All the angles are smaller in the AM1 model, except for the axial angles of the NO₂ structure, which seems widened.

The trend between the different isomers is the same as discussed before for the bond distances. Isomer 1 shows slightly longer bond lengths compared to isomer 2 and three for the Eu-N bond. However, the **Eu-O bonds** are not smaller in isomer 1, as observed in the DFT calculation. Eu-O bond lengths in the different isomers are almost the same in the AM1 calculation. The **axial angles** show a behaviour which was observed for the equatorial angles in the DFT calculation: In isomer 2 and 3 one axial angle is smaller than in isomer 1, one is almost the same and one is widened. For the **equatorial angles** the different isomers give quite the same values.

Substitution effects follow again the trend seen for the ab initio calculated structures: electron pushing groups elongate the Eu-N bond but compress the Eu-O bond. For the angles no clear conclusion can be done. Here steric effects of the different substitution groups might have an influence as well.

The results of the solvent calculation show that bonding of the solvent molecule to the Eu ion occur in a much less degree than in the DFT calculations. The biggest difference can be seen for isomer 2 of the NO₂ structure in case of the ETOH solvent, where a DFT calculation results in a 9-fold coordination. In the ab initio structure all ETOH molecules are bond to the Eu ion, while in the AM1 structure none of the ETOH molecules attach to the central ion. Comparing the AM1 gas phase and solvent calculations, the bond lengths are elongated in the ETOH and DCM calculations. In case of the DCM calculations, the axial angles are widened, but the equatorial angles remain the same for both solvents.

4.6 Absorption Spectra of the Complexes in Gas Phase

Absorption spectra were calculated for four homoleptic complexes with substituents H, NH₂, NO₂ and HSO₃ in 5-position of the 8-quinolinolate ligand.

For the H, NH₂ and NO₂ substituted complexes solvent influence on the absorption spectra was investigated via IEF-PCM model and with explicit solvent molecules. In case of the explicit solvent model the structures show three DCM or ETOH solvent molecules in the first coordination sphere as discussed in the geometry section on page 85.

Furthermore absorption spectra for two homoleptic EuQ₄X₂ (X=H₂O or ETOH) complexes were calculated. The solvent molecules are incorporated in the structure of the complex. The ligand Q is the unsubstituted 8-quinolinolate ligand. In this structure two ligands are coordinated in a bidentate fashion while the other two ligands are coordinated with the quinolinolate oxygen to the Eu ion only. To keep the charge neutral, one of the one fold coordinated ligands shows protonation on the quinolinolate nitrogen. The structures are discussed in the geometry section on page 86.

In the following the absorption spectra and interpretation of the vertical transition is discussed. Excitation calculations were performed for all three isomers of the complexes, however, for the interpretation only the energetically most stable form was used. In case of the gas phase calculation the isomers 2 of the unsubstituted complex, isomers 2 and 3 for the NH₂ and NO₂ and isomer 3 of the HSO₃ substituted complex have the lowest relative energy and were considered. In case of the explicit solvent calculation isomer 2 of the different complexes were used (see also Table 4.8 on page 83).

4.6.1 Unsubstituted complexes - Eu(Q)₃

The convoluted **gas phase** spectrum of **isomer 2** of the Eu(Q)₃ complex shows two peaks in the visible region as depicted in Figure 4.44. The stronger band at approximately 2.87 eV (431 nm) comes from two transitions where the first one lies at 2.8457 eV (f=0.0544 a.u.) and is the S₀-S₁ transition. The second one is the strongest one and could be identified as S₀-S₂ transition at 2.8715 eV (f=0.0909 a.u.) (see Tab. 4.9).

The S₀-S₁ transition is a combination of π - π^* and intraligand charge transfer (ILCT) excitations. The biggest contribution comes from the HOMO - LUMO transition, which is a ILCT from the phenoxy part of ligands 1 and 2 to the pyridino part of ligand 3. Table 4.9 gives an overview of the different excitations and its attribution. While in the HOMO orbital the charge is distributed in the phenoxy part of the ligand system including the oxygen atoms, the LUMO orbital does not show any charge on the oxygen atoms. In the LUMO orbital the electron density is mainly distributed on the pyridino part of ligand 3

and shows a small electron density in the pyridino part of ligand 2. Pictures of the orbitals are depicted in Figures 4.45 - 4.46. Further contributions to the S_0 - S_1 transition come from lower lying occupied orbitals (HOMO-1 and HOMO-2) to LUMO and LUMO+1 orbitals. The HOMO-1 orbital shows most of its electron density on ligands 2 and 3, same does the LUMO+1 orbital. The electron density on the HOMO-1 orbital is similar distributed as in the HOMO orbital. The only difference is the inverted sign of the orbital which is located on the phenoxy part of ligand 1. The HOMO-2 orbital is centered on ligand 3 mainly. Therefore transitions from HOMO-1 or HOMO orbitals to the LUMO+1 orbital are π - π^* transitions, those going from the HOMO or HOMO-1 orbital to the LUMO orbital or from HOMO-2 to LUMO+1 are attributed as ILCT transitions.

The behaviour that transition goes from the phenoxy part of the quinolinolate to the pyridino part was observed in the ligand excitation calculations before.

The S_0 - S_2 transition is the strongest transition in terms of oscillator strength and comes mainly from excitations arising from the HOMO, HOMO-1 and HOMO-2 orbitals and going to the LUMO, LUMO+1 and LUMO+2 orbitals. The strongest attribution however is the HOMO - LUMO+1 excitation which is attributed as π - π^* transition in ligands 1 and 2. This could be a reason for the slightly increased oscillator strength compared to the S_0 - S_1 transition, since π - π^* transitions show a higher oscillator strength than ILCT excitations.

The second peak in the convoluted spectrum lies at approximately at 3.98 eV (311 nm) and is based mainly on one vertical transition. This transition could be identified as S_0 - S_{10} transition (3.9853 eV, $f=0.0245$ a.u.). It is composed of excitations from lower lying occupied orbitals (HOMO-4 and HOMO-5) to higher lying unoccupied orbitals (LUMO+2, LUMO+3 and LUMO+4). The main contributions come from a HOMO - LUMO+3 excitation, which is a ILCT from ligands 1 and 2 to ligand 3 and from the HOMO-2 - LUMO+2 excitation, which is an ILCT. The LUMO+3 orbital shows, in contrary to the LUMO orbital discussed before, an electron density which is distributed not only on the pyridino part of ligand 3 but which extends over the whole ligand. However, no electron density is present on the pyridino N atom or the phenoxy O atom. The second strongest contribution comes from a HOMO-2 - LUMO+2 transition. The HOMO-2 orbital is located around the phenoxy part of ligand 3 while the LUMO+2 orbital is centered on the pyridino part of ligand 2 and shows also a small contribution of ligand 1. This transition is attributed as ILCT from ligand 3 to ligand 1. The other contributions consists of transitions from lower lying occupied orbitals where the electron density is centered strictly on one ligand only (HOMO-4 on ligand 1, HOMO-5 on ligand 3) and go as ILCT to higher lying unoccupied orbitals. If calculation are done with the **IEF-PCM** model in DCM and ETOH, the absorption bands shift to higher energy (from 431 nm in gas phase to 411 nm in DCM and 408 nm in ETOH). The S_0 - S_{10} transition shows a higher absorption in case of the solvent calculation if compared to the gas phase calculation. However, the absorption bands of the solvent spectra are not energetically shifted noteworthy

regarding the applied solvent.

In the **DCM** spectrum the first peak comes mainly from a S_0 - S_1 transition (2.9817 eV, $f=0.0988$ a.u.) and the S_0 - S_2 transition (3.0175 eV, $f=0.1108$ a.u.). The first excitation is a HOMO - LUMO ILCT excitation, the second one a π - π^* excitation, as seen for the gas phase spectrum before. The smaller, energetically higher lying peak, is the S_0 - S_{10} transition (4.0635 eV, $f=0.0467$ a.u.) and is a HOMO - LUMO+4 ILCT excitation from ligand 3 to ligand 1.

For the **EtOH** calculation the first transitions (S_0 - S_1 at 3.0065 eV, $f=0.1001$ a.u., and S_0 - S_2 at 3.0475 eV, $f=0.1070$ a.u.) show the same excitations as in the DCM calculation. The S_0 - S_{10} transition (4.0703 eV, $f=0.0359$ a.u.) however is mainly an HOMO - LUMO+5 transition. The excitation shows characteristics of a π - π^* transition and of a ILCT. The HOMO orbital is centered on ligand 1 and 2, while the LUMO orbitals are centered on ligand 1 only (LUMO+4) or ligand 2 only (LUMO+5).

In the spectrum in Figure 4.44 the orange line shows the experimental S_0 - S_1 energy (see [51]). The gas phase spectrum is calculated 0.48 eV too low. Applying the IEF-PCM model decreases the error to 0.31 eV.

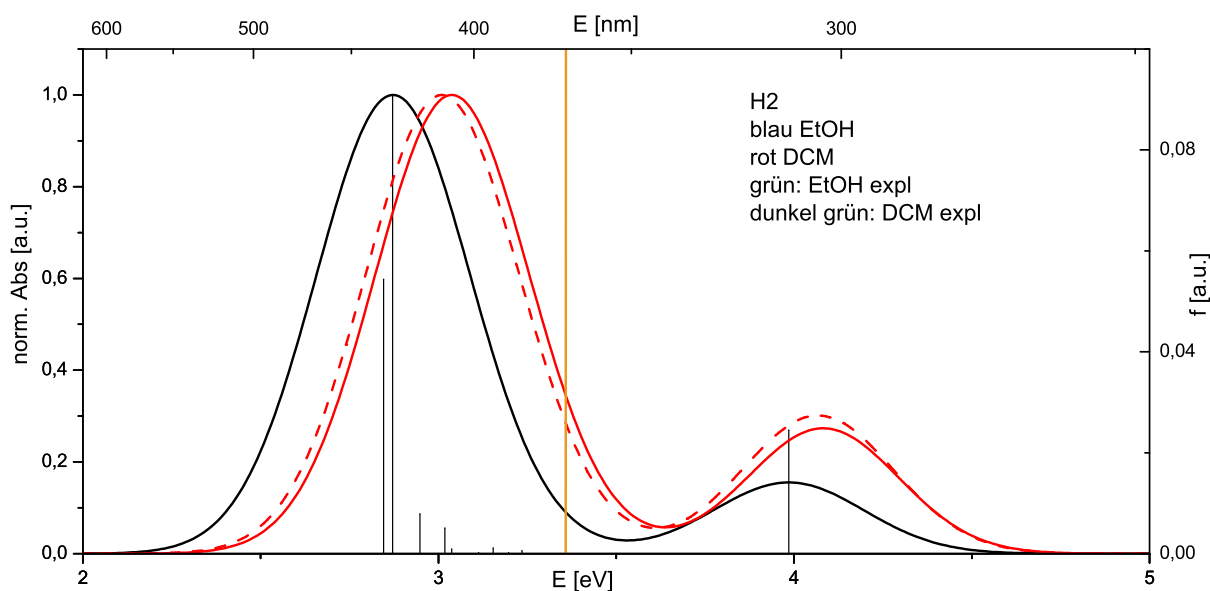


Figure 4.44: Calculated spectra of $\text{Eu}(\text{Q})_3$ isomer 2. The vertical black lines give the calculated gas phase transitions. Black: Gas phase spectrum; Red: IEF-PCM spectrum for DCM (dashed line) and for EtOH (solid line). The vertical orange line marks the experimental S_0 - S_1 transition at 370 nm (3.5 eV) as reported in [51]. Calculation on UB3LYP/TZVP/52MWB level of theory.

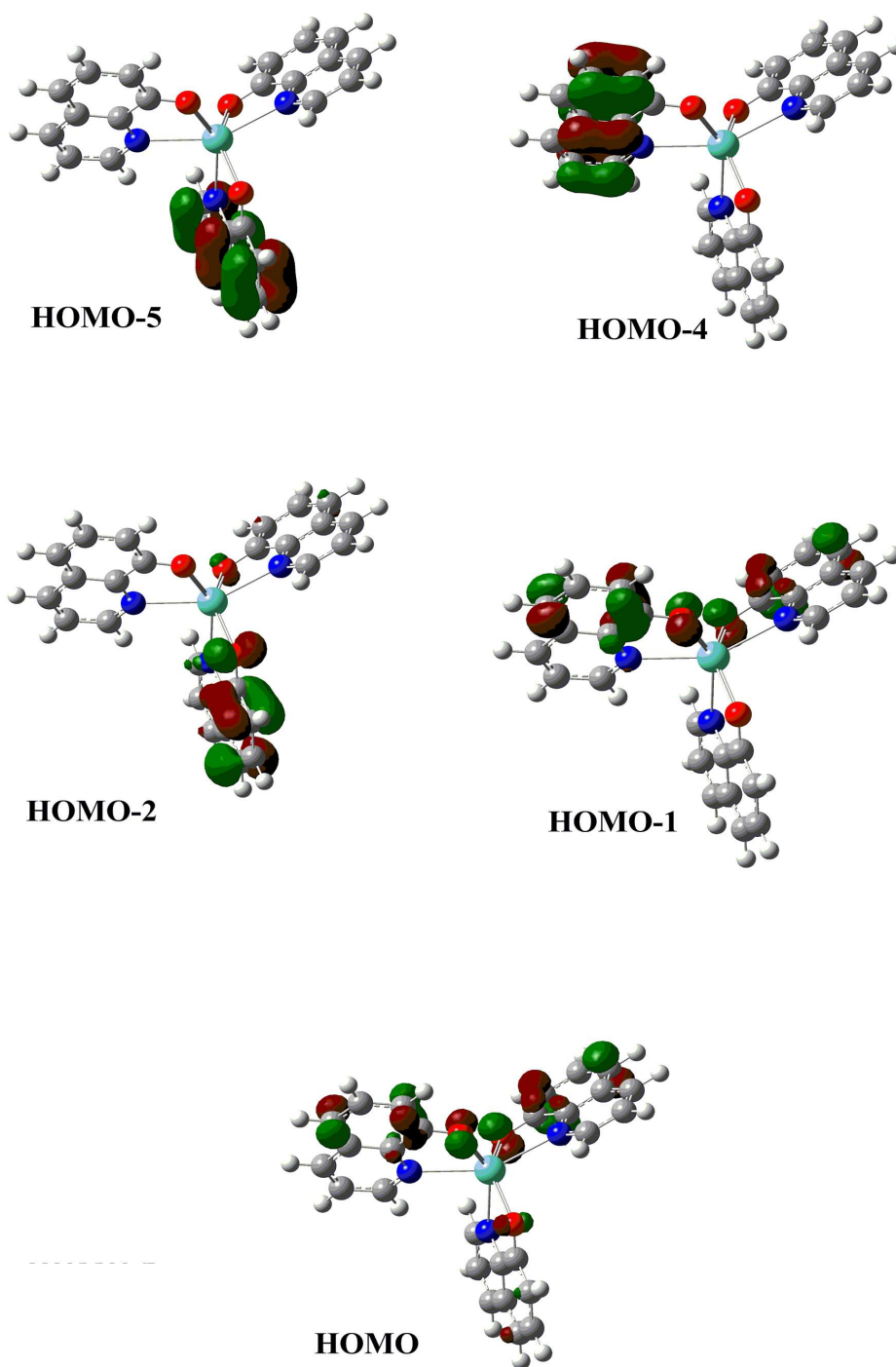


Figure 4.45: Occupied molecular orbitals of isomer 2 of the EuQ_3 complex. Calculated in gas phase on UB3LYP/TZVP/52MWB level of theory.

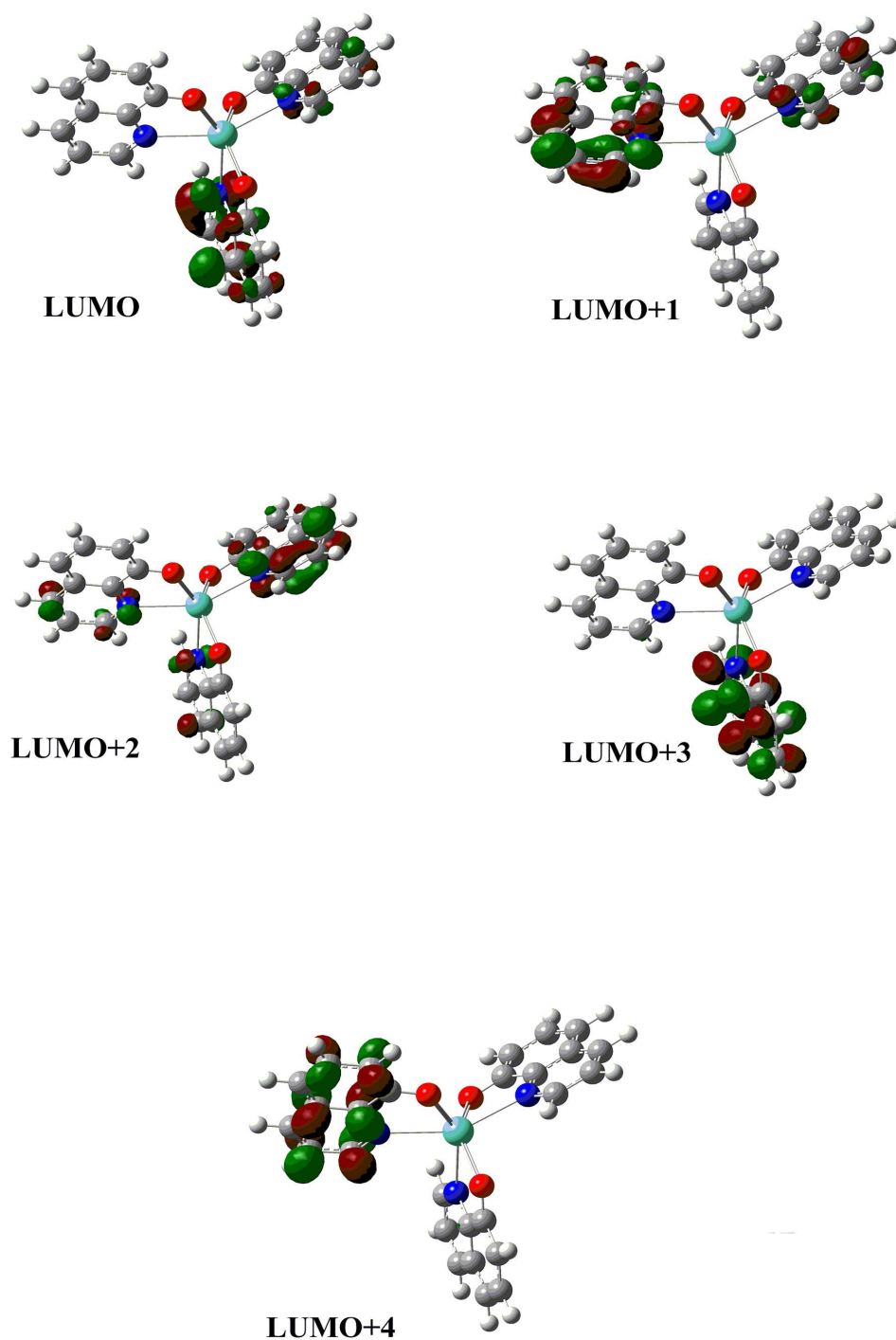


Figure 4.46: Unoccupied molecular orbitals of isomer 2 of the EuQ_3 complex. Calculated in gas phase on UB3LYP/TZVP/52MWB level of theory.

Table 4.9: Absorption energies, transition energies and band attribution of Eu(Q)₃ complex for isomer 2. Calculated in gas phase. Calculation on UB3LYP/TZVP/52MWB level of theory. If more than one attribution is present, the less important one is set in paranthesis.

$E_{\text{abs.}}$ [eV]	$E_{\text{trans.}}$ [eV]	Transition	f [a.u.]	Contribution	CI coefficient [a.u.]	Attribution
2.87	2.8457	S_0-S_1	0.0544	HOMO - LUMO	0.58680	ILCT
				HOMO-2 - LUMO	-0.21832	$\pi-\pi^*$
				HOMO-1 - LUMO+1	0.15860	$\pi-\pi^*$
				HOMO-1 - LUMO	0.13065	ILCT
				HOMO-2 - LUMO+2	0.12144	ILCT
				HOMO - LUMO+1	0.10503	$\pi-\pi^*$
2.8715	S_0-S_2	0.0909	HOMO - LUMO+1	0.55344	$\pi-\pi^*$	
			HOMO-1 - LUMO	-0.22528	ILCT	
			HOMO-1 - LUMO+2	-0.20777	ILCT ($\pi-\pi^*$)	
			HOMO-1 - LUMO+1	-0.17071	$\pi-\pi^*$	
			HOMO-2 - LUMO	-0.11295	$\pi-\pi^*$	
3.98	3.9853	S_0-S_{10}	0.0245	HOMO - LUMO+3	0.44944	ILCT
				HOMO-2 - LUMO+2	-0.36465	ILCT
				HOMO-5 - LUMO	0.27222	$\pi-\pi^*$
				HOMO-5 - LUMO+2	-0.12110	ILCT
				HOMO-2 - LUMO+4	-0.10637	ILCT
				HOMO-4 - LUMO+1	0.10607	$\pi-\pi^*$ (ILCT)

4.6.2 NH₂ substituted complexes - Eu(NH₂Q)₃

Isomer 2 of the Eu(NH₂Q)₃ complex shows two peaks in the visible region. The gas phase and IEF-PCM spectra are depicted in Figure 4.47. The stronger absorption band can be seen at 2.42 eV (511 nm) and comes from the S₀-S₁ and S₀-S₂ transition mainly. The **S₀-S₁** transition lies at 2.4006 eV (f=0.0605 a.u.) and is a HOMO - LUMO excitation. The HOMO orbital is a π orbital localised on the phenyl part of ligands 1 and 2 and shows some contribution of the oxygen and the NH₂ group, while the LUMO orbital is centered on the pyridino part of ligand 3. This excitation is comparable to the HOMO - LUMO transition in the unsubstituted quinoline complex discussed in the subchapter before. Other important contributions to the S₀-S₁ transition come from a HOMO-2 - LUMO excitation (π - π^* excitation in ligand 3) and HOMO-1 - LUMO+1 excitation (π - π^* transition in ligand 1 and ILCT from ligand 2 to ligand 1). The difference between the HOMO and HOMO-1 orbital is the inverted sign of the orbitals in ligand 1, as stated before for the unsubstituted complex.

The **S₀-S₂** transition lies at 2.4271 eV (f=0.0916 a.u.) and is stronger than the S₀-S₁ transition. Here the main contribution comes from a HOMO - LUMO+1, HOMO-1 - LUMO+2 and HOMO-1 - LUMO excitations. The first two excitations are π - π^* transitions with a smaller contribution from a ILCT and go from the phenoxy parts of ligand 1 and ligand 2 to the pyridino part of ligand 1 (HOMO - LUMO+1) and vice versa for the HOMO-1 - LUMO+2 excitation. The HOMO-1 - LUMO excitation is a pure ILCT transition from the HOMO-1 orbital located on ligands 1 and 2 to the LUMO orbital on ligand 3. The π - π^* characteristic of the two major contribution in the S₀-S₂ transition are responsible for the increased oscillator strength if compared to the S₀-S₁ transition.

The second absorption band is conducted at 3.59 eV (343 nm) and is a result of three vertical transitions, namely the S₀-S₁₀, S₀-S₁₁ and S₀-S₁₂ transition. This explains also the higher absorption if compared to the unsubstituted EuQ₃ complex (0.67 referring to the normalised stronger band at 2.42 eV for the Eu(NH₂Q)₃ complex). The **S₀-S₁₀** transition is composed of excitations from the HOMO and HOMO-2 orbitals to the LUMO+3 orbital. The HOMO - LUMO+2 excitation is a ILCT from ligands 2 and 3 to ligand 3. In contrary to the LUMO orbital, which is also purely located on the pyridino part of ligand 3 and plays the major role in the S₀-S₁ transition, the LUMO+3 orbital shows the electron density distributed over the whole ligand. The HOMO-2 orbital is located on the phenoxy part of ligand 3 and the HOMO-2 - LUMO+3 transition is therefore a π - π^* excitation where the electron density moves from the phenoxy part of ligand three to the whole ligand. The **S₀-S₁₁** transition (3.6070 eV, f=0.0428 a.u.) is a mixed ILCT and π - π^* excitation from ligand 1 and 2 to ligand 2. The **S₀-S₁₂** transition (3.6204 eV, f=0.0233 a.u.) in isomer 2 of the Eu(NH₂Q)₃ complex is an excitation from HOMO and HOMO-1 orbital which are centered on ligand 1 and 2 to the LUMO+5 orbital on ligand 2. Orbital pictures are depicted in Figures 4.48 - 4.49 and the energies and contributions of the excitations are presented in

table 4.10.

Comparing the gas phase spectra with the **IEF-PCM spectra** a small blueshift can be seen where the solvent spectra are calculated at higher energy. For the energetically higher lying band at 3.59 eV the solvent calculation shows an increase of absorption (0.90 for ETOH, 0.95 for DCM referring to the strongest peak at 2.42 eV). The reason for it is the relatively strong S_0 - S_{10} transition ($f=0.1086$ a.u. in EtOH, $f=0.1090$ a.u. in DCM, $f=0.0418$ in gas phase).

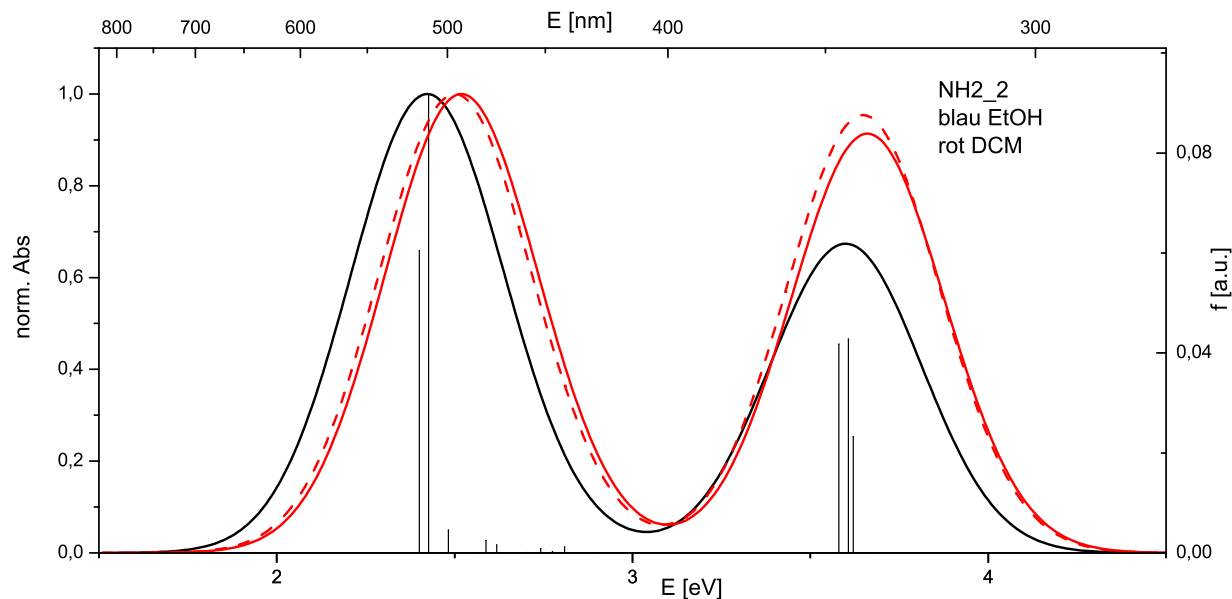


Figure 4.47: Calculated spectra of $\text{Eu}(\text{NH}_2\text{Q})_3$ isomer 2. The vertical black lines give the calculated gas phase transitions. Black: Gas phase spectrum; Red: IEF-PCM spectrum for DCM (dashed line) and for ETOH (solid line). Calculation on UB3LYP/TZVP/52MWB level of theory.

Table 4.10: Absorption energies, transition energies and band attribution of $\text{Eu}(\text{NH}_2\text{Q})_3$ complex for isomer 2. Calculated in gas phase. Calculation on UB3LYP/TZVP/52MWB level of theory. If more than one attribution is present, the less important one is set in paranthesis

$E_{\text{abs.}}$ [eV]	$E_{\text{trans.}}$ [eV]	Transition	f [a.u.]	Contribution	CI coefficient [a.u.]	Attribution
2.42	2.4006	S_0-S_1	0.0605	HOMO - LUMO	0.52509	ILCT
				HOMO-2 - LUMO	0.30528	$\pi-\pi^*$
				HOMO-1 - LUMO+1	0.17477	$\pi-\pi^*$ (ILCT)
				HOMO-2 - LUMO+2	-0.15383	ILCT
				HOMO-1 - LUMO	0.13373	ILCT
				HOMO - LUMO+2	0.12175	$\pi-\pi^*$ (ILCT)
	2.4271	S_0-S_2	0.0916	HOMO - LUMO+1	0.52547	$\pi-\pi^*$ (ILCT)
				HOMO-1 - LUMO+2	0.25714	$\pi-\pi^*$ (ILCT)
				HOMO-1 - LUMO	0.24377	ILCT
				HOMO-1 - LUMO+1	-0.16511	$\pi-\pi^*$ (ILCT)
				HOMO-2 - LUMO	-0.11261	$\pi-\pi^*$
3.59	3.5799	S_0-S_{10}	0.1086	HOMO - LUMO+3	0.56143	ILCT
				HOMO-2 - LUMO+3	0.32241	$\pi-\pi^*$
				HOMO-5 - LUMO	-0.16832	$\pi-\pi^*$
	3.6070	S_0-S_{11}	0.0428	HOMO - LUMO+4	0.49971	$\pi-\pi^*$ (ILCT)
				HOMO-1 - LUMO+4	-0.28938	$\pi-\pi^*$ (ILCT)
				HOMO-2 - LUMO+3	-0.18803	$\pi-\pi^*$
	3.6204	S_0-S_{12}	0.0233	HOMO - LUMO+5	-0.53468	$\pi-\pi^*$ (ILCT)
				HOMO-1 - LUMO+5	-0.27983	$\pi-\pi^*$ (ILCT)
				HOMO-4 - LUMO+2	-0.16362	ILCT

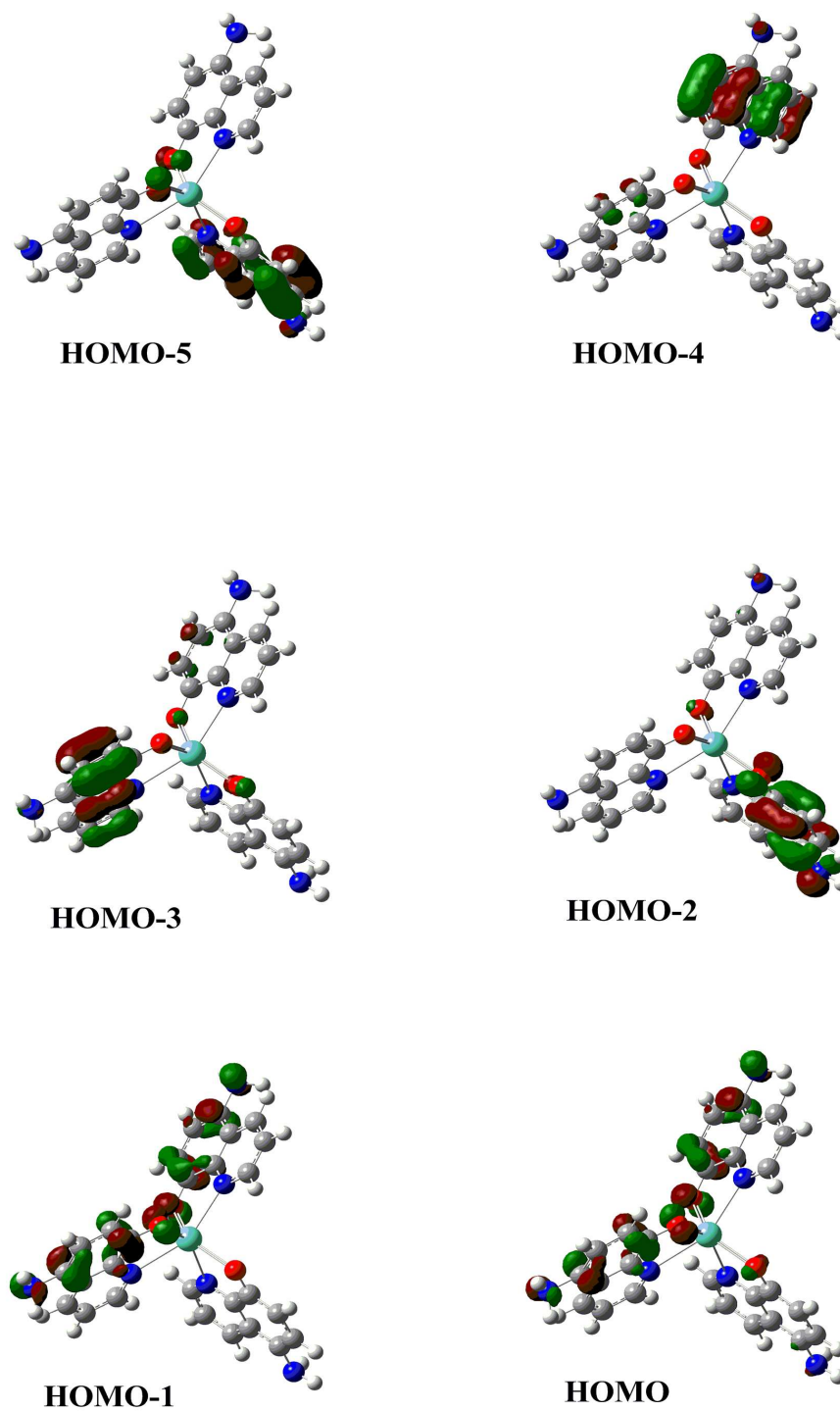


Figure 4.48: Occupied molecular orbitals of isomer 2 of the $\text{Eu}(\text{NH}_2\text{Q})_3$ complex. Calculated in gas phase on UB3LYP/TZVP/52MWB level of theory.

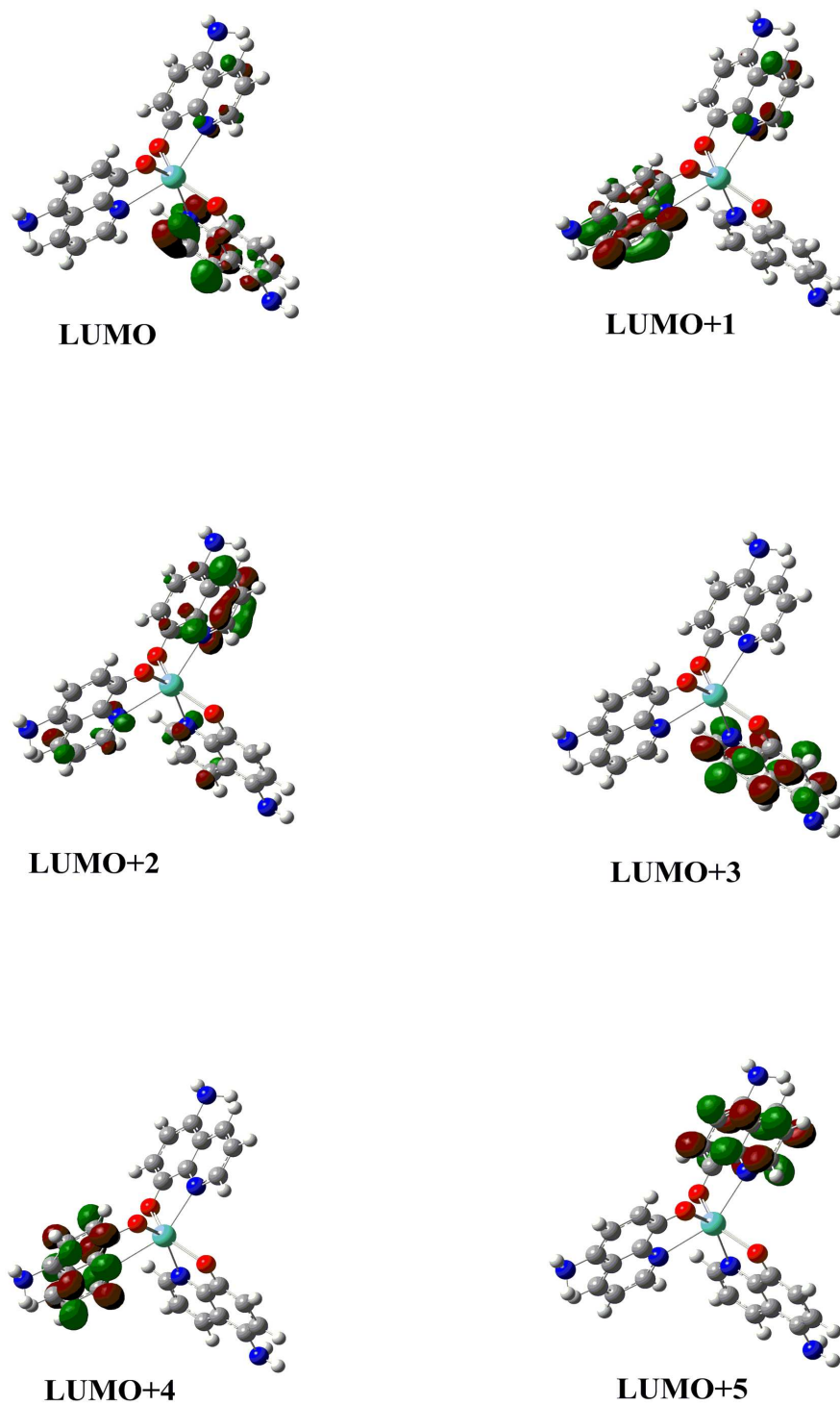


Figure 4.49: Unoccupied molecular orbitals of isomer 2 of the $\text{Eu}(\text{NH}_2\text{Q})_3$ complex. Calculated in gas phase on UB3LYP/TZVP/52MWB level of theory.

Isomer 3 of the $\text{Eu}(\text{NH}_2\text{Q})_3$ complex gives a similar absorption spectrum as seen before for the isomer 2. This is expected, since isomer 2 and 3 are enantiomers and the orbitals of isomer 2 and 3 are expected to have the same shape and size but are located on different ligands (see Figure 4.50). The result is that the position of the vertical transitions and their attribution are the same for isomer 2 and 3. However, the deviation from the ideal octahedral geometry results in small changes. In this way the S_0 - S_{13} transition is present in the spectrum of isomer 3, but absent in the spectrum of isomer 2. The result is a slightly higher absorption of the high energy band at 3.59 eV. The energies and contribution of the S_0 - S_{13} transition of isomer 3 is given in table 4.11.

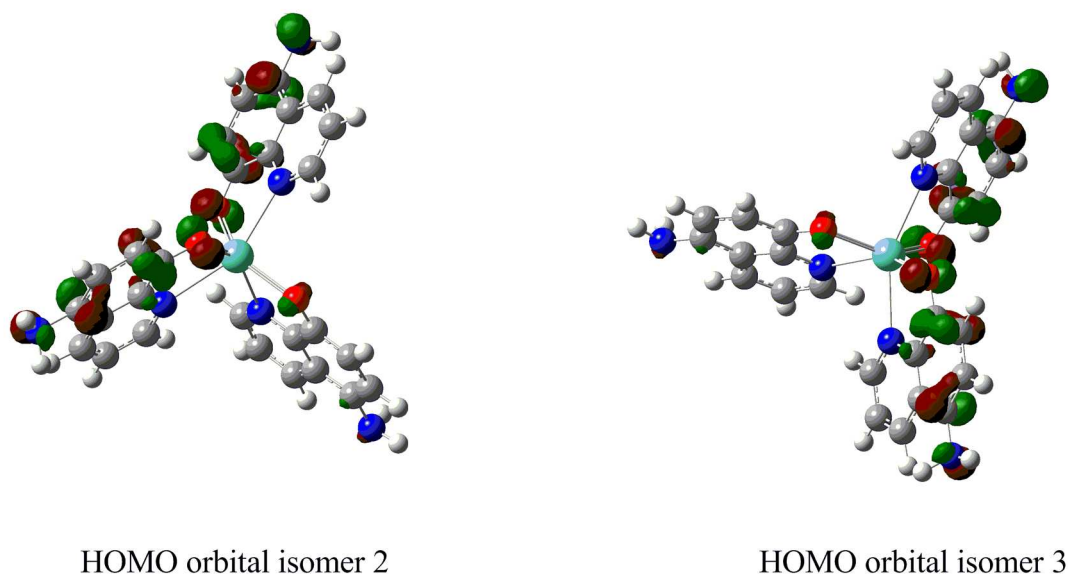


Figure 4.50: HOMO orbitals of the $\text{Eu}(\text{NH}_2\text{Q})_3$ complex: isomer 2 (left) and isomer 3 (right). Calculated on UB3LYP/TZVP/52MWB level of theory.

Table 4.11: Absorption energies, transition energies and band attribution of $\text{Eu}(\text{NH}_2\text{Q})_3$ complex for isomer 3. Calculated in gas phase. Calculation on UB3LYP/TZVP/52MWB level of theory. If more than one attribution is present, the less important one is set in paranthesis

$E_{\text{trans.}}$ [eV]	Transition	f [a.u.]	Dominant contribution	CI coefficient [a.u.]	Attribution
3.6845	S_0 - S_{13}	0.0250	HOMO-2 - LUMO+3	0.50365	π - π^*
			HOMO - LUMO+3	-0.35141	ILCT
			HOMO - LUMO+5	0.18259	π - π^* (ILCT)

4.6.3 NO₂ substituted complexes - Eu(NO₂Q)₃

The **gas phase** absorption spectrum of **isomer 2** of the Eu(NO₂Q)₃ complex is depicted in Figure 4.51 and shows one band at 3.07 eV (403 nm) which is blueshifted if compared to the experimental S₀-S₁ transition (2.79 eV, 445 nm see [49]). The error is 0.28 eV (around 10%) and smaller than in case of the unsubstituted EuQ₃ complex. The band at 3.07 eV shows four strong contributions which will be discussed in the following. MO pictures are given in Figures 4.52. The energies and attributions are summarised in table 4.12.

The energetically lowest lying contribution is the **S₀-S₁** transition at 2.9730 eV (f=0.0971 a.u.) and is a pure HOMO - LUMO excitation comprising a ILCT from ligand 1 and 2 to ligand 3. The HOMO orbital is centered on the phenoxy part of ligands 1 and 2 and shows a bigger contribution of the O atom but less electron density on the NO₂ group. The LUMO orbital is distributed over the whole quinolinolate in ligand 3 and shows contribution of the quinolinolate O and the NO₂ group. This is a difference to the distribution seen before in the EuQ₃ and Eu(NH₂Q)₃ complexes, where the LUMO orbital is centered on the pyridino part of ligand 3 only.

The **S₀-S₂** transition (0.2624 eV, f=0.2624) is the strongest transition and is composed of a HOMO - LUMO+1 and HOMO - LUMO+5 excitation. While in the HOMO - LUMO+1 excitation electron density migrates from the phenoxy part and distributes over the whole quinolinolate system in ligand 1 and 2, the HOMO - LUMO+5 excitation is mainly an π - π^* excitation from the phenoxy part of ligand 1 and 2 to the pyridino part of the same ligands. However, in the LUMO+5 orbital the electron density on the NO₂ group remains.

The **S₀-S₄** transition at 3.0995 eV (f=0.1174 a.u.) is composed of transitions from lower lying occupied orbitals to higher lying unoccupied orbitals. The most important contribution is a π - π^* excitation from the HOMO-2 to the LUMO orbital. Both orbitals are centered on ligand 3 and the excitation goes from the phenoxy part of ligand 3 to the pyridino part. Other contributions are π - π^* going from HOMO-1 - LUMO+1 and from the HOMO to the LUMO+2 orbitals. As described in the complex systems before, the difference between the HOMO and HOMO-1 orbital is the inverted sign of the orbitals in one of the ligands. The HOMO-1 - LUMO+1 and HOMO - LUMO+2 excitations go from ligand 1 to ligand 2 respectively.

The last noteworthy contribution to the peak at 3.07 eV is a HOMO-1 - LUMO+2 excitation and is

attributed as S_0-S_6 transition (3.2517 eV, $f=0.0575$ a.u.).

The **IEF-PCM** spectra do not show a shift regarding the energy of absorption, however, at 3.79 eV (325 nm) a second band appears for the DCM and ETOH spectra. This peak comes, in case of the **DCM** spectrum, from the S_0-S_{12} transition at 3.8042 eV ($f=0.1610$ a.u.) and shows mainly contribution from HOMO - LUMO+3 and HOMO-3 - LUMO+5 excitations. In the **ETOH** spectra a transition consisting of the same excitations is the S_0-S_{13} transition at 3.8083 eV ($f=0.1361$ a.u.). Other transitions attributing to the band at 3.79 eV in the ETOH calculation are the S_0-S_{11} (3.7846 eV, $f=0.0083$ a.u.) and S_0-S_{12} (3.7898 eV, $f=0.0011$ a.u.) transitions, but show only a minor contribution. In the 30 states which were calculated for the gas phase spectra the S_0-S_{10} and higher transitions are not displayed. It is highly possible that the second peak can be found if more states would be calculated for the gas phase spectrum.

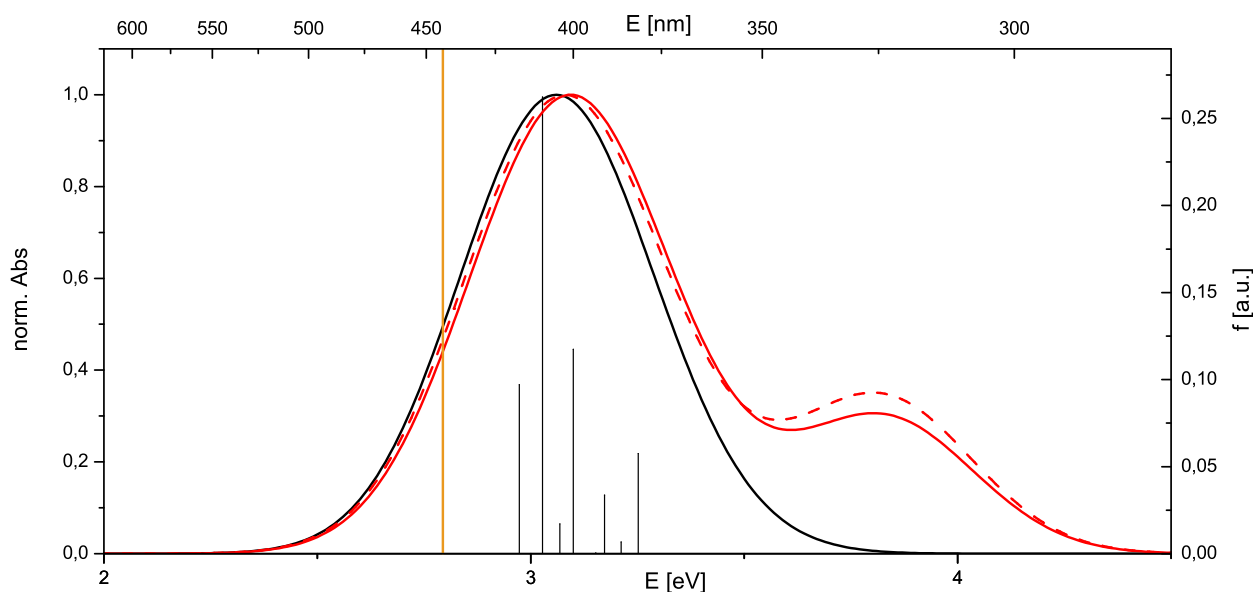


Figure 4.51: Calculated spectra of $\text{Eu}(\text{NO}_2\text{Q})_3$ isomer 2. The vertical black lines give the calculated gas phase transitions. Black: Gas phase spectrum; Red: IEF-PCM spectrum for DCM (dashed line) and for ETOH (solid line). The vertical orange line marks the experimental S_0-S_1 transition (see [49]). Calculation on UB3LYP/TZVP/52MWB level of theory.

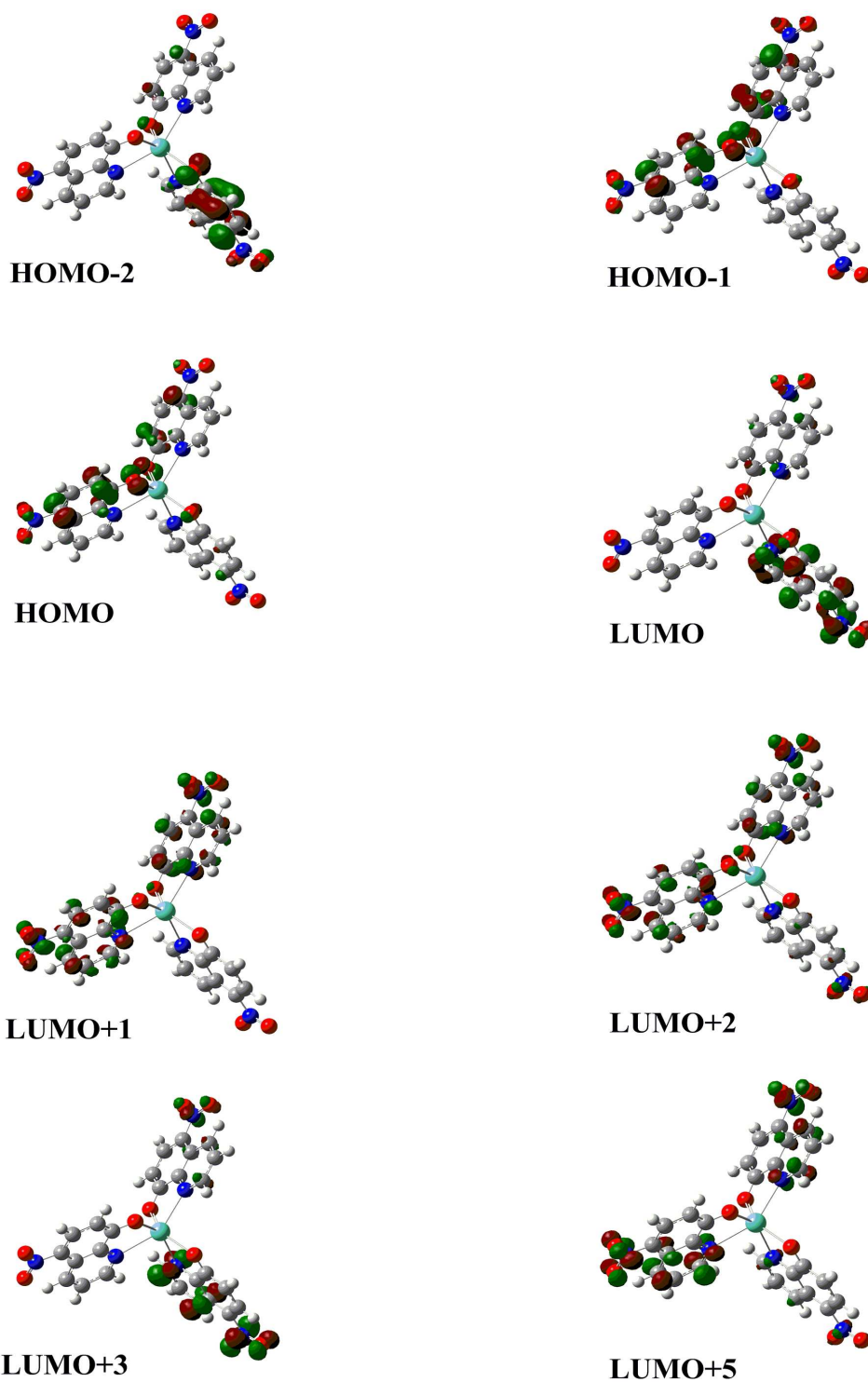


Figure 4.52: Molecular orbitals of isomer 2 of the $\text{Eu}(\text{NO}_2\text{Q})_3$ complex. Calculated in gas phase on UB3LYP/TZVP/52MWB level of theory.

Table 4.12: Absorption energies, transition energies and band attribution of $\text{Eu}(\text{NO}_2\text{Q})_3$ complex for isomer 2. Calculated in gas phase. Calculation on UB3LYP/TZVP/52MWB level of theory. If more than one attribution is present, the less important one is set in paranthesis

$E_{\text{abs.}}$ [eV]	$E_{\text{trans.}}$ [eV]	Transition	f [a.u.]	Contribution	CI coefficient [a.u.]	Attribution
3.07	2.9730	S_0-S_1	0.09711	HOMO - LUMO	0.67849	ILCT
	3.0273	S_0-S_2	0.2624	HOMO - LUMO+1	0.64372	$\pi-\pi^*$
HOMO - LUMO+5				-0.10465	$\pi-\pi^*$ (ILCT)	
3.0995	S_0-S_4	0.1174	HOMO-2 - LUMO	0.57679	$\pi-\pi^*$	
			HOMO-1 - LUMO+1	-0.28325	$\pi-\pi^*$	
			HOMO - LUMO+2	0.12849	$\pi-\pi^*$	
			HOMO - LUMO+1	0.11388	$\pi-\pi^*$	
			HOMO-2 - LUMO+3	-0.11217	$\pi-\pi^*$	
3.2517	S_0-S_6	0.0575	HOMO-1 - LUMO+2	0.66509	$\pi-\pi^*$	

As seen before for the NH₂ substituted complex, the orbitals of **isomer 2** and **3** of the Eu(NO₂Q)₃ substituted complex are located on different ligands but same in terms of shape and size. The change regarding the excitations is an accumulation of vertical transitions in the area around 3.09 eV (low energy band in the spectrum) and a therefore higher absorption for the low energy band. The high energy transitions which can be seen in the IEF-PCM solvent calculation of isomer 2 are also present in the gas phase calculation of isomer 3 and is identified as the S₀-S₁₀ transition. Contributions and energy of the S₀-S₁₀ transition are listed in Table 4.13.

Interestingly, pure n-π* excitations, which are present in the NO₂-8-hydroxyquinoline S₀-S₁ transition, are not present in the first 30 excitations of the complex orbitals.

Table 4.13: Absorption energies, transition energies and band attribution of Eu(NO₂Q)₃ complex for isomer 3. Calculated in gas phase. Calculation on UB3LYP/TZVP/52MWB level of theory. If more than one attribution is present, the less important one is set in paranthesis

E _{abs.} [eV]	E _{trans.} [eV]	Transition	f [a.u.]	Contribution	CI coefficient [a.u.]	Attribution
3.9	3.8970	S ₀ -S ₁₀	0.2182	HOMO - LUMO+3	0.54235	ILCT
				HOMO-2 - LUMO+3	-0.19984	π-π*
				HOMO-1 - LUMO+3	-0.19484	ILCT
				HOMO-2 - LUMO+4	-0.13206	ILCT
				HOMO - LUMO+4	-0.11735	π-π*

4.6.4 HSO₃ substituted complexes - Eu(HSO₃Q)₃

The spectrum of **isomer 3** of the Eu(HSO₃Q)₃ complex shows two absorption bands for the gas phase and the IEF-PCM calculated spectra as depicted in Figure 4.53

The first band at 2.44 eV (504 nm) comes from the S₀-S₂ and S₀-S₃ transition mainly. The S₀-S₂ transition lies at 2.4315 eV (f=0.0475 a.u.) and is 0.89 eV shifted to lower energy if compared to the experimental S₀-S₁ transition which lies at 3.354 eV (350 nm, see [49]). Pictures of the orbitals are depicted in figure 4.54 and the energies and attributions are given in Table 4.14.

The S₀-S₂ transition shows contributions mainly from HOMO - LUMO excitation. Hereby the electron density goes from the phenoxy part of ligand 1 to the pyridino part of ligand 2. A small contribution also comes from the electron density located on ligand 3. The HOMO-2 - LUMO excitation is a π-π* excitation in ligand 2 where the electron density changes from the phenoxy part to the pyridino part of the ligand. In both cases the orbitals do not show any density on the HSO₃ substituent. The next

strongest contribution comes from a π - π^* excitation which takes part on ligand 3. Here the electron density, which is located on the pyridino part of ligand 3 in the HOMO-1 orbital, goes to the phenoxy part in the LUMO+1 orbital.

The S_0 - S_3 transition at 2.4460 eV ($f=0.0944$ a.u.) is composed of excitations from HOMO - LUMO+1 and HOMO-1 to LUMO and LUMO+1 orbitals. The strongest contribution comes from the HOMO - LUMO+1 excitation and is attributed as ILCT going from ligand 1 to ligand 3. The HOMO-1 - LUMO excitation is a ILCT where the electron density goes from the phenoxy part of ligands 1 and 3 to the pyridino part of ligand 2. Equally strong is the contribution from the HOMO-1 - LUMO+1 excitation which is a π - π^* excitation from the phenoxy part in ligand 3 to the pyridino part of the same ligand.

The second band in the spectra at 3.87 eV (319 nm) comes from a single transition which could be identified as S_0 - S_{10} transition. The three main contribution to this transition go from the HOMO and HOMO-2 orbitals to the LUMO+3 and HOMO-5 to LUMO orbitals respectively. The HOMO-5 orbital is a π orbital centered on ligand 1 and so the HOMO-5 - LUMO excitation is attributed as an ILCT. The HOMO - LUMO+3 and HOMO-1 - LUMO+3 excitations are ILCT excitations from the occupied orbitals which are centered on the phenoxy part of ligands 1 and 3 to the LUMO+3 orbital which is distributed over the whole quinolinolate molecule in ligand 2. The difference between the HOMO and HOMO-1 orbital is - as found in the complexes discussed before - a change in sign at the orbitals centered on one ligand.

The **IEF-PCM** solvent model spectra show a shift of about 0.09 eV of the strongest band towards higher energy which lies at 2.53 eV. The second, weaker band does not show a shift but much less intensity (0.04 relative absorption referred to the strongest band in the gas phase calculation, and 0.008 relative absorption in the IEF-PCM calculations). However, a closer look shows that the equivalent of the gas phase S_0 - S_{10} transition which gives raise to the high energetic band, is the S_0 - S_{13} transition in the IEF-PCM calculations. This S_0 - S_{13} transition lies at 4.2223 eV (ETOH, $f=0.0047$ a.u.) and 4.2016 eV (DCM, $f=0.0044$ a.u.) and is therefore blueshifted if compared to the gas phase spectrum. The second strongest contribution to the small absorption band at higher energy in the IEF-PCM spectra is not the π - π^* HOMO - LUMO+3 excitation as seen in the gas phase spectrum, but it is an HOMO-1 - LUMO+3 excitation which has ILCT attribution. That means that the main three contributions to the S_0 - S_{13} transition in the IEF-PCM calculation are ILCT excitations which might explain the small absorbance.

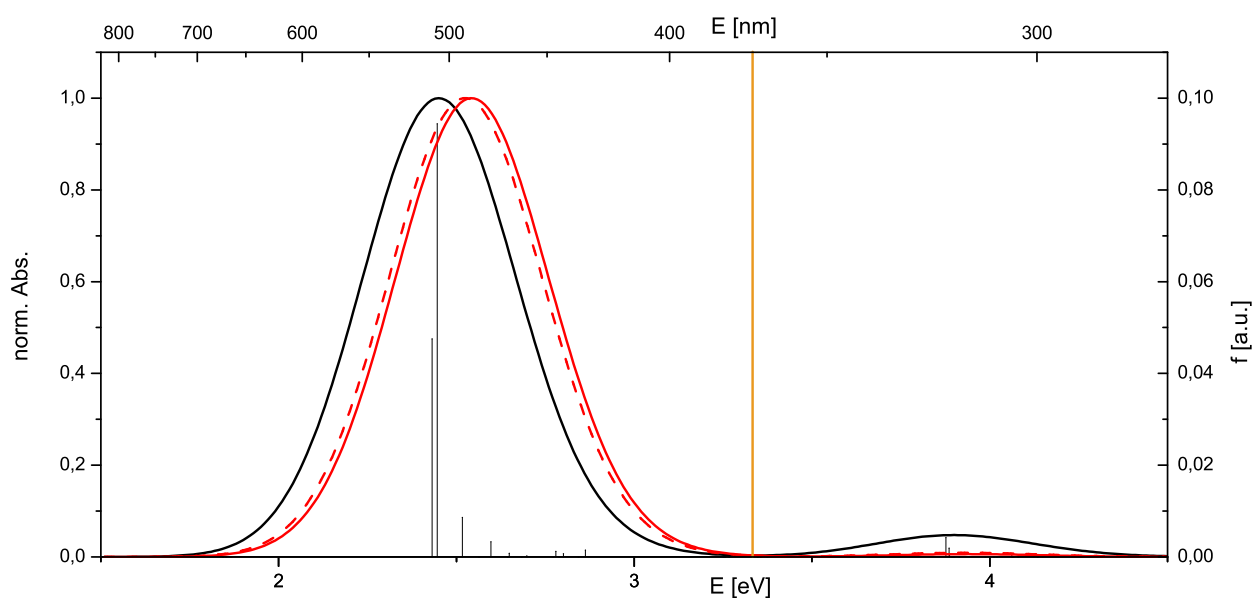


Figure 4.53: Calculated spectra of $\text{Eu}(\text{HSO}_3\text{Q})_3$ isomer 3. The vertical black lines give the calculated gas phase transitions. Black: Gas phase spectrum; Red: IEF-PCM spectrum for DCM (dashed line) and for ETOH (solid line). The vertical orange line marks the experimental S_0 - S_1 transition (see [49]). Calculation on UB3LYP/TZVP/52MWB level of theory.

Table 4.14: Absorption energies, transition energies and band attribution of Eu(HSO₃Q)₃ complex for isomer 3. Calculated in gas phase. Calculation on UB3LYP/TZVP/52MWB level of theory. If more than one attribution is present, the less important one is set in paranthesis

$E_{\text{abs.}}$ [eV]	$E_{\text{trans.}}$ [eV]	Transition	f [a.u.]	Contribution	CI coefficient [a.u.]	Attribution
3.87	2.4315	S_0-S_1	0.0475	HOMO - LUMO	0.53245	ILCT ($\pi-\pi^*$)
				HOMO-2 - LUMO	0.28703	$\pi-\pi^*$
				HOMO-1 - LUMO+1	-0.22785	$\pi-\pi^*$ (ILCT)
				HOMO - LUMO+2	-0.14999	$\pi-\pi^*$ (ILCT)
				HOMO-2 - LUMO+2	0.12268	ILCT
2.4460	S_0-S_2	0.0944	HOMO - LUMO+1	0.50465	ILCT ($\pi-\pi^*$)	
			HOMO-1 - LUMO	-0.23675	ILCT	
			HOMO-1 - LUMO+1	0.23516	$\pi-\pi^*$ (ILCT)	
			HOMO-1 - LUMO+2	0.21992	ILCT ($\pi-\pi^*$)	
			HOMO - LUMO+2	-0.13992	$\pi-\pi^*$ (ILCT)	
			HOMO - LUMO	0.10139	ILCT	
2.49	3.8769	S_0-S_{10}	0.0042	HOMO - LUMO+3	0.36054	ILCT
				HOMO-2 - LUMO+3	0.31346	$\pi-\pi^*$
				HOMO-5 - LUMO	-0.28913	ILCT

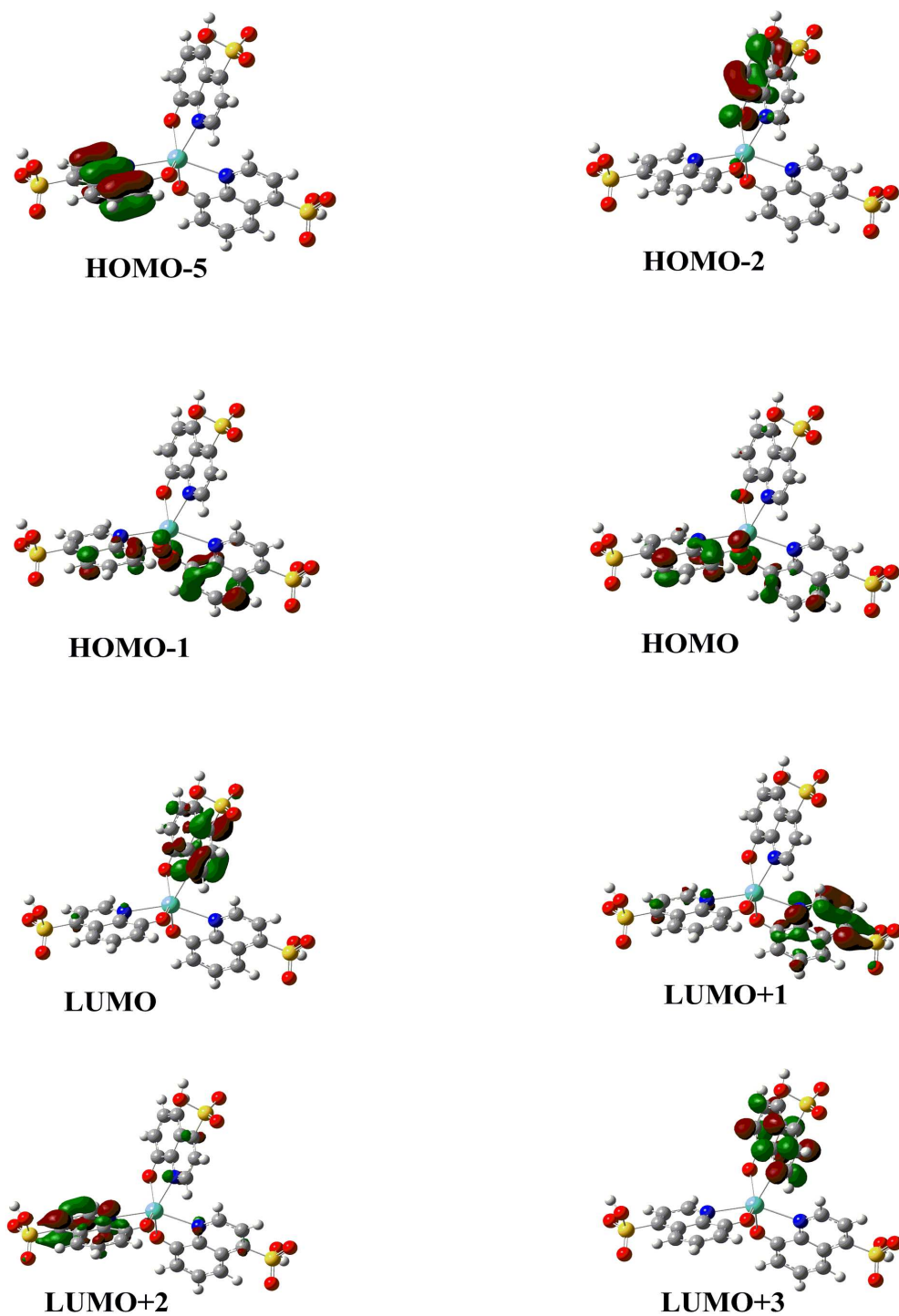


Figure 4.54: Molecular orbitals of isomer 3 of the $\text{Eu}(\text{HSO}_3\text{Q})_3$ complex. Calculated in gas phase on UB3LYP/TZVP/52MWB level of theory.

4.7 Explicit solvent models

The most important difference between explicit solvent calculation and gas phase calculation is the localisation of the electron density. In the gas phase calculation the HOMO and lower lying occupied orbitals are centered on 2 ligands. In the explicit solvent model calculation mixing of the ligands is only seen to a very small amount. In most cases the electron density is located on one ligand only. The HOMO and HOMO-1 orbitals are located on different ligands in the explicit solvent molecule calculation while in the gas phase calculation the HOMO and HOMO-1 orbital are located on the same ligands showing inverted sign.

In the following the difference between the gas phase and the explicit solvent calculations is discussed.

4.7.1 $\text{EuQ}_3(\text{X})_3$ (X=DCM, ETOH)

Isomer 2 of the $\text{EuQ}_3(\text{X})_3$ (X=DCM or ETOH) shows two peaks which show a hypsochromic shift compared to the gas phase calculation (2.87 eV gas phase, 3.12 eV ETOH and 2.95 eV DCM for the low energy absorption band). The results are summarised in Tables 4.15 - 4.16. If ETOH is used as solvent, the S_0 - S_1 transition is a pure HOMO - LUMO ILCT excitation. In the calculation for the DCM solvent also a HOMO-1 - LUMO+1 π - π^* excitation gives some small contribution to the S_0 - S_1 transition. Remarkable is that the first band consists of four important transitions in case of the ETOH solvent (S_0 - S_1 , S_0 - S_2 , S_0 - S_4 , S_0 - S_6) while in the gas phase calculation only the S_0 - S_1 and S_0 - S_2 transition have an oscillator strength above 0.01 a.u. In case of the DCM spectrum the first four excited states are representative for the high energy band. The oscillator strength for the S_0 - S_1 transition in the explicit solvent calculation are weaker compared to the gas phase calculation ($f=0.0544$ a.u. gas phase, $f=0.0266$ a.u. ETOH and DCM). The reason is most probably that the transition in case of the solvent calculations has more of a ILCT character than in the gas phase calculation.

Table 4.15: Absorption energies, transition energies and band attribution of $\text{EuQ}_3(\text{EtOH})_3$ complex for isomer 2. Calculation on UB3LYP/TZVP/52MWB level of theory. If more than one attribution is present, the less important one is set in paranthesis

$E_{\text{abs.}}$ [eV]	$E_{\text{trans.}}$ [eV]	Transition	f [a.u.]	Contribution	CI coefficient [a.u.]	Attribution
3.12	2.8385	S_0-S_1	0.0266	HOMO - LUMO	0.68371	ILCT
	3.0625	S_0-S_2	0.0353	HOMO - LUMO+2	0.63340	$\pi-\pi^*$
				HOMO - LUMO+1	0.17505	ILCT
HOMO - LUMO				0.10308	ILCT	
3.1251	S_0-S_4	0.0330	HOMO-1 - LUMO+1	0.49527	$\pi-\pi^*$	
			HOMO-1 - LUMO	-0.38912	ILCT	
			HOMO - LUMO+1	-0.18574	ILCT	
			HOMO - LUMO+2	0.13149	$\pi-\pi^*$	
3.2353	S_0-S_6	0.0425	HOMO-2 - LUMO	0.65655	$\pi-\pi^*$	
			HOMO - LUMO+1	0.12284	ILCT	
4.01	3.9927	S_0-S_{18}	0.0164	HOMO - LUMO+5	0.46449	$\pi-\pi^*$ (ILCT)
				HOMO - LUMO+4	-0.36849	ILCT ($\pi-\pi^*$)
				HOMO-3 - LUMO+2	0.24109	$\pi-\pi^*$ (ILCT)
				HOMO-3 - LUMO	-0.19860	ILCT ($\pi-\pi^*$)
				HOMO - LUMO+3	0.14820	ILCT
4.0713	S_0-S_{21}	0.0185	HOMO-1 - LUMO+4	0.47700	$\pi-\pi^*$ (ILCT)	
			HOMO-4 - LUMO	-0.34700	$\pi-\pi^*$	
			HOMO-1 - LUMO+5	0.31056	ILCT ($\pi-\pi^*$)	
			HOMO - LUMO+4	-0.13747	ILCT ($\pi-\pi^*$)	
			HOMO - LUMO+5	-0.11553	$\pi-\pi^*$ (ILCT)	

Table 4.16: Absorption energies, transition energies and band attribution of $\text{EuQ}_3(\text{DCM})_3$ complex for isomer 2. Calculation on UB3LYP/TZVP/52MWB level of theory. If more than one attribution is present, the less important one is set in paranthesis

$E_{\text{abs.}}$ [eV]	$E_{\text{trans.}}$ [eV]	Transition	f [a.u.]	Contribution	CI coefficient [a.u.]	Attribution
2.95	2.8755	S_0-S_1	0.0266	HOMO - LUMO	0.66184	ILCT
				HOMO-1 - LUMO+1	0.14740	$\pi-\pi^*$ (ILCT)
	2.9275	S_0-S_2	0.0731	HOMO - LUMO+1	0.46855	ILCT ($\pi-\pi^*$)
				HOMO-1 - LUMO	0.34398	ILCT
				HOMO-1 - LUMO+1	0.28504	$\pi-\pi^*$ (ILCT)
				HOMO - LUMO	-0.13362	ILCT
				HOMO-1 - LUMO+2	0.10574	ILCT ($\pi-\pi^*$)
	3.0309	S_0-S_3	0.0288	HOMO-2 - LUMO	0.45799	$\pi-\pi^*$
				HOMO-1 - LUMO	-0.41071	ILCT
				HOMO - LUMO+1	0.26098	ILCT ($\pi-\pi^*$)
	3.0730	S_0-S_4	0.0163	HOMO - LUMO+2	0.50494	$\pi-\pi^*$ (ILCT)
				HOMO-1 - LUMO+1	-0.26644	$\pi-\pi^*$ (ILCT)
				HOMO-2 - LUMO	-0.23510	$\pi-\pi^*$
				HOMO-1 - LUMO+2	-0.15914	ILCT ($\pi-\pi^*$)
				HOMO-1 - LUMO	-0.13076	ILCT
				HOMO - LUMO+1	0.12298	ILCT ($\pi-\pi^*$)

4.7.2 $\text{Eu}(\text{NH}_2\text{Q})_3(\text{X})_3$ (X=DCM or ETOH)

The spectra of isomer 2 of the $\text{Eu}(\text{NH}_2\text{Q})_3(\text{X})_3$ (X=DCM or ETOH) complex shows 2 peaks which are blue shifted if compared to the gas phase calculation (2.59 eV in ETOH, 2.47 eV in DCM and 2.42 eV in gas phase for the low energy absorption band). Transitions of the solvent spectra and their attribution are given in Tables 4.17 - 4.18. As seen before for the unsubstituted complex, the first band in the ETOH spectrum is a result of four transitions (S_0 - S_1 , S_0 - S_3 , S_0 - S_4 and S_0 - S_5) from which the first one is a pure HOMO - LUMO excitation. In case of the DCM spectrum also mixing of HOMO - LUMO+1 and HOMO-1 - LUMO+1 excitations occurs. In all cases the HOMO - LUMO excitation is a ILCT, however, the HOMO - LUMO+1 excitation in case of the DCM solvent calculation has $\pi - \pi^*$ attribution and makes 40% of the transition. Therefore the S_0 - S_1 transition shows the highest oscillator strength with $f=0.0615$ a.u. in the DCM calculation. In the gas phase calculation different excitations give contribution to the S_0 - S_1 transition from which the second and third most important have a $\pi - \pi^*$ characteristic and the oscillator strength is with $f=0.0605$ a.u. close to the DCM calculated one. In case of the ETOH calculation the pure HOMO - LUMO excitation is a ILCT and shows therefore a diminished oscillator strength ($f=0.0187$ a.u.). In case of the ETOH calculation one interesting point should be mentioned. The HOMO-3 orbital is the only one under all investigated calculations which shows an orbital on the solvent molecule as depicted in figure 4.55.

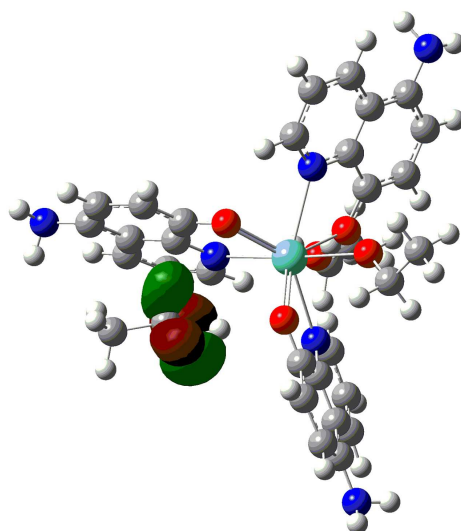


Figure 4.55: HOMO-3 orbital of isomer 2 of the $\text{Eu}(\text{NH}_2\text{Q})_3(\text{ETOH})_3$ complex. Calculated on UB3LYP/TZVP/52MWB level of theory.

Excitation from the HOMO-3 orbital goes therefore from the solvent to the complex. However, this excitation is only seen for the S_0 - S_{12} transition which gives rise to the high energy absorption band at 3.66 eV.

Table 4.17: Absorption energies, transition energies and band attribution of $\text{Eu}(\text{NH}_2\text{Q})_3(\text{EtOH})_3$ complex for isomer 2. Calculation on UB3LYP/TZVP/52MWB level of theory. If more than one attribution is present, the less important one is set in parenthesis

$E_{\text{abs.}}$ [eV]	$E_{\text{trans.}}$ [eV]	Transition	f [a.u.]	Contribution	CI coefficient [a.u.]	Attribution
2.59	2.2807	S_0 - S_1	0.0187	HOMO - LUMO	0.69152	ILCT
	2.5479	S_0 - S_3	0.0456	HOMO-2 - LUMO	0.65008	π - π^*
HOMO-1 - LUMO				0.11172	ILCT	
2.6124	S_0 - S_4	0.0689	HOMO - LUMO+2	0.57554	π - π^*	
			HOMO - LUMO+1	0.26986	ILCT	
			HOMO-1 - LUMO+1	0.14034	π - π^*	
			HOMO-1 - LUMO+2	-0.12762	ILCT	
2.6656	S_0 - S_5	0.0275	HOMO-1 - LUMO+1	0.59699	π - π^*	
			HOMO - LUMO+2	-0.21775	π - π^*	
			HOMO-1 - LUMO+2	-0.13081	ILCT	
			HOMO - LUMO+1	0.12565	ILCT	
3.66	3.6367	S_0 - S_{12}	0.0258	HOMO - LUMO+5	0.60211	π - π^*
				HOMO-3 - LUMO+2	-0.20165	ILCT
				HOMO-2 - LUMO+3	-0.15152	π - π^*
				HOMO - LUMO+4	-0.12768	ILCT
				HOMO - LUMO	-0.10535	ILCT
3.6527	S_0 - S_{13}	0.0559	HOMO-2 - LUMO+3	0.61219	π - π^*	
			HOMO-8 - LUMO	0.21751	π - π^*	
			HOMO - LUMO+5	0.14511	π - π^*	
			HOMO-1 - LUMO+4	0.10458	π - π^*	
3.6878	S_0 - S_{14}	0.0615	HOMO-1 - LUMO+4	0.58198	π - π^*	
			HOMO-4 - LUMO+1	0.22848	ILCT	
			HOMO - LUMO+4	0.22191	ILCT	

Table 4.18: Absorption energies, transition energies and band attribution of $\text{Eu}(\text{NH}_2\text{Q})_3(\text{DCM})_3$ complex for isomer 2. Calculation on UB3LYP/TZVP/52MWB level of theory. If more than one attribution is present, the less important one is set in paranthesis

$E_{\text{abs.}}$ [eV]	$E_{\text{trans.}}$ [eV]	Transition	f [a.u.]	Contribution	CI coefficient [a.u.]	Attribution
2.47	2.4426	S_0-S_1	0.0615	HOMO - LUMO	0.47006	ILCT
				HOMO - LUMO+1	-0.44932	$\pi-\pi^*$
				HOMO-1 - LUMO+1	-0.13919	ILCT
	2.5302	S_0-S_2	0.0415	HOMO-1 - LUMO	0.55164	$\pi-\pi^*$
				HOMO - LUMO+1	-0.31724	ILCT
				HOMO - LUMO	-0.16502	ILCT
				HOMO-1 - LUMO+1	0.10853	ILCT
3.51	3.2219	S_0-S_7	0.0196	HOMO - LUMO+2	0.69972	ILCT
	3.4338	S_0-S_9	0.0789	HOMO-2 - LUMO+2	0.65286	$\pi-\pi^*$
	3.6222	S_0-S_{10}	0.0348	HOMO - LUMO+4	0.58552	$\pi-\pi^*$
				HOMO-1 - LUMO+3	0.21616	$\pi-\pi^*$
				HOMO-5 - LUMO+1	-0.20430	$\pi-\pi^*$
				HOMO - LUMO+3	-0.11614	ILCT
				HOMO-5 - LUMO	0.10119	ILCT
	3.6310	S_0-S_{11}	0.0454	HOMO - LUMO+3	0.46961	ILCT
				HOMO-1 - LUMO+3	-0.39240	$\pi-\pi^*$
				HOMO - LUMO+2	0.21764	ILCT
				HOMO-4 - LUMO	-0.17828	ILCT

4.7.3 $\text{Eu}(\text{NO}_2\text{Q})_3(\text{X})_3$ (X=ETOH, DCM)

The $\text{Eu}(\text{NO}_2\text{Q})_3(\text{X})_3$ (X=ETOH, DCM) complex shows one band in the absorption spectrum of isomer 2. Same as in the before discussed spectra shows the band a hypsochromic shift if compared to the gas phase spectrum of the corresponding $\text{Eu}(\text{NO}_2\text{Q})_3$ complex (3.17 eV ETOH, 3.13 eV DCM and 3.07 eV gas phase). However in case of the NO_2 substituted complex, the S_0-S_1 transition is a pure HOMO - LUMO ILCT transition in the gas phase and DCM calculation while in the ETOH calculation also a HOMO - LUMO+1 ILCT with $\pi-\pi^*$ mixing excitation can be seen. This would let us expect that the different transitions exhibit a similar oscillator strength, however, the gas phase calculation shows the highest oscillator strength ($f=0.09711$ a.u.) followed by the DCM calculation ($f=0.0299$ a.u.) and the ETOH calculation shows the lowest oscillator strength with $f=0.0159$ a.u. Reason is that excitation in the

gas phase calculation goes from ligand 1 to ligand 3, while in the solvent calculation the HOMO orbital is expanded delocalised over ligand 1 and 2 respectively. Transitions and their attribution are given in Tables 4.19 - 4.20.

Table 4.19: Absorption energies, transition energies and band attribution of $\text{Eu}(\text{NO}_2\text{Q})_3(\text{ETOH})_3$ complex for isomer 2. Calculation on UB3LYP/TZVP/52MWB level of theory. If more than one attribution is present, the less important one is set in paranthesis

$E_{\text{abs.}}$ [eV]	$E_{\text{trans.}}$ [eV]	Transition	f [a.u.]	Contribution	CI coefficient [a.u.]	Attribution
3.17	2.9564	S_0-S_1	0.0159	HOMO-1 - LUMO	0.65810	ILCT
				HOMO - LUMO+1	-0.23682	ILCT ($\pi-\pi^*$)
	3.1138	S_0-S_3	0.1274	HOMO - LUMO+2	0.56831	ILCT ($\pi-\pi^*$)
				HOMO-1 - LUMO+1	0.31230	ILCT ($\pi-\pi^*$)
				HOMO - LUMO+4	-0.13584	ILCT ($\pi-\pi^*$)
				HOMO-2 - LUMO	0.10729	$\pi-\pi^*$
	3.1808	S_0-S_4	0.3226	HOMO-2 - LUMO	0.46833	$\pi-\pi^*$
				HOMO-1 - LUMO+1	-0.39048	ILCT ($\pi-\pi^*$)
				HOMO-1 - LUMO+2	-0.16601	$\pi-\pi^*$ (ILCT)
				HOMO-2 - LUMO+3	0.13676	$\pi-\pi^*$ (ILCT)
	3.3337	S_0-S_6	0.1290	HOMO-1 - LUMO+2	0.56474	ILCT ($\pi-\pi^*$)
				HOMO-1 - LUMO+1	-0.25255	ILCT ($\pi-\pi^*$)
				HOMO-1 - LUMO+5	0.14631	$\pi-\pi^*$ (ILCT)
				HOMO - LUMO+2	0.12529	ILCT ($\pi-\pi^*$)

Table 4.20: Absorption energies, transition energies and band attribution of $\text{Eu}(\text{NO}_2\text{Q})_3(\text{DCM})_3$ complex for isomer 2. Calculation on UB3LYP/TZVP/52MWB level of theory. If more than one attribution is present, the less important one is set in paranthesis

$E_{\text{abs.}}$ [eV]	$E_{\text{trans.}}$ [eV]	Transition	f [a.u.]	Contribution	CI coefficient [a.u.]	Attribution
3.13	2.9451	S_0-S_1	0.0299	HOMO - LUMO	0.69501	ILCT
	3.0466	S_0-S_2	0.1511	HOMO-1 - LUMO HOMO - LUMO+1	0.58962 0.32356	ILCT ILCT ($\pi-\pi^*$)
	3.0746	S_0-S_3	0.1152	HOMO - LUMO+1 HOMO-1 - LUMO	0.58434 -0.36112	$\pi-\pi^*$ (ILCT) ILCT
	3.1633	S_0-S_4	0.1707	HOMO-2 - LUMO HOMO-1 - LUMO+1 HOMO-2 - LUMO+3	0.49528 0.40931 -0.10893	$\pi-\pi^*$ ILCT ($\pi-\pi^*$) $\pi-\pi^*$
	3.1955	S_0-S_5	0.0841	HOMO - LUMO+2 HOMO-1 - LUMO+1 HOMO-2 - LUMO	0.45295 -0.44041 0.24928	$\pi-\pi^*$ (ILCT) $\pi-\pi^*$ (ILCT) $\pi-\pi^*$

4.7.4 $\text{Eu}(\text{Q})_4(\text{X})_2$ ($\text{X}=\text{H}_2\text{O}$ or ETOH)

The spectra of the $\text{Eu}(\text{Q})_4(\text{X})_2$ ($\text{X}=\text{H}_2\text{O}$ or ETOH) are depicted in Figure 4.56. The spectra show a main band at 3.01 eV (409 nm, ETOH) and 3.06 eV (402 nm, H_2O) and a smaller peak at 2.33 eV (529 nm, ETOH) and 3.36 eV (524 nm, H_2O). In both spectra the important contribution to the smaller peak at lower energy comes from a S_0-S_4 transition. In case of the H_2O spectrum the S_0-S_4 transition (2.3730 eV, $f=0.0232$ a.u.) results from the HOMO-3 - LUMO excitation which is a $\pi-\pi^*$ excitation from the phenoxy part of ligand 1 to the pyridino part. The second contribution comes from a HOMO-2 - LUMO excitation which is an ILCT from the phenoxy part of ligand 3 to ligand 1. The second band at higher energy is composed of five transitions. The strongest is the S_0-S_5 transition (2.9570 eV, $f=0.0609$ a.u.) and results mainly from a HOMO-1 - LUMO+1 ILCT and HOMO-1 - LUMO+2 $\pi-\pi^*$ excitation. The HOMO-1 - LUMO+1 excitation goes from the phenoxy part of ligand 2 to the pyridino part of ligand 3. The HOMO-1 - LUMO+2 excitation is a $\pi-\pi^*$ excitation from the phenoxy part of ligand 2 to the pyridino part of the same ligand. A small contribution of ligand 3 in the LUMO+2 orbital can be seen, so that a small contribution from an ILCT is present. The other transitions showing a mentionable higher oscillator strength are the S_0-S_6 , the S_0-S_8 and S_0-S_9 transition which show excitations from HOMO and HOMO-2 to higher lying unoccupied orbitals such as the LUMO+2 and LUMO+4 orbital. As seen in the explicit solvent model calculations before, the orbitals are located on one ligand only and mixed ILCT

and π - π^* transitions are rare. However, since four conjugated ligand systems are present in the structure, ILCT is by far the most important excitation in this complex, which can be seen in a decreased oscillator strength of the transitions.

The **ETOH** spectrum shows less transition lines in the area of the energetically higher lying peak. Most of the transition lines are shifted to lower energy if compared to the H₂O spectrum and so does the absorption band, although the shift is with 0.03 eV (weak band) and 0.06 eV (strong absorption peak) rather small.

The first noteworthy transition is same as in the H₂O spectrum. Main contribution to the **S₀-S₄** is an HOMO-3 - LUMO excitation as seen for the H₂O complex before. However, comparing the H₂O and ETOH calculation shows that the sign of the orbitals is inverted. The contributions to the main absorption band come from S₀-S₅, S₀-S₆, S₀-S₇, S₀-S₈ and S₀-S₉ transitions. The highest oscillator strength shows again the S₀-S₅ transition at 2.8898 eV (f= 0.0604 a.u.). However, for this transitions the contributions are different then in case of the H₂O calculation. Main contribution comes from a HOMO - LUMO+2 transition, going from the phenoxy part of ligand 2 to the pyridino part of the same ligand and is attributed as π - π^* excitation. This excitation corresponds to the HOMO-1 - LUMO+2 excitation in the H₂O calculation. The second contribution is the HOMO - LUMO+1 excitation which is an ILCT from ligand 2 to ligand 3 and corresponds to the HOMO-1 - LUMO+1 excitation in the H₂O calculation. The last contribution to the S₀-S₅ transition is the HOMO-1 - LUMO+2 excitation which is an ILCT going from ligand 3 to ligand 2.

The other transitions are excitations from HOMO and lower lying occupied orbitaly (HOMO-1 and HOMO-2) to the LUMO+1 and LUMO+2 orbitals. Interestingly none of the molecular orbitals is located on the solvent molecules. The most important orbitals are depicted in Figures 4.57 - 4.58. Transitions and their attribution is listed in Tables 4.21 and 4.22.

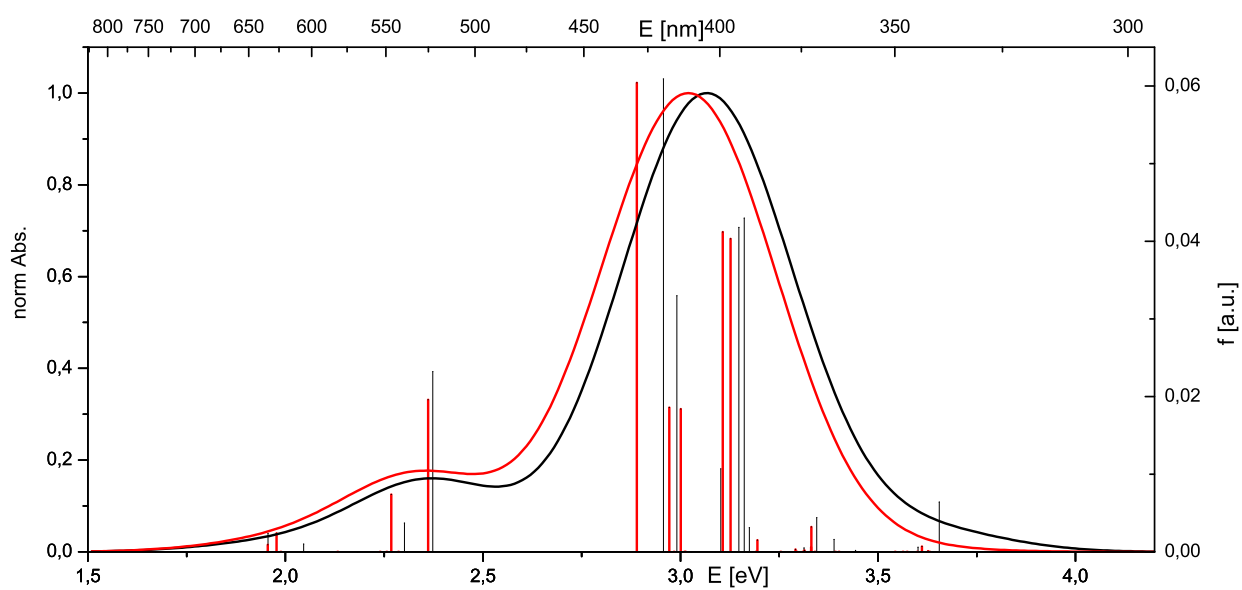


Figure 4.56: Calculated spectra of the $\text{EuQ}_4(\text{H}_2\text{O})_2$ (black) and $\text{EuQ}_4(\text{ETOH})_2$ (red) complexes. Vertical lines show the calculated transitions and correspond to the ETOH calculation (blue lines) and the H_2O calculation (black lines) respectively. Calculation on UB3LYP/TZVP/52MWB level of theory.

Table 4.21: Absorption energies, transition energies and band attribution of $\text{EuQ}_4(\text{H}_2\text{O})_2$ complex. Calculation on UB3LYP/TZVP/52MWB level of theory.

$E_{\text{abs.}}$ [eV]	$E_{\text{trans.}}$ [eV]	Transition	f [a.u.]	Contribution	CI coefficient [a.u.]	Attribution
2.36	2.3730	S_0 - S_4	0.0299	HOMO-3 - LUMO	0.64678	π - π^*
				HOMO-2 - LUMO	-0.15717	ILCT
3.06	2.9570	S_0 - S_5	0.0609	HOMO-1 - LUMO+1	0.48234	ILCT
				HOMO-1 - LUMO+2	-0.45701	ILCT
	2.9911	S_0 - S_6	0.0330	HOMO - LUMO+1	0.67350	ILCT
				HOMO-2 - LUMO+1	-0.11018	π - π^*
				HOMO - LUMO+2	0.10797	ILCT
	3.14477	S_0 - S_8	0.0481	HOMO-2 - LUMO+1	0.54462	π - π^*
				HOMO - LUMO+3	-0.24023	π - π^*
				HOMO - LUMO+4	0.21323	ILCT
				HOMO - LUMO+1	0.14299	ILCT
				HOMO-1 - LUMO+1	0.11464	ILCT
				HOMO-1 - LUMO+2	0.11394	π - π^*
	3.1615	S_0 - S_9	0.0430	HOMO - LUMO+3	0.42430	π - π^*
				HOMO - LUMO+4	-0.37738	ILCT
				HOMO-2 - LUMO+1	0.30417	π - π^*
				HOMO-1 - LUMO+2	0.10914	π - π^*

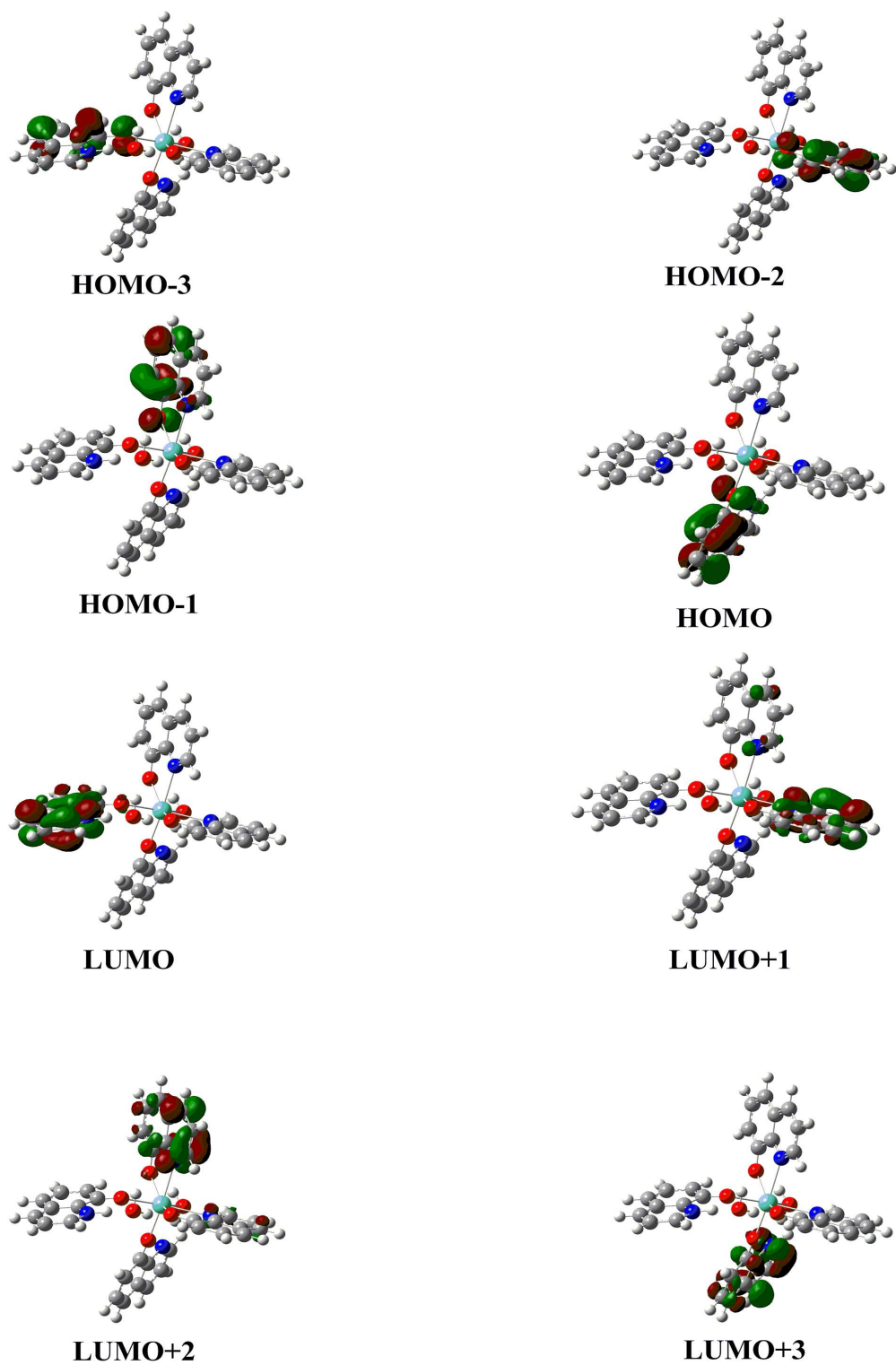


Figure 4.57: Molecular orbitals of the $\text{EuQ}_4(\text{H}_2\text{O})_2$ complex. Calculated on UB3LYP/TZVP/52MWB level of theory.

Table 4.22: Absorption energies, transition energies and band attribution of EuQ₄(EtOH)₂ complex. Calculation on UB3LYP/TZVP/52MWB level of theory.

$E_{\text{abs.}}$ [eV]	$E_{\text{trans.}}$ [eV]	Transition	f [a.u.]	Contribution	CI coefficient [a.u.]	Attribution
2.33	2.3612	S ₀ -S ₄	0.0196	HOMO-3 - LUMO	0.63261	π - π^*
				HOMO-2 - LUMO	0.22067	ILCT
3.01	2.8898	S ₀ -S ₅	0.0604	HOMO - LUMO+2	0.57816	π - π^*
				HOMO - LUMO+1	-0.30445	ILCT
				HOMO-1 - LUMO+2	0.12583	ILCT
2.9720	S ₀ -S ₆	0.0186	0.0186	HOMO-1 - LUMO+1	0.046878	ILCT
				HOMO - LUMO+1	-0.45069	ILCT
				HOMO - LUMO+2	-0.19656	π - π^*
				HOMO-2 - LUMO+1	0.13122	π - π^*
3.0009	S ₀ -S ₇	0.0184	0.0184	HOMO-1 - LUMO+1	0.48526	ILCT
				HOMO - LUMO+1	0.44192	ILCT
				HOMO - LUMO+2	0.22405	π - π^*
3.1073	S ₀ -S ₈	0.0412	0.0412	HOMO-1 - LUMO+3	0.61177	π - π^*
				HOMO - LUMO+3	-0.19309	ILCT
				HOMO-1 - LUMO+1	0.13204	ILCT
3.1268	S ₀ -S ₉	0.0403	0.0403	HOMO-2 - LUMO+1	0.64821	π - π^*
				HOMO-1 - LUMO+1	-0.12604	ILCT

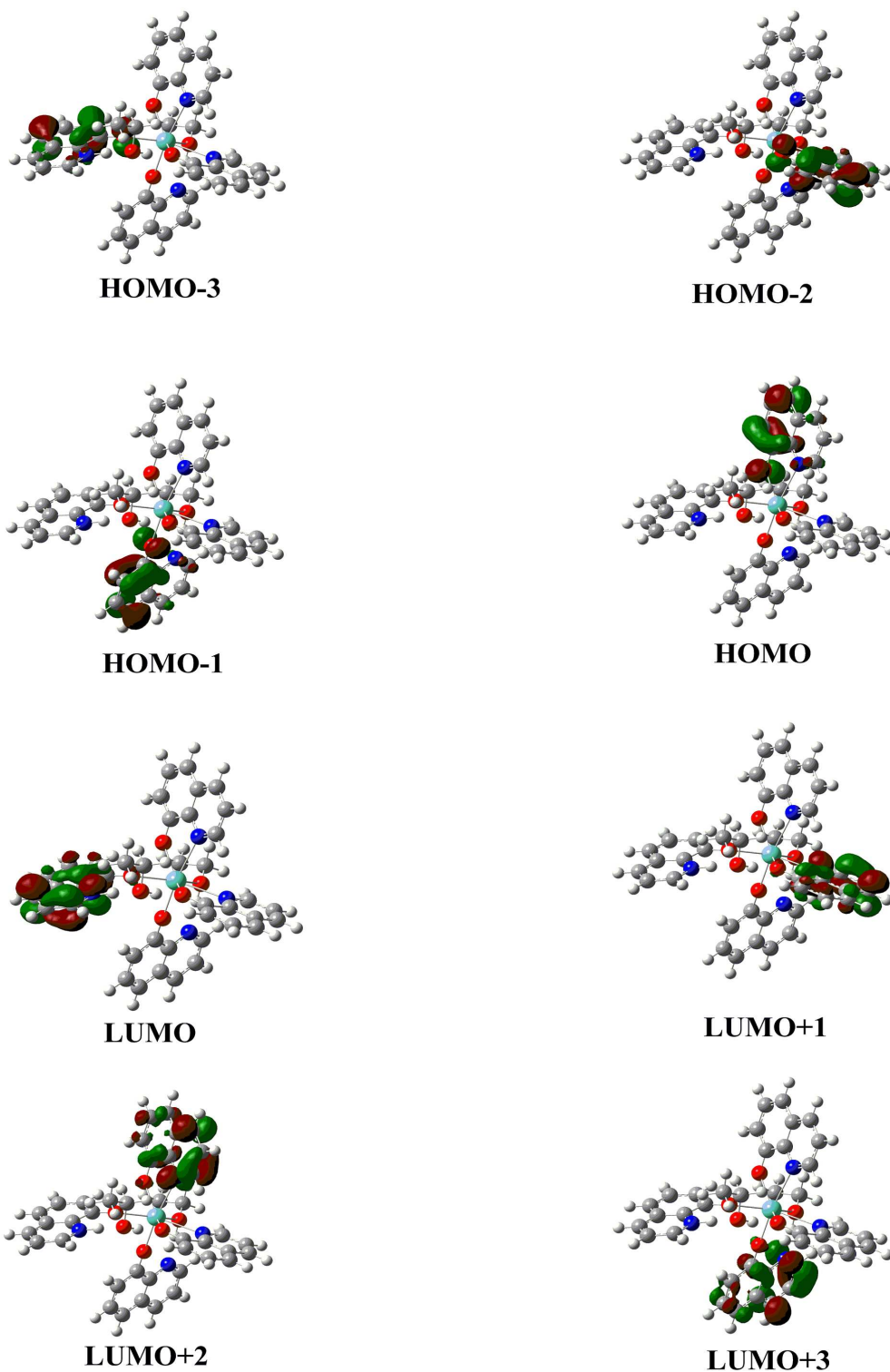


Figure 4.58: Molecular orbitals of the $\text{EuQ}_4(\text{ETOH})_2$ complex. Calculated on UB3LYP/TZVP/52MWB level of theory.

4.8 Jablonski Diagram for Complex Structures

The excitation of most interest is the HOMO - LUMO excitation which gives the strongest contribution to the S_0 - S_1 transition in the complex spectra. In Figure 4.59 the HOMO - LUMO gap of the different complexes is depicted. Although four complexes are by far a too small number to find a trend regarding the influence of the substituent on the HOMO - LUMO gap energy, one can clearly see that the HOMO orbital of the complex bearing the electron donating NH_2 group lies at energetically higher compared to the unsubstituted EuQ_3 complex. At the same time the energy of the LUMO orbital stays almost unaltered, resulting in a smaller HOMO - LUMO gap (2.97 eV) upon NH_2 substitution. For the electron pulling HSO_3 and NO_2 substituents both the LUMO and HOMO orbitals are lower in energy by different amounts if compared to the unsubstituted complex. However, the HOMO - LUMO energy is the same as in case of the unsubstituted complex in case of the HSO_3 substituted complex, or slightly smaller in the NO_2 substituted one.

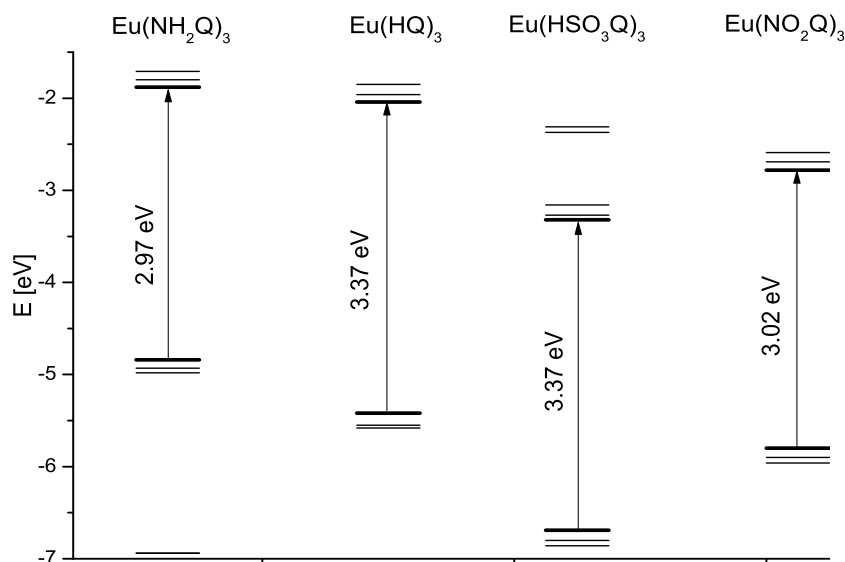


Figure 4.59: HOMO - LUMO energies of isomer 2 of the different complexes. Calculation in gas phase on UB3LYP/TZVP/52MWB level of theory.

As described in chapter 4.6 The S_0 - S_1 transition depends also on other excitations, such as excitations going from lower lying occupied orbitals to higher lying unoccupied orbitals. The trend for the S_0 - S_1 energies of the different complex does therefore not follow necessarily the trend observed for the HOMO - LUMO gap. Figure 4.60 depicts the S_0 - S_1 energies for the different complexes in gas phase and in solution.

The gas phase calculation gives S_0 - S_1 energies which are underestimated if compared to the solvent models. Applying the IEF-PCM solvent model gives similar energies for ETOH and DCM calculations. This was also discussed before for the complex spectra, where the energetically lower lying absorption

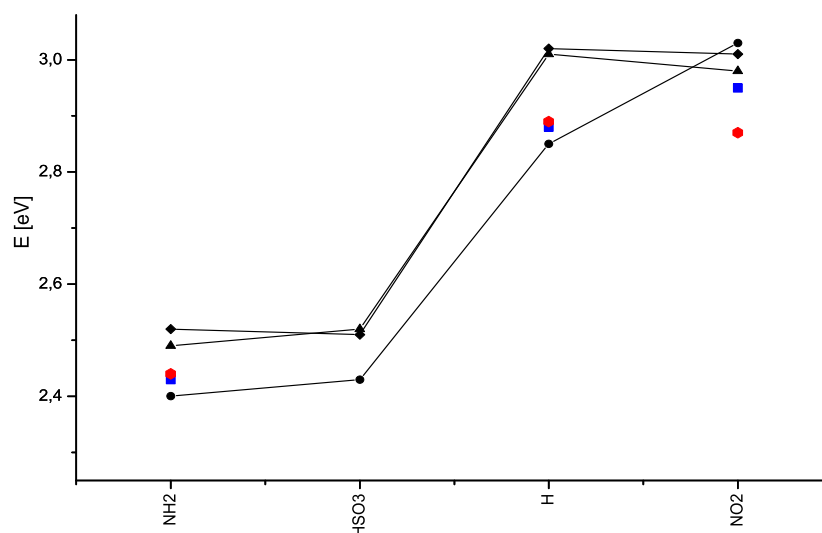


Figure 4.60: Energies of isomer 2 of the S_0 - S_1 energies of the different complexes in gas phase and IEF-PCM and explicit solvent model. Calculated on UB3LYP/TZVP/52MWB level of theory.

band shows only a small shift between the gas phase and the IEF-PCM spectra. S_0 - S_1 energies calculated with the explicit solvent model show energies which lie between the IEF-PCM and the gas phase energies. An exception is the $\text{Eu}(\text{NO}_2)_3(\text{EtOH})_3$ calculation which underestimates the energy. Here the reason could be a stronger influence of the more bulky EtOH solvent molecule on the geometry of the complex. The NH_2 substituted complex shows the lowest energy, while the strong electron pulling NO_2 substituent shows the highest S_0 - S_1 energy. However, all calculated complexes absorb in the visible range of the spectrum.

Two triplet energies (T_{1S^*} and T_{1T}) were calculated for the complex structures. The T_{1S^*} energy, which corresponds to an optimised singlet geometry. The triplet energy is calculated using a singlet wavefunction in the excitation calculation, that means the coefficients are not optimised as in calculations which employ a triplet wavefunction. The second triplet energy is the T_{1T} energy, which is gained from a single point calculation based on an optimised triplet state geometry using a optimised triplet wavefunction. Figure 4.61 displays the different energies in form of a Jablonski-Diagram.

Figure 4.62 depicts the different triplet energies for isomer 2 of the complexes calculated in gas phase. It can clearly be seen that the triplet energies follow the trend of the S_0 - S_1 energies and show the lowest energy for the NH_2 substituted ligand and the highest for the NO_2 substituted ligand. However, none of the calculated triplet energies lies above the 5D_0 energy of the Eu(III) ion. It is known that the 5D_0 energy of the Eu ion can change slightly depending on the ligands in the complex [49]. However, the difference is in the range of 0.03 eV which is smaller than the deviation seen for the triplet energies of

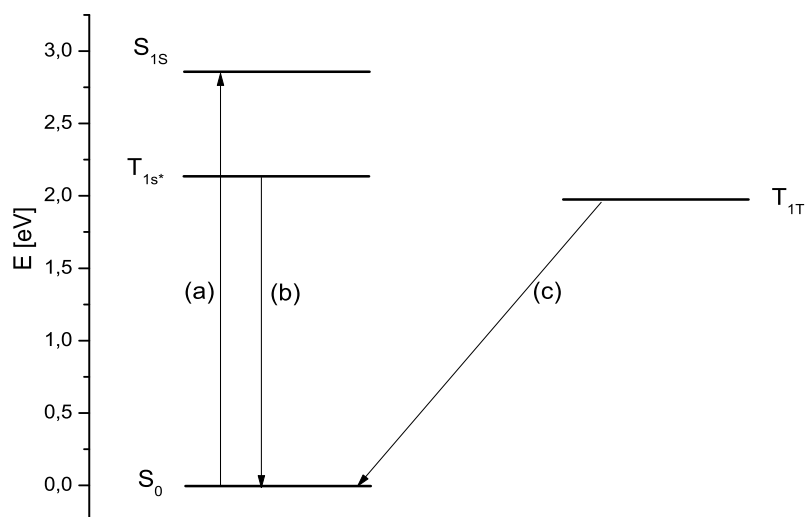


Figure 4.61: Jablonski diagram for isomer 2 of the EuQ_3 complex. Calculated in gas phase on UB3LY/TZVP/52MWB level of theory. (a) Absorption energy for the S_0 - S_1 transition, (b) vertical phosphorescence from T_{1S^*} to S_0 , (c) adiabatic phosphorescence from T_{1T} to S_0 .

the NH_2 or HSO_3 complexes.

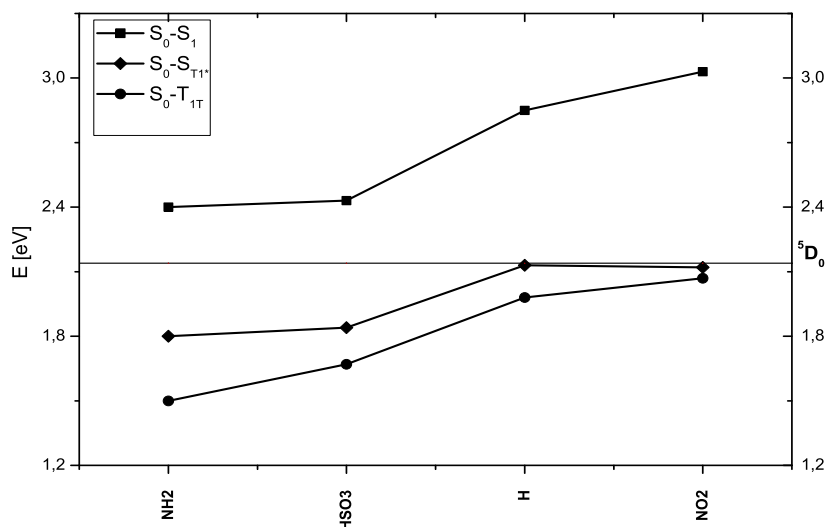


Figure 4.62: Triplet state energies and S_0 - S_1 energy of the different complexes in gas phase. Calculated on UB3LY/TZVP/52MWB level of theory. The vertical line represents the 5D_0 energy of the Eu(III) ion.

In Figures 4.63 and 4.64 the triplet energies of isomer 2 of the different complexes is depalyed for the IEF-PCM calculation. While the T_{1T} energy seems not to be effected in case of the DCM calculation (except the unsubstituted complex), the T_{1S^*} energy is shifted approximately 0.1 eV to higher energies if compared to the gas phase triplet energies. Only the NO_2 substituted complex shows a smaller shift with 0.03 eV to higher energy if compared with the gas phase spectrum. Interestingly the energies of the

unsubstituted complex show the biggest change in energy if the IEF-PCM solvent model is applied. In the ETOH calculation both, the T_{1S^*} and T_{1T} energies are shifted 0.10 eV to higher energy if compared to the gas phase calculation. Exception is again the NO_2 substituted complex, which shifts to 0.05 eV lower energy if compared to the gas phase calculation.

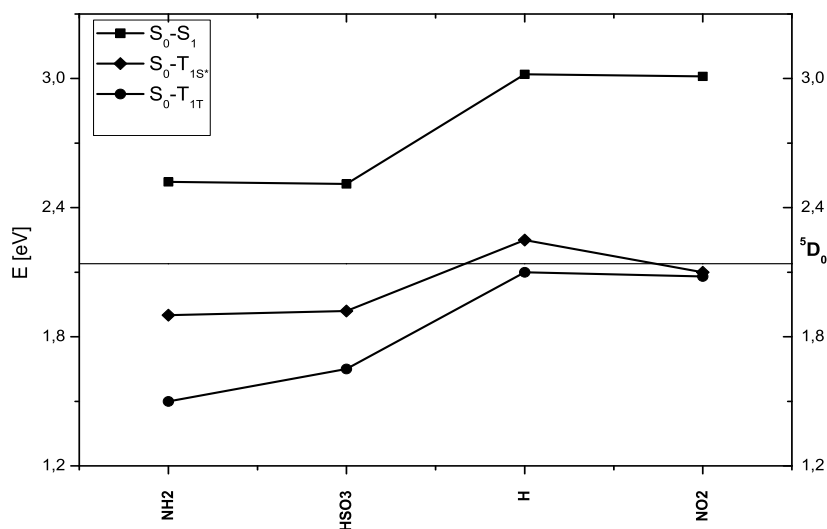


Figure 4.63: Triplet state energies and S_0-S_1 energy of the different complexes calculated with IEF-PCM model for DCM. Calculation on UB3LY/TZVP/52MWB level of theory. The vertical line represents the 5D_0 energy of the Eu(III) ion.

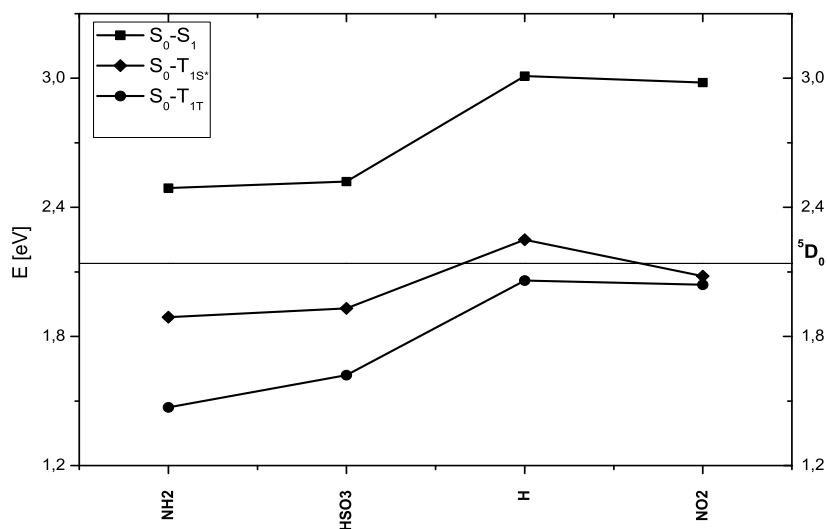


Figure 4.64: Triplet state energies and S_0-S_1 energy of the different complexes calculated with IEF-PCM model for ETOH. Calculation on UB3LY/TZVP/52MWB level of theory. The vertical line represents the 5D_0 energy of the Eu(III) ion.

Figure 4.65 shows the energy level of the occupied and unoccupied orbitals for isomer 2 of four different

complexes in gas phase. Depending on the electron pulling or pushing ability of the substituent the orbital energies are shifted. In case of the donor substituent NH_2 the HOMO and LUMO orbital is shifted towards higher energy if compared to the unsubstituted complex. Same applies for the SOMO orbital in the triplet state, which lies energetically higher than the SOMO orbital of the unsubstituted species. For the acceptor substituents (HSO_3 and NO_2) the orbital energies are lowered for the HOMO and LUMO (singlet groundstate) and for the SOMO orbital (triplet state) if compared to the unsubstituted complex. Same as could be seen before for the ligand system, the lowering of the frontier orbitals in the singlet state is more distinct for the HOMO orbital in case of the acceptor substituents.

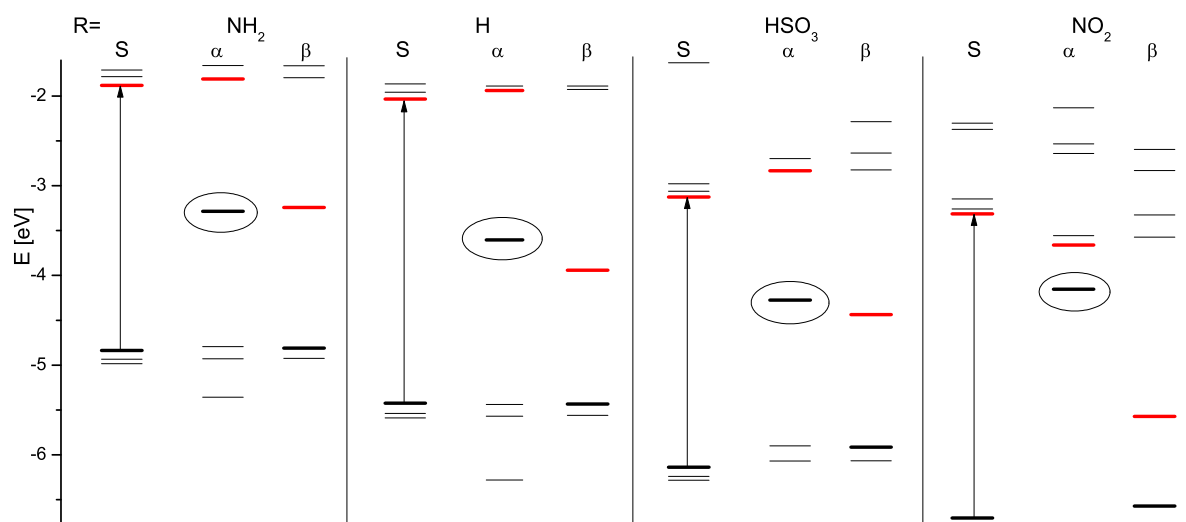


Figure 4.65: HOMO (black), LUMO (red) and SOMO (circled) orbitals of the 5 substituted EuQ_3 complexes. Calculation in gas phase on UB3LYP/52MWB/TZVP level of theory.

4.9 Conclusion

The main aim of the work was to find a method which computes structural and energetic properties of 8-hydroxyquinoline ligands and Eu-8-oxoquinolinolate complexes with high accuracy. Furthermore the question which triplet state energy has to be computed to get reliable values close to the experimental triplet state energy of the complexes has to be answered. The influence of donor and acceptor substituents on the absorption behaviour and shift of HOMO or SOMO and LUMO orbitals and interrelated changes in the structure of the molecules was another aspect which was matter of investigation. The most important question however is the question for a correlation between the energies calculated for the ligands and the complex structures. A good correlation of those energies would make it dispensable to calculate the complex structures and would make it possible to predict energies of the complexes just with results obtained from the ligand calculations.

4.9.1 Error introduced in the calculation

As mentioned before DFT method was used exhaustingly for similar problems before [17, 18, 19]. To validate the method, results are compared to experimental data. Regarding the structure of the ligands, the calculated structure parameters of the unsubstituted 8-hydroxyquinoline are compared to structure data from an XRD experiment. The average error for the bond length is 0.01 Å and for the angles 1.96°. The difference between experimental and calculated results are depicted in Table 4.23.

Table 4.23: Error of the calculated structure in 8-hydroxyquinoline. XRD structure values versus calculated values. Increased values in the calculated structure are accented bold.

Type of bond	XRD bond length [Å]	Error [Å]	Error [%]
C(1)-C(2)	1.41	0.02	1.4
C(1)-N(10)	1.38	0.02	1.5
C(2)-O(11)	1.39	0.03	2.2
Type of angle	XRD angle [°]	Error [°]	Error [%]
C(2)-C(1)-N(10)	119.1	0.45	0.4
C(1)-C(2)-C(3)	121.2	1.41	1.2
C(1)-C(2)-O(11)	120.3	1.92	1.6

The maximum error of 2.2% for the bond lengths and 1.6% for the angles shows that DFT method in combination with B3LYP functional and 6-31G*/52MWB basis set is accurate enough to calculate optimised structures. Generally the structure parameters are underestimated with the applied method.

An important information regarding the quality of the results can be obtained by comparing the experimental and calculated results for the vertical excitation energies. Table 4.24 lists the error for the experimental and calculated absorption energies of the quinoline ligands.

Table 4.24: S_0 - S_1 energies for the substituted quinoline ligands and average error experiment vs. calculation Substitution in 5-position of the quinolone backbone.

Ligand and Solvent	Abs. _{exp} [eV]	Abs. _{calc} ^{G.P.} [eV]	Abs. _{calc} ^{IEF-PCM} [eV]
H in ETOH	3.92	3.84	3.94
Error [%]		2.00	0.51
	5.07	5.33	5.50
Error [%]		5.12	8.48
CHO in ETOH	3.13	3.61	3.46
Error [%]		15.30	10.50
	3.75	3.82	3.95
Error [%]		1.87	5.33
	4.73	4.75	4.92
Error [%]		0.42	4.01
	5.14	5.19	5.29
Error [%]		0.97	2.92
NO₂ in ETOH	3.49	3.41	3.57
Error [%]		2.29	2.29
	4.43	4.40	4.92
Error [%]		0.68	11.06
	5.19	5.48	5.68
Error [%]		5.59	9.44
NO₂ in DCM	3.49	3.41	3.57
Error [%]		2.29	2.29
	4.36	4.41	4.92
Error [%]		1.15	12.84
	5.16	5.48	5.68
Error [%]		6.20	10.08

Interestingly the energies for the NO₂ substituted quinoline ligands show a bigger deviation from the experimental results. However those for the unsubstituted ligand come quite close to the expected values. An error of 13% as seen for the NO₂ calculation in DCM might seem high on the first sight but

considering solvtn effects in the calculation increases the quality of the results in all cases and drops the error below 10% which is acceptable. As can be seen in Table 4.24, the method overestimates the absorption energies. The exceptions are the transitions for the 8-hydroxyquinoline and the 5-nitro-8-hydroxyquinoline. Over all, the method gives values which are reproduceable and can predict energies for other ligand systems.

Table 4.25: Average error of the singlet and triplet energies for the complexes. Bold values show a hypsochromic shift in the spectra.

Complex	Exp. transition	E_{exp} [eV]	E_{GP} [eV]	$E_{\text{DCM}}^{\text{PCM}}$ [eV]	$E_{\text{ETOH}}^{\text{PCM}}$ [eV]	$E_{\text{DCM}}^{\text{Expl.}}$ [eV]	$E_{\text{ETOH}}^{\text{Expl.}}$ [eV]	Calc. Transition
H	S_0-S_1	3.35	2.85	3.02	3.01	2.88	2.84	S_0-S_1 (ILCT)
	Error [%]		14.9	9.9	10.2	14.0	15.2	
	T_1-S_0	2.20	2.13	2.25	2.25	2.17	2.17	$T_{1S^*}-S_0$
Error [%]		3.2	2.3	2.3	1.4	1.4		
			1.98	2.1	2.06	2.61	2.02	$T_{1T}-S_0$
Error [%]			10.0	4.6	6.4	18.6	8.2	
NO₂	S_0-S_1	2.79	3.03	3.01	2.98	2.95	2.75	S_0-S_1 (ILCT)
	Error [%]		8.6	7.9	6.8	5.7	1.4	
HSO₃	S_0-S_1 ($\pi-\pi^*$)	3.35	2.43	2.51	2.52			S_0-S_1 (ILCT/$\pi-\pi^*$)
	Error [%]		27.6	25.1	24.87			
	S_0-S_1 (ILCT)	3.18	2.43	2.51	2.52			S_0-S_1 (ILCT/$\pi-\pi^*$)
Error [%]		23.6	21.0	20.8				

In case of the EuQ₃ complexes the error for the gas phase calculations is with > 10% quite high. Applying the IEF-PCM solvent model however brings the error down to less than 10% which is acceptable. Comparing the error for the different complex systems shows that the difference to the experimental results is reproduceable and the error is of systematic kind. The explicit solvent calculations show an error which scatter. Reason is that only one structure with explicit solvent was computed. A more distinct investigation of the solvent influence by computing different structures with explicit solvent molecules would be important to be able to comment on singlet and triplet state energies. The HSO₃ derivative shows an error of more than 20% in most cases. Here the protonated HSO₃ group was used for the calculation. In the experiment (see [49]) the SO₃⁻ group is coordinated by Eu(III) ions [52]. This results in a different charge distribution on the SO₃⁻ group than in the the protonated HSO₃ group.

For the unsubstituted EuQ₃ complex triplet state energies are reported [49]. It is interesting to know which if the T_{1S*} triplet state, which is based on the optimised singlet geometry, or the T_{1T} triplet state,

based on optimised triplet geometry, comes closest to the experimental values. The errors are smaller for the absorption energies and are around 2% for the $T_{1S^*}-S_0$ energy and around 4-6% for the $T_{1T}-S_0$ energy. In this case the $T_{1S^*}-S_0$ energy gives results closer to the experiment. This fact is also quite interesting in terms of computational efficiency, since an optimised triplet state geometry is not necessary to compute the T_{1S^*} energy.

4.9.2 Geometry of the ligand and complex structures

Substituent influence in the **ligand systems** can be summarised as following. Molecules with acceptor substituents show elongated C(1)-C(2) and C(2)-O(11) bond lengths if compared to donor substituted ligands. The opposite trend is true for the C(1)-N(10) bond length.

In the **complex structures** donor substituents elongate the Eu-N bond length, while the electron withdrawing NO_2 substituent contracts the bond. Axial angles are smaller if electron donating substituents are present in the complex structure. The opposite trend is observed for the equatorial angles.

Unfortunately it is not possible to give a statement about the influence of the electron donating or withdrawing capability of different substituents in the quinoline ligand on the energetics of the ligand. The influence is more an interaction of structural and energetic aspects which can not be investigated separately.

4.9.3 Singlet and Triplet state energies of the ligands and complexes

In the 5-substituted quinoline **ligand systems** the biggest contribution to the S_0-S_1 comes from a HOMO - LUMO excitation. Exception are the CHO and NO_2 substituted ligands.

In the unsubstituted ligand the HOMO - LUMO excitation is a $\pi-\pi^*$ excitation which goes from the phenoxy part of the hydroxyquinoline to the pyridino part. This kind of excitation can be found in all other ligand systems. In case of the CHO and NO_2 ligands $n-\pi^*$ excitations show the most important contribution to the S_0-S_1 transition. Here the excitation goes from a lower lying occupied orbital (HOMO-1 in case of CHO and HOMO-3 in case of NO_2) to the LUMO or LUMO+1 orbital. For the CHO substituent the HOMO - LUMO excitation goes from the phenoxy part to the pyridino part, as observed for other ligands. For the NO_2 substituent the excitation goes from a π orbital which is located on the phenoxy part and the NO_2 group to the whole ligand system. However, a notable part of the electron density stays on the phenoxy part.

In case of the **complex systems** the HOMO - LUMO excitation gives the biggest contribution to the S_0-S_1 transition and is in all cases a ILCT. The HOMO orbital is located on two ligands while the LUMO orbital lies on another ligand only. Excitation goes from the phenoxy part of the two ligands (HOMO) to

the pyridino part of the ligand where the LUMO orbital is located. An exception is the NO₂ substituted complex, where the LUMO orbital spreads over the phenoxy part of the ligand. In this way the behaviour of the excitations in the ligand and complex systems is similar.

For both, the ligand and the complex systems, the acceptor groups shift the HOMO orbital in the singlet state towards lower energy if compared to the unsubstituted species. However, in case of the complexes structural aspects can have a bigger influence as seen for the HSO₃ substituted complex. Here the HSO₃ substituted complex shows a bigger shift of the HOMO orbital than the complex bearing the stronger electron accepting NO₂ group in the structure. The donor groups also show the same effect in the ligand and complex systems and push the LUMO orbital towards higher energy. However, there is no clear correlation between the energy difference of the HOMO and LUMO orbitals of the ligand and complex systems and it is not enough to calculate the ligands only to predict the energy for the complex systems. A correlation exists however between the Mulliken charges on the hydroxy-oxygen of the ligand systems and the complexes. The average charge on the oxygen atom in the complexes is about 0.45e more negative than in the ligands. The charges are presented in Table 4.26.

Table 4.26: Mulliken Charges of the ligands and complexes for their singlet and triplet state. Calculation on UB3LYP/TZVP and UB3LYP/MWB52/TZVP level of theory.

Substituent:	NH ₂	H	HSO ₃	NO ₂
Ligand (S)	-0.2426	-0.2366	-0.2182	-0.2083
Complex (S)	-0.6892	-0.6780	-0.6766	-0.6633
$\Delta_{Lig.-Compl.}$	0.45	0.44	0.46	0.45
Ligand (T)	-0.2020	-0.2015	-0.1931	-0.1851
Complex (T)	-0.6574	-0.6389	-0.6838	-0.6531
$\Delta_{Lig.-Compl.}$	0.46	0.44	0.49	0.47

This is an interesting observation, since by knowing the Mulliken charge on the hydroxy oxygen atom of the ligand one can approximate the charge of the O atoms in the complex structure. For the investigated complexes this charge is directly related to the Eu-O bond length, as depicted in figure 4.66 for the singlet state and in Figure 4.67 for the triplet state of the complexes in gas phase.

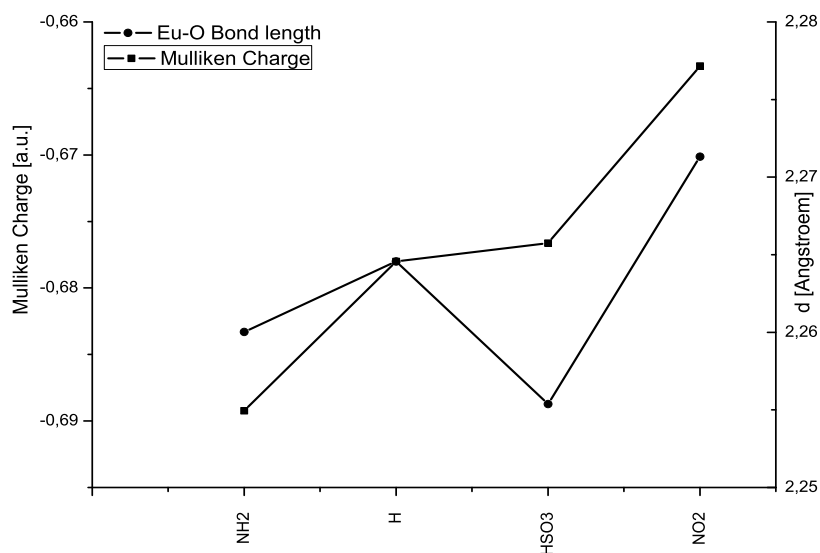


Figure 4.66: Mulliken charges and the Eu-O bond lengths for different complexes in gas phase in their singlet state. Calculated on UB3LYP/51MWB/TZVP level of theory (Charges) and UB3LYP/52MWB/6-31G* level of theory (Bond length).

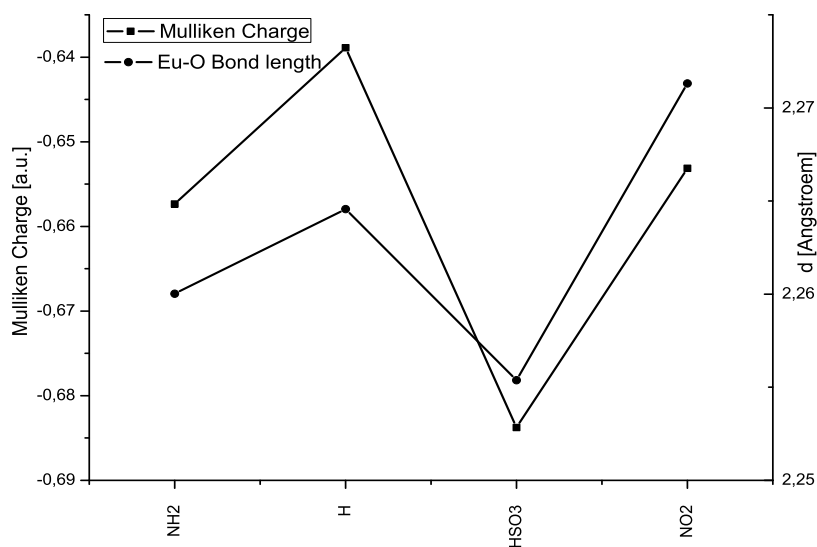


Figure 4.67: Mulliken charges and the Eu-O bond lengths for different complexes in gas phase in their triplet state. Calculated on UB3LYP/51MWB/TZVP level of theory (Charges) and UB3LYP/52MWB/6-31G* level of theory (Bond length).

According to the Mulliken charges the bond length of the HSO₃ substituted ligand should be longer by approximately 0.1 Å. As mentioned before the HSO₃ substituent is sterically demanding in the complex structure and values for bond lengths can deviate from expected values. In the triplet state the bond length correlates better with the Mulliken charges. Why the HSO₃ substituent in the triplet state shows the most negative charge is unclear. However, it seems that in the triplet state no prediction can be made

corresponding the electron donating/accepting ability of the substituent and the charge on the hydroxy oxygen atom.

The correlation between the ligand and complex Mulliken charge becomes even more interesting when the Mulliken charges are compared with the S_0-S_1 energies for the singlet structure and the triplet energies for the triplet structure as depicted in Figures 4.68 and 4.69.

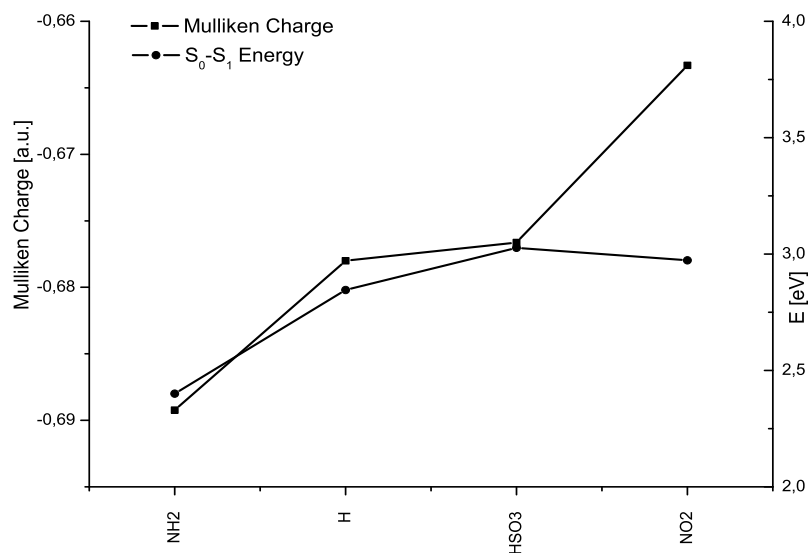


Figure 4.68: Mulliken charges and S_0-S_1 energies for different complexes in gas phase in their singlet state. Calculated on UB3LYP/52MWB/TZVP level of theory.

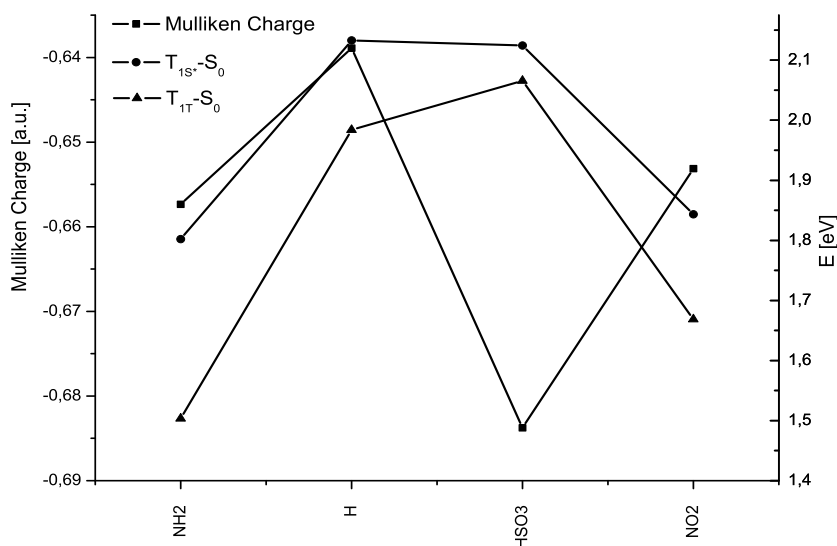


Figure 4.69: Mulliken charges and $T_{1S^*}-S_0$ and $T_{1T}-S_0$ energies for different complexes in gas phase in their singlet state. Calculated on UB3LYP/52MWB/TZVP level of theory.

The absorption energy follows the trend of the Mulliken charges. A strong electron donor (e.g. NH_2) means a more negative charge on the hydroxy-O, smaller Eu-O bond length and smaller absorption energy.

The above discussed trends can be used as guideline for tuning the complex energies. Ligand calculations can be used to give a rough estimation about Mulliken charges, bond lengths and the corresponding energies. To get exact values the complex structures must be computed. Regarding the triplet state energies of the complexes, it seems as if it is not necessary to optimise the triplet geometry. Triplet state energies calculated on an optimised singlet ground state geometry (T_{1S^*}) come close to the experimental values.

Chapter 5

Summary and Outlook

The TD-DFT method in combination with the B3LYP functional is a wide used method to compute energetical and photochemical properties of Eu-oxoquinolinolate complexes (EuQ₃) [17]. Hereby the Eu(III) ion is modeled by an ECP which handles the 4f electron in the core. This approximation is feasible since 4f electrons do not contribute to the bonding in the complex [53].

For optimisation of the ground state structures of the 8-hydroxyquinoline ligands the 6-31G* basis set gave results with an accuracy of 0.1 Å if compared to experimental XRD results [43]. For optimising the complex structures the 6-31G* basis set for the ligand atoms in combination with the 52MWB ECP published by Dolg et al. [22] for the Eu-ion was applied. Energy was refined with a single point calculation on TZVP level for the ligands and 52MWB ECP for the Eu-ion. IEF-PCM solvation model has been tested for its capability to compute accurately the singlet and triplet energies of different 8-hydroxyquinoline ligands and Eu-8-oxoquinolinolate complexes. The applied method was evaluated against experimental results.

The error between experimental S₀-S₁ energies and calculated ones lies in an acceptable range (less than 5% for the ligand systems and less than 10% for the complexes). Applying the IEF-PCM solvent model increases the quality of the results. Placing explicitly solvent molecules around the complex structure can model the ninefold coordinated Eu complex as reported in literature but also increases the error of the singlet and triplet energies if the structures are not selected carefully.

The absolute electronegativity of the ligands and other electronic parameters were computed and used to sort the different substituents according to their electron donating or accepting ability.

The geometries of the ligand and complex structures are discussed in terms of substituents and substitution position in the ligand backbone. Complexes were also calculated with the semiempirical AM1 model using a sparkle for the Eu ion. The difference in AM1 and DFT geometries is marginal and it

could be demonstrated that the computationally less expensive AM1 model gives geometries which are accurate enough to serve as optimised geometry for further TD-DFT calculations.

The absorption spectra for a total of 50 8-hydroxyquinoline ligand molecules bearing different substituents was calculated. The spectra were interpreted and it could be demonstrated that the π - π^* excitation from the HOMO to the LUMO orbital gives the strongest contribution to the S_0 - S_1 transition. Exceptions are ligands with nitro and formyl groups as substituent, where the S_0 - S_1 transition shows contribution from n - π^* excitations. In this cases excitations go from lower lying occupied orbitals such as HOMO-1 or HOMO-3 to the LUMO and LUMO+1 orbital.

There is evidence that strong electron acceptors shift the HOMO orbital towards lower energy while the donor substituents shift the LUMO orbital towards higher energy. The effect however is more pronounced for the donor substituents. In this way the absorption wavelength can be tuned.

Structural and energetical trends which were observed for the ligand systems can be found in the complex calculations as well. The most important contribution to the S_0 - S_1 transition for the complexes is a ILCT from the HOMO to the LUMO orbitals. Placing explicit solvent molecules around the complex has the effect that the occupied orbitals are not located on two ligands anymore but rather focused in one ligand. This has the effect that π - π^* excitations with ILCT mixing, which were observed in the gas phase and IEF-PCM calculations become strict π - π^* excitations with a higher oscillator strength in the explicit solvent calculation.

Same as in the ligand systems, the HOMO orbitals are lowered by introducing acceptors in the structure, while LUMO orbital energy is increased by donor substitution in case of the complexes. Bulky ligands have a higher impact on the energetics of the complexes. The protonated sulfonic acid group e.g. shows abnormalities regarding the Eu-N and Eu-O bond lengths. This structural changes also have an influence on the singlet and triplet state energies.

Mulliken charges were investigated for the 8-oxoquinolates and it could be demonstrated that the difference between the charges on the hydroxy-O in the ligand system and the quinolate-O in the complex lies around 0.44 - 0.49e. This makes it possible to give a rough estimation of the Mulliken charge if only the ligand systems are calculated. At the same time there is a correlation between the Mulliken charge on the oxygen in the complex, the Eu-O bond length in the complex, the S_0 - S_1 energies and the triplet energies. This makes it possible to give a rough estimation about the energies of the complex by only calculating the ligands.

Different triplet states were computed to find out which method reproduces the experimental energies in the best way. It could be demonstrated that the triplet state energies computed with a singlet wavefunction based on a singlet ground state geometry shows the smallest deviation from the experiment. This allows to skip the optimisation of the triplet geometry.

To get a deeper understanding of the influence of the substituents on the singlet and triplet energies of the complexes it would be necessary to calculate a bigger set on test molecules for the ligand system, bearing different electron donors or acceptors. The existing results give an idea about differences regarding the structural and energetic changes depending on substituents. However, the available data are a much too small number to comment on absolute trends. For the same reason it is necessary to calculate a bigger number of complex structures with different donor and acceptor substituents. In case of the complex systems the pyridino substituted and formyl substituted ligands are of high interest. The pyridino ligand shows good characteristics regarding the absorption energies and triplet state energies. Calculations on the formyl substituted ligand would be interesting because it is the only one beside the nitro substituted ligand which shows $n-\pi^*$ excitations.

For future work it would be interesting to perform calculations on the complex system using a full-electron basis set for the Eu ion. In this case relativistic effects must be included separately e.g. by applying the ZORA method and spin-orbit coupling must be accounted for. It would also be interesting to investigate other methods than TD-DFT to calculate the excited states. ZINDO or CC calculations could be challenging but would give more information on the photochemistry of the complexes.

Bibliography

- [1] M. C. De Rosa et al., *J. Am. Chem. Soc.*, 2004, **126**, 7619 – 7626.
- [2] A. Lobnik et al., *Sens. and Act. B: Chemical*, 2001, **74**, 200 – 206.
- [3] J. Kido and Y. Okamoto, *Chem. Rev.*, 2002, **102**, 2357 – 2368.
- [4] S. M. Borisov and I. Klimant, *J. Fluoresc.*, 2008, **18**, 581 – 589.
- [5] S. Kappaun et al., *Org. Biomol. Chem.*, 2006, **4**, 1503 – 1511.
- [6] G. S. Kottas et al., *Eur. J. Inor. Chem.*, 2007, **22**, 3465 – 3468.
- [7] S. Kappaun et al., *Chem. Mat.*, 2007, **19**, 1209 – 1211.
- [8] O. M. Khreis et al., *Org. Electr.*, 2001, **2**, 45 – 51.
- [9] N. M. Shavaleev et al., *Inorg. Chem.*, 2008, **47**, 9055 – 9068.
- [10] S. Stanimirov and I. Petkov, *Spectrochim. Acta*, 2009, **A72**, 1127 – 1133.
- [11] J. P. Leonard and T. Gunnlaugsson, *J. Fluor.*, 2005, **15**, 585 – 595.
- [12] J. Hofkens et al., *Spectrochim. Acta*, 2001, **A57**, 2093 – 2107.
- [13] S. Min-Min et al., *Mat. Chem. and Phys.*, 2009, **115**, 841 – 845.
- [14] X. Ouyang, H. Zeng, and Y. Xie, *Front. Chem. China*, 2007, **2**, 407 – 413.
- [15] D. Imbert et al., *Chem. Comm.*, 2005, **11**, 1423 – 1434.
- [16] G. H. Diecke, H. M. Crosswhite, and H. Crosswhite, *Spectra and Energy Levels of Rare Earth Ions in Crystals*, Wiley, 1968.
- [17] T. Dziembowska et al., *Spectrochim. Acta*, 2003, **59**, 2175 – 2189.
- [18] F. Nunez-Zarur and R. Vivas-Reyes, *J. Mol. Struc.: THEOCHEM*, 2008, **850**, 127 – 134.
- [19] W. Wang et al., *J. Mol. Struc.: THEOCHEM*, 2008, **867**, 116 – 121.
- [20] M. Atanasov et al., *Inorg. Chem.*, 2005, **44**, 2954 – 2963.
- [21] L. Perrin, L. Maron, and E. O., *Farad. Disc.*, 2003, **124**, 25 – 39.
- [22] M. Dolg et al., *Theor. Chem. Acc.*, 1989, **75**, 173 – 194.

- [23] R. O. Freire, G. B. Rocha, and A. M. Simas, *Inorg. Chem.*, 2005, **44**, 3299 – 3310.
- [24] C. J. Cramer, *Essentials of Computational Chemistry, Theories and Models*, Wiley, 2nd ed., 2004.
- [25] F. Jensen, *Introduction to Computational Chemistry*, Wiley, 2nd ed.
- [26] W. Kutzelnigg, *Einführung in die Theoretische Chemie*, Wiley, 2002.
- [27] P. Hohenberg and W. Kohn, *Phys. Rev.*, 1964, **136**, B864 – B871.
- [28] W. Kohn and L. J. Sham, *Phys. Rev.*, 1965, **140**, A1133 – A1138.
- [29] M. J. Frisch et al., *Gaussian Inc., Wallingford CT*, 2004, **7**.
- [30] M. Olivucci, *Computational Photochemistry*, Vol. 16, Elsevier, 2005.
- [31] O. Tapia and J. Bertrand, *Solvent Effects and Chemical Reactivity*, Vol. 17 of *Understanding Chemical Reactivity*, Kluwer Academic Publisher, 2002.
- [32] M. Cossi et al., *Chem. Phys. Lett.*, 1996, **255**, 327 – 335.
- [33] P. E. Smith and M. B. Pettitt, *J. Phys. Chem.*, 1994, **98**, 9700 – 9711.
- [34] L. Onsager, *J. Am. Chem. Soc.*, 1936, **58**, 1486 – 1493.
- [35] Y. Luo et al., *Chem. Phys. Lett.*, 1997, **275**, 145 – 150.
- [36] B. Menucci and R. Cammi, *Continuum Solvation Models in Chemical Physics: From Theory to Applications*, Wiley, 2007.
- [37] P. Scherdtfeger, *Relativistic Electronic Structure Theory: Part 1 Fundamentals*, Elsevier, 2002.
- [38] S. Wilson, P. F. Bernath, and R. Mc. Weeney, *Handbook of Molecular Physics and Quantum Chemistry*, Wiley, 2003.
- [39] J. P. Steward, *web: <http://OpenMOPAC.net>*.
- [40] G. Schaftenaar and J. H. Noordik, *J Comp. Aid. Mol. Des.*, 2000, **14**, 123 – 134.
- [41] S. Kontur, *Voigt.f90*.
- [42] R. O. Freire et al., *J. Mol. Mod.*, 2005, **12**, 16 – 23.
- [43] P. Roychowdhury, *Acta Cryst. B: Structural Science*, 1978, **34**, 1047 – 1048.
- [44] B. Hoge and J. Bader, *J. Fluor. Chem.*, 2007, **128**, 857–861.
- [45] R. G. Parr and P. R. G., *J. Am. Chem.*, 1983, **105**, 7512 – 7516.
- [46] C. W. Tang and van Slyke S. A., *Appl. Phys. Lett.*, 1987, **51**, 913 – 915.
- [47] G. A. Crosby and J. J. Whan, R. E. Freeman, *J. Phys. Chem.*, 1962, **66**, 2493 – 2499.
- [48] G. A. Crosby, R. E. Whan, and R. M. Alire, *J. Chem. Phys.*, 1961, **34**, 743 – 748.
- [49] V. Tsaryuk et al., *J. Photochem. Photobiol. A: Chemistry*, 2006, **177**, 314 – 323.

- [50] M. A. Katkova et al., *Inorg. Chim. Act.*, 2009, **362**, 1393 – 1395.
- [51] W. Watson et al, *Inorg. Chem.*, 1975, **14**, 2675 – 2680.
- [52] V. Tsaryuk, *Private Communication*, 2010.
- [53] I. Georgieva et al., *Inorg. Chem.*, 2007, **46**, 10926 – 10936.

Appendix

Appendix A

Tables

Bond	experimental value [\AA]	calculated at $\theta_1 = 0^\circ$ [\AA]	calculated at $\theta_1 = 180^\circ$ [\AA]
C(8')-C(8)	1.411	1.433(8)	1.430(2)
C(8)-C(7)	1.412	1.382(4)	1.380(9)
C(7)-C(6)	1.431	1.413(8)	1.414(6)
C(6)-C(5)	1.357	1.375(2)	1.379(5)
C(5)-C(4')	1.443	1.419(9)	1.419(1)
C(4')-C(8')	1.449	1.431(8)	1.425(8)
C(8')-N(1)	1.383	1.360(3)	1.360(4)
C(4')-C(4)	1.423	1.418(8)	1.418(7)
C(4)-C(3)	1.443	1.374(4)	1.377(1)
C(3)-C(2)	1.428	1.416(7)	1.416(2)
C(2)-N(1)	1.350	1.317(8)	1.319(5)
C(8)-O(9)	1.390	1.358(9)	1.350(9)

Table A.1: Comparison of experimental and calculated **bond lengths** of 8-hydroxyquinoline. Experimental datas are taken from [43]. Calculation on UB3LYP/6-31G* level of theory.

Angle	experimental value [°]	calculated $\theta_1=0^\circ$ [°]	calculated $\theta_1=180^\circ$ [°]
C(8)-C(8')-C(4')	119.3	119.8(7)	118.3(1)
C(8)-C(8')-N(1)	119.1	116.3(4)	118.6(5)
C(4')-C(8')-N(1)	121.5	123.7(8)	123.0(2)
C(8')-C(8)-C(7)	121.2	119.7(9)	119.9(6)
C(8')-C(8)-O(9)	120.3	118.3(8)	116.9(3)
C(7)-C(8)-O(9)	118.2	121.8(1)	123.0(9)
C(8)-C(7)-C(6)	117.8	119.7(6)	120.8(5)
C(7)-C(6)-C(5)	123.0	121.8(8)	120.8(6)
C(6)-C(5)-C(4')	119.8	119.5(6)	119.7(1)
C(5)-C(4')-C(8')	118.7	119.1(2)	120.2(8)
C(5)-C(4')-C(4)	122.7	124.7(0)	122.9(1)
C(8')-C(4')-C(4)	118.6	116.1(7)	116.7(9)
C(4')-C(4)-C(3)	119.2	119.7(6)	119.7(0)
C(4)-C(3)-C(2)	117.4	119.1(4)	118.5(8)
C(3)-C(2)-N(1)	124.1	123.2(3)	124.1(0)
C(2)-N(1)-C(8')	119.0	117.9(0)	117.7(8)

Table A.2: Comparison of experimental and calculated **angles** of 8-hydroxyquinoline. Experimental datas are taken from [43]. Calculation on UB3LYP/6-31G* level of theory.

2-Position										
R	R'	C(8')-C(8) [Å]	C(8')-N(1) [Å]	C(8)-O(9) [Å]	O(9)-H(10) [Å]	N(1)-C(8')-C(8) [°]	C(8')-C(8)-O(9) [°]	Dieder [°]	Wagging [°]	Rotation [°]
NH ₂	OH	1.4311	1.3599	1.3632	0.9702	118.82	116.87		44.28	23.32
CN	OH	1.4355	1.3540	1.3544	0.9706	118.41	116.78			
HSO ₃	OH	1.4298	1.3592	1.3567	0.9705	118.95	116.57			
NO ₂	OH	1.4341	1.3556	1.3530	0.9706	118.70	116.80			
Ph	OH	1.4343	1.3542	1.3597	0.9704	118.68	116.90	14.45		
Py	OH	1.4315	1.3546	1.3519	0.9714	118.83	116.56	26.86		
3-Position										
R	R'	C(8')-C(8) [Å]	C(8')-N(1) [Å]	C(8)-O(9) [Å]	O(9)-H(10) [Å]	N(1)-C(8')-C(8) [°]	C(8')-C(8)-O(9) [°]	Dieder [°]	Wagging [°]	Rotation [°]
NH ₂	OH	1.4307	1.3609	1.3602	0.9703	118.97	116.99		47.67	25.27
CN	OH	1.4322	1.3611	1.3558	0.9705	118.64	116.88			
HSO ₃	OH	1.4321	1.3621	1.3558	0.9705	118.53	116.90			
NO ₂	OH	1.4320	1.3618	1.3553	0.9705	118.57	116.91			
Ph	OH	1.4321	1.3603	1.3590	0.9704	118.94	116.98	38.40		
Py	OH	1.4329	1.3580	1.3477	0.9713	118.56	116.63	52.52		

Table A.3: Geometry parameters of the ligand system in its **singlet** groundstate. R is the substitution in **2- and 3-position**, R' is the substitution in 8-position of the quinoline molecule. Calculation on UB3LYP/6-31G* level of theory.

R	R'	C(8')-C(8) [Å]	C(8')-N(1) [Å]	C(8)-O(9) [Å]	O(9)-H(10) [Å]	N(1)-C(8')-C(8) [°]	C(8')-C(8)-O(9) [°]	Dieder [°]	Wagging [°]	Rotation [°]
NH ₂	OH	1.4342	1.3610	1.3595	0.9703	117.92	116.69		46.66	24.59
CN	OH	1.4346	1.3583	1.3558	0.9705	118.28	116.74			
HSO ₃	OH	1.4347	1.3578	1.3559	0.9705	117.63	116.69			
NO ₂	OH	1.4356	1.3560	1.3556	0.9706	117.21	116.61	27.77		
Ph	OH	1.4344	1.3600	1.3594	0.9704	117.66	116.78	55.75		
Py	OH	1.4370	1.3547	1.3446	0.9715	118.12	116.33	72.92		
SO ₃ ⁻	OH	1.4322	1.3636	1.3718	0.9699	117.97	117.28			

Table A.4: Geometry parameters of the ligand system in its **singlet** groundstate. R is the substitution in **4-position**, R' is the substitution in 8-position of the quinoline molecule. Calculation on UB3LYP/6-31G* level of theory.

R	R'	C(8')- C(8) [Å]	C(8')- N(1) [Å]	C(8)- O(9) [Å]	O(9)- H(10) [Å]	O(9)- C(10) [Å]	N(1)-C(8')-C(8) [°]	C(8')-C(8)-O(9) [°]	Dieder [°]	Wagging [°]	Rotation [°]
CH ₃	OH	1.4311	1.3609	1.3618	0.9692		117.99	116.61			
NH ₂	MeO	1.4372	1.3595	1.3603		1.4153	118.31	115.71		56.05	29.59
NH ₂	OH	1.4318	1.3602	1.3642	0.9700		118.32	117.21		55.98	29.55
CN	MeO	1.4419	1.3581	1.3458		1.4223	118.14	115.44			
CN	OH	1.4360	1.3585	1.3505	0.9713		118.18	116.79			
CHO	MeO	1.4448	1.3572	1.3448		1.4222	117.39	115.38			
CHO	OH	1.4387	1.3577	1.3495	0.9711		117.40	116.80			
HSO ₃	OH	1.4378	1.3574	1.3499	0.9710		117.53	116.65			
MeO	MeO	1.4389	1.3594	1.3594		1.4156	118.57	115.60			
MeO	OH	1.4336	1.3598	1.3634	0.9701		118.59	117.06			
NO ₂	MeO	1.4438	1.3564	1.3423		1.4239	116.61	115.48	13.50		
NO ₂	OH	1.4373	1.3571	1.3475	0.9711		116.61	116.84	12.64		
Ph	OH	1.4328	1.3604	1.3583	0.9704		117.74	117.10	53.40		
Py	OH	1.4403	1.3542	1.3391	0.9719		117.67	116.31	63.89		
5,7DiMe	OH	1.4311	1.3609	1.3618	0.9692		117.99	116.61			
H	MeO	1.4392	1.3601	1.3550		1.4177	118.62	115.43			
H	OH	1.4338	1.3603	1.3589	0.9706		118.66	116.93			

Table A.5: Geometry parameters of the ligand system in its **singlet** groundstate. R is the substitution in **5-position**, R' is the substitution in 8-position of the quinoline molecule. Calculation on UB3LYP/6-31G* level of theory.

6-Position											
R	R'	C(8')- C(8) [Å]	C(8')- N(1) [Å]	C(8)- O(9) [Å]	O(9)- H(10) [Å]	O(9)- C(10) [Å]	N(1)-C(8')-C(8) [°]	C(8')-C(8)-O(9) [°]	Dieder [°]	Wagging [°]	Rotation [°]
NH ₂	OH	1.4345	1.3576	1.3585	0.9703		118.91	116.88		48.83	25.85
CN	OH	1.4360	1.3578	1.3542	0.9707		118.54	116.75			
HSO ₃	OH	1.4372	1.3581	1.3534	0.9708		118.45	116.77			
NO ₂	OH	1.4372	1.3577	1.3536	0.9708		118.53	116.76			
Ph	OH	1.4330	1.3594	1.3586	0.9704		118.96	116.90	38.33		
Py	OH	1.4402	1.3541	1.3423	0.9712		118.01	116.43	53.23		
7-Position											
R	R'	C(8')- C(8) [Å]	C(8')- N(1) [Å]	C(8)- O(9) [Å]	O(9)- H(10) [Å]	O(9)- C(10) [Å]	N(1)-C(8')-C(8) [°]	C(8')-C(8)-O(9) [°]	Dieder [°]	Wagging [°]	Rotation [°]
NH ₂	OH	1.4314	1.3607	1.3455	0.9847		118.67	119.79		60.39	89.96
CN	OH	1.4344	1.3590	1.3435	0.9748		118.13	117.41			
HSO ₃	OH	1.4449	1.3568	1.3323	0.9846		117.42	116.58			
NO ₂	MeO	1.4379	1.3617	1.3501		1.4379	117.32	117.54	33.03		
NO ₂	OH	1.4446	1.3561	1.3244	0.9927		117.84	120.77			
Ph	OH	1.4336	1.3614	1.3567	0.9730		118.33	116.22	49.10		
Py	OH	1.4348	1.3566	1.3534	0.9701		117.50	116.90	59.69		

Table A.6: Geometry parameters of the ligand system in its **singlet** groundstate. R is the substitution in **6- and 7-position**, R' is the substitution in 8-position of the quinoline molecule. Calculation on UB3LYP/6-31G* level of theory.

2-Position										
R	R'	C(8')-C(8) [Å]	C(8')-N(1) [Å]	C(8)-O(9) [Å]	O(9)-H(10) [Å]	N(1)-C(8')-C(8) [°]	C(8')-C(8)-O(9) [°]	Dieder [°]	Wagging [°]	Rotation [°]
NH ₂	OH	1.4353	1.3335	1.3527	0.9710	118.62	117.45		37.75	19.81
CN	OH	1.4466	1.3256	1.3443	0.9719	118.80	116.82			
HSO ₃	OH	1.4345	1.3350	1.3446	0.9718	119.27	117.03			
NO ₂	OH	1.4471	1.3260	1.3406	0.9721	119.02	116.78			
Ph	OH	1.4476	1.3214	1.3502	0.9714	118.83	116.85	0.04		
Py	OH	1.4518	1.3267	1.3297	0.9744	118.80	116.34	4.29		
3-Position										
R	R'	C(8')-C(8) [Å]	C(8')-N(1) [Å]	C(8)-O(9) [Å]	O(9)-H(10) [Å]	N(1)-C(8')-C(8) [°]	C(8')-C(8)-O(9) [°]	Dieder [°]	Wagging [°]	Rotation [°]
NH ₂	OH	1.4147	1.3525	1.3575	0.9703	119.82	118.30		45.43	24.27
CN	OH	1.4211	1.3516	1.3441	0.9716	118.94	118.08			
HSO ₃	OH	1.4275	1.3465	1.3431	0.9718	118.72	117.75			
NO ₂	OH	1.4207	1.3545	1.3393	0.9721	118.65	118.13			
Ph	OH	1.4195	1.3492	1.3506	0.9709	119.505	118.28	29.92		
Py	OH	1.4278	1.3530	1.3243	0.9745	118.69	117.58	33.35		

Table A.7: Geometry parameters of the ligand system in its **triplet** state. R is the substitution in **2- and 3-position**, R' is the substitution in 8-position of the quinoline molecule. Calculation on UB3LYP/6-31G* level of theory.

R	R'	C(8')-C(8) [Å]	C(8')-N(1) [Å]	C(8)-O(9) [Å]	O(9)-H(10) [Å]	N(1)-C(8')-C(8) [°]	C(8')-C(8)-O(9) [°]	Dieder [°]	Wagging [°]	Rotation [°]
NH ₂	OH	1.4333	1.3372	1.3559	0.9706	118.57	117.54		48.29	25.01
CN	OH	1.4347	1.3393	1.3434	0.9718	118.53	117.25			
HSO ₃	OH	1.4402	1.3353	1.3426	0.9721	118.07	116.91			
NO ₂	OH	1.4403	1.3374	1.3389	0.9724	117.14	116.90			
Ph	OH	1.4336	1.3386	1.3498	0.9712	117.79	117.28			
Py	OH	1.4477	1.3344	1.3240	0.9747	117.25	116.37	36.93		
SO ₃ ⁻	OH	1.4353	1.3375	1.3631	0.9704	118.43	117.88	36.95		

Table A.8: Geometry parameters of the ligand system in its **triplet** state. R is the substitution in **4-position**, R' is the substitution in 8-position of the quinoline molecule. Calculation on UB3LYP/6-31G* level of theory.

R	R'	C(8')- C(8) [Å]	C(8')- N(1) [Å]	C(8)- O(9) [Å]	O(9)- H(10) [Å]	O(9)- C(10) [Å]	N(1)-C(8')-C(8) [°]	C(8')-C(8)-O(9) [°]	Dieder [°]	Wagging [°]	Rotation [°]
CH ₃	OH	1.4323	1.3360	1.3554	0.9700		118.17	116.91			
NH ₂	OH	1.4501	1.3355	1.3473		1.4209	118.26	115.23		41.17	21.19
NH ₂	MeO	1.4389	1.3392	1.3521	0.9709		118.41	117.30		41.31	21.28
CN	OH	1.4544	1.3331	1.3447		1.4243	116.62	119.95			
CN	MeO	1.4443	1.3347	1.3498	0.9714		118.77	117.27			
CHO	OH	1.4533	1.3366	1.3499		1.4240	117.79	115.62			
CHO	MeO	1.4436	1.3379	1.3501	0.9715		117.92	117.61			
HSO ₃	OH	1.4407	1.3326	1.3489	0.9715		118.35	117.42			
MeO	MeO	1.4451	1.3370	1.3466		1.4216	118.60	115.62			
MeO	OH	1.4330	1.3412	1.3516	0.9709		118.78	117.81			
NO ₂	MeO	1.4475	1.3345	1.3463		1.4267	117.17	117.29	6.90		
NO ₂	OH	1.4564	1.3340	1.3407	0.9720		117.20	115.38	6.30		
Ph	OH	1.4395	1.3393	1.3528	0.9711		118.01	117.51	32.13		
Py	OH	1.4515	1.3369	1.3281	0.9743		117.22	116.88	37.57		
5,7DiMe	OH	1.4323	1.3360	1.3554	0.9700		118.17	116.91			
H	MeO	1.4481	1.3318	1.3454		1.4228	118.99	115.37			
H	OH	1.4374	1.3350	1.3503	0.9712		119.18	117.56			

Table A.9: Geometry parameters of the ligand system in its **triplet** state. R is the substitution in **5-position**, R' is the substitution in 8-position of the quinoline molecule. Calculation on UB3LYP/6-31G* level of theory.

6-Position											
R	R'	C(8')- C(8) [Å]	C(8')- N(1) [Å]	C(8)- O(9) [Å]	O(9)- H(10) [Å]	O(9)- C(10) [Å]	N(1)-C(8')-C(8) [°]	C(8')-C(8)-O(9) [°]	Dieder [°]	Wagging [°]	Rotation [°]
NH ₂	OH	1.4356	1.3379	1.3563	0.9704		119.61	116.72		41.95	22.50
CN	OH	1.4690	1.3316	1.3443	0.9724		118.65	115.86			
HSO ₃	OH	1.4619	1.3198	1.3437	0.9724		118.64	116.66			
NO ₂	OH	1.4742	1.3198	1.3361	0.9735		118.42	115.86			
Ph	OH	1.4593	1.3214	1.3508	0.9716		119.29	115.89	21.97		
Py	OH	1.4696	1.3238	1.3229	0.9747		118.48	115.36	24.71		
7-Position											
R	R'	C(8')- C(8) [Å]	C(8')- N(1) [Å]	C(8)- O(9) [Å]	O(9)- H(10) [Å]	O(9)- C(10) [Å]	N(1)-C(8')-C(8) [°]	C(8')-C(8)-O(9) [°]	Dieder [°]	Wagging [°]	Rotation [°]
NH ₂	OH	1.4322	1.3377	1.3365	0.9901		119.41	120.85		59.76	89.92
CN	OH	1.4225	1.3458	1.3422	0.9756		119.18	119.18			
HSO ₃	OH	1.4357	1.3380	1.3373	0.9850		118.73	118.35			
NO ₂	MeO	1.4331	1.3499	1.3313		1.4361	120.13	127,24	30.357		
NO ₂	OH	1.4289	1.3475	1.3276	0.9944		115.53	117.04	0.01		
Ph	OH	1.4301	1.3442	1.3479	0.9744		119.13	117.32	39.70		
Py	OH	1.4412	1.3421	1.3244	0.9790		118.16	117.16	38.47		

Table A.10: Geometry parameters of the ligand system in its **triplet** state. R is the substitution in **6- and 7-position**, R' is the substitution in 8-position of the quinoline molecule. Calculation on UB3LYP/6-31G* level of theory.

2-Position						
R	R'	μ_S [eV]	IP [eV]	E_{ca} [eV]	η_S	χ_S
NH ₂	OH	-3.6612	7.1095	-0.2129	3.4483	3.6612
CN	OH	-3.6771	8.2130	0.8588	4.5359	3.6771
HSO ₃	OH	-3.5733	8.3327	1.1861	4.7594	3.5733
NO ₂	OH	-3.4880	8.3430	1.3670	4.8550	3.4880
Ph	OH	-3.5159	7.3417	0.3100	3.8258	3.5159
Py	OH	-2.8956	10.8580	5.0667	7.9623	2.8956
3-Position						
R	R'	μ_S [eV]	IP [eV]	E_{ca} [eV]	η_S	χ_S
NH ₂	OH	-3.6753	7.1920	-0.1586	3.5167	3.6753
CN	OH	-3.6803	8.2527	0.8920	4.5723	3.6803
HSO ₃	OH	-3.5874	8.2351	1.0603	4.6477	3.5874
NO ₂	OH	-3.4043	8.3433	1.5347	4.9390	3.4043
Ph	OH	-3.5342	7.4923	0.4238	3.9581	3.5342
Py	OH	-2.8110	10.7589	5.1369	7.9479	2.8110

Table A.11: Chemical Potential (μ_S), Ionisation Potential (IP), Electron Affinity (E_{ca}), Absolute Electronegativity (χ_S) and Hardness parameter (η_S) of the ligands. R is the substituent in **2- and 3-position**, R' is the substituent in 8-position. Calculated on UB3LYP/TZVP level of theory.

R	R'	μ_s [eV]	IP [eV]	E_{ea} [eV]	η_s	χ_s
NH ₂	OH	-3.7656	7.2540	-0.2772	3.4884	3.7656
CN	OH	-3.5811	8.2055	1.0433	4.6244	3.5811
HSO ₃	OH	-3.4979	8.2032	1.2074	4.7053	3.4979
NO ₂	OH	-3.2721	8.2642	1.7200	4.9921	3.2721
Ph	OH	-3.5216	7.4653	0.4220	3.9437	3.5216
Py	OH	-2.8948	10.9482	5.1587	8.0535	2.8948
SO ₃ ⁻	OH	-3.6403	4.4531	-2.8275	0.8128	3.6403

Table A.12: Chemical Potential (μ_s), Ionisation Potential (IP), Electron Affinity (E_{ea}), Absolute Electronegativity (χ_s) and Hardness parameter (η_s) of the ligands. R is the substituent in **4-position**, R' is the substituent in 8-position. Calculated on UB3LYP/TZVP level of theory.

R	R'	μ_s [eV]	IP [eV]	E_{ea} [eV]	η_s	χ_s
NH ₂	OH	-3.4304	6.7869	-0.0739	3.3565	3.4304
NH ₂	MeO	-3.4457	6.6453	-0.2461	3.1996	3.4457
CN	OH	-3.7472	8.2811	0.7866	4.5338	3.7472
CN	MeO	-3.6711	8.0714	0.7293	4.4003	3.6711
CHO	OH	-3.6885	8.2231	0.8462	4.5347	3.6885
CHO	MeO	-3.6158	8.0212	0.7896	4.4054	3.6158
HSO ₃	OH	-3.7306	8.3682	0.9070	4.6376	3.7306
MeO	OH	-3.6361	7.1556	-0.1165	3.5196	3.6361
MeO	MeO	-3.6475	7.0013	-0.2938	3.3537	3.6475
NO ₂	OH	-3.5169	8.4422	1.4084	4.9253	3.5169
NO ₂	MeO	-3.4386	8.2299	1.3528	4.7913	3.4386
Ph	OH	-3.5027	7.2763	0.2709	3.7736	3.5027
Py	OH	-3.1264	11.2115	4.9587	8.0851	3.1264
5,7DiMe	OH	-3.8368	7.5218	-0.1518	3.6850	3.8368
H	MeO	-3.8266	7.5896	-0.0636	3.7630	3.8266
H	OH	-3.9043	7.7913	-0.0174	3.8869	3.9043

Table A.13: Chemical Potential (μ_s), Ionisation Potential (IP), Electron Affinity (E_{ea}), Absolute Electronegativity (χ_s) and Hardness parameter (η_s) of the ligands. R is the substituent in **5-position**, R' is the substituent in 8-position. Calculated on UB3LYP/TZVP level of theory.

6-Position						
R	R'	μ_s [eV]	IP [eV]	E_{ea} [eV]	η_s	χ_s
NH ₂	OH	-3.6210	7.0820	-0.1600	3.4610	3.6210
CN	OH	-3.7596	8.3178	0.7987	4.5583	3.7596
HSO ₃	OH	-3.6796	8.3109	0.9517	4.6313	3.6796
NO ₂	OH	-3.4805	8.4373	1.4762	4.9568	3.4805
Ph	OH	-3.5114	7.4132	0.3904	3.9018	3.5114
Py	OH	-3.0181	11.1393	5.1032	8.1213	3.0181
7-Position						
R	R'	μ_s [eV]	IP [eV]	E_{ea} [eV]	η_s	χ_s
NH ₂	OH	-3.6666	7.2546	-0.0785	3.5881	3.6666
CN	OH	-3.7650	8.3341	0.8042	4.5692	3.7650
HSO ₃	OH	-3.6275	8.2376	0.9825	4.6100	3.6275
NO ₂	MeO	-3.3675	8.0938	1.3588	3.3675	3.3675
NO ₂	OH	-3.4303	8.0938	1.3588	4.7263	3.4303
Ph	OH	-3.6054	7.3977	0.1869	3.7923	3.6054
Py	OH	-2.9880	11.1663	5.1903	8.1783	2.9880

Table A.14: Chemical Potential (μ_s), Ionisation Potential (IP), Electron Affinity (E_{ea}), Absolute Electronegativity (χ_s) and Hardness parameter (η_s) of the ligands. R is the substituent in **6- and 7-position**, R' is the substituent in 8-position. Calculated on UB3LYP/TZVP level of theory.

2-Position					
R	R'	S ₀ -S ₁ [eV]	T _{1S*} -S ₀ [eV]	T _{1T} -S ₀ [eV]	T _{1S} -S ₀ [eV]
NH ₂	OH	3.69	2.69	2.58	2.98
CN	OH	3.59	2.48	2.43	2.79
HSO ₃	OH	3.71	2.57	2.48	2.89
NO ₂	OH	3.22	2.43	2.40	2.75
Ph	OH	3.69	2.52	2.46	2.84
Py	OH	2.32	1.99	2.05	2.41
3-Position					
R	R'	S ₀ -S ₁ [eV]	T _{1S*} -S ₀ [eV]	T _{1T} -S ₀ [eV]	T _{1S} -S ₀ [eV]
NH ₂	OH	3.79	2.62	2.55	2.92
CN	OH	3.63	2.50	2.46	2.81
HSO ₃	OH	3.70	2.57	2.47	2.88
NO ₂	OH	3.06	2.35	2.34	2.67
Ph	OH	3.80	2.58	2.54	2.92
Py	OH	2.05	1.88	2.05	2.39

Table A.15: Singlet and triplet energies of the ligand systems. R is the Substituent in **2- and 3-position**, R' is the Substituent in 8-position. Calculated in gas phase on UB3LYP/TZVP level of theory.

R	R'	S ₀ -S ₁ [eV]	T _{1S*} -S ₀ [eV]	T _{1T} -S ₀ [eV]	T _{1S} -S ₀ [eV]
NH ₂	OH	4.09	2.67	2.61	2.96
CN	OH	3.34	2.36	2.31	2.68
HSO ₃	OH	3.43	2.45	2.36	2.76
NO ₂	OH	2.78	2.16	2.09	2.50
Ph	OH	3.72	2.58	2.49	2.90
Py	OH	2.05	2.01	2.10	2.56
SO ₃ ⁻	OH	3.34	2.68	2.62	3.01

Table A.16: Singlet and triplet energies of the ligand systems. R is the Substituent in **4-position**, R' is the Substituent in 8-position. Calculated in gas phase on UB3LYP/TZVP level of theory.

R	R'	S ₀ -S ₁ [eV]	T _{1S*} -S ₀ [eV]	T _{1T} -S ₀ [eV]	T _{1S} -S ₀ [eV]
NH ₂	OH	3.31	2.34	2.18	2.64
CN	OH	3.92	2.52	2.47	2.80
CN	MeO	3.89	2.54	2.48	2.81
CHO	OH	3.46	2.50	2.45	2.73
CHO	MeO	3.47	2.51	2.47	2.74
HSO ₃	OH	4.10	2.71	2.65	3.00
MeO	OH	3.56	2.52	2.44	2.84
MeO	MeO	3.55	2.56	2.48	2.87
NO ₂	OH	3.57	2.39	2.36	2.62
NO ₂	MeO	3.55	2.39	2.35	2.61
Ph	OH	3.73	2.55	2.41	2.85
Py	OH	2.46	2.24	2.29	2.70
5,7DiMe	OH	3.72	2.53	2.51	2.84
H	MeO	3.91	2.69	2.62	3.02
H	OH	3.94	2.66	2.59	2.99

Table A.17: Singlet and triplet energies of the ligand systems. R is the Substituent in **5-position**, R' is the Substituent in 8-position. Calculated in gas phase on UB3LYP/TZVP level of theory.

6-Position						
R	R'	S ₀ -S ₁ [eV]	T _{1S*} -S ₀ [eV]	T _{1T} -S ₀ [eV]	T _{1S} -S ₀ [eV]	
NH ₂	OH	3.67	2.60	2.48	2.86	
CN	OH	3.89	2.56	2.51	2.88	
HSO ₃	OH	3.97	2.67	2.56	3.01	
NO ₂	OH	3.23	2.35	2.32	2.66	
Ph	OH	3.79	2.56	2.48	2.87	
Py	OH	2.39	2.14	2.18	2.65	
7-Position						
R	R'	S ₀ -S ₁ [eV]	T _{1S*} -S ₀ [eV]	T _{1T} -S ₀ [eV]	T _{1S} -S ₀ [eV]	
NH ₂	OH	3.82	2.61	2.54	2.93	
CN	OH	3.92	2.61	2.57	2.91	
HSO ₃	OH	3.96	2.73	2.62	3.02	
NO ₂	MeO	3.52	2.55	2.37	2.85	
NO ₂	OH	3.22	2.36	1.89	2.57	
Ph	OH	3.75	2.56	2.49	2.86	
Py	OH	2.28	2.12	2.23	2.65	

Table A.18: Singlet and triplet energies of the ligand systems. R is the Substituent in **6- and 7-position**, R' is the Substituent in 8-position. Calculated in gas phase on UB3LYP/TZVP level of theory.

2-Position					
R	R'	S ₀ -S ₁ [eV]	T _{1S*} -S ₀ [eV]	T _{1T} -S ₀ [eV]	T _{1S} -S ₀ [eV]
NH ₂	OH	3.78	2.74	2.57	2.97
CN	OH	3.35	2.40	2.29	2.63
HSO ₃	OH	3.49	2.49	2.34	2.74
NO ₂	OH	2.74	2.21	2.08	2.40
Ph	OH	3.58	2.51	2.41	2.79
Py	OH	2.74	2.29	2.11	2.47
3-Position					
R	R'	S ₀ -S ₁ [eV]	T _{1S*} -S ₀ [eV]	T _{1T} -S ₀ [eV]	T _{1S} -S ₀ [eV]
NH ₂	OH	3.68	2.58	2.47	2.82
CN	OH	3.47	2.45	2.34	2.68
HSO ₃	OH	3.56	2.52	2.35	2.76
NO ₂	OH	2.73	2.17	2.06	2.35
Ph	OH	3.72	2.57	2.47	2.85
Py	OH	2.82	2.38	2.22	2.57

Table A.19: Singlet and triplet energies of the ligand systems. R is the Substituent in **2- and 3-position**, R' is the Substituent in 8-position. Calculated with IEF-PCM solvation model (DCM) on UB3LYP/TZVP level of theory.

R	R'	S ₀ -S ₁ [eV]	T _{1S*} -S ₀ [eV]	T _{1T} -S ₀ [eV]	T _{1S} -S ₀ [eV]
NH ₂	OH	4.03	2.69	2.60	2.96
CN	OH	3.16	2.30	2.18	2.54
HSO ₃	OH	3.30	2.41	2.25	2.65
NO ₂	OH	2.50	2.01	1.81	2.22
Ph	OH	3.66	2.57	2.44	2.85
Py	OH	2.80	2.45	2.24	2.67
SO ₃ ⁻	OH	3.73	2.60	2.46	2.88

Table A.20: Singlet and triplet energies of the ligand systems. R is the Substituent in **4-position**, R' is the Substituent in 8-position. Calculated with IEF-PCM solvation model (DCM) on UB3LYP/TZVP level of theory.

R	R'	S ₀ -S ₁ [eV]	T _{1S*} -S ₀ [eV]	T _{1T} -S ₀ [eV]	T _{1S} -S ₀ [eV]
NH ₂	OH	3.18	2.31	2.05	2.53
CN	OH	3.87	2.55	2.46	2.80
CN	MeO	3.87	2.58	2.49	2.82
CHO	OH	3.59	2.49	2.41	2.69
CHO	MeO	3.59	2.52	2.44	2.71
HSO ₃	OH	4.00	2.70	2.62	2.96
MeO	OH	3.44	2.49	2.33	2.73
MeO	MeO	3.47	2.54	2.39	2.79
NO ₂	OH	3.41	2.30	2.22	2.46
NO ₂	MeO	3.39	2.31	2.23	2.47
Ph	OH	3.63	2.53	2.38	2.80
Py	OH	3.00	2.59	2.43	2.81
5,7DiMe	OH	3.65	2.53	2.47	2.79
H	MeO	3.86	2.66	2.54	2.94
H	OH	3.87	2.70	2.58	2.98

Table A.21: Singlet and triplet energies of the ligand systems. R= Substituent in **5-position**, R'= Substituent in 8-position. Calculated with IEF-PCM solvation model (DCM) on UB3LYP/TZVP level of theory.

6-Position						
R	R'	S ₀ -S ₁ [eV]	T _{1S*} -S ₀ [eV]	T _{1T} -S ₀ [eV]	T _{1S} -S ₀ [eV]	
NH ₂	OH	3.53	2.56	2.38	2.76	
CN	OH	3.79	2.55	2.46	2.82	
HSO ₃	OH	3.91	2.68	2.53	2.97	
NO ₂	OH	2.91	2.19	2.08	2.42	
Ph	OH	3.72	2.56	2.45	2.84	
Py	OH	2.96	2.55	2.32	2.77	
7-Position						
R	R'	S ₀ -S ₁ [eV]	T _{1S*} -S ₀ [eV]	T _{1T} -S ₀ [eV]	T _{1S} -S ₀ [eV]	
NH ₂	OH	3.77	2.61	2.49	2.89	
CN	OH	3.86	2.62	2.54	2.87	
HSO ₃	OH	3.95	2.74	2.61	3.00	
NO ₂	MeO	3.24	2.48	2.26	2.72	
NO ₂	OH	3.00	2.21	1.74	2.36	
Ph	OH	3.72	2.57	2.47	2.84	
Py	OH	2.95	2.61	2.47	2.83	

Table A.22: Singlet and triplet energies of the ligand systems. R is the Substituent in **6- and 7-position**, R' is the Substituent in 8-position. Calculated with IEF-PCM solvation model (DCM) on UB3LYP/TZVP level of theory.

2-Position					
R	R'	S ₀ -S ₁ [eV]	T _{1S*} -S ₀ [eV]	T _{1T} -S ₀ [eV]	T _{1S} -S ₀ [eV]
NH ₂	OH	3.78	2.74	2.57	2.97
CN	OH	3.32	2.39	2.26	2.60
HSO ₃	OH	3.47	2.48	2.32	2.71
NO ₂	OH	2.69	2.17	2.02	2.33
Ph	OH	3.57	2.50	2.40	2.78
Py	OH	2.80	2.31	2.11	2.48
3-Position					
R	R'	S ₀ -S ₁ [eV]	T _{1S*} -S ₀ [eV]	T _{1T} -S ₀ [eV]	T _{1S} -S ₀ [eV]
NH ₂	OH	3.67	2.57	2.46	2.81
CN	OH	3.46	2.44	2.32	2.66
HSO ₃	OH	3.54	2.52	2.33	2.75
NO ₂	OH	2.69	2.14	2.01	2.29
Ph	OH	3.71	2.57	2.46	2.84
Py	OH	2.91	2.42	2.25	2.59

Table A.23: Singlet and triplet energies of the ligand systems. R is the Substituent in **2- and 3-position**, R' is the Substituent in 8-position. Calculated with IEF-PCM solvation model (ETOH) on UB3LYP/TZVP level of theory.

R	R'	S ₀ -S ₁ [eV]	T _{1S*} -S ₀ [eV]	T _{1T} -S ₀ [eV]	T _{1S} -S ₀ [eV]
NH ₂	OH	4.03	2.70	2.60	2.96
CN	OH	3.14	2.29	2.16	2.51
HSO ₃	OH	3.29	2.41	2.23	2.63
NO ₂	OH	2.47	1.99	1.77	2.18
Ph	OH	3.65	2.57	2.43	2.84
Py	OH	2.89	2.46	2.26	2.68
SO ₃ ⁻	OH	3.69	2.59	2.44	2.86

Table A.24: Singlet and triplet energies of the ligand systems. R is the Substituent in **4-position**, R' is the Substituent in 8-position. Calculated with IEF-PCM solvation model (ETOH) on UB3LYP/TZVP level of theory.

R	R'	S ₀ -S ₁ [eV]	T _{1S*} -S ₀ [eV]	T _{1T} -S ₀ [eV]	T _{1S} -S ₀ [eV]
NH ₂	OH	3.16	2.30	2.03	2.50
CN	OH	3.87	2.55	2.46	2.79
CN	MeO	3.88	2.58	2.49	2.82
CHO	OH	3.61	2.49	2.40	2.68
CHO	MeO	3.60	2.52	2.44	2.71
HSO ₃	OH	3.99	2.70	2.61	2.96
MeO	OH	3.43	2.48	2.32	2.71
MeO	MeO	3.46	2.54	2.37	2.77
NO ₂	OH	3.41	2.28	2.19	2.43
NO ₂	MeO	3.39	2.29	2.21	2.45
Ph	OH	3.62	2.53	2.37	2.79
Py	OH	3.07	2.60	2.44	2.82
H	MeO	3.87	2.70	2.58	2.98
5,7DiMe	OH	3.65	2.53	2.47	2.79
H	OH	3.85	2.65	2.53	2.93

Table A.25: Singlet and triplet energies of the ligand systems. R is the Substituent in **5-position**, R' is the Substituent in 8-position. Calculated with IEF-PCM solvation model (ETOH) on UB3LYP/TZVP level of theory.

6-Position						
R	R'	S ₀ -S ₁ [eV]	T _{1S*} -S ₀ [eV]	T _{1T} -S ₀ [eV]	T _{1S} -S ₀ [eV]	
NH ₂	OH	3.52	2.55	2.36	2.74	
CN	OH	3.78	2.55	2.45	2.81	
HSO ₃	OH	3.91	2.68	2.38	2.82	
NO ₂	OH	2.88	2.17	2.03	2.37	
Ph	OH	3.72	2.56	2.44	2.83	
Py	OH	3.04	2.57	2.33	2.78	
7-Position						
R	R'	S ₀ -S ₁ [eV]	T _{1S*} -S ₀ [eV]	T _{1T} -S ₀ [eV]	T _{1S} -S ₀ [eV]	
NH ₂	OH	3.76	2.61	2.48	2.88	
CN	OH	3.86	2.62	2.54	2.86	
HSO ₃	OH	3.96	2.74	2.60	2.99	
NO ₂	MeO	3.20	2.47	2.24	2.69	
NO ₂	OH	2.98	2.19	1.72	2.33	
Ph	OH	3.72	2.58	2.46	2.84	
Py	OH	3.04	2.63	2.51	2.84	

Table A.26: Singlet and triplet energies of the ligand systems. R is the Substituent in **6- and 7-position**, R' is the Substituent in 8-position. Calculated with IEF-PCM solvation model (ETOH) on UB3LYP/TZVP level of theory.

R, isomer:		H isomer 1	NH ₂ isomer 2	NH ₂ isomer 3	NO ₂ isomer 2	NO ₂ isomer 3	HSO ₃ isomer 3
r[Å]	Eu-N1	2.6360	2.6208	2.6208	2.5973	2.6208	2.6308
r[Å]	Eu-N2	2.6360	2.6251	2.5862	2.6029	2.5862	2.5919
r[Å]	Eu-N3	2.6360	2.5862	2.6251	2.5669	2.6251	2.6273
r[Å]	Eu-O1	2.2509	2.2619	2.2619	2.2705	2.2619	2.2473
r[Å]	Eu-O2	2.2509	2.2488	2.2694	2.2613	2.2694	2.2637
r[Å]	Eu-O3	2.2509	2.2694	2.2488	2.2821	2.2488	2.2552
∠[°]	axial	149.95	137.40	137.40	138.07	137.40	147.10
∠[°]	axial	149.95	153.68	153.68	150.18	153.68	135.11
∠[°]	axial	149.95	149.37	149.37	149.05	149.37	150.97
∠[°]	equatorial	66.90	66.91	66.91	66.24	66.91	66.39
∠[°]	equatorial	66.90	66.98	67.53	66.26	67.53	67.00
∠[°]	equatorial	66.90	67.53	66.98	66.83	66.98	66.30

Table A.27: Geometry of the complexes in its **singlet** state. R is the substitution in 5-position of the ligand. Calculation in **gas phase** on UB3LYP/6-31G* level of theory.

R, isomer:		H isomer 1	NH ₂ isomer 2	NH ₂ isomer 3	NO ₂ isomer 2	NO ₂ isomer 3	HSO ₃ isomer 3
r[Å]	Eu-N1	2.5261	2.6360	2.6165	2.6053	2.6049	2.6197
r[Å]	Eu-N2	2.6378	2.4739	2.6021	2.5718	2.5714	2.5968
r[Å]	Eu-N3	2.6243	3.6072	2.4971	2.5334	2.5332	2.4986
r[Å]	Eu-O1	2.3482	2.2437	2.6165	2.2624	2.2624	2.2463
r[Å]	Eu-O2	2.2519	2.3751	2.6021	2.2658	2.2665	2.5968
r[Å]	Eu-O3	2.2442	2.2528	2.3488	2.3358	2.3360	2.4986
∠[°]	axial	153.40	147.15	133.98	145.61	145.39	130.38
∠[°]	axial	146.07	141.01	145.50	138.59	151.47	139.00
∠[°]	axial	150.06	148.04	151.37	152.06	138.64	148.85
∠[°]	equatorial	67.64	66.77	66.94	66.16	66.16	66.43
∠[°]	equatorial	66.59	67.89	67.20	66.81	66.81	66.94
∠[°]	equatorial	67.03	66.80	67.68	66.92	66.96	67.18

Table A.28: Geometry of the complexes in its **triplet** state. R is the substitution in 5-position of the ligand. Calculation in **gas phase** on UB3LYP/6-31G* level of theory.

R, isomer:		H isomer 1	NH ₂ isomer 2	NH ₂ isomer 3	NO ₂ isomer 2	NO ₂ isomer 3	HSO ₃ isomer 2
r [Å]	Eu-N1	2.5120	2.5100	2.5101	2.5087	2.5086	2.5161
r [Å]	Eu-N2	2.5119	2.5095	2.5083	2.5086	2.5072	2.5141
r [Å]	Eu-N3	2.3753	2.5083	2.5095	2.5073	2.5086	2.5161
r [Å]	Eu-O1	2.5122	2.3723	2.3723	2.3764	2.3762	2.3713
r [Å]	Eu-O2	2.3753	2.3708	2.3756	2.3753	2.3797	2.3756
r [Å]	Eu-O3	2.3754	2.3758	2.3709	2.3795	2.3755	2.3713
∠ [°]	axial	148.41	135.56	135.49	136.13	136.37	135.60
∠ [°]	axial	148.65	153.39	153.14	152.19	150.46	150.26
∠ [°]	axial	147.85	154.12	153.63	154.38	154.65	155.23
∠ [°]	equatorial	64.32	64.23	64.24	63.94	63.93	63.90
∠ [°]	equatorial	64.32	64.39	64.50	64.05	64.17	64.22
∠ [°]	equatorial	64.32	64.50	64.39	64.14	64.04	64.02

Table A.29: Geometry of the complexes in its **singlet** state. R is the substitution in 5-position of the ligand. Calculation in **gas phase** on HF-AM1 level of theory.

R, isomer:		H isomer 1	NH ₂ isomer 2	NH ₂ isomer 3	NO ₂ isomer 2	NO ₂ isomer 3	HSO ₃ isomer 3
r [Å]	Eu-N1	2.5101	2.4639	2.4639	2.5082	2.5097	2.4658
r [Å]	Eu-N2	2.4616	2.5104	2.5093	2.4623	2.5082	2.5120
r [Å]	Eu-N3	2.5111	2.5093	2.5104	2.5084	2.5078	2.5137
r [Å]	Eu-O1	2.3755	2.4155	2.4156	2.3771	2.3778	2.4195
r [Å]	Eu-O2	2.4206	2.3733	2.3736	2.4161	2.3810	2.3730
r [Å]	Eu-O3	2.3758	2.3737	2.3733	2.3801	2.3710	2.3721
∠ [°]	axial	147.49	138.27	138.22	136.02	135.07	137.65
∠ [°]	axial	149.88	163.46	163.36	143.68	152.61	161.77
∠ [°]	axial	141.41	140.42	140.13	160.59	154.19	139.91
∠ [°]	equatorial	64.31	63.87	63.87	63.97	63.90	63.85
∠ [°]	equatorial	63.87	64.16	64.22	63.70	64.13	64.05
∠ [°]	equatorial	64.20	64.22	64.16	64.08	64.20	63.91

Table A.30: Geometry of the complexes in its **triplet** state. R is the substitution in 5-position of the ligand. Calculation in **gas phase** on HF-AM1 level of theory.

R		H	NH ₂	NO ₂
r [Å]	Eu-N1	2.6038	2.5268	2.5930
r [Å]	Eu-N2	2.6250	2.6263	2.6137
r [Å]	Eu-N3	2.5600	2.6141	2.5493
r [Å]	Eu-O1	2.2862	2.2944	2.2878
r [Å]	Eu-O2	2.2451	2.2538	2.2566
r [Å]	Eu-O3	2.2861	2.2778	2.2924
∠ [°]	axial	142.55	142.21	141.00
∠ [°]	axial	148.33	147.49	148.19
∠ [°]	axial	158.16	151.90	152.26
∠ [°]	equatorial	66.99	68.02	66.30
∠ [°]	equatorial	66.92	66.95	66.02
∠ [°]	equatorial	67.95	66.82	67.22
r [Å]	Eu-DCM1	4.8048	3.7596	4.7982
r [Å]	Eu-DCM2	4.6416	4.8353	5.0252
r [Å]	Eu-DCM3	5.7171	5.7406	5.6545

Table A.31: Geometry of the complexes in its **singlet** state for **isomer2**. R is the substitution in 5-position of the ligand. Calculation on UB3LYP/6-31G* level of theory with three **explicit DCM** solvent molecules.

R		H	NH ₂	NO ₂
r [Å]	Eu-N1	2.5947	2.4913	2.5318
r [Å]	Eu-N2	2.4912	2.6270	2.6124
r [Å]	Eu-N3	2.5656	2.5657	2.5559
r [Å]	Eu-O1	2.2814	2.3687	2.3450
r [Å]	Eu-O2	2.3660	2.2538	2.2582
r [Å]	Eu-O3	2.2827	2.2712	2.2809
∠ [°]	axial	139.44	144.80	143.47
∠ [°]	axial	146.83	139.10	145.35
∠ [°]	axial	138.40	156.26	158.36
∠ [°]	equatorial	66.99	67.59	67.03
∠ [°]	equatorial	67.69	66.90	66.05
∠ [°]	equatorial	67.79	67.85	67.11
r [Å]	Eu-DCM1	4.6548	4.5045	4.8730
r [Å]	Eu-DCM2	4.7805	4.7296	4.9834
r [Å]	Eu-DCM3	5.3533	6.5315	6.3677

Table A.32: Geometry of the complexes in its **triplet** state for **isomer2**. R is the substitution in 5-position of the ligand. Calculation on UB3LYP/6-31G* level of theory with three **explicit DCM** solvent molecules.

R		H	NH ₂	NO ₂
r [Å]	Eu-N1	2.6271	2.7170	2.6856
r [Å]	Eu-N2	2.6495	2.6428	2.6648
r [Å]	Eu-N3	2.7087	2.6952	2.6320
r [Å]	Eu-O1	2.2955	2.3813	2.3837
r [Å]	Eu-O2	2.4067	2.3044	2.3147
r [Å]	Eu-O3	2.3495	2.3684	2.3571
∠ [°]	axial	144.48	146.95	140.84
∠ [°]	axial	128.76	146.31	151.29
∠ [°]	axial	129.15	147.46	143.09
∠ [°]	equatorial	66.89	63.77	64.19
∠ [°]	equatorial	64.89	66.20	65.06
∠ [°]	equatorial	64.74	64.29	64.50
r [Å]	Eu-ETOH1	4.1515	2.4924	2.6889
r [Å]	Eu-ETOH2	2.5675	4.0481	2.9800
r [Å]	Eu-ETOH3	2.6178	2.5481	2.6363

Table A.33: Geometry of the complexes in its **singlet** state for **isomer2**. R is the substitution in 5-position of the ligand. Calculation on UB3LYP/6-31G* level of theory with three **explicit ETOH** solvent molecules.

R		H	NH ₂	NO ₂
r [Å]	Eu-N1	2.6792	3.5808	2.6548
r [Å]	Eu-N2	2.5326	2.4762	2.6591
r [Å]	Eu-N3	2.6429	2.6073	2.6460
r [Å]	Eu-O1	2.3503	2.2900	2.4318
r [Å]	Eu-O2	2.3956	2.3561	2.3148
r [Å]	Eu-O3	2.3884	2.4013	2.3577
∠ [°]	axial	134.76	139.71	141.17
∠ [°]	axial	142.09	131.51	136.08
∠ [°]	axial	149.13	133.77	117.70
∠ [°]	equatorial	65.38	66.40	64.65
∠ [°]	equatorial	67.24	67.93	65.06
∠ [°]	equatorial	65.45	65.80	64.36
r [Å]	Eu-ETOH1	2.6002	2.5850	2.6627
r [Å]	Eu-ETOH2	4.1054	4.1708	2.9419
r [Å]	Eu-ETOH3	2.5925	4.5049	2.6488

Table A.34: Geometry of the complexes in its **triplet** state for **isomer2**. R is the substitution in 5-position of the ligand. Calculation on UB3LYP/6-31G* level of theory with three **explicit ETOH** solvent molecules.

R		H	NH ₂	NO ₂
r [Å]	Eu-N1	2.5100	2.5120	2.5106
r [Å]	Eu-N2	2.5107	2.5120	2.5115
r [Å]	Eu-N3	2.5070	2.4944	2.5078
r [Å]	Eu-O1	2.3824	2.3790	2.3838
r [Å]	Eu-O2	2.3755	2.3730	2.3776
r [Å]	Eu-O3	2.3810	2.3814	2.3826
∠ [°]	axial	132.56	135.49	132.77
∠ [°]	axial	152.15	149.88	152.37
∠ [°]	axial	152.25	146.72	151.54
∠ [°]	equatorial	64.37	64.21	63.97
∠ [°]	equatorial	64.32	64.24	63.88
∠ [°]	equatorial	64.61	64.65	64.19
r [Å]	Eu-DCM1	4.6053	4.6097	4.6279
r [Å]	Eu-DCM2	4.6321	5.0251	4.6376
r [Å]	Eu-DCM3	4.7641	4.7320	4.7678

Table A.35: Geometry of the complexes in its **singlet** state for **isomer2**. R is the substitution in 5-position of the ligand. Calculation on HF-AM1 level of theory with three **explicit DCM** solvent molecules.

R		H	NH ₂	NO ₂
r [Å]	Eu-N1	2.5101	2.5123	2.5141
r [Å]	Eu-N2	2.5122	2.5133	2.5113
r [Å]	Eu-N3	2.5055	2.5096	2.5098
r [Å]	Eu-O1	2.3831	2.3786	2.3817
r [Å]	Eu-O2	2.3832	2.3800	2.3839
r [Å]	Eu-O3	2.3820	2.3807	2.3893
∠ [°]	axial	138.58	134.71	133.82
∠ [°]	axial	140.60	140.79	144.03
∠ [°]	axial	134.45	118.50	119.84
∠ [°]	equatorial	64.33	64.15	63.63
∠ [°]	equatorial	64.35	64.28	63.83
∠ [°]	equatorial	64.53	64.34	64.13
r [Å]	Eu-ETOH1	3.7180	3.7498	3.7417
r [Å]	Eu-ETOH2	4.2469	4.5541	3.7518
r [Å]	Eu-ETOH3	3.7526	3.7224	4.7353

Table A.36: Geometry of the complexes in its **singlet** state for **isomer2**. R is the substitution in 5-position of the ligand. In the NH₂ complex the ETOH forms a bond to the Eu (highlighted bold). Calculation on HF-AM1 level of theory with three **explicit ETOH** solvent molecules.

R, isomer		Singlet*	EuQ ₄ (H ₂ O) ₂ Triplet	Eu(NO ₂ Q) ₄ (EtOH) ₂ Triplet
r [Å]	Eu-N1	4.8333	4.9854	5.0364
r [Å]	Eu-N2	2.6686	2.6610	2.6827
r [Å]	Eu-N3	2.6543	2.6304	2.6766
r [Å]	Eu-N4	4.1658	4.1392	4.2056
r [Å]	Eu-O1	2.3481	2.4275	2.6445
r [Å]	Eu-O2	2.3776	2.3716	2.3108
r [Å]	Eu-O3	2.3781	2.3562	2.3410
r [Å]	Eu-O4	2.2340	2.2219	2.2230
∠ [°]	axial	144.39	144.64	138.04
∠ [°]	axial	144.82	143.62	138.50
∠ [°]	axial	174.50	171.77	163.00
∠ [°]	equatorial	64.86	64.95	64.62
∠ [°]	equatorial	64.53	65.28	64.18
r [Å]	Eu-Solvent	4.3047	4.3891	4.3997
r [Å]	Eu-Solvent	2.5202	2.5031	2.4975

Table A.37: Geometry of the EuQ₄X₂ complexes for the **singlet** and **triplet** structures. Calculated on UB3LYP/6-31G* level of theory. (*) All complexes show the same geometry in the singlet state.

Gas phase	H	NH ₂	NO ₂	HSO ₃
S ₀ -S ₁	2.85	2.40	3.01	2.44
T _{1S*} -S ₀	2.13	1.80	2.12	1.85
T _{1T} -S ₀	1.98	1.50	2.07	1.67
IEF-PCM DCM	H	NH ₂	NO ₂	HSO ₃
S ₀ -S ₁	3.02	2.52	3.01	2.51
T _{1S*} -S ₀	2.25	1.90	2.10	1.92
T _{1T} -S ₀	2.10	1.50	2.08	1.65
IEF-PCM ETOH	H	NH ₂	NO ₂	HSO ₃
S ₀ -S ₁	3.01	2.49	2.98	2.52
T _{1S*} -S ₀	2.25	1.89	2.08	1.93
T _{1T} -S ₀	2.06	1.47	2.04	1.62

Table A.38: Singlet and triplet state energies in eV for the complexes in **gas phase** and with **IEF-PCM** solvation model. Calculated on UB3LYP/TZVP level of theory.

LV

expl.DCM	H	NH ₂	NO ₂
S ₀ -S ₁	2.88	2.43	2.95
T _{1S*} -S ₀	2.17	1.83	2.95
T _{1T} -S ₀	2.01	1.92	2.16
expl. ETOH	H	NH ₂	NO ₂
S ₀ -S ₁	2.84	2.28	2.75
T _{1S*} -S ₀	2.17	1.86	2.08
T _{1T} -S ₀	2.02	1.42	1.88
	S ₀ -S ₁	T _{1S*} -S ₀	T _{1T} -S ₀
EuQ ₄ (H ₂ O) ₂	1.96	1.67	1.58

Table A.39: Singlet and triplet state **energies in eV** for the complexes in gas phase and with **explicit solvation model**. Calculated on UB3LYP/TZVP level of theory.

Appendix B

List of Tables

List of Tables

3.1	Dielectric constant of the solvents	38
3.2	Eu sprakle parameters	39
4.1	Experimental and calculated geometry parameters of 8-hydroxyquinoline	42
4.2	Absorption energy of 8HQ	61
4.3	Experimental and calculated absorption energies of 8HQ	61
4.4	Experimental and calculated absorption energies of 5-CHO-8HQ	63
4.5	Absorption energy of 5-CHO-8HQ	65
4.6	Experimental and calculated absorption energies of 5-NO ₂ -8HQ	68
4.7	Absorption energy of 5-NO ₂ -8HQ	70
4.8	Relative energy of the complexes	83
4.9	Absorption energies for Eu(Q) ₃ complex	94
4.10	Absorption energies for Eu(NH ₂ Q) ₃ complex (isomer 2)	97
4.11	Absorption energies for Eu(NH ₂ Q) ₃ complex (isomer 3)	100
4.12	Absorption energies for Eu(NO ₂ Q) ₃ complex (isomer 2)	104
4.13	Absorption energies for Eu(NO ₂ Q) ₃ complex (isomer 3)	105
4.14	Absorption energies for Eu(HSO ₃ Q) ₃ complex	108
4.15	Absorption energies for EuQ ₃ (ETOH) ₃ complex	111
4.16	Absorption energies of EuQ ₃ (DCM) ₃ complex	112
4.17	Absorption energies of Eu(NH ₂ Q) ₃ (ETOH) ₃ complex	114
4.18	Absorption energies of Eu(NH ₂ Q) ₃ (DCM) ₃ complex	115
4.19	Absorption energies of Eu(NO ₂ Q) ₃ (ETOH) ₃ complex	116
4.20	Absorption energies of Eu(NO ₂ Q) ₃ (DCM) ₃ complex	117
4.21	Absorption energies of EuQ ₄ (H ₂ O) ₂ complex	120
4.22	Absorption energies of EuQ ₄ (ETOH) ₂ complex	122
4.23	Error of calculation vs. XRD structure - ligands	129
4.24	Error of calculated singlet energies vs. experimental results - ligands	130
4.25	Error of calculated singlet and triplet energies vs. experimental results - complexes	131

4.26 Mullien charges of ligands and complexes	133
A.1 Experimental vs. calculated geometry of 8HQ - bond length	XVII
A.2 Experimental vs. calculated geometry of 8HQ - angles	XVIII
A.3 Geometry parameter of ligand system: substitution in 2- and 3-position (singlet)	XIX
A.4 Geometry parameter of ligand system: substitution in 4-position (singlet)	XX
A.5 Geometry parameter of ligand system: substitution in 5-position (singlet)	XXI
A.6 Geometry parameter of ligand system: substitution in 6- and 7-position (singlet)	XXII
A.7 Geometry parameter of ligand system: substitution in 2- and 3-position (triplet)	XXIII
A.8 Geometry parameter of ligand system: substitution in 4-position (triplet)	XXIV
A.9 Geometry parameter of ligand system: substitution in 5-position (triplet)	XXV
A.10 Geometry parameter of ligand system: substitution in 6- and 7-position (triplet)	XXVI
A.11 Electronic parameter of ligand system: substitution in 2- and 3-position	XXVII
A.12 Electronic parameter of ligand system: substitution in 4-position	XXVIII
A.13 Electronic parameter of ligand system: substitution in 5-position	XXIX
A.14 Electronic parameter of ligand system: substitution in 6- and 7-position	XXX
A.15 Singlet and triplet energies of ligand system: substitution in 2- and 3-position (gas phase)	XXXI
A.16 Singlet and triplet energies of ligand system: substitution in 4-position (gas phase)	XXXII
A.17 Singlet and triplet energies of ligand system: substitution in 5-position (gas phase)	XXXIII
A.18 Singlet and triplet energies of ligand system: substitution in 6- and 7-position (gas phase)	XXXIV
A.19 Singlet and triplet energies of ligand system: substitution in 2- and 3-position (DCM)	XXXV
A.20 Singlet and triplet energies of ligand system: substitution in 4-position (DCM)	XXXVI
A.21 Singlet and triplet energies of ligand system: substitution in 5-position (DCM)	XXXVII
A.22 Singlet and triplet energies of ligand system: substitution in 6- and 7-position (DCM)	XXXVIII
A.23 Singlet and triplet energies of ligand system: substitution in 2- and 3-position (ETOH)	XXXIX
A.24 Singlet and triplet energies of ligand system: substitution in 4-position (ETOH)	XL
A.25 Singlet and triplet energies of ligand system: substitution in 5-position (ETOH)	XLI
A.26 Singlet and triplet energies of ligand system: substitution in 6- and 7-position (ETOH)	XLII
A.27 DFT-Geometry parameters of complex systems in gas phase (singlet)	XLIII
A.28 DFT-Geometry parameters of complex systems in gas phase (triplet)	XLIV
A.29 AM1-Geometry parameters of complex systems in gas phase (singlet)	XLV
A.30 Am1-Geometry parameters of complex systems in gas phase (triplet)	XLVI
A.31 DFT-Geometry parameters of complex systems with three DCM molecules (singlet)	XLVII
A.32 DFT-Geometry parameters of complex systems with three DCM molecules (triplet)	XLVIII
A.33 DFT-Geometry parameters of complex systems with three ETOH molecules (singlet)	XLIX
A.34 DFT-Geometry parameters of complex systems with three ETOH molecules (triplet)	L

A.35 AM1-Geometry parameters of complex systems with three DCM molecules (singlet) . . .	LI
A.36 AM1-Geometry parameters of complex systems with three ETOH molecules (singlet) . . .	LII
A.37 DFT-Geometry parameters of EuQ_4X_2 complex ($\text{X}=\text{H}_2, \text{ETOH}$)	LIII
A.38 Singlet and triplet energies for complex system (gas phase and IEF-PCM)	LIV
A.39 Singlet and triplet energies for complex system (expl. solvent)	LV

Appendix C

List of Figures

List of Figures

2.1	Scheme of HF calculation	11
2.2	Shape of STO and GTO functions	12
4.1	Isomers of 8-hydroxyquinolin	40
4.2	PES along the C-C-O-H torsion mode in 8-hydroxyquinoline	41
4.3	Torsion angle of Py group in Py substituted 8-hydroxyquinoline	43
4.4	Bond length of C(8')-C(8) bond in 8-hydroxyquinoline (singlet)	45
4.5	Bond length of C(8')-N(1) bond in 8-hydroxyquinoline (singlet)	46
4.6	Bond length of C(8)-O(9) bond in 8-hydroxyquinoline (singlet)	47
4.7	Bond length of O(9)-H(10) bond in 8-hydroxyquinoline (singlet)	47
4.8	N(1)-C(8')-C(8) angle in 8-hydroxyquinoline (singlet)	48
4.9	C(8')-C(8)-O(9) angle in 8-hydroxyquinoline (singlet)	48
4.10	Bond length of C(8')-C(8) bond in 8-hydroxyquinoline (triplet)	49
4.11	Bond length of C(8')-N(1) bond in 8-hydroxyquinoline (triplet)	50
4.12	Bond length of C(8)-O(9) bond in 8-hydroxyquinoline (triplet)	51
4.13	Bond length of O(9)-H(10) bond in 8-hydroxyquinoline (triplet)	51
4.14	N(1)-C(8')-C(8) angle in 8-hydroxyquinoline (triplet)	52
4.15	C(8')-C(8)-O(9) angle in 8-hydroxyquinoline (triplet)	52
4.16	Difference in singlet and triplet structure of 8HQ: C(8')-C(8) bond	53
4.17	Difference in singlet and triplet structure of 8HQ: C(8')-N(1) bond	53
4.18	Difference in singlet and triplet structure of 8HQ: C(8)-O(9) bond	54
4.19	Difference in singlet and triplet structure of 8HQ: O(9)-H(10) bond	54
4.20	Electronic parameter for substituents in 5-position of the 8HQ backbone	56
4.21	IP and E_{ea} values for different substituents in 5-position of the 8HQ backbone	57
4.22	Experimental and calculated spectra of 8HQ	59
4.23	HOMO and LUMO orbitals of 8HQ	60
4.24	Experimental and calculated spectra of 5-CHO-8HQ	63
4.25	Molecular orbitals of 5-CHO-8HQ	64

4.26	Experimental and calculated spectra of 5-NO ₂ -8HQ	68
4.27	Molecular orbitals of 5-NO ₂ -8HQ	69
4.28	Singlet energies of the ligands (gas phase)	71
4.29	HOMO - LUMO splitting for the ligand system	73
4.30	HOMO - LUMO splitting for Py and NO ₂ substituted ligands	74
4.31	HOMO - LUMO splitting for NH ₂ and Ph substituted ligands	74
4.32	HOMO - LUMO splitting for HSO ₃ and CN substituted ligands	75
4.33	Jablonski diagram for ligands	77
4.34	Triplet state energies for ligands (gas phase)	77
4.35	Triplet state energy for ligands (IEF-PCM ETOH)	78
4.36	Triplet state energies for ligands (IEF-PCM DCM)	79
4.37	HOMO, LUMO and SOMO orbital energy for ligands	80
4.38	Sheme of the "Antenna-Effect"	81
4.39	Structure of the complex isomers	82
4.40	Structure of EuQ ₃	83
4.41	Structure of Eu(Q) ₄ (H ₂ O) ₂	84
4.42	Structure of ninefold coordinated EU(NO ₂ Q) ₃ (ETOH) ₃ complex	86
4.43	Structure of Eu(NO ₂ Q) ₃ (DCM) ₃	87
4.44	Spectra of Eu(Q) ₃ complex	91
4.45	Occupied orbitals of EuQ ₃ complex	92
4.46	unoccupied orbitals of EuQ ₃ complex	93
4.47	Spectra of Eu(NH ₂ Q) ₃ complex	96
4.48	Occupied orbitals of Eu(NH ₂ Q) ₃ complex	98
4.49	Unoccupied orbitals of Eu(NH ₂ Q) ₃ complex	99
4.50	HOMO orbitals of isomer 2 and 3 of Eu(NH ₂ Q) ₃ complex	100
4.51	Spectra of Eu(NO ₂ Q) ₃ complex	102
4.52	Molecular orbitals of Eu(NO ₂ Q) ₃ complex	103
4.53	Spectra of Eu(HSO ₃ Q) ₃ complex	107
4.54	Molecular orbitals of Eu(HSO ₃ Q) ₃ complex	109
4.55	HOMO-3 orbital of Eu(NH ₂ Q) ₃ (ETOH) ₃ complex	113
4.56	Absorptionspectra of EuQ ₄ (X) ₂ complexes (X=H ₂ O, ETOH)	119
4.57	Molecular orbitals of EuQ ₄ (H ₂ O) ₂ complex	121
4.58	Molecular orbitals of EuQ ₄ (ETOH) ₂ complex	123
4.59	HOMO - LUMO splitting of different complexes	124
4.60	Singlet energies of different complexes (gas phase and PCM-solvent model	125

4.61 Jablonski diagram for complexes	126
4.62 Triplet state energies of different complexes (gas phase)	126
4.63 Triplet state energies of different complexes (DCM)	127
4.64 Triplet state energies of different complexes (ETOH)	127
4.65 HOMO, LUMO and SOMO orbital energies of different complexes	128
4.66 Correlation of Mulliken charge and Eu-O bond length - singlet	134
4.67 Correlation of Mulliken charge and Eu-O bond length - triplet	134
4.68 Correlation of Mulliken charge and singlet energies	135
4.69 Correlation of Mulliken charge and triplet energies	135

Appendix D

List of Symbols

β^0	Bonding parameter in CNDO
Δ	Laplace operator
$\delta_{\mu,\nu}$	Kronecker delta
η_S	Chemical Hardness
κ	Debye-Hückel parameter
λ	Switching function; $0 \leq \lambda \leq 1$
μ	Dipole moment operator
μ^{elec}	electronic part of dipole momentum
μ^{nuc}	nuclear part of dipole momentum
μ_S	Chemical Potential
μ, ν	Indices referring to electrons
$\rho(r)$	Electron density
Ω	Transition energy
ω	frequency
ϕ	Atomic orbital function (GTO or STO)
Φ_{HF}	Ground state Slater determinant
Φ_i	Excited state Slater determinant
$\phi(r)$	Electrostatic potential
s	Absolute Electronegativity
χ	Spin orbital function
Ψ	Single electron wavefunction
$\sigma_{x,y,z}$	Pauli spin matrices
ζ	Spin polarisation function
∇	Nabla operator
$A(r)$	Magnetic potential

a	Annihilation operator
a [†]	Creation operator
a_0	Bohr radius
B	Magnetic field
C	Coefficient matrix
c	Speed of light
E	Energy matrix
E_C	Correlation term of E _{XC}
E_{ea}	Electron Affinity
E_X	Exchange term of E _{XC}
E_{XC}	Exchange and correlation functional in DFT
e	Charge of one electron
F	Fock matrix
F ^{KS}	Kohn-Sham operator
<i>f</i>	Reaction field factor
G	Free energy
H	Hamiltonian operator
H	Hessian matrix
H [ρ](x,t)	One particle Hamiltonian in TD-DFT
h	Planck's constant
\hbar	Planck's constant divided by 2π
$h(r_\mu, r_\nu)$	Hole function
I	Unity matrix
IP	Ionisation Potential
κ, L	Indices referring to nuclei
M	Nucleus mass
m_e	Electron mass
P	Density matrix
P	One-particle density matrix
p	Momentum operator
q	Charge in terms of elementary charge
$R_{\kappa, L}$	Distance between two nuclei
r	Radius
r	Local operator
$r_{\mu, \nu}$	Distance between two electrons

S	Overlap matrix
S_0	Singlet groundstate
S_1	First excited singlet state
S^*	Excited singlet state
T	Kinetic energy operator
T_{UEG}	Kinetic energy operator for the uniform electron gas
T_{1T}	Optimised triplet state
T_{1S}	Optimised triplet state based on S_0 geometry
T_{1S^*}	Triplet state based on S_0 geometry, calculated with optimised singlet wavefunction coefficients.
T^*	Triplet state
U	Special potential energy operator in CNDO approach
V	Potential energy operator
V	Perturbation term in MP theory
v	velocity
x,y,z	Cartesian coordinates
Z	Charge of the nucleus